PHD

The Involvement of Phosphoinositide 3-kinase in Murine Lung Branching Morphogenesis and Insights into Protein Mediated Drug Delivery

Carter, Edward

Award date:
2014

Awarding institution:
University of Bath

The Involvement of Phosphoinositide 3-kinase in Murine Lung Branching Morphogenesis and Insights into Protein-mediated Drug Delivery

Edward Philip Carter

A thesis submitted for the degree of Doctor of Philosophy

University of Bath
Department of Pharmacy and Pharmacology

May 2014

Acknowledgements

Firstly I would like to express my sincere gratitude to my supervisors Steve Ward, David Tosh, Malcolm Watson and Randall Mrsny for their consistent enthusiasm, patience and friendship throughout my PhD. Without their support I would not have experienced many of the opportunities presented to me as part of my PhD. Thanks should also be given to the Medical Research Council and Novartis for funding my project for the past four years.

I would also like to thank Professor David Warburton and Dr Denise Al Alam at the Saban Research Institute, Los Angeles for inviting me to their lab to learn valuable techniques as well as providing guidance in the field of lung development. I am also grateful to Professor Wayne Lencer and Drs Ramiro Massol and Yvonne Welscher at Boston Children's Hospital for hosting me in their lab during a collaborative project.

Finally I would like to thank all the people at the university who have made this process both enjoyable and memorable. Special thanks goes to John Foster, Matt Blunt, Jenny Ball, Sophie Archer, Benoit Roux, Ana Maria Cravo and Floriane Laurent for their help and friendship over the years.

Abstract

Epithelial branching morphogenesis is a critical step in the development of many epithelial organs including the lungs and the salivary glands. Many of the signalling pathways that orchestrate this process show a resurgence in the diseased state. We sought to determine the role of a common disease pathway, the phosphoinositide 3-kinase (PI3K) pathway, in the branching program of the lung. We utilised *ex-vivo* cultures of embryonic murine lungs that best recapitulates the developmental process. Inhibition of PI3Kα, or its downstream signalling components Akt and mammalian target of rapamycin, was able to greatly enhance the branching potential of embryonic lungs, implying a negative role for PI3K in the lung branching morphogenesis. Moreover inhibition of PI3K was sufficient to alter the morphogenic properties of fibroblast growth factor 7 on isolated murine lung epithelium from a cystic to a branching response.

We also investigated protein mediated drug delivery tools to provide a means of enhancing the delivery of PI3K based therapeutics. Cell-penetrating peptides (CPPs) are small proteins that are able to transport a drug cargo across the membrane of a cell. However, given that many CPPs are derived from viral proteins and venoms we sought to determine if common CPPs could induce an immune response. CPPs we capable of delivering a protein cargo into the interior of epithelial cells without inducing an immune response as measured by a lack of NFκB activation and no observable increase in interleukin-6 or -8 secretion.

We finally explored the potential of repurposing bacterial toxins for therapeutic applications. The toxins *Pseudomonas aeruginosa* exotoxin A (PEx) and Cholix (Chx) are natively capable of entering cells and subsequently being transported to either the cytoplasm of non-polarised cells, or undergoing transcytosis across polarised cells. We were able to identify that the C16:1 ceramide chain variant of the ganglioside GM1 is capable of enhancing the intracellular transport of PEx to the Golgi network. Moreover, we demonstrated that PEx is able to transport an siRNA cargo across polarised monolayers of Caco-2 cells and deliver said cargo into cells present in the basolateral compartment.

Abbreviations

AEC	Alveolar Epithelial Cell
BMP	Bone Morphogenic Protein
BSA	Bovine Serum Albumin
CHO	Chinese Hamster Ovary
$CHO^{CD91-/-}$	Chinese Hamster Ovary cells deficient in CD91
Chx	Cholix Toxin
COPD	Chronic Obstructive Pulmonary Disease
CPP	Cell Penetrating Peptide
CTB	Cholera Toxin Subunit B
DAG	Diacylglycerol
DAPI	4', 6-diamidino-2-phenylindole
DTx	Diphtheria Toxin
DUSP	Dual Specificity Phosphatase
E	Embryonic Day
EF2	Elongation Factor 2
EMT	Epithelial-Mesenchymal Transition
ER	Endoplasmic Reticulum
FBS	Foetal Bovine Serum
FGF	Fibroblast Growth Factor
FGFR	Fibroblast Growth Factor Receptor
FRS2	Fibroblast Growth Factor Receptor Substrate 2
GEF	Guanine Nucleotide Exchange Factor
GFP	Green Fluorescent Protein
GPCR	G-Protein Coupled Receptor
GSK	Glycogen Synthase Kinase
IL	Interleukin
$Ins(1,4,5)P_3$	Inositol 1,4,5-trisphosphate
JNK	c-Jun N-terminal Kinase
MAPK	Mitogen Activated Protein Kinase
MEF	Murine Embryonic Fibroblasts
$MEF^{GM1-/-}$	Murine Embryonic Fibroblasts deficient in GM1
MMP	Matrix Metalloproteinase

mTOR	Mammalian Target of Rapamycin
mTORC	Mammalian Target of Rapamycin Complex
MTT	(4,5-dimethylthiazol-2-yl)- 2,5-diphenyl tetrazolium bromide
PDK1	3-Phosphoinositide-Dependent Protein Kinase 1
PEx	*Pseudomonas Aeruginosa* Exotoxin A
PFA	Paraformaldehyde
PH3	Phosphorylated Histone H3
PI3K	Phosphoinositide 3-kinase
$PI(4,5)P_2$	Phosphatidylinositol 4,5-bisphosphate
$PI(3,4,5)P_3$	Phosphatidylinositol 3,4,5-trisphosphate
PKC	Protein Kinase C
PLCγ	Phospholipase-Cγ
PTEN	Phosphatase and Tensin Homolog
RTK	Receptor Tyrosine Kinase
S6K	Ribosomal S6 Kinase
Shh	Sonic Hedgehog
SHIP	SH2-domain containing Inositol-5-phosphotase
SMA	Smooth Muscle Actin
SPC	Surfactant Protein C
SSB	Sjögren Syndrome Antigen B
TGF	Transforming Growth Factor
TNF	Tumour Necrosis Factor
TSC	Tuberous Sclerosis Complex
VEGFR	Vascular Endothelial Growth Factor Receptor

Table of Contents

Table of Figures

Table of tables

Chapter 1: Introduction

1.1 The mammalian lung

The mammalian lung is a remarkable organ, elegantly adapted for the process of gas exchange between the body and outside world. In order to effectively feed a respiring body with sustaining oxygen the lung requires two key design features: a very large surface area, approximately the size of a tennis court; and a very thin tissue barrier, separating the outside world with the circulatory system (Weibel, 2009). The first of these is achieved through the generation of an elaborate network of branching airway tubes that supply the 480 million gas exchanging alveoli with oxygen and blood (Ochs et al., 2004). The second of these requirements is accomplished by the alveoli, the primary gas-exchanging structure of the lung. Two specialised alveolar epithelial cell (AEC) types comprise an alveolus and function to maximise gas exchange. Type I cells make up approximately 96% of the alveolus surface and are extremely thin, minimising the space between the blood and atmosphere. Type II cells make up the other 4% and serve to replenish damaged type I cells and secrete surfactant proteins that reduce surface tension across the alveolus (Castranova et al., 1988).

Changes in the ability of this organ to effectively exchange gas, either through developmental complications or acquired disease, are therefore detrimental to the health of an individual and to society. In 2011 three of the ten leading causes of death in the world were a result of lung related diseases ().

As our understanding of the cellular processes involved in disease has increased similarities between the diseased environment and the developmental state of the organ are becoming apparent. Increased insight into the development of the lung will further increase our understanding of disease process and will lead to novel regenerative therapies. Alongside insights into the disease process, novel delivery methods need to be developed for emerging therapeutics that either cannot be administered by conventional means, require help in reaching their cellular target or need to be directed to their site of action to prevent systemic toxicity.

1.2 Lung development and disease

Asthma

Asthma is an airway inflammatory disease characterised by intermittent airway obstruction and is one of the most prevalent chronic diseases in the developed world (Barnes, 2004). Symptoms of asthma are mediated by increased mucus production and hyper responsive airway smooth muscle. Studies have identified that the airway-remodelling characteristic of asthma (goblet cell metaplasia, airway smooth muscle hyperplasia) are already established in infants before the onset of symptoms (Warner et al., 1998). Considering that airway smooth muscle is formed and is active during the development of the lung (Schittny et al., 2000), any abnormalities in this process may persist in the infant thus predisposing them to childhood asthma.

Chronic obstructive pulmonary disease

Chronic obstructive pulmonary disease (COPD) is an obstructive lung disease characterised by chronically reduced airflow. A major component of COPD is emphysema, the progressive loss of the respiratory surface area. Although there is a strong association with smoking and the development of emphysema, genetic factors can also be influential. For instance, α-1 antitrypsin deficiency predisposes individuals to emphysema. α-1 antitrypsin is produced from epithelial cells of the airways and acts as an inhibitor of neutrophil elastase. Deficiency of this gene therefore allows unimpeded neutrophil elastase function. This leads to the break down of elastin present in the alveoli, impairing their function and causing emphysema-like symptoms (Stockley and Turner, 2013). Mice deficient in Smad3, a major signalling component of the transforming growth factor (TGF) β pathway, exhibit impaired lung alveolarisation. This deficiency leads to the mice displaying an emphysema-like phenotype later in adulthood (Chen et al., 2005). Impairment in the development of the alveoli, or how they are maintained, may therefore reduce an individual's resilience to airway irritants later in life.

Pulmonary fibrosis

Pulmonary fibrosis is characterised by the progressive build up of connective tissue in the lung leading to loss of function and eventual death due to heart

failure; the primary driving force behind this disease is the generation of myofibroblasts within the lung (Scotton and Chambers, 2007). These cells proliferate and produce extracellular matrix that remodel the lung, destroying the gas exchange surface. The source of these cells is currently not well understood but TGFβ is considered to be an essential factor. TGFβ overexpression in the lungs of adult rats leads to an aggressive fibrosis (Sime et al., 1997). Similarly, mice deficient in Smad3 (and thus reduced TGFβ signalling) exhibited a resistance to bleomycin-induced fibrosis (Zhao et al., 2002). As loss of TGFβ signalling also leads to emphysema (Chen et al., 2005), appropriate levels of this factor are critical for the function of the lung. This is also true for the development of this organ as reduced TGFβ signalling impairs lung alveolarisation (Chen et al., 2005). Equally, overexpression of TGFβ in the epithelium of embryonic lung either through adenoviral overexpression or application of exogenous TGFβ inhibits the growth of the airway network (Xing et al., 2008; Zhao et al., 1999).

Cancer

Many epithelial cancers involve the aggressive proliferation and migration of cancerous cells into the surrounding environment. Studies from prostate (Pritchard et al., 2009; Schaeffer et al., 2008), breast (Zvelebil et al., 2013) and lung cancers (De Leij et al., 1987; Rudin et al., 2012) have identified that many pathways activated in the epithelial cells during the development of these organs become reactivated in the cancerous setting. As an example, two genes commonly found to be dysregulated in breast cancer, *Tbx3* and *Gata-3*, are essential in the development of the mammary gland. Deletion of either severely impairs the formation of the ductal tree and reduces epithelial cell differentiation (Asselin-Labat et al., 2007; Davenport et al., 2003). SOX2 is commonly upregulated in small cell lung cancer (Rudin et al., 2012). This transcription factor is also found during the development of the lung, overexpression of which results in an increased number of epithelial cell progenitor cells and impairs the development of the airway network (Gontan et al., 2008). Together, these studies would imply that epithelial cancers could result from a reversion to their developmental state.

Epithelial-mesenchymal transition

Epithelial-mesenchymal transition (EMT) is a process whereby epithelial cells lose their epithelial characteristics and adopt those of a mesenchymal cell (Figure 1.1). EMT is found during a number of developmental processes including gastrulation (Nieto et al., 1994), and neural crest formation (Duband et al., 1995; Theveneau et al., 2013). Incomplete EMT in the development of the neural crest is a cause of cleft palate in infants (Nawshad and Hay, 2003; Yu et al., 2009). Epithelial cancers are thought to undergo an EMT like event in the acquisition of a migratory phenotype, invading the surrounding tissue and giving rise to secondary tumours (Birchmeier et al., 1996). Moreover, EMT has been identified as a potential source of disease promoting myofibroblasts in lung fibrosis. This comes from the observations that a portion of cells taken from the lungs of mice with experimental fibrosis, and epithelial cells isolated from patients with idiopathic pulmonary fibrosis, express markers of both epithelial and mesenchymal cells, indicative of a cell undergoing EMT (Kim et al., 2006; Marmai et al., 2011).

One of the most well studied promoters of EMT is the pro-fibrotic cytokine TGFβ (Miettinen et al., 1994; Willis et al., 2005). TGFβ can induce characteristic features of EMT in cultured epithelial cells such as the loss of the adherens junction protein E-Cadherin and the gain of the mesenchymal proteins vimentin and fibronectin. The transcription factors slug and snail are crucial for this process and act downstream of TGFβ to directly inhibit E-Cadherin transcription and promote fibroblast protein transcription (Cano et al., 2000; Naber et al., 2013). Prolonged exposure to TGFβ also induces the expression of smooth muscle actin (αSMA) and the production of extracellular matrix proteins (Shirakihara et al., 2011), hallmarks of the fibrotic process. TGFβ is therefore an attractive target for fibrosis. Indeed, p38 kinase inhibitor pirfenidone, and the only currently licenced drug for pulmonary fibrosis, exerts its anti-fibrotic actions partly through the suppression of TGFβ activity (Iyer et al., 1999). Moreover, pirfenidone can reduce TGFβ-induced EMT in cultured epithelial cells (Hisatomi et al., 2012). However the use of pirfenidone for pulmonary fibrosis in the clinic is controversial based on a somewhat limited efficacy and a large number of adverse side effects (Anon., 2013; Takeda et al., 2014). New, more potent therapies for pulmonary fibrosis may

emerge from an enhanced understanding of the mechanisms that govern the EMT process in both development and disease.

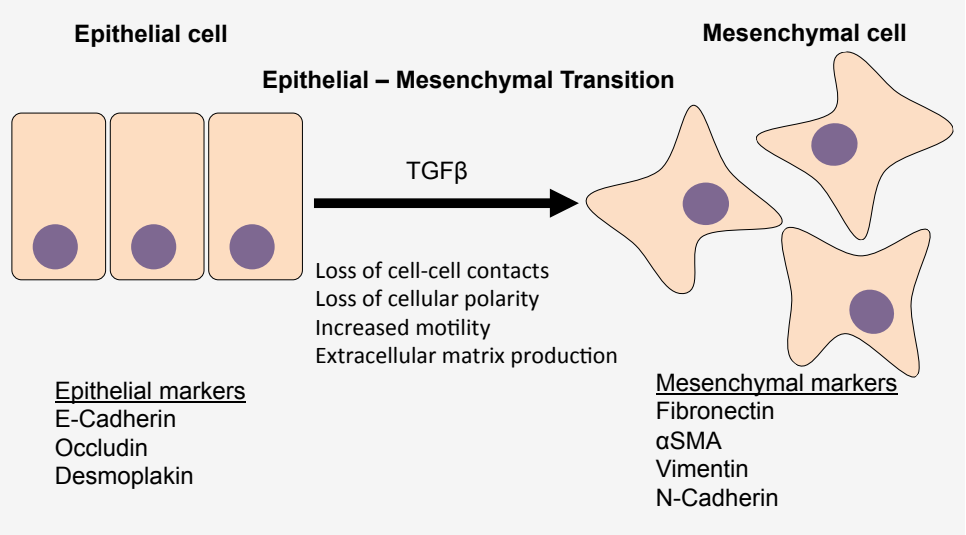

Figure 1.1. Characteristic features of epithelial–mesenchymal transition. Diagram illustrating the main cellular changes in morphology and protein expression during epithelial-mesenchymal transition in response to TGFβ.

1.3 Lung development

The embryonic development of the lung can be split into five separate stages based on morphological appearance and function: i) embryonic, ii) pseudoglandular, iii) canalicular, iv) saccular and v) alveolar (Figure 1.2) (Joshi and Kotecha, 2007; Warburton et al., 2010):

Embryonic (embryonic day (E) 9 – 12 in murine embryos, 3 – 7 weeks in human pregnancy): The lung initially develops as an outgrowth of the ventral foregut, the laryngotracheal groove. The trachea forms from invading cells of the foregut endoderm. This tracheal line subsequently develops into two primary bronchi by the end of this stage.

Pseudoglandular (E12 – 16 in murine embryos, 5 – 17 weeks in human pregnancy): During this stage the primitive epithelial tubes of the lung undergo successive rounds of highly coordinated branching. Cells of the branching epithelium invade the surrounding mesenchyme in a stereotypical fashion culminating in a network of airway tubules resembling the architecture of the adult

organ (Figure 1.3A) (Metzger et al., 2008). 23 generations of airways are formed in humans and 12 in mice (Weibel and Gomez, 1962). Interactions between the branching epithelium and the surrounding mesenchymal tissue tightly control at what point branches form and separate from one another.

Canalicular (E15 – 17 in murine embryos, 16 – 26 weeks in human pregnancy): Once the branched network of airway epithelial tubes has formed there is a substantial vascularisation of the airways. Terminal bronchioles and alveolar ducts comprising the acini of the lung also begin to form and epithelial cells begin to differentiate from the immature type II AECs cells of the pseudoglandular stage to mature type I and type II AECs.

Saccular (E17 – Birth in murine embryos, 26 – 36 weeks in human pregnancy): Thinning of the acinar structures occurs accompanied by the formation of saccular structures. Epithelial cells further differentiate into mature type I and type II AECs

Alveolar (Birth to postnatal day 20 in mouse, 36 weeks of pregnancy to 8 years of age in humans): The majority of the gas-exchanging surface is formed at this stage and continues following the birth of a mammal. A human infant is born with approximately 20-50 million alveoli that will develop into 480 million by adulthood (Kotecha, 2000; Ochs et al., 2004).

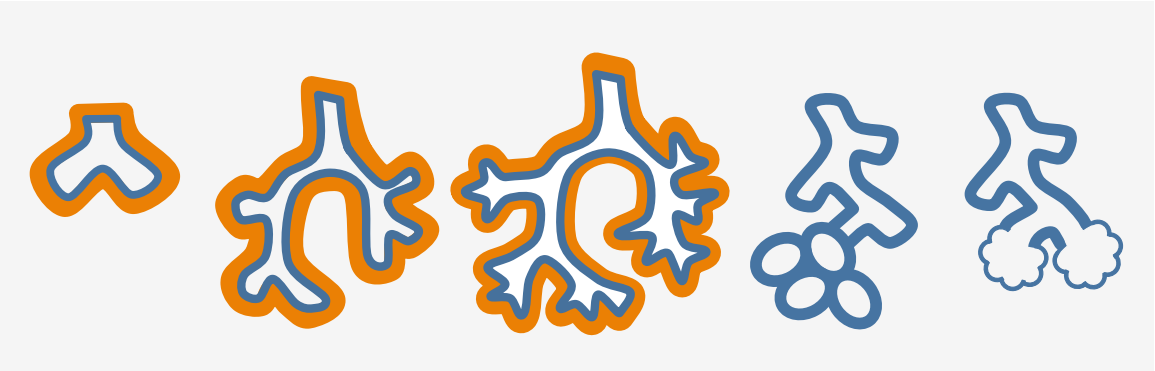

Embryonic	Pseudoglandular	Canalicular	Saccular	Alveolar
Mouse: E 9-12	E 12-15	E 15-17	E 17-Birth	Birth – PN20
Human: Wks 3-7	Wks 5-17	Wks 16-26	Wks 26-36	Wks 36 – 8 years

Figure 1.2. Stages of mammalian lung development. Illustrations of the main morphological changes that define the different stages of lung development. Approximate time for each stage in human and murine development is given. Lung epithelial tissue is highlighted in blue and mesenchyme in orange. E – Embryonic day; PN – postnatal.

1.4 Lung branching morphogenesis

Epithelial branching morphogenesis is a process critical for the development of many epithelial organs such as the lung, pancreas, mammary and salivary glands. Remarkably, lungs are sufficiently identical between mice so as to suggest a pre-determined pattern of lung growth. Indeed, the apparent complexity of the branched network can be adequately modelled through the repetition of simple patterns (fractal mathematics) (Mandelbrot, 1983).

Analysis of the branched structure of the lung revealed that with each successive generation of the airway tree, the diameter of each airway reduces by a constant factor (Weibel and Gomez, 1962). Surprisingly, this factor is optimum for airflow in a branched system, minimising the work required to overcome flow resistance and dead space volume (Murray, 1926; Weibel, 2009).

The branching of the lung can be further simplified by the discovery in mice that there are only three modes of branching repeated throughout the pseudoglandular stage: domain branching, planar bifurcation and orthogonal bifurcation (Figure 1.3). In domain branching, daughter branches form along the proximal part of a parent branch. This process occurs from the start of the lung branching program and is found throughout the pseudoglandular stage. From E12 onwards, planar bifurcation is found, during this process the tip of an expanding branch splits into two daughter branches, which continue to develop along the same plane as the parent. The final branching process, orthogonal bifurcation, occurs from E13 onwards and is similar to planar bifurcation in that two daughter branches are formed from the tip of a parent. However, following bifurcation the two daughter branches rotate and continue to develop along a different plane from the parent (Metzger et al., 2008). This provides answers as to how the lung can create such a vast network of branches in such a small area.

This branching program therefore requires substantial regulation to coordinate where branches should form and regulate their size to maximise on the space available for growth. Equally, the branching program needs to achieve the optimal number of terminal buds. Too few a number and there would not be enough

terminal branches to give rise to an effective number of alveoli. Too many and there would be insufficient space for the alveoli to dilate into at the latter part of their development, thus compromising their effectiveness. To achieve this delicate balance there is considerable cross talk between the branching epithelium and the surrounding mesenchyme using a plethora of communication factors.

Peristaltic waves in branching morphogenesis

As the branched network of the lung is formed the developing lumen is filled with fluid that is constantly been forced though the branched network by peristaltic waves of contraction (Schittny et al., 2000). These constant waves of contraction are propagated by airway smooth muscle lining the proximal branches and appear to regulate branching morphogenesis. Increasing the peristalsis of cultured lung explants through the addition of nicotine conferred an increased branching response. Similarly, reducing peristalsis through addition of the calcium channel blocker nifedipine reduced branching (Jesudason et al., 2006; Jesudason et al., 2005). Calcium waves underpin this airway peristalsis as evidenced by studies observing waves of calcium propagating along the airways moments prior to a contractile wave (Featherstone et al., 2006). Alterations to the levels of calcium present in lung explant cultures affect the branching response (Finney et al., 2008), potentially through affecting these peristaltic waves.

Airway smooth muscle cells are derived from fibroblast growth factor (FGF) 10 producing cells of the mesenchyme. During the branching process, bone morphogenic protein (BMP) 4 and sonic hedgehog (Shh) are produced in the epithelium in response to FGF10 stimulation. These factors signal back to the FGF10 producing cells promoting their migration and differentiation to airway smooth muscle cells, which line the proximal airways (Mailleux et al., 2005; Weaver et al., 2003). Approximately 6% of the FGF10 producing cells end up as these airway smooth muscle cells with the rest forming either vascular smooth muscle cells (4%), lipofibroblast cells (30%) or other fibroblast cells (60%) (Agha et al., 2014).

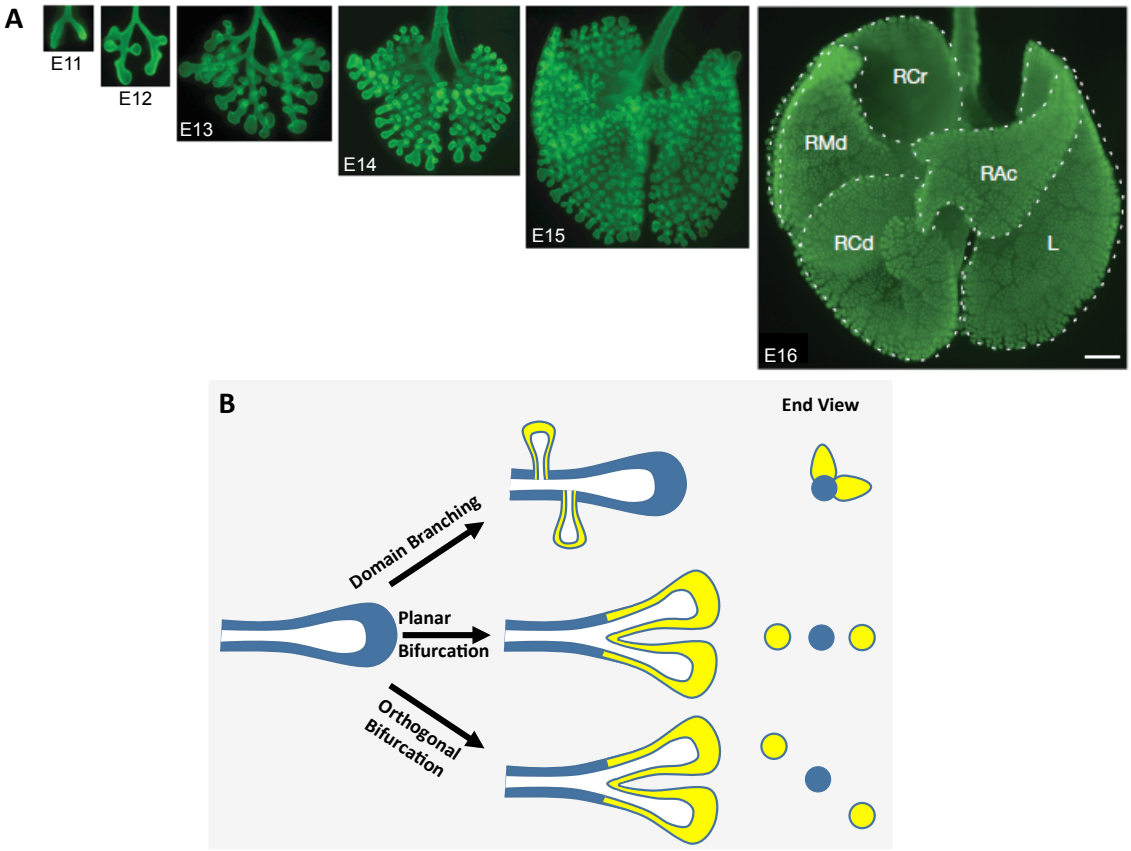

Figure 1.3. Murine lung branching morphogenesis. A. Expression of the epithelial marker E-Cadherin in lungs taken from murine embryos during the pseudoglandular stage of lung development. Scale bar = 500 µm. **B.** Schematic demonstrating the three types of branching found during lung development: domain branching, planar bifurcation and orthogonal bifurcation. Parent branches are coloured in blue and daughter branches in yellow. The resulting plane of the daughter branches with respect to the parent is represented in the right part of the panel. RCr –right cranial, RMd – right middle, RAc – right accessory, RCd – right caudal, L – left. Figure adapted from (Metzger et al., 2008)

1.5 Fibroblast growth factors

FGFs comprise a family of 23 factors that bind four types of tyrosine kinase receptors (FGFR1-4) (Zhang et al., 2006). The FGFR contains three extracellular immunoglobulin-like domains and a binding sequence for heparan sulphate molecules. Alternative splicing of the first of these immunoglobulin-like domains confers multiple receptors with different ligand specificity, summarised in table 1.1 (Miki et al., 1992). Moreover, this splicing event allows for tissue specific expression of alternate FGFRs. As an example, two of the splice variants of FGFR2, FGFR2b and FGFR2c are preferentially expressed in the epithelium and mesenchyme respectively (Orr-Urtreger et al., 1993). The ability for many FGFs to

interact with heparan sulphate molecules is also important for their function as heparan sulphate can limit FGF diffusion, thus restricting the action of an FGF to a specific site on a tissue (Flaumenhaft et al., 1990; Makarenkova et al., 2009).

FGF Family	FGF	FGFR selectivity
FGF1 subfamily	FGF1	All FGFRs
	FGF2	FGFR 1c, 3c > 1b, 4 > 2c > 2b
FGF4 subfamily	FGF4	
	FGF5	FGFR 1c > 3c, 4 > 2c > 1b, 2b
	FGF6	
FGF7 subfamily	FGF3	
	FGF7	FGFR 2b > 1b > 4
	FGF10	
	FGF22	
FGF8 subfamily	FGF8	
	FGF17	FGFR 3c > 4 > 2c > 1c > 3b
	FGF18	
FGF9 subfamily	FGF9	
	FGF16	FGFR 3c > 2c > 1c, 3b > 4
	FGF20	
FGF19 subfamily	FGF19	
	FGF21	FGFR 1c > 2c, 3c, 4
	FGF23	
FGF11 subfamily	FGF11	
	FGF12	No known activity
	FGF13	
	FGF14	

Table 1.1. Selectivity of FGF family members to FGFR isoforms. Adapted from (Ornitz et al., 1996; Zhang et al., 2006)

FGFR signalling

Formation of the FGF: FGFR complex stabilises receptor dimerization and induces receptor trans-phosphorylation. This in turn recruits a number of signalling effectors including phospholipase-C γ (PLCγ) (Mohammadi et al., 1991), and fibroblast growth factor receptor substrate 2 (FRS2) (Kouhara et al., 1997; Ong et al., 2000). PLCγ produces diacylglycerol (DAG) and inositol 1,4,5-trisphosphate [Ins(1,4,5)P_3] from phosphatidylinositol 4,5-bisphosphate [PI(4,5)P_2] present in the plasma membrane (Carpenter and Ji, 1999). Ins(1,4,5)P_3 induces the release of calcium from intracellular stores, thus activating calcium dependent kinases such as Ca^{2+}/calmodulin-dependent protein kinase, whereas DAG activates protein kinase C (PKC). Once recruited to the receptor FRS2 is phosphorylated, which is

dependent on the further recruitment of the adaptor protein Shb (Cross et al., 2002). Following phosphorylation, FRS2 recruits the adaptor protein Grb2 (Kouhara et al., 1997), which in turn recruits the guanine nucleotide exchange factor (GEF) SOS, and the scaffolding molecule Gab1 (Kanai et al., 1997). SOS activates the GTPase Ras thus initiating the mitogen activated protein kinase (MAPK) cascade through Raf, MEK and ERK (Kouhara et al., 1997). Gab1 recruits the lipid kinase phosphoinositide 3-kinase (PI3K) (Ong et al., 2001). Together these signalling events govern a range of cellular processes, notably cell proliferation, differentiation and migration. This signalling cascade is summarised in figure 1.4.

FGFR signalling is mediated by a number of factors that negatively feedback to several elements of the FGFR cascade. Grb2 recruits the ubiquitin ligase Cbl, which targets FGFR for internalisation (Wong et al., 2002). Further feedback inhibition comes from the induction of the negative regulators sprouty, dual specificity phosphatase (DUSP) and Sef. Sprouty is produced in response to ERK signalling (Ding et al., 2003), and is phosphorylated by FRS2-recruited SRC kinase (Li et al., 2004; Rubin et al., 2005). Sprouty exerts its inhibitory action on FGFR signalling by competing with SOS for Grb2 binding (Lao et al., 2006), and directly inhibiting Raf (Yusoff et al., 2002). DUSPs dephosphorylate, and thus inactivate, ERK. As with sprouty, DUSP transcription can be initiated by MAPK signalling downstream of FGFR (Mandl et al., 2005; Smith et al., 2006b). Moreover, phosphorylation of DUSP by ERK can increase the stability of the protein, thus increasing its activity (Brondello et al., 1999). Sef is a transmembrane protein that is transcribed in response to FGFR signalling. Sef directly interacts with FGFR resulting in impaired receptor phosphorylation (Kovalenko et al., 2003).

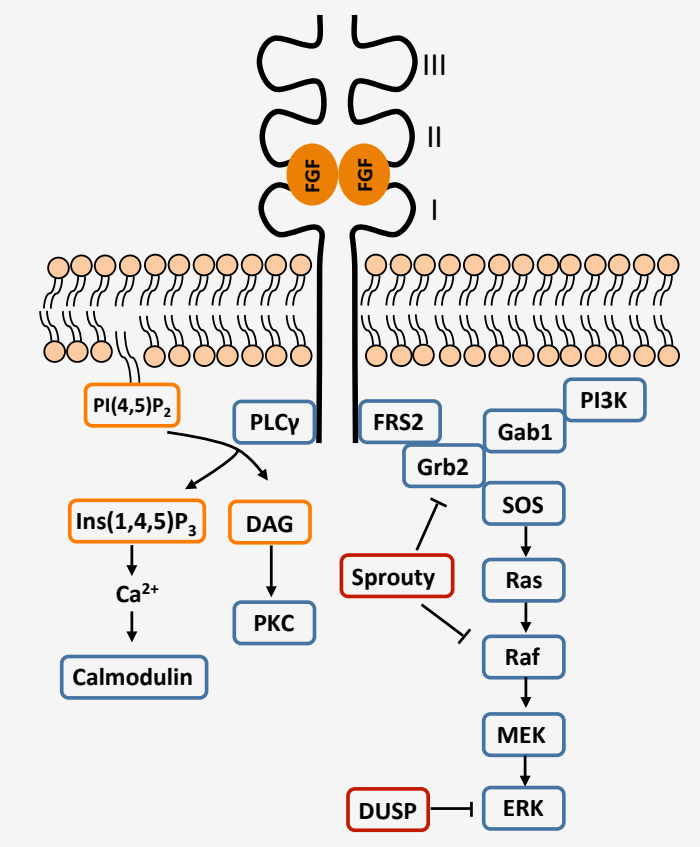

Figure 1.4. FGF receptor structure and signalling. Schematic of FGFR showing FGF molecules bound to the three extracellular immunoglobulin-like domains, which results in receptor dimerisation. Following activation, and receptor trans-phosphorylation PLCγ is recruited. PLCγ converts $PI(4,5)P_2$ to $Ins(1,4,5)P_3$ and DAG. $Ins(1,4,5)P_3$ releases calcium from intracellular stores, which in turn activates calcium dependent calmodulin. DAG activates PKC. FRS2 is also recruited to active FGFR. FRS2 further recruits Grb2 and Gab1. Grb2 recruits SOS, which initiates Ras/Raf/MEK/ERK signalling. Gab1 promotes PI3K recruitment and activation. Sprouty and DUSP are transcribed in response to ERK signalling and regulate FGFR signalling at the indicated sites.

FGFs in disease

FGFRs have key roles in cell proliferation, survival, differentiation, migration and angiogenesis making them an important signalling event in many cancers (Turner and Grose, 2010). This is highlighted by their potential use as biomarkers for cancer prognosis. As an example, a high level of FGF2 in the serum of patients with small cell lung caner is an indicator of poor prognosis (Ruotsalainen et al., 2002). FGFRs can become overactive in cancer through a number of mechanisms. Non-small cell lung cancer cells have been demonstrated to acquire autocrine FGF signalling which promotes the growth and survival of the cancer cells (Marek et al., 2009). Cancer cells can also adopt mutations that give rise to FGFRs that are either constitutively active themselves or recruit constitutively

active signalling components (Liao et al., 2013). Isoform switching of FGFRs have also been reported in cancer cells, and during fibrosis, thus sensitising cells to FGFs that they would otherwise not interact with (Shirakihara et al., 2011; Yan et al., 1993). Finally, cancer cells can supress negative regulators of FGFR signalling, such as sprouty, to increase FGFR signalling and drive pathogenesis (Sutterlüty et al., 2007).

FGFRs are therefore an attractive target for a number of diseases, particularly cancer. The FGFR shares high sequence homology with the vascular endothelial growth factor receptor (VEGFR) (Manning et al., 2002; Turner and Grose, 2010). As a result, many FGFR tyrosine kinase inhibitors are also VEGFR inhibitors. For instance, the tyrosine kinase inhibitor PD173074 binds to the ATP binding pocket of both VEGFR and FGFR (Mohammadi et al., 1998). This may actually be advantageous, as a dual VEGFR and FGFR inhibitor would effectively block both angiogenesis and cancer cell proliferation. However, the use of FGFR inhibitors in the clinic may be hampered by the acquisition of resistance following prolonged treatment, which has been reported in a number of tumour cell lines (Chell et al., 2013). Moreover, the lack of inhibitor specificity between isoforms of FGFR may further limit the use of these compounds in the clinic.

FGFs and branching morphogenesis

FGFs have been identified as crucial signalling factors in the branching program of animals with conserved roles from *Drosophila* to mammals. Integral to the branching process is FGF10 and its receptor FGFR2b, present on the branching epithelium (Figure 1.5A). Knockouts of the *Drosophila* homologs of these proteins, *branchless* and *breathless*, fail to produce a tracheal network as a result of impaired cellular migration from tracheal pits (Klämbt et al., 1992; Sutherland et al., 1996). Similarly, lungs from mice deficient in either FGF10 or FGFR2b develop an initial trachea and primary lung buds but lack any distal lung branching (De Moerlooze et al., 2000; Min et al., 1998). Functionally, FGF10 is produced from sites in the mesenchyme ahead of an epithelial branch. FGF10 then acts as an attractant for the epithelial cells of a branch by signalling through epithelial FGFR2b. The expression of these FGF10 producing cells changes dynamically

around the branching epithelium conferring where branches will form and in which direction they will develop (Bellusci et al., 1997; Park et al., 1998).

A level of regulation for FGF10 signalling comes from the induction of the negative regulator sprouty, specifically the sprouty2 isoform, in the branching epithelium. The *Drosophila* homologue of sprouty2, *sprout*y, is induced by *branchless* and blocks signalling in the proximal regions of the branch. Deletion of *sprouty* results in overactive *branchless* signalling and increased tracheal branching (Hacohen et al., 1998). In the mouse, sprouty2 is found in the distal tips of developing branches and is induced by FGF10 signalling. Antisense knockdown of sprouty2 in murine lung explants stimulates epithelial branching (Tefft et al., 1999), whereas overexpression reduces (Mailleux et al., 2001).

FGF9, produced from the mesothelium and acting through mesenchymal FGFR2c is also implicated in the regulation of branching. FGF9 null mice exhibit reduced mesenchymal growth and impaired branching (Colvin et al., 2001). Addition of FGF9 to lung explants and isolated lung mesenchyme increases the expression of FGF10 suggesting that FGF9 directly influences FGF10 expression in the branching lung.

FGF7 is found in the lung mesenchyme later in the pseudoglandular stage, from E14.5 onwards (Finch et al., 1995; Mason et al., 1994), nevertheless it appears to contribute to lung branching. Addition of FGF7 to isolated lung epithelium promotes the growth of large cystic structures from the initial epithelium (Cardoso et al., 1997). Antisense knockdown of FGF7 in cultures of rat lung explants impairs branching (Post et al., 1996). However, mice lacking FGF7 do not exhibit any lung abnormalities suggesting a redundancy for FGF7 in the branching program (Guo et al., 1996).

FGF7 is structurally similar to FGF10 and both act through the epithelial FGFR2b (Igarashi et al., 1998). Despite this, both factors produce strikingly different morphological effects when applied to cultures of isolated lung epithelium. FGF10 produces a directed branching response, whereas FGF7 promotes a large uniform growth of the epithelium (Bellusci et al., 1997; Cardoso et al., 1997). FGF10 and

FGF7 are also required for epithelial branching in the developing salivary gland. However, the actions of these factors differ from the lung. FGF7 induces an initial budding response from the salivary gland epithelium whereas FGF10 promotes elongation of epithelial buds (Makarenkova et al., 2009). The reason for this apparent disparity between the two factors may lie in how FGF10 signalling is regulated during branching morphogenesis.

Restriction of FGF10 signalling to branch sites

The FGF10 receptor FGFR2b is ubiquitously expressed across the lung epithelium (Cardoso et al., 1997), the signalling of FGF10 therefore has to be restricted to sites of branching. This is achieved by two means. Firstly, FGF10 producing cells only appear ahead of a developing branch (Bellusci et al., 1997), FGF10 would therefore be concentrated at the closest part of the epithelium and be reduced elsewhere through diffusion. However, this tendency for FGF10 producing cells to only appear ahead of sites of branching may be dispensable for the branching process as ubiquitous expression of FGF10 across the lung mesenchyme fails to perturb branching morphogenesis (Volckaert et al., 2013). Equally, the addition of recombinant FGF10 to cultures of isolated epithelium is able to induce branching despite its concentration being equal across the culture (Xing et al., 2008). Secondly, FGF10 signalling is restricted to sites of branching through binding to locally expressed heparan sulphate (Izvolsky et al., 2003) (Figure 1.5B). This explains how FGF10 and FGF7 can promote different effects in isolated lung epithelium as FGF7 natively lacks a heparan-binding domain. Addition of exogenous heparan sulphate to cultures of isolated lung or salivary gland epithelium perturbs the endogenous heparan gradient, allowing FGF10 to act uniformly across the epithelium. This results in FGF10 producing a uniform growth of the lung epithelium, or a budding response in salivary gland epithelium, comparable to the related factor FGF7 (Izvolsky et al., 2003; Patel et al., 2008). Similarly, deletion of the heparan-binding component of FGF10 creates a factor whose morphogenic response is equal to that of FGF7 (Makarenkova et al., 2009).

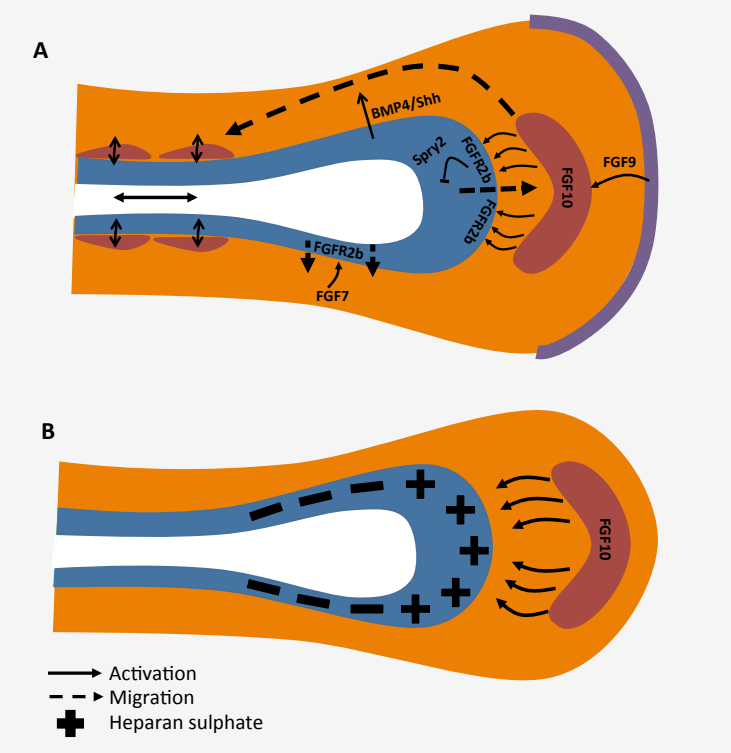

Figure 1.5. FGF signalling in branching morphogenesis. A. Schematic illustration of FGF signalling in the branching lung. Epithelium is represented in blue, mesenchyme in orange and mesothelium in purple. FGF10 producing cells/ airway smooth muscle cells are labelled in red. Mesothelium derived FGF9 regulates the expression of FGF10-producing cells that in turn promote epithelial branching. BMP4/Shh produced from the epithelium in response to FGF10 induces the migration and differentiation of FGF10 producing cells into airway smooth muscle. These smooth muscle cells line the proximal part of a branch and undergo periodic waves of contraction, forcing fluid back and forth along the lumen. FGF7 is produced elsewhere in the mesenchyme and induces the growth of the epithelium. **B**. Illustration showing restriction of FGF10 signalling to a site of branching through production of FGF10 ahead of a developing branch and local expression of heparan sulphate from the epithelium.

1.6 Phosphoinositide 3-kinase

Phosphoinositide (PI) lipids constitute a major component of the plasma membrane. The phosphorylation state of the six carbon atoms that comprise the intracellular inositol ring, particularly at positions 3, 4 and 5, are tightly regulated by a number of lipid kinases and phosphatases to generate seven types of PI derivatives (Figure 1.6). Of these lipid kinases, the PI3K family is the most widely studied due to its crucial role in a number of cellular events and the recognition that PI3K dysfunction is apparent in a number of diseases. Three distinct subfamilies of PI3K exist; classes I, II and III, based on their substrate specificities and structures.

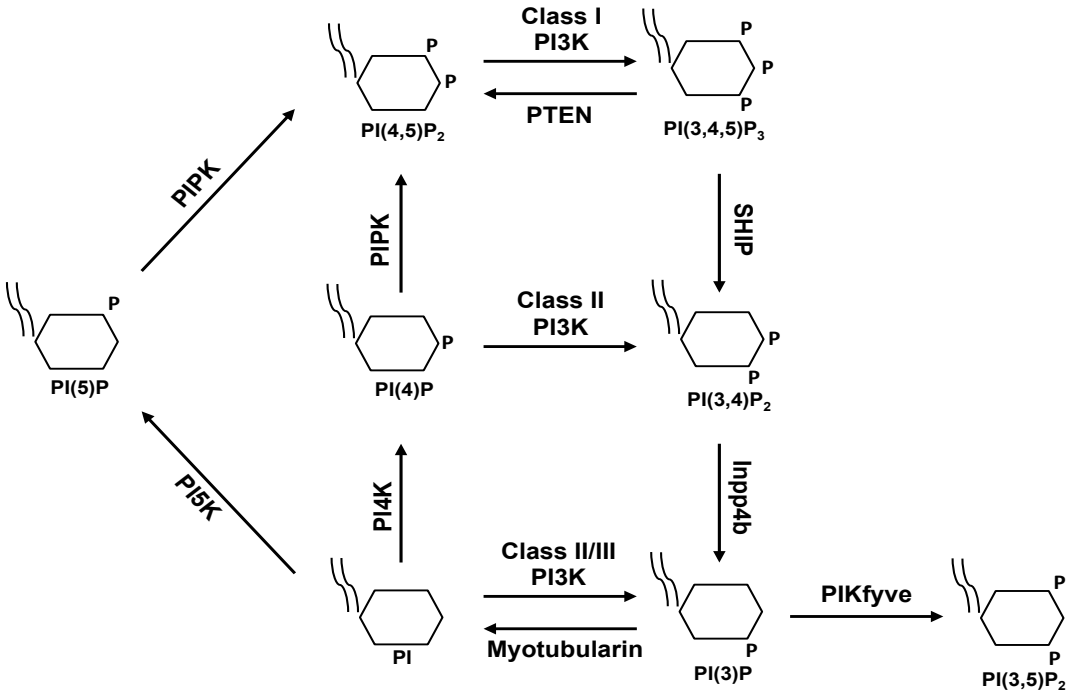

Figure 1.6. Phosphorylated derivatives of phosphoinositide and their regulation by lipid kinases and phosphatases. Figure adapted from (Okkenhaug, 2013).

Class I PI3K

Each member of the class I PI3K family is composed of a regulatory and a catalytic subunit. The class IA family contains five regulatory subunits encoded by three genes: *PIK3r1*, which encodes for p85α and its alternative transcripts p55γ and p50α; *PIK3r2*, which encodes for p85β; and *PIK3r3*, which encodes p55γ. These regulatory subunits pair with one of three catalytic subunits (p110α, β, δ) encoded by three separate genes (*PIK3CA*, *PIK3CB*, *PIK3CD*). The class IB catalytic subunit p110γ (encoded by *PIK3CG*) couples with either the p84/p87 or p101 regulatory subunits (encoded by *PIK3R5* and *PIK3R6* respectively) (Foster et al., 2012). Four distinct isoforms of the class I PI3K family therefore exist, PI3Kα, PI3Kβ, PI3Kδ and PI3Kγ. All PI3K p110 catalytic subunits can interact with, and be activated by, the GTPase Ras (Rodriguez-Viciana et al., 1994). PI3Kα/β/δ signals downstream of receptor tyrosine kinases (RTKs), such as FGFR (Ong et al., 2001), whereas PI3Kγ signals downstream of G-protein coupled receptors (GPCRs) (Bohnacker et al., 2009). There does appear to exist some redundancy between the isoforms as PI3Kβ can also signal through GPCRs (Guillermet-Guibert et al., 2008). PI3Kα and PI3Kβ are ubiquitously expressed in mammals whereas PI3Kδ and PI3Kγ are predominantly expressed in leukocytes (Sasaki et

al., 2000; Vanhaesebroeck et al., 1997). PI3Kδ and PI3Kγ can also be found in fibroblasts (Conte et al., 2011), and PI3Kγ can be found in cells of the heart and endothelium (Crackower et al., 2002; Patrucco et al., 2004).

Class I PI3K family phosphorylates the D3 position on the inositol ring of $PI(4,5)P_2$ to generate $PI(3,4,5)P_3$. $PI(3,4,5)P_3$ acts as a docking site for a number of pleckstrin homology (PH) domain containing proteins including Akt and a range of scaffolding proteins and GEFs (Figure 1.7) (Park et al., 2008). The generation of $PI(3,4,5)P_3$ is tightly regulated by the lipid phosphatases phosphatase and tensin homolog (PTEN) and SH2-domain containing inositol-5-phosphotase (SHIP). PTEN is a 3' phosphatase, producing $PI(4,5)P_2$ from $PI(3,4,5)P_3$ whereas SHIP is a 5' phosphatase producing $PI(3,4)P_2$ (Harris et al., 2008).

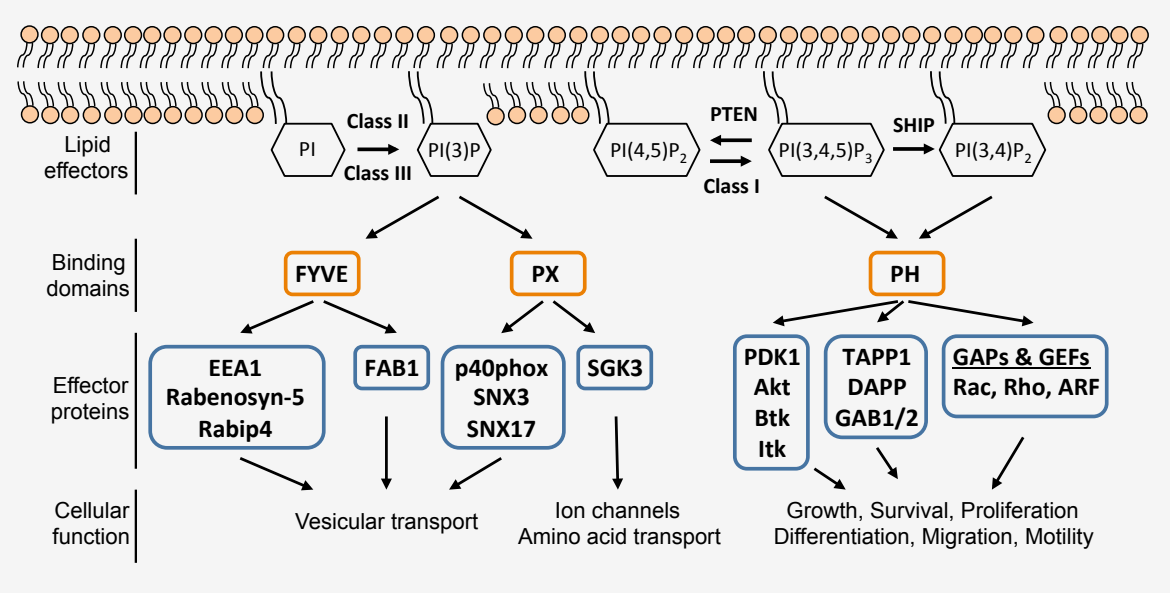

Figure 1.7. The PI3K signalling cascade. The class II and III PI3K family members produce PI(3)P from PI, which recruits a number of proteins that contain either an FYVE or PX binding domain. The class I PI3K family members produce $PI(3,4,5)P_3$ from $PI(4,5)P_2$. The phosphatase PTEN reverses this reaction whereas the phosphatase SHIP produces $PI(3,4)P_2$ from $PI(3,4,5)P_3$. Both $PI(3,4,5)P_3$ and $PI(3,4,)P_2$ recruit a number of proteins that contain a PH binding domain. Figure adapted from (Foster et al., 2012).

Class II and III PI3K

Mammalian cells contain three isoforms of the class II PI3K, C2α, C2β and C2γ. Class II PI3K phosphorylate either PI or PI(4)P to create PI(3)P or PI(3,4)P_2 respectively (Misawa et al., 1998), although their preferred substrate is PI. The sole class III PI3K member, Vps34, uses PI as its substrate to produce PI(3)P (Schu et al., 1993) (Figure 1.5). PI(3)P is regulated by the 3' phosphatase myotubularin which converts PI(3)P back into PI (Taylor et al., 2000). Moreover PI(3)P can be sequestered into intracellular vacuoles, leading to its degradation (Wurmser and Emr, 1998). PI(3,4)P_2 is regulated by the 4' phosphatase inpp4b, which generates further PI(3)P (Norris et al., 1997).

PI(3)P recruits a number of proteins that contain either a PX or FYVE binding domain (Figure 1.7). Many of these proteins, including early endosome antigen-1 (Patki et al., 1997), Fab1 (Rusten et al., 2006), and SNX3 (Xu et al., 2001), have been identified to have critical roles in vesicular transport within cells. Others, such as the PX containing kinase SGK3, are involved in amino acid transport and nutrient uptake (Palmada et al., 2005; Tessier and Woodgett, 2006). Amino acids are also capable of activating Vps34, which in turn can activate mammalian target of rapamycin (mTOR) (Nobukuni et al., 2005). PI(3)P can also be phosphorylated at the D5 position by PIKfyve to generate PI(3,5)P_2, which also has important roles in endosomal transport (Ikonomov et al., 2006).

PI3K/Akt/mTOR signalling

Of the signalling effectors recruited by PI(3,4,5)P_3 the PI3K/Akt/mTOR cascade is the best understood (Figure 1.8). Following generation by PI3K, PI(3,4,5)P_3 recruits 3-phosphoinositide-dependent protein kinase 1 (PDK1) and Akt. PDK1 phosphorylates, and thereby activates, Akt at the threonine 308 position (Alessi et al., 1997; Franke et al., 1995). The product of SHIP, and of the class II PI3Ks, PI(3,4)P_2 is also involved in the recruitment and activation of Akt (Franke et al., 1997).

Following activation, Akt affects a number of signalling proteins, including tuberous sclerosis complex (TSC), FOXO, Bad and glycogen synthase kinase (GSK) 3β (Manning and Cantley, 2007). TSC is phosphorylated by Akt (Inoki et al., 2002;

Potter et al., 2002), which releases the small GTPase Rheb from the inhibitory actions of TSC. Rheb then activates mTOR (Gao et al., 2002; Garami et al., 2003). mTOR exist as a complex of proteins that function as serine/threonine kinases. Two complexes exist, the rapamycin sensitive mTOR complex (mTORC) 1, and the rapamycin insensitive mTORC2. mTORC2 can phosphorylate Akt at the serine 473 position (Facchinetti et al., 2008; Sarbassov et al., 2005). This leads to the complete activation of Akt, which exhibits fivefold more activity than phosphorylation at threonine 308 alone (Sarbassov et al., 2005). mTORC1 activates ribosomal S6 kinase (S6K) and inactivates the transcriptional repressor 4E-BP1 thus promoting protein translation.

As well as activating protein translation, S6K can regulate the activity of the PI3K/Akt/mTOR signalling cascade by inactivating mTORC2, thus reducing Akt phosphorylation at serine 473 (Julien et al., 2010). Moreover, S6K induces the downregulation of insulin receptor substrate 1 present at RTKs, which in turn reduces PI3K recruitment and signalling (Haruta et al., 2000; O'Reilly et al., 2006). S6K has also been identified to directly phosphorylate mTOR, thus providing an element of positive feedback (Holz and Blenis, 2005).

FOXO is a transcription factor that is phosphorylated in response to Akt activation. This phosphorylation retains FOXO in the cytoplasm of the cell and prevents FOXO from activating its target genes. FOXO controls the expression of several negative regulators of the cell cycle and several pro-apoptotic genes such as p27 and Bim (Lam et al., 2006). Thus, inhibition of FOXO by Akt can promote cell survival and growth. Akt also promotes cell cycle progression through the inactivation of the pro-apoptotic protein BAD (Datta et al., 1997), and inactivation of GSK3β, which normally targets the cell cycle factor cyclin D for proteolysis (Diehl et al., 1998). Recently, FOXO has been shown to increase the transcription of the mTORC2 protein rictor, which serves to promote Akt activation (Lin et al., 2014).

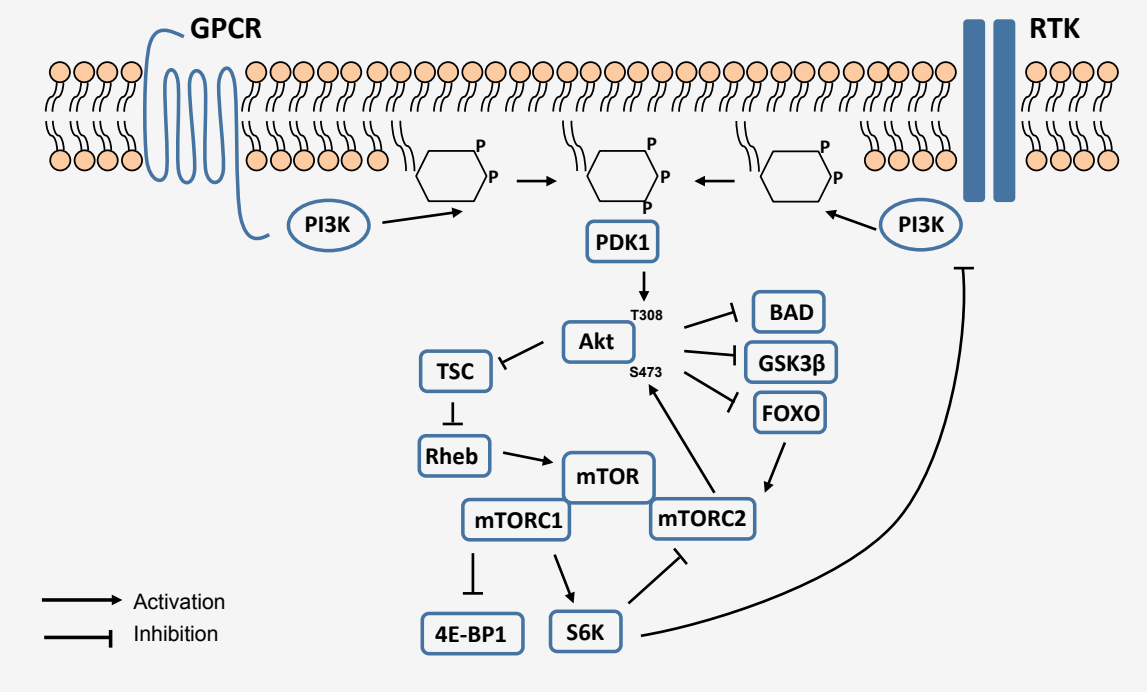

Figure 1.8. PI3K/Akt/mTOR signalling pathway. Once activated by either GPCRs or RTKs PI3K phosphorylates the D3 position of $PI(4,5)P_2$ creating $PI(3,4,5)P_3$. PDK1 and Akt are then recruited to the cell membrane. PDK1 phosphorylates threonine 308 on Akt thus activating this kinase. Akt then inactivates TSC removing the inhibitory effect on the small GTPase Rheb. Once released from TSC, Rheb activates mTOR. mTORC2 can feed back and fully activate Akt at the serine 473 position. mTORC1 activates S6K which negatively regulates mTORC2, and PI3K signalling from RTKs.

PI3K signalling in disease

Hyperactive PI3K signalling, particularly via PI3Kα, is a hallmark of many cancers. Generally there are two methods of PI3K activation in cancer; over-activation of RTKs and mutations in elements of the PI3K pathway (Engelman, 2009). Many anticancer agents that act through inhibition of RTKs rely on their ultimate inhibition of PI3K for therapeutic effect (Engelman et al., 2005; Yakes et al., 2002). For example, non-small cell lung cancer cell lines sensitive to the epidermal growth factor receptor inhibitor gefitinib exhibit enhanced PI3K signalling whereas those insensitive to gefitinib do not (Engelman et al., 2005). Mutations in the *PIK3CA* gene are found in many cancers (Samuels et al., 2004), this leads to PI3Kα over-activation through at least two mechanisms. Firstly, in the wild type PI3Kα the p85 regulatory subunit can inhibit the catalytic activity of the p110α subunit. This inhibitory effect is lost in a number of *PIK3CA* mutations leading to enhanced PI3K activity (Huang et al., 2007). Secondly, mutations can occur that promote constitutive activation by mimicking PI3K binding to Ras (Zhao and Vogt,

2008). Inhibition of PI3Kα is therefore an attractive target for the treatment of cancer. Indeed, knockdown or inhibition of PI3Kα, but not PI3Kβ, severely impairs the function of small cell lung cancer cells isolated from patients (Wojtalla et al., 2013). Expression of PI3Kδ and PI3Kγ has also been noted in cell types outside of their normal expression pattern that may contribute to the cancer progression (Edling et al., 2010; Sawyer et al., 2003). Aside from Class I PI3K signalling, the class II PI3K C2β has been implicated in the migration of epithelial cells (Domin et al., 2005; Maffucci et al., 2005), thus suggesting a role for this isoform in cancer progression.

Due to their preferential expression and multiple roles in cells of the immune system, PI3Kδ and PI3Kγ are commonly found to be influential in the progression of inflammatory diseases of the lung (Foster et al., 2012). Emphysema requires neutrophil recruitment to the lung for the production of neutrophil elastase. Neutrophil recruitment can be abrogated through inhibition of PI3Kγ suggesting that inhibition of PI3Kγ would be capable of reducing the progression of emphysema (Thomas et al., 2005). During an allergic asthma attack mast cells undergo degranulation, releasing numerous factors that act to promote airway contraction, a process that heavily relies on PI3Kδ (Ali et al., 2008). Similarly, inactivation of PI3Kδ, by genetic means or pharmacologically, reduces the hyperactive response to the airway allergen ovalbumin and reduces airway inflammation and remodelling (Lee et al., 2006; Nashed et al., 2007).

PI3K activity has also been implicated in the pathology of lung fibrosis (Hinz and Gabbiani, 2010). Inhibition of either PI3Kα or PI3Kγ reduces the proliferation of myofibroblasts and airway smooth muscle cells and inhibits the production of collagen in response to TGFβ (Conte et al., 2011; Moir et al., 2011). Treatment of rats with the PI3Kγ inhibitor AS605240 conferred a protection from bleomycin-induced fibrosis (Wei et al., 2010), although this response may be largely due to the immunosuppressant actions of PI3Kγ inhibition rather than anti-fibrotic.

The importance of PI3K in disease is highlighted by the fact that there are currently eighteen compounds targeting PI3K signalling in clinical trials, the majority targeting cancer (Foster et al., 2012). Future insights into how PI3K acts

during the disease process will surely lead to more of these compounds entering trials and the clinic for a wider range of conditions.

PI3K signalling in branching morphogenesis

PI3K has been implicated in the branching program of many organs but the precise role for this kinase has yet to be fully established. Inhibition of PI3K with the pan class I inhibitor LY294002 inhibits branching in cultures of murine embryonic salivary gland. This inhibition could be partially rescued with the application of the main product of PI3K, $PI(3,4,5)P_3$ (Larsen et al., 2003). Inhibition of PI3K was also able to reduce epithelial budding in response to FGF7, but had no effect on the elongation response elicited by FGF10, in cultures of isolated salivary gland epithelium (Steinberg et al., 2005). Together, these data would suggest that PI3K regulates branching at the epithelial level. Similar findings have been reported from the branched urogenital sinus tissue. Inhibition of PI3K signalling, with LY294002, reduced branching of cultured murine urogenital sinus tissue. Conversely, mice deficient in the negative regulator PTEN, and thus exhibiting enhanced PI3K signalling, also showed a decrease in branching (Ghosh et al., 2011).

Two downstream signalling effectors of PI3K, Akt and Rac1, localised to the sites of, and were required for, branch initiation and elongation during the formation of mammary epithelial branches in response to hepatocyte growth factor (Zhu and Nelson, 2013). Consistent with the pharmacological data in cultured cells, mice expressing homozygous knockdown of PI3Kα under the control of a mammary gland specific promoter exhibited impaired mammary branching. Conversely, knockdown of PI3Kβ enhanced mammary branching (Utermark et al., 2012). Data from mammary glands may therefore point towards divergent roles for PI3K isoforms in the branching process.

Conflicting results exist for PI3K in the branching program of the lung as well. Murine lung explants cultured with LY294002 show reduced branching implying a requirement for PI3K-dependent signalling in branching as observed with salivary glands and urogenital sinus tissue (Wang et al., 2005). However, in isolated lung epithelium derived from mice deficient in PTEN, branching in response to FGF10

was significantly impaired compared to wild type epithelium (Xing et al., 2008). Information from mice with conditional deletions of PTEN also presents a conflicting role for PTEN, and by extension PI3K, in lung branching morphogenesis. Mice with a lung specific deletion of PTEN under control of the Nkx2.1 promoter exhibited no branching abnormalities. These mice did show enhanced epithelial cell proliferation conferring protection from naphthalene-induced lung injury in the adult (Tiozzo et al., 2009). Conversely, mice with a lung specific deletion of PTEN under the control of the surfactant protein C (SPC) promoter, exhibited reduced epithelial branching. As with the PTEN knockouts under the control of Nkx2.1, these mice showed an enhanced capacity for epithelial proliferation, which led to spontaneous adenocarcinoma (Yanagi et al., 2007).

PTEN has also been identified as having an important role in the formation of epithelial tube lumen. PTEN is recruited to the apical surface of polarising epithelial cells, which enriches $PI(4,5)P_2$ at the apical membrane and $PI(3,4,5)P_3$ at the basolateral (Martin-Belmonte et al., 2007). The exogenous application of $PI(4,5)P_2$ to the basolateral surface of epithelial cells induces the recruitment of apical proteins thus perturbing the polarisation, and morphogenesis of the epithelium. This is also true for the exogenous application of $PI(3,4,5)P_3$, which converts the apical surface to basolateral (Gassama-Diagne et al., 2006).

Little is currently known about the class II and III PI3K family members in branching morphogenesis. This is due to a lack of pharmacological tools with which to study these kinases and the embryonic lethality of the class III Vsp34 knockout mice (Zhou et al., 2011). Knockout mice for the class II PI3K isoforms C2α and C2β exist and are viable beyond early embryonic development. C2α knockout mice show poor postnatal development and exhibit sever renal failure. However whether there was a branching defect in the development of the kidneys that may have contributed to the renal failure was not examined (Harris et al., 2011). C2β knockout mice appear viable, are fertile, and do not exhibit any gross abnormalities (Harada et al., 2005). A requirement for both C2α and C2β in the formation of endothelial tubular formation has been demonstrated with siRNA

approaches (Biswas et al., 2013; Tibolla et al., 2013), which may imply a role for these isoforms in epithelial branching as well.

Pharmacological intervention of PI3K/mTOR signalling

Aberrant signalling of PI3K in many diseases, particularly cancer, makes PI3K an attractive target for therapeutic intervention. This has spurred the development of many pharmacological tools with which to dissect the role of PI3K signalling in cellular processes. The first compounds identified to target PI3K signalling were the pan class I inhibitors wortmannin and LY294002 (Arcaro and Wymann, 1993; Vlahos et al., 1994). Although extremely useful in exploring the PI3K pathway their numerous off-target effects, particularly their inhibitory actions on mTOR signalling (Brunn et al., 1996; Davies et al., 2000), limits the use of these compounds. X-ray crystallography data of LY294002 bound to the ATP binding pocket of p110γ has helped in the design of new inhibitors with increased selectivity against each isoform of PI3K and many of its downstream effectors (Walker et al., 2000) (Table 1.2).

Debate exists as to the optimal site of intervention in the PI3K/Akt/mTOR signalling cascade to achieve optimum therapeutic output. Direct inhibition of PI3K prevents Akt activation through $PI(3,4,5)P_3$. However, Akt can also be phosphorylated at threonine 308 and serine 473 by IKBKE independently of PI3K (Guo et al., 2011). Direct Akt inhibition is also a possibility. Although, Akt inhibition may actually increase PI3K signalling by removing the negative regulation of PI3K induced through mTORC1 activation (Haruta et al., 2000; O'Reilly et al., 2006). Moreover, Akt inhibition may potentiate mTORC2 activity by removing the inhibitory effect on FOXO, which in turn can increase the transcription of the mTORC2 protein rictor (Lin et al., 2014). mTOR is another potential site of inhibition but again this has the caveat of potentially enhancing PI3K activity by removing the negative feedback loop induced through S6K. Furthermore, mTORC1 inhibition would increase Akt activation by removing the inhibitory effect on mTORC2 (Julien et al., 2010) (Figure 1.8). Inhibition of PI3K and mTORC1/2 would potentially produce the best therapeutic effect, as this approach would shut down the PI3K/Akt/mTOR signalling cascade and these positive feedback loops.

Pharmacological intervention of PI3K signalling may be tempered in the clinic by off-target and systemic effects of the compounds. A particular concern is the action of PI3K directed therapies on the cardiovascular system (McLean et al., 2013). As an example, LY294002 exhibits inotropic effects on the heart through off target effects on potassium channels (Sun et al., 2004). Another concern is whether an effective therapeutic window can be achieved with PI3K targeted compounds, especially as PI3K compounds are being combined with other inhibitors to increase their therapeutic effect (Shimizu et al., 2012). The introduction of compounds with enhanced selectivity may overcome some toxicity through a reduction in off-target effects. However, as mentioned, the inhibition of multiple sites in the PI3K signalling cascade may have better therapeutic output. Compounds that target both PI3K and mTOR come with the caveat of potentially increased toxicity due to the non-selective nature of the compounds (Fruman and Rommel, 2014). One compound that may overcome this caveat is the Semaphore compound SF1126. SF1126 is a derivative of LY290042 and therefore inhibits both PI3K and mTOR signalling. SF1126 benefits from the addition of an RGD peptide, which improves compound solubility and targets the compound to the pro-angiogenic integrins αvβ3/α5β1 present within the tumour environment (Garlich et al., 2008). SF1126 is currently in phase I clinical trials for solid tumours and multiple myeloma (Foster et al., 2012).

Compound	IC_{50} value (nM)					Reference
	PI3K isoform				mTOR	
	p110α	p110β	p110δ	p110γ		
LY294002	183	98	227	1967	5000	(Brunn et al., 1996)
ZSTK474	16	44	4.6	49	>100,000	(Kong and Yamori, 2007)
PIK75	5.8	1300	76	510	1000	(Knight et al., 2006)
BYL719	5	1200	290	250	>9100	(Furet et al., 2013)
A66	32	>12500	>1250	3480	>5000	(Jackson et al., 2005)
GSK2636771	2000	13	79	1000	3200	(Sanchez et al., 2012)
TGX-221	5000	5	100	>10,000	N/A	(Jackson et al., 2005)
IC-87114	>100,000	1820	70	1240	N/A	(Bilancio et al., 2006)
AS-605240	3400	>20,000	>20,000	190	N/A	(Bilancio et al., 2006)
AZD8055	>1000	>1000	>1000	>1000	0.8	(Chresta et al., 2010)
	Akt1		Akt2		Akt3	
Akt inhibitor VIII	58		210		2120	(Lindsley et al., 2005)

Table 1.2 IC_{50} values of some commonly used PI3K/Akt/mTOR inhibitors. Individual IC_{50} values derived from *in-vitro* assays with either purified or recombinant protein.

1.7 Targeted drug delivery

Many challenges exist in the effective delivery of a therapeutic to an intended site of action. The target may be intracellular and therefore only accessible to cell-permeant small molecules. The target tissue may also be largely inaccessible, as is the case for pancreatic cancer where the poorly perfused tumour acts as an effective obstacle for drug delivery (Olive et al., 2009). Further, balancing a therapeutic concentration of an agent in the target tissue while minimising toxic systemic effects is a constant challenge. These obstacles have lead to the development of drug carriers that can facilitate the delivery of a therapeutic agent and protect its journey through the body to a site of action.

Drug delivery carriers, such as liposomes, encapsulate a drug molecule and can be modified in a variety of ways to tailor their function. For instance, carriers can exhibit photo-thermal properties allowing for direct targeting of tumours regardless of the overall distribution of the carrier (O'Neal et al., 2004). The versatility of carriers can also be used to protect the carrier itself from the body. For example, a

common modification of a carrier is the coating with polyethylene glycol, which reduces the clearance of the carrier by phagocytic cells (Owens and Peppas, 2006). This modification also extends the circulation time of the carrier thus increasing the likelihood of delivery to the site of action. Once a drug carrier has reached its intended target and penetrated into a cell the drug carrier can become trapped within lysosomes. These acidic organelles are filled with proteases that may destroy the drug carrier and the drug itself, greatly reducing the effectiveness of the therapeutic. Again, carriers can be modified to aid in their release from lysosomes into the cytoplasm of a cell. Polyethylenimine has an inherent buffering capacity that acts as a 'proton sponge' inside lysosomes ultimately causing the rupture of a lysosome that releases the carrier into the cytosol (Akinc et al., 2005).

The following sections will discuss two emerging strategies for targeted drug delivery, cell penetrating peptides (CPPs) and bacterial toxins. These tools will help overcome many of the delivery challenges faced by both small molecule compounds, oligonucleotides and macromolecule therapeutics.

1.8 Cell-penetrating peptides

CPPs are small peptides comprising an amino acid sequence with either a large proportion of cationic amino acids, such as lysine or arginine, or have sequences that contain an alternating pattern of polar and nonpolar amino acids. CPPs are noted for having the remarkable ability to facilitate the transport of macromolecules across the membrane barrier of a cell to reach the cell cytoplasm. By being covalently attached, or by forming electrostatic complexes to a cargo, these peptides offer the exciting potential for use as an efficient delivery system for small therapeutics that are otherwise cell membrane impermeable, such as proteins or oligonucleotides (Milletti, 2012). CPPs also provide an added bonus of protecting a labile cargo from enzymatic degradation, such as endonucleases in the case of siRNA delivery (Crombez et al., 2009), on its journey from administration to the intended site of action.

Broadly speaking, CPPs can be classified into three groups based on their chemical properties: cationic, amphipathic and hydrophobic (Milletti, 2012).

Cationic CPPs, such as HIV-TAT (Frankel and Pabo, 1988), are composed of at least eight positively charged amino acid residues, which are required for their uptake into a cell (Futaki et al., 2001). Amphipathic CPPs, such as Antennapedia (Berlose et al., 1996), are CPPs that contain both polar and non-polar regions. Finally, hydrophobic CPPs are CPPs that contain only apolar amino acid residues, such as the PFVYLI peptide (Watkins et al., 2009).

There are currently several CPP based drugs in clinical trials that show promising results. These include RT001, a botulinum toxin A topical gel, for the removal of wrinkles (Glogau et al., 2012); AZX100, a cell-permeant HSP20 mimic, for the treatment of keloid and surgical scarring (ClinicalTrials.gov identifiers NCT00811577, NCT00825916 and NCT00892723); and p28, an Azurin-derived peptide, for metastatic refractory solid tumours (ClinicalTrials.gov identifier NCT00914914).

Mechanisms of CPP cell entry

Although there has been many examples of CPP mediated drug delivery in the literature and in the clinic, the precise mechanisms by which CPPs can enter a cell are still not fully understood. This has arisen from conflicting results in the literature, describing different cell entry routes for the same CPP. CPP entry may therefore be largely dependent on the experimental conditions; cell type, cargo, incubation period, analytical tools etc. (Richard et al., 2003; Tünnemann et al., 2006). Alternatively, CPPs may utilise multiple mechanisms at once to enter the interior of a cell (Guterstam et al., 2009). Despite these complications there appears to be two primary mechanisms for CPP entry into cells: direct translocation and endocytosis.

Direct translocation: The first studies to investigate the mechanisms by which CPPs enter cells identified that they enter passively through temperature and receptor independent processes that are insensitive to inhibitors of endocytosis (Derossi et al., 1994; Vivès et al., 1997). However, these studies were reliant on the imaging of fixed cells, a technique which was later demonstrated to produce artefacts concerning CPP entry and localisation (Richard et al., 2003). Nevertheless, direct translocation across the membrane has been demonstrated

using live imaging techniques and biophysical approaches (Guterstam et al., 2009; Jiao et al., 2009).

Direct translocation is proposed to occur when positively charged residues of CPPs interact with negatively charged phospholipids of the cell membrane. This interaction results in the invagination of the cell membrane. Disruption of the cell membrane then releases the CPP into the cytoplasm (Alves et al., 2008; Derossi et al., 1994; Joanne et al., 2009) (Figure 1.9A). Alternatively, CPPs have been proposed to translocate directly across the lipid bilayer (Rothbard et al., 2005). Positively charged CPPs again interact with negatively charged phospholipids forming a transient ion pair complex that is able to diffuse across the cell membrane. This diffusion is driven by the membrane potential which favours the movement of positively charged substances into cells. In support of this, depolarising a cell membrane significantly reduces, whereas hyperpolarising increases, CPP entry into a cell (Rothbard et al., 2005) (Figure 1.9A).

Endocytosis: Endocytosis of CPPs has been demonstrated to occur through three pathways: caveolae- and clathrin- mediated endocytosis and macropinocytosis (Figure 1.9B). Caveolae mediated endocytosis involves the interaction of a CPP with a lipid raft; cholesterol-interacting calveolin proteins then oligomerise forming an endocytotic vesicle around the CPP (Rothberg et al., 1992). Clathrin-mediated endocytosis is mediated by the adaptor protein AP2 which recruits clathrin to the membrane resulting in the formation of an endocytotic vesicle (Keen et al., 1979; Pearse, 1976).

Live cell imaging of fluorescently labelled CPPs has demonstrated that CPPs co-localise with cholera toxin, an indicator of caveolae-mediated endocytosis, at the cell membrane. Further, these tagged CPPs did not co-localise with transferrin, a marker of clathrin-mediated endocytosis, suggesting that calveolin mediated endocytosis is the predominant entry mechanism for CPPs (Fittipaldi et al., 2003; Jones et al., 2005). However, others have presented contradicting results, suggesting dependence on clathrin, and not caveolae, for CPP entry. CPP entry into cells was shown to be unaffected by inhibitors of caveolae-mediated endocytosis (nystatin and filipin III) but reduced by inhibitors of clathrin-mediated

endocytosis (chlorpromazine and potassium depletion) (Richard et al., 2005). Moreover, CPP entry has also been shown to localise with transferrin (Richard et al., 2003).

Macropinocytosis is neither caveolae nor clathrin-dependent and involves the encapsulation of a CPP by actin-containing membrane protrusions, forming a macropinosome. This is supported by the CPP-induced formation of lamellipodia (Gerbal-Chaloin et al., 2007). Additionally, CPP entry is reduced when cells are pre-treated with 5-(N-ethyl-N-isopropyl) amiloride, an inhibitor of the Na^+/H^+ antiporter required for macropinocytosis (Nakase et al., 2004; Nakase et al., 2007).

Following endocytosis of a CPP into a cell CPPs can become trapped in endosomal compartments, preventing cargo release into the cytoplasm. This is supported by studies utilising endosomolytic compounds such as chloroquine to release a trapped CPP, which greatly increased the effectiveness of a CPP (Rudolph et al., 2003). As a result, many of the CPPs in development today contain modifications to increase their endosomal escape. These modifications include the addition of histidine motifs to a CPP, which acts a proton sponge (Lo and Wang, 2008; Lundberg et al., 2007). Alternatively, CPPs have been attached to the intracellular transport domain of a bacterial toxin. The transport domain of a bacterial toxin allows the CPP to be transported through multiple compartments of a cell ultimately leading to the release of the CPP into the cytosol (Mohammed et al., 2012).

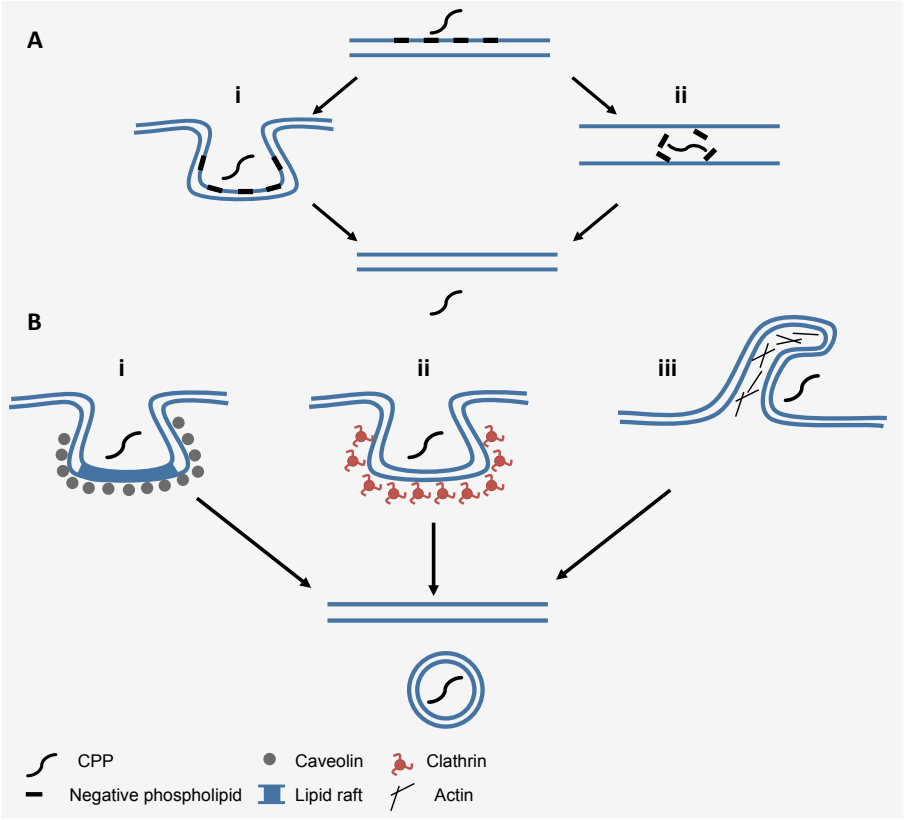

Figure 1.9. Mechanisms of CPP cell entry. A. *Direct translocation*. CPPs interact with negatively charged phospholipids on the cell membrane. Interactions of the positively charged CPPs with negatively charged phospholipids either causes invagination of the membrane i) or results in the CPP being transported across the membrane relative to membrane potential ii). The CPP is then released into the cytoplasm of the cell. **B**. *Endocytosis*. CPPs either interact with i) caveolin containing lipid rafts or ii) instigate the recruitment of clathrin to the membrane. iii) Alternatively, the actin is reorganised, forming lamellipodia, enveloping the CPP by the process of macropinocytosis. The CPP is then endocytosed into the cell and is retained in endosomes.

Immunogenicity of CPPs

Like other drug carriers, CPPs have been modified over the years to increase their effectiveness. The CPPs in development today are usually based on sequences from the originally identified natural CPPs. The HIV-TAT peptide is derived from the human immunodeficiency viral protein trans-activator of transcription. This protein natively serves to increase the transcription of all HIV derived genes in a host cell but was identified as having the ability to form a complex with a cargo and transport it across a cell membrane (Frankel and Pabo, 1988). Although yet to be proved, it has been suggested that the CPP function of the full length TAT peptide may serve to allow secreted TAT peptide to enter non-infected cells and prime them for transcription of viral proteins following subsequent infection. Another CPP, Antennapedia, was derived from a transcription factor isolated from

Drosophila (Berlose et al., 1996). Similar to the HIV-TAT peptide, it is currently unknown if the biological action of the Antennapedia protein is influenced by its CPP properties. However it is believed that any biological role would reflect the capability of homeodomain proteins such as Antennapedia to be released from one cells and influence another in a paracrine fashion (Berlose et al., 1996).

CPPs have also been derived from various scorpion, snake and wasp venoms (Gurrola et al., 2010; Rádis-Baptista and Kerkis, 2011). In this context the CPP action of the protein appears to be required for the function of the venom. The scorpion toxin imperatoxin A contains a CPP motif that allows translocation of the toxin across cardiomyocyte membranes. Following penetration into cardiomyocytes the toxin can promote the release of calcium through the activation of ryanodine receptors present on intracellular calcium stores thereby exhibiting inotropic effects on the heart (Gurrola et al., 2010).

Given their foreign nature there is potential for CPPs to be toxic to cells. Indeed studies have identified that, at high concentrations, CPPs can greatly affect the viability of cells (Hansen et al., 2012; Kilk et al., 2009; Watkins et al., 2009). This effect occurs at concentrations of CPPs above those required for efficient entry of a CPP into a cell. Nevertheless there still remains the possibility that CPPs may be recognised by the body as foreign, which could result in the initiation of an immune response. If CPPs were capable of initiating an immune response this would be detrimental to their use in the clinic. It is therefore quite surprising that this has not been investigated given the current interest in CPP based therapies and that a number are entering clinical trials. In fact, to date only a few studies have examined if CPPs can initiate an immune response.

In one study involving the THP-1 cell line, the CPP PepFect, which is based on the more commonly used CPP Transportan, was shown to efficiently deliver and induce the expression of a DNA plasmid containing a green fluorescent protein (GFP) expression vector (Suhorutsenko et al., 2011). This delivery with PepFect did not elicit the production of pro-inflammatory cytokines from the THP-1 cells. Similarly, intravenous injection of PepFect into mice did not cause an elevation in serum levels of pro-inflammatory cytokines (Suhorutsenko et al., 2011). In another

study, the nasal delivery of complexes of insulin and the CPP Penetratin to rats was assessed for an immunogenic response. Following the delivery of these complexes to rats there was no increase in pro-inflammatory cytokines in either nasal lavage fluid or blood plasma (Khafagy et al., 2013). This study would suggest that CPPs produce no inflammatory reaction either at the site of administration or systemically immediately following CPP delivery or for many days after.

One study has presented evidence for an immune response from CPPs. In this study the successfully delivery of a p38 siRNA duplex conjugated to either the CPP HIV-TAT or Penetratin to murine lungs was evaluated. Intratracheal administration of Penetratin covalently coupled to an siRNA was found to increase the levels of the pro-inflammatory cytokines tumour necrosis factor α (TNFα), interleukin (IL)-1β and interferon γ in murine lungs six hours post administration (Moschos et al., 2007). Interestingly, neither HIV-TAT conjugated to an siRNA nor HIV-TAT or Penetratin alone induced a similar immune response in the mice. This may suggest that some CPPs induce an immune response whereas others do not. Alternatively, this may reflect potential differences between CPPs in their modes of uptake and transport within cells, which can also be dependent on the type of cargo and method of association (covalent or non-covalent) (Lundin et al., 2008; Madani et al., 2011; Milletti, 2012). It is therefore possible that the Penetratin–siRNA complex transported to a region within cells where either the Penetratin sequence, or the siRNA itself (Sioud, 2006), was recognised by pattern recognition receptors.

1.9 Bacterial toxins as therapeutic tools

Microorganisms secrete toxins as virulence factors to aid in their evasion of the bodies' defences. These toxins are generally harmful and sometimes fatal but also have the potential to be repurposed for therapeutic applications. A common approach is the creation of 'immunotoxins'. Immunotoxins are hybrids composed of an antibody linked to a toxin that has had their cell-binding domain removed. This creates a therapeutic that has high target specificity and high toxicity.

The most commonly used bacterial toxins for therapeutic applications are diphtheria toxin (DTx) produced from *Corynebacterium diphtheria* (Marsh, 1988), *Pseudomonas aeruginosa* exotoxin A (PEx) (FitzGerald et al., 1986), and more recently Cholix toxin (Chx) produced from *Vibrio cholerae* (Sarnovsky et al., 2010). These three toxins share a similar intoxication pathway and protein structures composed of three distinct domains. Domain one is responsible for receptor binding and toxin entry into cells. The receptor for DTx is a heparin-binding EGF-like growth factor precursor (Naglich et al., 1992) and PEx binds to low density lipoprotein receptor-1 (CD91) (Kounnas et al., 1992). The receptor for Chx is currently unknown, although given its sequence homology with PEx it may also bind CD91 (Jørgensen et al., 2008). Domain two is required for the transport of the toxin from endosomal compartments to the cytosol in non-polarised cells. Domain three is the enzymatic portion of the toxin, which inhibits protein translation within cells leading to the induction of apoptosis. These domains can be manipulated for therapeutic use; domain I can be replaced with an antibody or another protein to produce a cell selective 'immunotoxin'. Alternatively, the third domain can be removed and replaced with a therapeutic cargo, aiding the delivery of such a cargo into the cell cytosol (Figure 1.10). This has been demonstrated by combining the translocation domain of PEx with a CPP and a GFP cargo. The addition of the translocation domain greatly enhanced the endosomal escape of GFP compared to the CPP-GFP complex alone (Mohammed et al., 2012).

In 2008 the first immunotoxin was approved for clinical use. Denileukin diftitox is an immunotoxin composed of DTx coupled to IL-2, thus specifically targeting DTx to cells expressing the IL-2 receptor, and is used for the treatment of cutaneous T cell lymphoma. Denileukin diftitox produced a 30% clinical response in patients, with 10% showing complete remission (Olsen et al., 2001). The success of this immunotoxin has lead to the generation of many more that are currently in clinical trials (Dosio et al., 2014). These include a phase III trial of Moxetumomab pasudotox, an anti-CD22 antibody coupled to PEx, for the treatment of hairy cell leukaemia (ClinicalTrials.gov identifier NCT01829711) and a phase I/II trial of cintredekin besudotox, an immunotoxin composed of IL-13 coupled to PEx, for the treatment of adrenocortical carcinoma (ClinicalTrials.gov identifier NCT01832974). As well as being used as single agents, immunotoxins may also be used in

combination with other therapeutics to have a greater net effect. For example, the combined application of the PI3K inhibitor ZSTK474 and a PEx based immunotoxin targeting prostate cancer cells had a greater therapeutic effect on prostate cancer in mice than either treatment alone (Baiz et al., 2013).

These immunotoxins appear to be initially well tolerated by the body. However, following prolonged exposure (around three weeks) the body produces neutralising antibodies against the immunotoxin (Posey et al., 2002). Strategies to overcome this obstacle include co-administering an immunosuppressant with the immunotoxin (Hassan et al., 2004), or altering the protein sequence of the immunotoxin to remove antigenic epitopes (Onda et al., 2011; Onda et al., 2008). Immunosuppressive approaches have had limited success (Hassan et al., 2004), whereas altered immunotoxins have managed to prolong the use of an immunotoxin before the development of neutralising antibodies (Onda et al., 2008; Onda et al., 2011). An alternative strategy is to use a second immunotoxin based on another bacterial toxin once a neutralising response has developed for the first. This has been proven in principle by a study indicating that neutralising antibodies directed at a PEx based immunotoxin do not affect the function of a similar immunotoxin based on Chx (Sarnovsky et al., 2010).

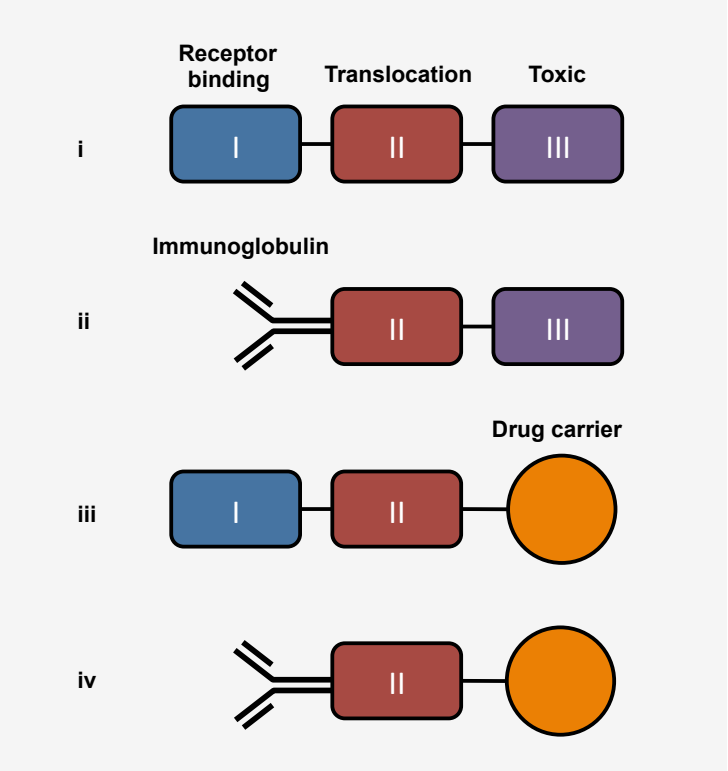

Figure 1.10. Bacterial toxins as therapeutic agents. i) The bacterial toxins DTx, PEx and Chx are polypeptides composed of three domains; a receptor binding domain (I), a translocation domain (II) and an enzymatic domain (toxic; III). These domains can be altered a to create a variety of therapeutic agents. Domain I can be replaced with an antibody, producing a cell specific immunotoxin (ii). Alternatively, the toxic domain can be replaced with a drug cargo creating a cell permeable drug delivery vehicle (iii). Finally, ii and iii can be combined to create a cell-specific drug delivery vehicle (iv).

DTx and PEx intoxication pathway

The intoxication pathways for DTx and PEx are well defined in non-polarised cells and are similar in that they both require receptor-mediated endocytosis and subsequent release into the cytosol for their action. This section will focus on the intoxication pathways for DTx and PEx, as the current pathway for Chx is currently unknown. Following entry into cells by receptor mediated endocytosis DTx and PEx are cleaved by the protease furin into two fragments, the active form of the toxin (fragment A, containing domains II and III) and the receptor binding element (fragment B) (Gordon et al., 1995). This step appears to be essential for the toxic activity of DTx and PEx as transfection of furin into furin-deficient cells is sufficient to overcome their innate resistance to DTx and PEx (Gordon et al., 1995). PEx and DTx also requires a second reduction step before the two fragments can be separated (McKee and FitzGerald, 1999; Ryser et al., 1991). After being encased

in acidic endosomes DTx undergoes a conformational change, the B fragment inserts itself into the membrane of the endosome creating a pore. The A fragment can then be released directly into the cytosol (Lemichez et al., 1997; Papini et al., 1993; Zalman and Wisnieski, 1984) (Figure 1.11). PEx requires subsequent translocation to the trans Golgi network and endoplasmic reticulum (ER) before being release into the cytosol.

Once in endosomes, PEx is transported to the Golgi network either through an Arf1/Rab9 or Syn16/Rab6 dependent mechanism, which appears to be cell-type dependent (Smith et al., 2006a). Once in the Golgi the REDL sequence present on PEx interacts with the KDEL receptor to direct the transport PEx to the ER. The REDL sequence of PEx is similar to that of the KDEL sequence, an ER retention and retrieval signal in mammalian cells (Giannotta et al., 2012; Lewis and Pelham, 1990). Consistent with a requirement for this REDL sequence, the toxicity of PEx is enhanced if the number of KDEL receptors are increased, or *visa versa* (Jackson et al., 1999). However, the REDL sequence is not crucial for the transport of PEx as a toxin construct with the REDL sequence removed is still capable of accessing the cytoplasm (Mohammed et al., 2012). Once in the ER PEx undergoes its reduction step, releasing fragments A and B. Fragment A then associates with the ER pore Sec61, affecting its gating properties and allowing fragment A to exit into the cytosol (Wirth et al., 2003).

Upon entry into the cytosol the enzymatic A fragment of DTx and PEx inactivates elongation factor 2 (EF2) through the ADP-ribosylation of a modified histidine residue, termed diphthamide, present on EF2 (Collier, 1975; Foley et al., 1995; Iglewski et al., 1977) (Figure 1.11). EF2 catalyses the movement of a polypeptide chain along a ribosome, inactivation of EF2 therefore halts protein synthesis. This results in the depletion of the anti-apoptotic protein Mcl-1 that is rapidly turned over, thus, initiating cell apoptosis (Du et al., 2010).

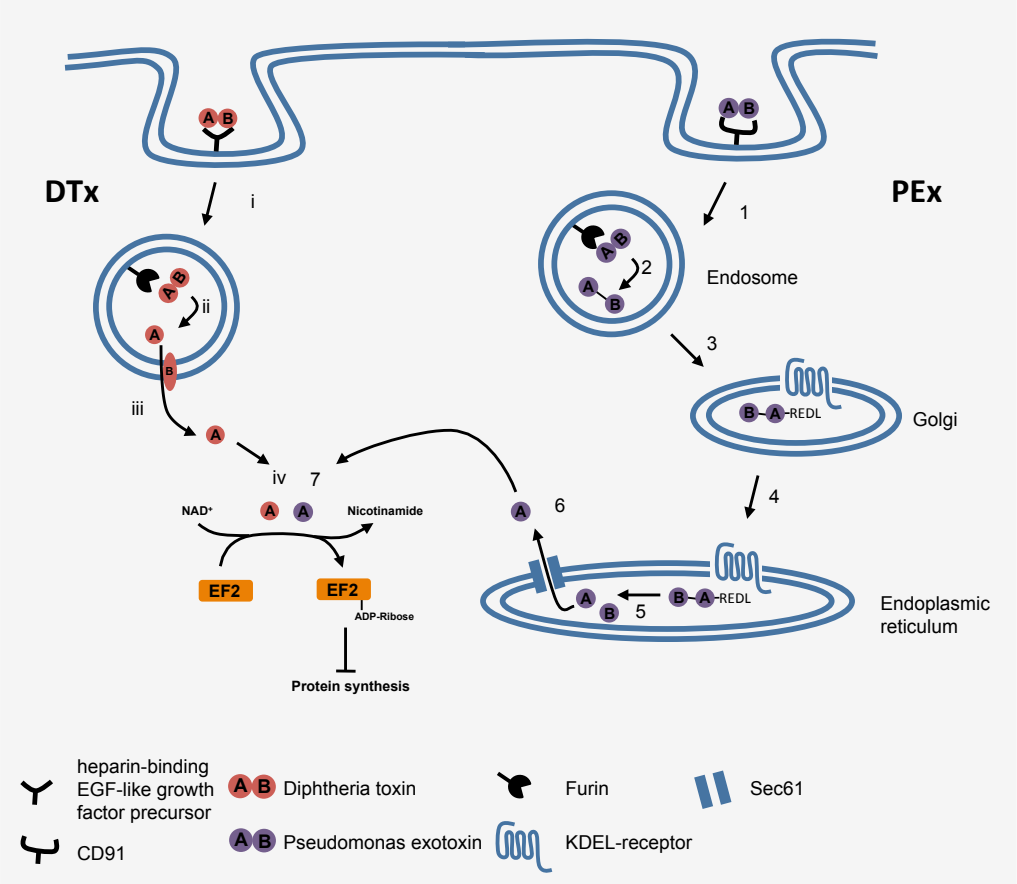

Figure 1.11. DTx and PEx intoxication pathway in non-polarised cells. *DTx intoxication*. i) DTx binds to heparin-binding EGF-like growth factor precursor and is internalised into cells. ii) Once in endosomes the protease furin cleaves DTx into fragments A and B. iii) The acidic nature of the endosome causes a conformational change in fragment B, which inserts itself into the endosomal membrane, allowing fragment A to exit into the cytosol. *PEx intoxication*. 1) PEx binds to CD91 and is internalised. 2) Once in endosomes PEx is cleaved by furin. However, a disulphide bond still covalently links the two fragments. 3) PEx is transported to the Golgi network where the REDL sequence of fragment A is recognised by the KDEL-receptor. 4) The two fragments are then transported to the endoplasmic reticulum. 5) Inside the endoplasmic reticulum the disulphide bond connecting fragments A and B is reduced, separating the two fragments. 6) Fragment A interacts with Sec61, releasing fragment A into the cytosol. iv) & 7) Fragment A of DTx and PEx catalyse the ADP ribosylation of elongation factor 2 (EF2) resulting in arrest of protein synthesis.

Directing toxin transport within a cell

Studies have suggested that as little as one molecule of toxin is sufficient to induce apoptosis in a cell (Yamaizumi et al., 1978). However, significantly more than this is required for the intoxication of cells (Kreitman and Pastan, 1998). This would suggest that <1% of the internalised toxin is not transported to the cytoplasm but instead ends up in other intracellular compartments, potentially lysosomes (Smith et al., 2006a). This has implications for the use of these toxins

as drug delivery vehicles as substantial amounts of a drug may be lost to degradative pathways, thereby rendering the therapeutic ineffective.

PEx has been shown to take two possible routes to the Golgi network, an Arf1 dependent route that can transport PEx to either the Golgi or to lysosomes from late endosomes, and a Syn16 dependent route that transports PEx straight from early endosomes to the Golgi network (Smith et al., 2006a). It could be conceived that altering PEx to only take the Syn16 route would increase the amount delivered to the cytosol by avoiding lysosomal degradation. However, inhibition of the Arf1-dependent route, and thus presumably increasing the amount of PEx in the Syn16 route, did not increase the sensitivity of the cells to PEx (Smith et al., 2006a). Nevertheless, identifying the interactions that govern the route a toxin takes within a cell may lead to improved toxins that have greater delivery to the cytosol.

A potential candidate is the ganglioside GM1, the native receptor for cholera toxin (Holmgren et al., 1975). GM1 is composed of an extracellular oligosaccharide that binds cholera toxin, and a ceramide domain that anchors the lipid in the membrane. Both of these domains exist in multiple forms that can influence the transport of GM1 within the cell (Chinnapen et al., 2012; Hakomori, 2003). For example, cholera toxin is transported to the Golgi network in cells loaded with the C16:0 ceramide chain variant of GM1 but transports to lysosomes in cells loaded with the C18:0 variant (Chinnapen et al., 2012). As PEx also binds to GM1 (R. Mrsny. Unpublished observations) there is the potential for this bacterial toxin to also utilise GM1 as a sorting mechanism within cells.

Drug administration using bacterial toxins

A major obstacle for the delivery of macromolecules (for example insulin) is the initial administration of the agent to the body. Macromolecules are too large to cross the epithelial barriers present at the skin, intestine, or airways. The intestinal route also has the added obstacle of passing through the stomach, which due to its acidic nature would likely render a therapeutic useless. Many macromolecules therefore need to be administered directly to the blood stream by intravenous administration. This is not ideal as it requires experienced hands and comes with a

social stigma that reduces patient compliance (Hanas and Ludvigsson, 1997). Oral, or other, formulations of macromolecule-based drugs would therefore be well received by the medical community.

As well as a potential use as a drug carrier to specific target cells and intracellular compartments, bacterial toxins such as PEx and Chx also have the potential to aid in the administration of therapeutics to the body. *Pseudomonas aeruginosa* is an opportunistic pathogen of the airways that releases PEx as a method of immune evasion. PEx passively crosses the polarised epithelial layer that comprises the mucosal lining of the airways and subsequently enters and induces apoptosis in non-polarised cell types, particularly antigen presenting cells, present in the submucosal space (Daugherty et al., 2000; Mrsny et al., 2002). It is hoped that by exploiting this mechanism of transcytosis by PEx, therapeutics could be developed that allow delivery via mucosal routes such as the airway and intestine (i.e. inhalation or oral delivery). This would ultimately involve the replacement of the third domain of PEx with a therapeutic (Figure 1.10 iii). PEx would then be able to transport its therapeutic cargo across a polarised epithelial surface and deliver it to the other side. The toxin could be further modified to either allow the delivery of the therapeutic to non-polarised cells or for the therapeutic to be cleaved from the toxin to allow it to act systemically.

1.10 Project aims and objectives

The experimental work in this thesis is divided into three sections. The first part will dissect the role of the disease relevant pathway PI3K in the embryonic development of the lung airways. The second part will investigate the use of CPPs as delivery mechanisms to epithelial cells with a focus on their potential immunogenic properties. The final part will examine the transport of bacterial toxins within cells to explore their prospective use as drug carriers. These elements come together with the intent to provide an improved understanding of potential therapeutic targets for pulmonary diseases, potential delivery of novel medicines into the cytoplasm of epithelial cells using CPP strategies, and the possibility of delivering biopharmaceuticals to the submucosal space using bacterial-derived delivery mechanisms.

i) Developmental pathways are regularly reactivated in the disease state where they can contribute to the remodelling of an organ, as is the case in fibrosis (Shi et al., 2009), or can increase the aggressive properties of epithelial cancers (De Leij et al., 1987). PI3K has been identified as a critical mediator in many of these disease processes. However comparatively little is known about PI3K in the development of the lung with current research producing conflicting results (Wang et al., 2005; Xing et al., 2008). This part of the thesis will utilise a pharmacological toolkit of specific inhibitors for PI3K and its downstream signalling components to dissect the role of this kinase in branching morphogenesis. This work aims to:

- Examine the role of PI3K in the process of EMT, which is relevant to both developmental and pathogenic mechanisms.
- Establish models of embryonic lung branching and explore approaches to manipulate the signalling pathways involved, e.g. pharmacological and lentiviral gene delivery.
- Using these approaches the role of PI3K will be examined in a physiologically relevant model of airway branching.
- Explore possible mechanisms of PI3K involvement in branching morphogenesis.

ii) CPPs are a useful tool to deliver otherwise cell impermeable therapeutics into cells (Milletti, 2012). However, as many of the CPPs currently in development are based on naturally derived CPPs there is the potential for these CPPs to elicit an immune response in the body that would be detrimental to their use in the clinic. Surprisingly there is currently little evidence related to the potential of CPPs to elicit an immune response. This part of the thesis seeks to explore this possibility by:

- Demonstrate the delivery of a cargo to epithelial cell lines by three commonly used CPPs; HIV-TAT, Antennapedia and Transportan, *in-vitro*.
- Establish if these CPPs can induce an immune response from the cells by measuring the activation of immune-related pathways *in-vitro*.

iii) Bacterial toxins are commonly used as immunotoxins, targeting specific cell types for effective destruction (Dosio et al., 2014). There is also the potential to use elements of these toxins as drug carriers either into cells (Mohammed et al., 2012), or across epithelial monolayers for oral or inhalation administration (Mrsny et al., 2002). However, question still remain concerning the amount of drug that can be delivered into a cell and whether bacterial toxins can effectively transport a therapeutic across epithelial barriers. This part of the thesis will investigate the utility of using bacterial toxins for this purpose by:

- Identify if the ganglioside GM1 can affect the trafficking of bacterial toxins within non-polarised cells.
- Assess the transport of bacterial toxins across polarised epithelial cells and examine the subsequent delivery of a therapeutic to a non-polarised cell population on the other side.

Chapter 2: Materials and Methods

2.1 Compounds

The pan class I PI3K inhibitors ZSTK474 and LY294002, the PI3Kα inhibitors A66 and PIK-75, the PI3Kβ inhibitor TGX-221, the mTORC1/2 inhibitor AZD8055 (, the mTORC1 inhibitor rapamycin, the c-Jun N-terminal kinase (JNK) inhibitor SP600125 and the FGFR inhibitor PD173074 were purchased from Selleckchem (Suffolk, UK). Akt inhibitor VIII was acquired from Merck chemicals (Dramstadt, Germany). The PI3Kβ inhibitor GSK2636771 was obtained from Axon Medchem (Groningen, The Netherlands). The PI3Kα inhibitor BYL719 was provided by Novartis (Basel, Switzerland). The GSK3β inhibitor 1M was a gift from Professor Melanie Welham (University of Bath) (Bone et al., 2009).

2.2 Cell Culture

Human A549 (alveolar), A431 (epidermal), Caco-2 (intestinal) and HEK293T (kidney) epithelial cells were maintained in DMEM: F12 cell culture medium (Gibco, Paisley, UK) supplemented with 10% foetal bovine serum (FBS) (Source Bioscience, Nottingham, UK), 2 mM L-glutamine (Gibco), 100 U/ml penicillin and 100 µg/ml streptomycin (Gibco). Murine 3T3 fibroblasts and J774.2 macrophages were also maintained in DMEM: F12 medium. Wild type Chinese hamster ovary (CHO) cells and CHO cells deficient in CD91 ($CHO^{CD91-/-}$), a gift from David Fitzgerald (National Cancer Institute, Bethesda, USA), were maintained in MEM medium (Gibco) supplemented with 10% FBS, 2 mM L-glutamine, 100 U/ml penicillin and 100 µg/ml streptomycin. All cells were grown in a 37°C 95% air/ 5% CO_2 incubator.

Murine embryonic fibroblasts (MEF) deficient in the ganglioside GM1 ($MEF^{GM1-/-}$) and A431 cells expressing GFP tagged Rab5, Rab7, Rab 11, Sec61 or Golgin 97 were maintained at Professor Wayne Lencer's laboratory (Boston Children's Hospital, Boston, USA) in DMEM cell culture medium (Gibco) supplemented with 10 % FBS.

For EMT experiments A549 cells were cultured to ~70% confluence then serum starved overnight prior to the application of 5 ng/ml TGFβ (Peprotech, London,

UK). A549 cells were cultured for a further 48 hours in serum free conditions prior to analysis.

Polarised monolayers of Caco-2 cells were grown by initially seeding 70,000 cells onto Transwell polycarbonate filters (0.4 μm pore size; Corning, Amsterdam, The Netherlands). Cells were then cultured for a period of 14-21 days until complete polarisation was achieved as indicated by consistent trans-epithelial electrical resistance values that were substantially above background.

2.3 Embryonic lung isolation

All animal experiments were performed within UK Home Office regulations and with the approval of the University of Bath ethics committee. E12.5 embryos were removed from timed pregnant CD1 mice and placed into ice cold plain DMEM: F12 medium. Using a Leica MZ75 stereomicroscope the organ tree containing the heart, lungs, stomach, liver and pancreas was initially separated from the surrounding embryonic tissue (Figure 2.2). Whole embryonic lungs were then carefully removed from the organ tree and placed into ice cold DMEM: F12 cell culture medium.

Whole lung explant culture

Isolated whole lung explants were placed on top of a nuclepore track etched membrane (8 μm pore size; Fisher scientific, Paisley, UK) suspended on top of DMEM: F12 culture medium supplemented with 0.5% FBS (Del Moral and Warburton, 2010). Whole lung cultures were then placed in a 37°C incubator gassed with 95% air/ 5% CO_2 for 48 hours. Images of lung growth were collected every 24 hours by a Canon EOS 1100D digital SLR camera attached to an Olympus CKX41 inverted light microscope. Airway branching was quantified by calculating the percentage increase in the number of terminal branches over 24 and 48 hours relative to the number at isolation using the equation:

$$\% \text{ Increase in branching} = (\text{Terminal branches}_{24/48 \text{ hours}} - \text{Terminal branches}_{0 \text{ hours}}) \div \text{Terminal branches}_{0 \text{ hours}} \times 100.$$

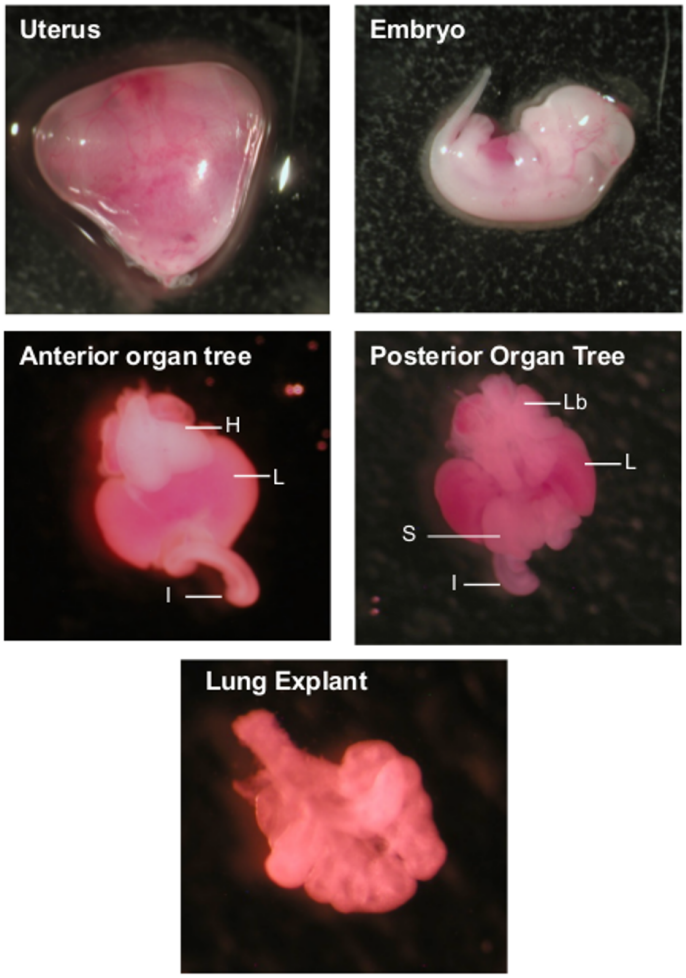

Figure 2.1. Embryonic murine lung isolation. Images representing the separate stages of murine embryonic lung isolation are shown. Initially, E12.5 murine embryos are removed from their respective uteri. The organ tree is then dissected from the embryo from which the whole embryonic lung is removed. H – Heart, L – Liver, I – Intestine, Lb – Lung bud, S – Stomach.

Whole lung explant time-lapse imaging

E12.5 murine lung explants were prepared as above and placed on top of Transwell polycarbonate filters (3 μm pore size; Corning) inserted into DMEM: F12 culture medium supplemented with 0.5% FBS. Transwell plates were then placed onto a Zeiss Axio Observer.Z1 microscope attached to a Hamamatsu CCD digital camera with incubator system XLmulti S1. Lung explants were maintained at 37°C in a 95% air/ 5% CO_2 atmosphere over 48 hours. Images were collected every 15 minutes and compiled into a time-lapse movie using Zeiss blue 2012 image software.

Embryonic lung epithelium isolation and culture

Isolated lung epithelial cultures were prepared by taking freshly isolated E12.5 whole lung explants and placing them into complete FBS in a glass petri dish. Fine insulin needles were then used to carefully remove the mesenchymal tissue from the epithelial branch tips. These epithelial tips were then separated from the remaining lung explant and placed into a growth factor reduced Matrigel (BD Bioscience, Oxford, UK) dome mixed 1:1 with DMEM: F12 cell culture medium supplemented with 0.5% FBS (Figure 2.2). Matrigel domes containing isolated epithelium were then allowed to polymerise at 37°C for 30 minutes before being covered with DMEM: F12 cell culture medium supplemented with 0.5% FBS and either 100 ng/ml FGF7 (Miltenyi Biotech, Surrey, UK), 100 ng/ml FGF1 (Miltenyi Biotech), 250 ng/ml FGF10 (Miltenyi Biotech) or 10-100 ng/ml FGF2 (Peprotech). Epithelial isolates were cultured for 96 hours with the culture medium being changed every 48 hours. Images of isolate growth were acquired at the start and end of culture.

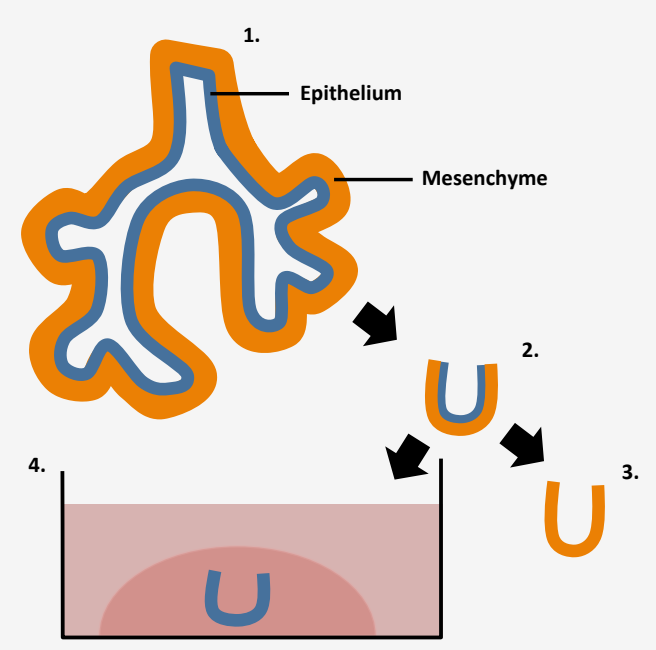

Figure 2.2. Schematic of murine embryonic lung epithelium isolation and culture. (1) E12.5 murine lung explants are dissected from timed pregnant females. (2) Epithelial tips are stripped of mesenchymal tissue using fine needles. (3) The mesenchyme is subsequently discarded and (4) the isolated epithelium is positioned inside a Matrigel dome and placed into culture.

siRNA transfection of epithelial isolates

SMART pool siRNA targeting either the catalytic p110α (*PIK3CA*) or p110β (*PIK3CB*) subunits of PI3K or the regulatory p85α (*PIK3R1*) or p85β (*PIK3R2*) subunits were purchased from Dharmacon (Leicestershire, UK). Sequences are provided in table 2.1.

To aid siRNA delivery into isolated lung epithelium three different transfection reagents were examined: lipofectamine 2000 (Invitrogen, Paisley, UK), jetPRIME (Source Bioscience) and 3D-Fect (OZ Biosciences, Marseille, France). Complexes of transfection reagent with 10-50 nM siRNA were prepared following manufactures instructions prior to incubation with fresh mesenchyme-stripped murine lung epithelium.

When using siRNA complexed with lipofectamine/jetPRIME, lung epithelial isolates were placed in solutions of transfection complexes on glass slides and incubated at 37°C in a humidified atmosphere for 2 hours. The isolates were then removed from transfection complex, placed into Matrigel domes and cultured as outlined in section 2.3.3. When using siRNA complexed with 3D-Fect the transfection complexes were combined with the Matrigel dome prior to the addition of a lung epithelial isolate.

The resulting cultures were grown for 96 hours then the isolates were released from their Matrigel dome using BD Matrigel recovery solution (BD Bisocience). Subsequently, RNA was extracted from the isolates using Trizol reagent (Invitrogen). Chloroform was used to separate the RNA, which was then precipitated using propan-2-ol. Following centrifugation the resulting RNA pellet was washed with 75% ethanol, dried, then suspended in RNAse free water before RNA content was quantified using a nanophotometer (Implen, Munich, Germany).

Target	Sequences
PIK3CA	GGACAGCUGUUUCAUAUAG GCAAGUAUAUUCUGAAAGU GAUCUCAACUCGCCUCAUA UAAAGAAACUCCAUGCUUA
PIK3CB	GAAUCAAACUGCUGUAUAU GGAAUAAACUUGAAGAUGU CAACAACCCUUUCCAAAUU GAACCGAGCUCCUGUGUAA
PIK3R1	CUAAAAUGCACGGCGAUUA GAAGUCAAGCAUUGCGUCA UAAUAAACCACUACCGGAA ACGCGAAGGCAACGAGAAA
PIK3R2	CCACAGCUCUGGCCAAUGG GACAGUGAAUGCUACAGUA GGACAAGAGCCGCGAAUAU GGAUGGAUCUUCUGAGUCA

Table 2.1 List of PI3K siRNA sequences

2.4 Lentiviral generation

The lentivirus expression system allows for the stable expression of a desired gene in cells that are otherwise difficult to transfect. Difficulties in transfection may arise due to the toxicity associated with chemical transfection reagents or their inherent resistance to transfection (Lois et al., 2002). The lentiviral system is based on the human immunodeficiency virus and utilises four plasmids; pREV, pGAG/Pol, pVSVG, and a final plasmid for the vector to be inserted into the host cell. pREV and pGAG/Pol encodes for viral proteins required for efficient viral packaging. pVSVG encodes a viral protein required for effective infection of the viral particles into the host cells (Dull et al., 1998). These plasmids are combined and transfected into HEK293T cells that in turn generate and release viral particles into the cell culture medium. This media can then be collected and used to infect desired cells.

Bacterial transformation and plasmid preparation

When required, 1 µg of plasmid DNA was added to chemically competent Stbl3 *E.coli* (Invitrogen) on ice. This was incubated for 30 minutes before being heat shocked at 42 °C for 30 seconds. SOC media (Invitrogen) was added to the vial on ice before being incubated for 1 hour at 37°C with agitation. The contents of the

vial were subsequently streaked onto an agar (Fisher Scientific) plate containing 100 µg/ml ampicillin (Sigma-Aldrich, Poole, UK) and incubated overnight in a 37°C oven. Resulting bacterial colonies containing the plasmid DNA were selected the following day and cultured in 5 ml of ampicillin containing (100 µg/ml) LB broth (Fisher Scientific) for 8 hours. 50 µl of this culture was then placed into a further 50 ml of ampicillin containing LB broth which was left to grow overnight at 37°C. Plasmids were then isolated from the bacterial culture using Qiagen midi prep kits (Qiagen, Manchester, UK) following the manufactures instructions.

Lentiviral particle production

HEK293T cells were grown to 50-70% confluence in a T75 cell culture flask. Four hours prior to transfection the cell culture medium was replaced with fresh DMEM: F12 culture medium supplemented with 10% FBS and 25 mM HEPES (pH 7.4).

Plasmids composed of 7.71 µg pREV, 7.71 µg pGAG/Pol, 3 µg pVSVG and 12.84 µg of pCLPS containing a GFP expression vector were combined with H_2O to a final DNA concentration of 0.5 µg/µl. Plasmids were added to DMEM: F12 cell culture medium containing Mirus LT1 transfection reagent (Cambridge Bioscience, Cambridge, UK) and incubated for 45 minutes at room temperature. The resulting complexes were then added directly to HEK293T cells and incubated at 37°C in a 5% CO_2 incubator. After 48 hours, the resulting viral containing cell culture medium was collected, centrifuged to remove cellular debris, divided into aliquant volumes and stored at -80°C until use.

Lentiviral infection of cells and embryonic lungs

A549 cells were grown to 20-30% confluence prior to infection with viral particles. Cell culture medium was removed and replaced with fresh cell culture medium mixed with virus-containing medium (3:2). 24 hours after infection the infection medium was replaced with fresh cell culture medium. 24 hours thereafter the cells were analysed for expression of the viral construct.

Following isolation of embryonic murine lungs, explants were cultured at the air liquid interface in cell culture medium containing viral medium (1:1). Viral medium was removed 24 hours after infection and the explants were analysed for vector

expression 24 hours thereafter. For isolated lung epithelium, fresh isolates were cultured in lentiviral medium for 1 hour prior to being embedded in Matrigel.

2.5 CPP complex formation

The CPPs HIV-TAT, Antennapedia and Transportan were sourced from Cambridge Bioscience (Table 2.2). Electrostatic, non-covalent, CPP: cargo complexes were formed by mixing solutions of either HIV-TAT (100 μM), Antennapedia (100 μM) or Transportan (50 μM) with either untagged or rhodamine tagged bovine serum albumin (BSA-568; 5 μM; Sigma-Aldrich), or VivoTag680-tagged Sjögren syndrome antigen B (SSB; 50nM) siRNA (Merck, Pennsylvania, USA)(Wei et al., 2011) by vigorous pipetting. The resulting solutions were then incubated at 37°C for 30 minutes to allow for complex formation. Prior to complex formation solutions of HIV-TAT were sonicated for 5 minutes to dissociate homogenous complexes.

CPP: cargo complexes were diluted 1:5 in serum free culture medium then applied to cells at final concentrations of 20 μM: 1 μM (CPP: BSA-568 Cargo) for HIV-TAT and Antennapedia and 10 μM: 1 μM for Transportan. For CPPs in complex with SSB siRNA, a final concentration of 10 nM siRNA was applied to cells. Cells were incubated with CPP: cargo complexes for 1 hour prior to the addition of serum containing culture medium.

Cell Penetrating Peptide	Amino Acid Sequence	Molecular Weight (Da)
HIV-TAT	GRKKRRQRRRPQ	1720
Antennapedia	RQIKIWFQNRRMKWKK	2247
Transportan	GWTLNSAGYLLGKINKALAALAKKIL	2842

Table 2.2. Amino acid sequences of cell penetrating peptides

2.6 MTT cell viability assay

(4,5-dimethylthiazol-2-yl)- 2,5-diphenyl tetrazolium bromide (MTT) can be used to assess the viability of cells. MTT is converted to formazan by mitochondrial

succinic dehydrogenase in metabolically active, viable cells. Dissolving the formazan with DMSO releases an intense colour, which is proportional to cell viability.

Cell culture medium was removed from cells at the required time and replaced with fresh cell culture medium containing 0.5 mg/ml MTT (Invitrogen). MTT-containing cell culture medium is then removed after a further three hours of culture and replaced with DMSO to dissolve the produced formazan. Absorbance at 550 nm was then recorded.

2.7 IL-6/8 ELISA

ELISA based kits (eBioscience, Hatfield, UK) were used as per the manufacturers guidelines to determine the levels of IL-6 and IL-8 present in collected cell supernatant. Supernatant from cells cultured with 2 ng/ml TNFα (Peprotech) were used as a positive control.

2.8 Preparation of labelled bacterial toxins

Labelled bacterial toxins were provided by Professor Randall Mrsny (University of Bath). Briefly, a TEV protease cleavage site (ENLFQS), located between two cysteine residues forming a disulphide bond, followed by a histidine tag was introduced at the C-terminal end of non-toxic versions of PEx and Chx. PEx and Chx were rendered non-toxic through amino acid substitutions at E553D for PEx and E581A for Chx. These protein constructs were then expressed in *E.coli* bacteria before being purified using immobilised metal ion affinity chromatography on a HisTrap FF column connected to an AKTA FPLC system (GE healthcare, Buckinghamshire, UK). This method isolates proteins labelled with a histidine tag.

Purified protein was then incubated with the TEV protease AcTEV (Invitrogen) and the reducing agent DTT. This step separates the histidine tag from the toxin protein and reduces the disulphide bond between the two introduced cysteine residues, thus providing a free terminal cysteine residue with which to conjugate a

cargo. Toxin protein was isolated from the separated histidine tag through a superdex 200 HR10/30 gel filtration column (GE healthcare).

Proteins containing a free cysteine residue can be linked to a cargo that contains a maleimide group. Maleimide-containing Alexa Fluor 488 or 568 (Invitrogen), or VivoTag680-tagged SSB siRNA was added in excess to solutions of isolated toxin protein and incubated at room temperature for two hours to initiate the coupling of the cargo to the protein. Labelled toxin was finally isolated from remaining free cargo by gel filtration before protein concentration was measured using a NanoDrop 2000c (Fisher).

Cholera toxin subunit B (CTB) labelled with either Alexa Fluor 488 or Alexa Fluor 568 was sourced from Invitrogen.

GM1 loading into GM1 deficient MEF cells

$MEF^{GM1-/-}$ cells were grown to 70% confluence on 12 mm glass coverslips prior to lipid loading. The cell culture medium was replaced with HBSS containing 0.034% free fatty acid BSA (Sigma-Aldrich) and cooled to 10°C. 5 μM GM1 C16:1, or 7.5 μM GM1 C18:0 (Provided by Professor Wayne Lencer) was prepared in HBSS containing 0.034% free fatty acid BSA and then added to the cells (Chinnapen et al., 2012). Cells were then incubated at 10°C for 1 hour before un-adhered lipids were washed away with DMEM cell culture medium containing 10% FBS. Cells were finally warmed to 37°C before the addition of labelled bacterial toxins as outlined below.

Bacterial toxin transport in non-polarised cells

A431 cells expressing either EGFP tagged Rab5, Rab7, Rab11, Sec61 or Golgin97 were grown to 70% confluence on 12 mm glass coverslips. Cell culture medium was replaced with HBSS containing 20 μg/ml of either PEx-568, Chx-568, or 40 nM CTB-568. Cells were incubated at 37°C in a humidified atmosphere for 2 hours before the toxin-containing HBSS was removed. Excess toxin was washed from cells using DMEM cell culture medium containing 10% FBS. Cells were then washed once with HBSS before been processed for immunofluorescence imaging as outlined in section 2.11.

2.9 Bacterial toxin transcytosis assay

Monolayers of Caco-2 cells were prepared as described in section 2.2. Cell culture medium was replaced in both the apical and basolateral compartments with HBSS and the cells were allowed to equilibrate for 30 minutes at 37°C prior to the addition of bacterial toxins to the apical compartment. HBSS in the basolateral compartment was then collected and replaced at 15, 30, 60, 120 and 240 minutes of incubation. Where appropriate collected basolateral samples were measured for fluorescent content using a FLUOstar omega plate reader (BMG labtech, Aylesbury, UK).

Dextran permeability assay

Dextran is a high molecular weight polymer of glucose that is incapable of efficiently crossing polarised cells. Dextran can therefore be used to assess the integrity of epithelial monolayers. Following application of dextran to the apical compartment of a Transwell insert the amount of dextran present in the basolateral compartment is proportional to the integrity of the cell monolayer.

Subsequent to a transcytosis assay, 200 µl of 0.5 mg/ml FITC-labelled 4 kDa dextran (Sigma-Aldrich) was added to the apical compartment of a transwell. The cells were then incubated at 37°C for 30 minutes before the basolateral compartment was collected and assayed for fluorescent content.

Analysis

Fluorescent values were obtained for dextran from each monolayer-containing well (Dex_{Total}), a well devoid of cells (Dex_{Blank}), and the background HBSS fluorescence (Background). These values were then used to calculate the relative permeability of each Transwell (Perm factor) using the equation:

$$\text{Perm factor} = (Dex_{Total} - \text{Background}) \div (Dex_{Blank} - \text{Background})$$

Fluorescent values were obtained for labelled toxin from each time point ($Fluor_{Total}$) and the background fluorescence. Using these values and the corresponding dextran permeability factor (Perm factor) a final fluorescent value relative to the

amount of labelled toxin present in the basolateral compartment that had crossed by transcytosis ($Fluor_{Toxin}$) was calculated using the equation:

$$Fluor_{Toxin} = (Fluor_{Total} – Background) – ((Fluor_{Total} – Background) \times Perm\ factor))$$

Incorporation of bacterial toxins into non-polarised cells following transcytosis

Coverslips containing attached J774.2 macrophages were placed in the basolateral compartment of Transwell chambers containing monolayers of Caco-2 cells in the apical compartment. 20 µg of either PEx-488 or PEx-siRNA was then added to the apical compartment in DMEM: F12 culture medium supplemented with 10% FBS. Cells were incubated up to 48 hours at 37°C before the basolateral cells were processed for immunofluorescence (2.11) or Western blotting (section 2.12).

2.10 FACS analysis

To analyse fluorescent content, adherent cells were removed from cell culture plastic by incubation with 0.05% trypsin at 37°C. Cell suspensions were then washed by centrifugation, with the cell pellet being suspended in PBS. Cell suspensions were finally centrifuged and suspended in 500 µl PBS supplemented with 2% FBS and transferred to FACS tubes. Fluorescent content was then assessed by flow cytometry using a BD FACS Canto flow cytometer (BD Bioscience)

2.11 Immunofluorescence

Sample preparation

Lung explant cultures were removed from nucleopore track etched membranes and placed into the fixative MEMFA (3.8% formaldehyde, 0.15 M MOPS, 2 mM EGTA, 1 mM MgSO4, pH7.4) for 1 hour. MEMFA solution was thoroughly washed from the lungs using PBS before the fixed lung explants were permeabilised with 1% Triton-X 100 for 1 hour (Sigma-Aldrich).

E12.5 embryonic branch tips stripped of mesenchyme were fixed in 4% paraformaldehyde (PFA) for 20 minutes and permeabilised with 0.05% saponin for a further 20 minutes. Alternatively, when examining desmin and αSMA expression, samples were fixed/permeabilised with ice-cold acetone:methanol (1:1) for 5 minutes.

Isolated epithelial cultures were first removed from their Matrigel dome through incubation with ice-cold Matrigel recovery solution for 40 minutes. Freed epithelial isolates were washed in PBS before being fixed with 4% PFA for 20 minutes and permeabilised with 0.05% saponin for a further 20 minutes.

Adherent cells cultured on either glass coverslips or Transwell filters were fixed for 20 minutes in 4% PFA before being permeabilised with 0.05 % saponin for a further 20 minutes where appropriate.

Immunofluorescence staining

Following permeabilisation samples were blocked with 2% BSA in PBS for 1 hour and incubated with primary antibody (Table 2.3) diluted in 2% BSA in PBS for 1 hour at room temperature (overnight at 4°C for whole lung explants). Primary antibody was then removed and excess washed away using 2% BSA in PBS. Samples were then incubated with an appropriate secondary antibody (Table 2.4) (diluted 1/200) as indicated for 2 hours. Secondary antibodies were subsequently removed and excess washed away using 2% BSA in PBS. Samples were finally incubated in a 1 μg/ml solution of 4', 6-diamidino-2-phenylindole (DAPI, Sigma-Aldrich) for 20 minutes to label the cell nuclei. Where indicated cellular F-actin was labelled by incubating the samples for a further 20 minutes with 1 μM rhodamine-conjugated phalloidin (Sigma-Aldrich). Excess DAPI and/or rhodamine-conjugated phalloidin were removed by washing the samples in PBS before mounting with MOWIOL solution onto microscope slides.

Fluorescent images were acquired using a Zeiss LSM 510 confocal microscope. Overview images of whole lung explants were acquired using tile-scan settings creating a patchwork of 9x9 images each taken with a 40x objective. Isolated murine lung epithelium and cell cultures were imaged using a 63x objective unless

otherwise stated. Images of $MEF^{GM1-/-}$ cells and A431 cells expressing EGFP tagged proteins were acquired using a Zeiss Spinning Disk Confocal microscope with Slidebook software (Intelligent Imaging Innovations, CO).

Isolated lung epithelium confocal analysis

Fluorescent images acquired from isolated lung epithelium labelled for Ki67 and with DAPI were collected. Channels were separated and each image adjusted to remove background and noise before being converted to a binary image using ImageJ software. Merged nuclei were then divided using the 'watershed' program before the number of nuclei was quantified using the 'analyse particles' function, discounting any particle less than 5 pixels in size. This was repeated for each channel. The resulting values were converted to give a percentage of Ki67 positive cells relative to the total number of cells in a single image.

Analysis of CPP mediated BSA-568 cell uptake

To quantify and compare the delivery of BSA-568 by different CPPs confocal images were acquired utilising the same fluorescent settings for each condition. Mean fluorescent intensities for rhodamine from each image were then measured using the Zeiss LSM image browser software. This value was then adjusted relative to the number of cells in the image to give a value representative of the amount of BSA-568 incorporated per cell. This could then be used to calculate the fold change of BSA-568 delivery between different CPPs.

Co-localisation analysis using iMAB software

A quantitative value for co-localisation can be calculated from fluorescent images composed of two or more signals. Mander's coefficient represents the fraction of co-localising objects in each compartment of a dual-channel fluorescent image (Manders et al., 1993).

Fluorescent images were acquired from $MEF^{GM1-/-}$ cells incubated with fluorescently labelled bacterial toxin and stained for the Golgi marker GM130. iMAB image software (Dr Ramiro Massol, Boston Children's Hospital, Boston, USA) was used to generate masks encompassing the fluorescent signal for labelled bacterial toxin ($Mask_{Toxin}$) and the signal for the GM130

immunofluorescence. These two masks were then overlaid and a third mask was generated over sites where there was co-localisation ($Mask_{Co\text{-}local}$). Using the fluorescent intensities measured from each mask a Mander's co-localisation coefficient with respect to the fraction of signal from the bacterial toxin present in the Golgi could then be generated. This was calculated by the equation:

Mander's Coeff. = Intensity from $Mask_{Co\text{-}local}$ ÷ Intensity from $Mask_{Toxin}$

2.12 Western Blotting

Sample preparation

Whole lung explants were removed from culture and lysed by rotating at 4°C for 2 hours in lysis buffer (50 mM Tris-HCl, 150 mM NaCl, 1% Nonidet P40, 1 mM sodium vanadate, 1 mM sodium molybdate, 10 mM sodium fluoride, 40 µg/ml PMSF, 0.7 µg/ml pepstatin A, 10 µg/ml aprotinin, 10 µg/ml leupeptin and 10 µg/ml soybean trypsin inhibitor). Lysed lung explants were then centrifuged at 10,000 rcf at 4°C for 10 minutes to remove debris and the protein containing supernatant collected. Samples were diluted in sample buffer (60 mM Tris-HCl pH 6.8, 2% SDS, 10% glycerol, 5% 2-mercaptoethanol, 0.01% bromophenol blue) and boiled for 5 minutes prior to electrophoresis.

Adherent cell were cultured for the required length of time before the media was discarded and excess washed with ice cold PBS. Cells were then removed from tissue culture plastic with the aid of a cell scraper following the addition of lysis buffer. Lysates were then centrifuged and boiled with sample buffer as described above.

Immunoblotting

Samples were loaded onto a 10% SDS-PAGE gel positioned in a gel tank containing running buffer (25 mM Tris-Base, 192 mM glycine, 0.1% SDS). Proteins were stacked at 70V for 20 minutes then resolved at 150V for roughly an hour until blue sample buffer could be seen at the base of the gel. Proteins were transferred onto nitrocellulose membrane (Fisher Scientific) at 40 mA per membrane for 1

hour using semi-dry transfer buffer (48 mM Tris-Base, 39 mM glycine, 0.0375% SDS, 20% methanol) and apparatus.

The resulting protein-containing membrane was blocked in 5% milk in TBS tween (20 mM Tris-HCl, 150 mM NaCl, 0.1% Tween 20) for 1 hour. Following the blocking step membranes were incubated in primary antibody (Table 2.3), diluted in TBS tween containing 1% BSA and 0.01% sodium azide, overnight at 4°C. The primary antibody was then removed and the membrane washed several times in TBS tween before the membrane was incubated for 1 hour in a species appropriate horseradish peroxidase conjugated secondary antibody (Table 2.4; diluted 1 in 10,000). The membrane was finally washed in TBS tween and protein bands visualised using an EZ-ECL chemiluminescence detection kit (Geneflow, Staffordshire, UK) and developed using either a ImageQuant developer (GE healthcare) or an X-ray film developer (Photon Imaging Systems, Swindon, UK).
Where appropriate membranes were stripped of their initial antibodies by incubating the membrane in stripping buffer (100 mM 2-mercaptoethanol, 2% SDS, 62.5 mM Tris-HCl, pH 6.7) for 30 minutes at 60°C. Excess 2-mercaptoethanol was removed through repeated washing with TBS tween for 1 hour before being re-blocked in 5% milk in TBS tween and then re-probed with additional primary antibodies.

Antibody	Species	Manufacturer	Catalogue Number	Dilution
E-Cadherin	Mouse	BD Bioscience	610182	1/100 IF 1/1000 WB
Phosphorylated Akt (Ser473)	Rabbit	Cell Signalling	4060S	1/1000 WB
Phosphorylated S6 ribosomal protein (Ser235/236)	Rabbit	Cell Signalling	2211S	1/1000 WB
ERK1	Rabbit	Santa Cruz	SC-93	1/1000 WB
SOX9	Rabbit	Millipore	AB5535	1/100 IF
Pro-SPC	Rabbit	Seven Hills	WRAB-9337	1/100 IF
TTF-1/ Nkx2.1	Rabbit	Seven Hills	WRAB-1231	1/100 IF
Ki67	Mouse	BD Bioscience	610968	1/100 IF
Phospho-Histone H3 (PH3)	Mouse	Millipore	05-806	1/100 IF
FGFR1/ flg	Mouse	Santa Cruz	SC-121	1/50 IF
Desmin	Mouse	Dako	M076029-2	1/100 IF
Occludin	Mouse	Invitrogen	33-1500	1/100 IF
β-Catenin	Rabbit	Cell Signalling	9582P	1/100 IF
Fibronectin	Mouse	Sigma-Aldrich	F7387	1/100 IF
Platelet endothelial cell adhesion molecule-1/ CD31	Rat	Millipore	CBL1337	1/50 IF
αSMA	Mouse	Sigma-Aldrich	A5228	1/100 IF
Slug	Rabbit	Cell Signalling	9585S	1/100 IF
Phosphorylated NFκB p65 (Ser563)	Rabbit	Cell Signalling	3033	1/1000 WB
SSB	Rabbit	Sigma-Aldrich	HPA012385	1/500 WB
GM130	Mouse	BD Bioscience	610823	1/200 IF

Table 2.3 List of primary antibodies used for immunofluorescence (IF) and/or western blotting (WB)

Antibody	Species	Manufacturer
HRP-conjugated anti Rabbit	Goat	DAKO
HRP-conjugated anti Mouse	Goat	DAKO
FITC-conjugated anti Rabbit	Goat	Vector Labs
FITC-conjugated anti Mouse	Horse	Vector Labs
Texas Red-conjugated anti Mouse	Horse	Vector Labs
Texas Red-Conjugated anti Rat	Goat	Vector Labs
Alexa Fluor 647-Conjugated anti Mouse	Goat	Invitrogen
Alexa Fluor 568-conjugated anti Rabbit	Donkey	Invitrogen

Table 2.4 List of secondary antibodies used for immunofluorescence and Western blotting.

2.13 Gelatin Zymography

Gelatin zymography is an electrophoretic technique enabling the semi-quantitative analysis of the amount and size of proteinases present in a sample based on their digestion of a protease substrate, such as gelatin, that is incorporated into an SDS-PAGE gel.

Supernatants were collected from stimulated cells and mixed with sample buffer (60 mM Tris-HCl pH 6.8, 2% SDS, 10% glycerol, 0.01% bromophenol blue). Samples were then loaded into a 10% SDS-PAGE gel containing 1% w/v porcine skin gelatin (Sigma-Aldrich). Proteins were then stacked at 50V for 20 minutes then resolved at 150V for a further hour. The gel was then placed into developing buffer (50 mM Tris-base pH 7.5, 200 mM NaCl, 5 µM ZnCl, 5 mM CaCl) containing 2.5% w/v Triton X-100 for 1 hour to remove SDS from the gel and renature proteinases present within the sample. Renatured gels were then placed developing solution and developed overnight at 37°C. Protein present in the gel was then visualised by incubating the gel with SimplyBlue™ SafeStain (Invitrogen) for 1 hour. An absence of blue protein stain in the gel was indicative of proteinase activity.

2.14 Statistical analysis

Data are represented as mean values ± standard error of the mean (SEM). Statistical analysis was performed using GraphPad Prism 6 software. Significant differences between experimental and control groups was determined by one-way ANOVA followed by Dunnet's *post hoc* test for experiments with three or more groups and Student's T-test for experiments with two groups.

Lung explant experiments where branching was measured over 24 and 48 hours was analysed for significance by two-way ANOVA with repeated measures followed by Dunnet's *post hoc* test where appropriate.

A statistically significant difference was accepted if $P<0.05$. Significance is indicated on graphical representations of the data by the marks: * $P<0.05$, ** $P<0.01$, *** $P<0.001$.

Chapter 3: Phosphoinositide 3-kinase in Lung Branching Morphogenesis

3.1 Background

An indication for the severity of a cancer is the ability for the cancerous epithelial cells to migrate away from the initial tumour, forming secondary tumours. Migration of epithelial cells is commonly found during development particularly in the formation of epithelial branches, where epithelial cells invade the surrounding mesenchymal tissue in a highly stereotyped fashion. It is therefore unsurprising that signalling events in epithelial cancers are also found in the development of the lung (De Leij et al., 1987). Similarities between the development of an organ and disease are not limited to cancer; a developmental link to fibrosis (Shi et al., 2009), COPD (Chen et al., 2005), and asthma (Warner et al., 1998) has also been established. Understanding how these signalling events influence the behaviour of the cells in their developmental setting may therefore lead to increased understanding of the disease state and novel therapeutic approaches.

A common pathway dysregulated during many pathologies is the PI3K signalling pathway (Engelman, 2009; Wojtalla et al., 2013). This pathway has also been found to be active during the branching program of the lung (Wang et al., 2005). However, the precise role for PI3K in this branching program of the lung has yet to be fully established with some work reporting a positive role for PI3K (Wang et al., 2005), and others a negative role (Xing et al., 2008). Moreover, much of the work on PI3K in epithelial branching to date has been conducted in other branching organs, namely the mammary and salivary glands (Larsen et al., 2003; Utermark et al., 2012). Comprehensive understanding of how PI3K functions in the branching program of the lung will consequently help influence therapeutics directed at PI3K in lung cancers and other developmentally relevant diseases such as fibrosis.

EMT is a process relevant to both cancer and fibrosis as it gives rise to motile epithelial cells that secrete extracellular matrix. PI3K has been reported to be active during hypoxia and TGFβ induced EMT in a number of epithelial cell lines. PI3K inhibition has been suggested to prevent the induction of EMT in epithelial cell lines although an isoform dependence in this process has yet to be elucidated (Bakin et al., 2000; Chen et al., 2012; Yan et al., 2009).

The aim of this current chapter was first to examine PI3K in the induction of EMT in lung epithelial cells using more selective inhibitors of PI3K and its separate isoforms. Secondly, we aimed to establish physiologically relevant models of embryonic lung branching, which could be manipulated either genetically or pharmacologically to assess the role of PI3K in the branching process.

3.2 PI3K contributes to TGFβ EMT in A549 alveolar epithelial cells

EMT can be easily induced in non-polarised epithelial cells through the application of TGFβ. This is characterised in A549 cells by the loss of the epithelial protein E-Cadherin at the cell surface and the subsequent gain of the mesenchymal protein fibronectin following exposure to TGFβ over 48 hours (Figure 3.1A,B). Moreover, once these cells had acquired a mesenchymal phenotype they begin to secrete MMP-9 (~92 kDa) and MMP-2 (~72 kDa) as identified by gelatin zymography (Figure 3.1C). The application of the pan class I PI3K inhibitor ZSTK474 prior to the addition of TGFβ appeared to slightly reduce the impact of TGFβ induced E-Cadherin loss at the cell surface (Figure 3.1A). However, western blot analysis revealed that E-Cadherin protein levels were comparable between TGFβ alone and TGFβ plus ZSTK474 (Figure 3.1B). This would suggest that PI3K inhibition did not prevent the loss of E-Cadherin protein but instead reduced the re-localisation of the protein from the cell surface. Cells cultured with both TGFβ and ZSTK474 also continued to express fibronectin. Interestingly, MMP-2 and MMP-9 production was markedly reduced with pre-treatment of ZSTK474 (Figure 3.1C).

To identify the isoform of PI3K involved in EMT we applied the PI3Kα selective inhibitor PIK-75 and the PI3Kβ selective inhibitor TGX-221 to A549 cells prior to the addition of TGFβ. As with ZSTK474, PIK-75 and TGX-221 both appeared to reduce TGFβ induced E-cadherin loss from the cell surface, although western blot analysis suggested comparable protein levels (Figure 3.2A,B). Moreover PIK-75, but not TGX-221, was able to reduce the production of MMP-2 and MMP-9 (Figure 3.2C). These data would therefore suggest an involvement of PI3Kα in the process of EMT.

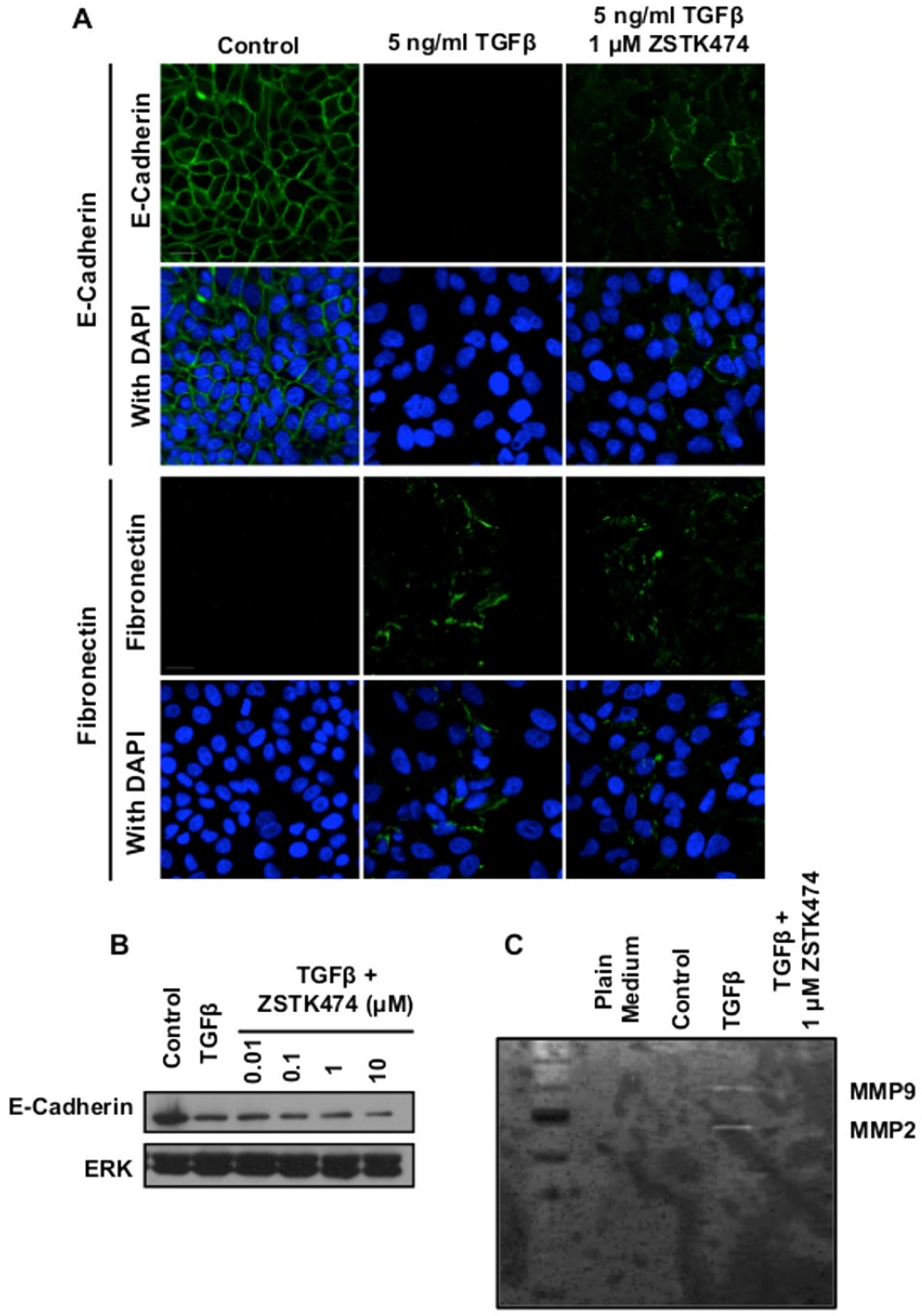

Figure 3.1 Inhibition of PI3K with ZSTK474 prevents complete induction of EMT in A549 cells. A. Confocal images of E-Cadherin (Top panels) and fibronectin (bottom panels) expression in A549 cells cultured for 48 hours with either 0.1% DMSO (Control), 5 ng/ml TGFβ or 5 ng/ml TGFβ with 1 μM ZSTK474. Scale bar = 20 μm. Images are representative of three independent experiments. **B.** Western blot analysis of E-Cadherin and ERK expression in A549 cells cultured for 48 hours with 5 ng/ml TGFβ alone or with either 0.01, 0.1, 1 or 10 μM ZSTK474. **C.** Gelatin zymography of cell supernatants collected from A549 cells after 48 hours of culture with 5 ng/ml TGFβ alone or with 1 μM ZSTK474. Protein and zymography bands are representative of three separate experiments.

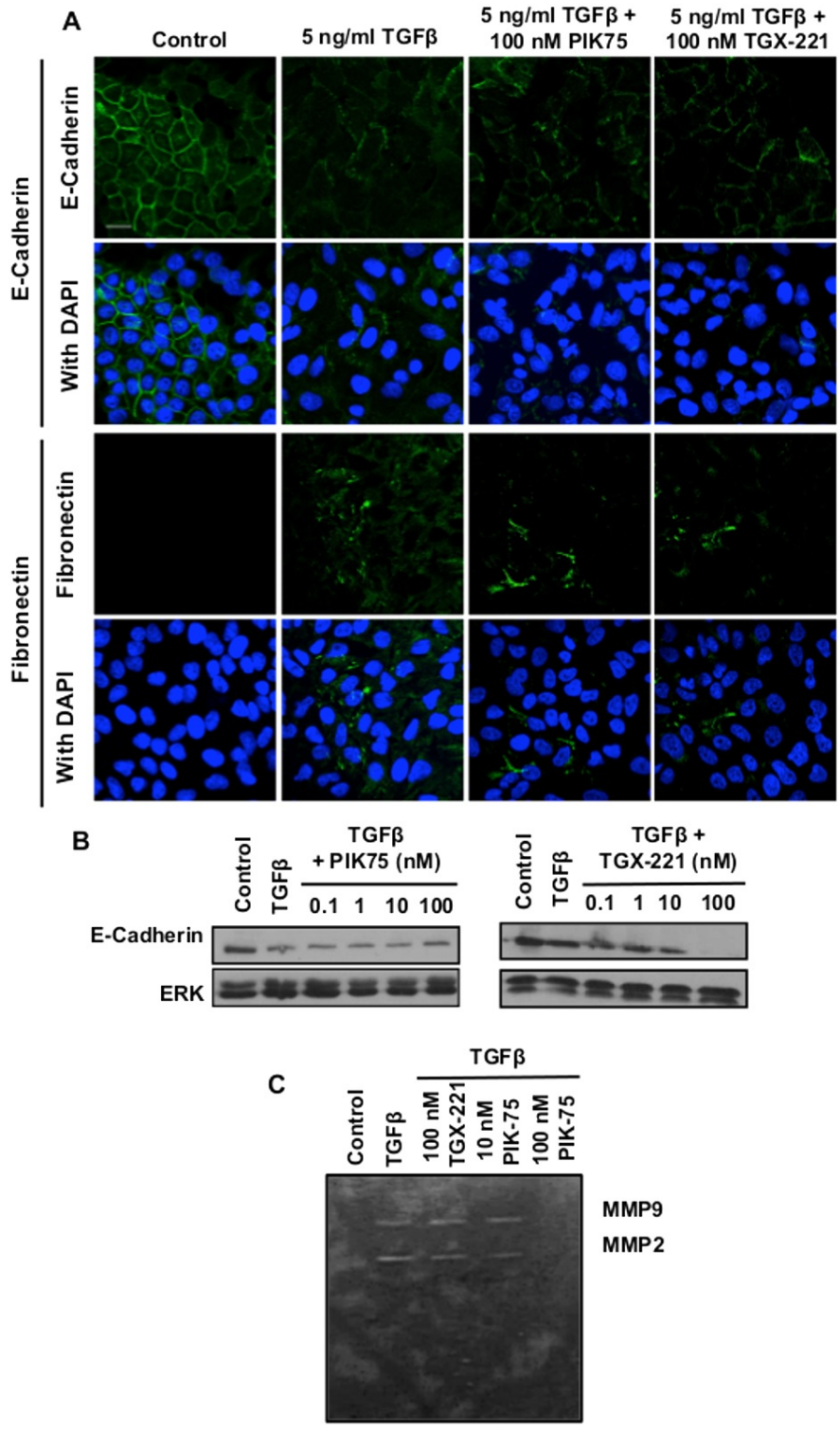

Figure 3.1 Inhibition of PI3Kα, but not PI3Kβ, prevents complete induction of EMT in A549 cells. A. Confocal images of E-Cadherin (Top panels) and fibronectin (bottom panels) expression in A549 cells cultured for 48 hours with either 0.1% DMSO (Control), 5 ng/ml TGFβ or 5 ng/ml TGFβ with either 100 nM PIK-75 or 100 nM TGX-221. Scale bar = 20 μm. Images are representative of two independent experiments. **B.** Western blot analysis of E-Cadherin and ERK expression in A549 cells cultured for 48 hours with 5 ng/ml TGFβ alone or with 0.1, 1, 10 or 100 nM of either PIK-75 or TGX-221. **C.** Gelatin zymography of cell supernatants collected from A549 cells after 48 hours of culture with 5 ng/ml TGFβ alone or with 100 nM of either PIK-75 or TGX-221. Protein and zymography bands are representative of two separate experiments.

3.3 Cultures of murine embryonic lungs recapitulate the branching process

Lung branching morphogenesis is a complex process requiring a number of signalling factors and the co-operative growth of a number of cell types. To effectively model this process in order to assess the role of PI3K we established a model of branching using embryonic lungs to best recapitulate the branching process. Lungs were isolated from embryos taken during the early days of the pseudoglandular stage of lung development (E12.5) and placed into culture at the air-liquid interface as this method has been reported to adequately recapitulate the branching process in a manner that can be easily manipulated (Del Moral and Warburton, 2010) (Figure 3.3A). Over 48 hours the epithelial branches enlarged and became more numerous as evidenced by an increase in the number of terminal branches (Video 3.1; Figure 3.3B,C). Further, these explant cultures exhibited periodic waves of contraction along the proximal branches (Video 3.2), consistent with reported observations (Schittny et al., 2000). Confocal analysis of the lung explants after 48 hours of culture revealed that these cultures contained numerous cell types and a morphology consistent with the embryonic lung during the pseudoglandular stage of development. Primitive epithelial tubules are found throughout the explants that are positive for the adherens junction E-Cadherin (Figure 3.3D,F). The expression of the tight junction marker occludin was also observed at the centre of epithelial branches implying the presence of a luminal surface (Figure 3.3E). This expression pattern for tight junctions has also been reported in the developing salivary glands (Hieda et al., 1996). Further, the distal ends of the epithelial tubes express the transcription factor SOX9 (Figure 3.3D), a known marker of distal lung epithelium (Rockich et al., 2013; Turcatel et al., 2013). These epithelial tubes develop within mesenchymal tissue observed by the expression of the mesenchymal marker Slug (Figure 3.3E). Moreover, the epithelial branches are surrounded by vasculature indicated by the tissue staining for the endothelial cell surface marker CD31 (Figure 3.3F). Again, the mutual development of the vasculature with the branching epithelium is consistent with the reported interactions between these two cell types (Lazarus et al., 2011).

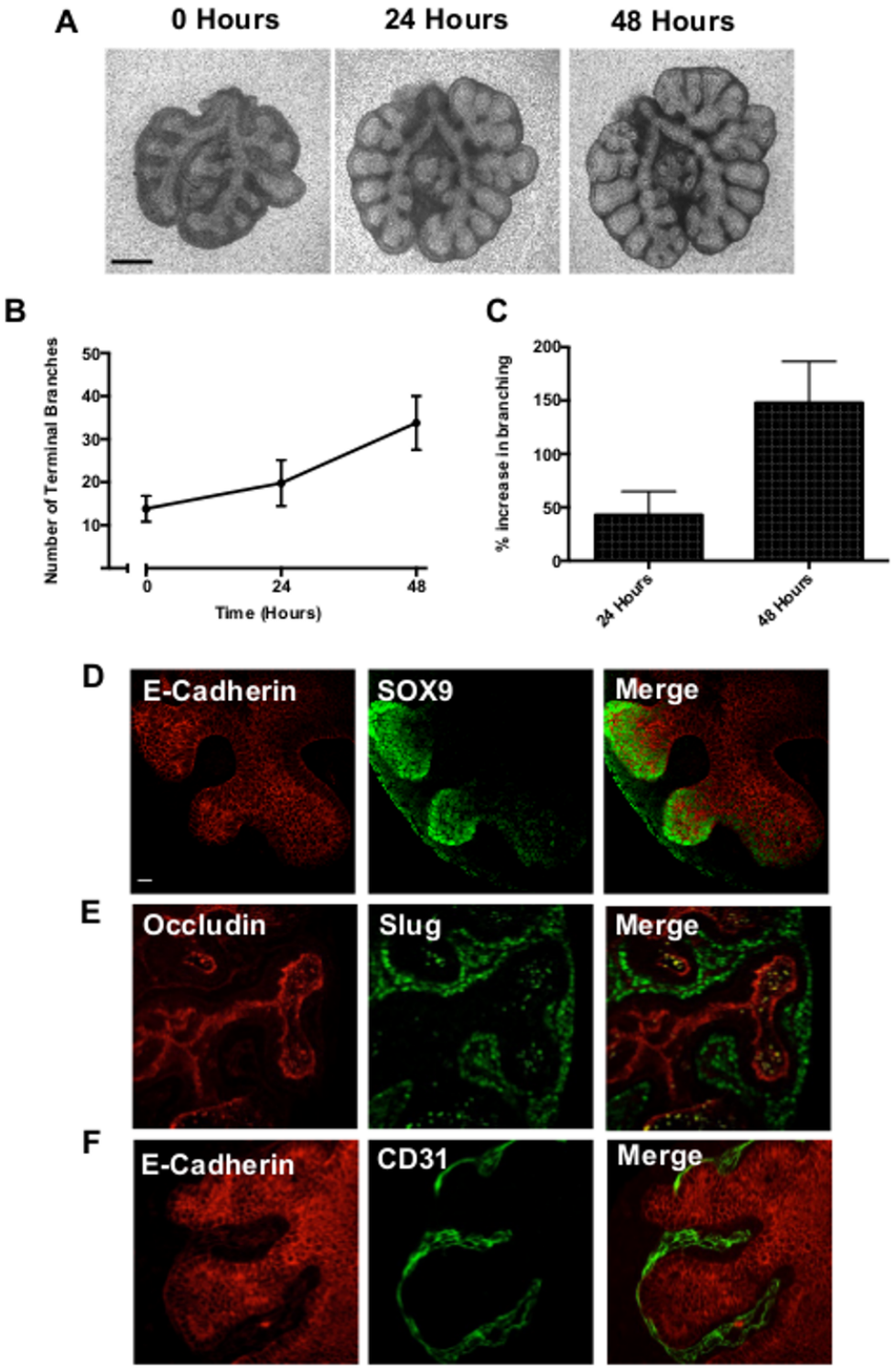

Figure 3.3. Culture of whole embryonic murine lungs recapitulates the developmental state. A. Light microscope images of E12.5 murine lung explants cultured over 48 hours at the air liquid interface. Images presented are representative of at least twelve explants. Scale bar = 0.5 mm. **B** Quantification of the number of terminal branches over 48 hours. Bars show mean ± s.e.m from n=12. **C.** Percentage increase in the number of terminal branches at 24 and 48 hours relative to the number of branches present at isolation. Bars show mean ± s.e.m from n=12. **D-F**. Confocal images of E-Cadherin (**D, F**, left panels), SOX9 (**D**, middle panel), occludin (**E**, left panel), Slug (**E**, middle panel) and CD31 (**F**, middle panel) expression in lung explants following 48 hours of culture. Images are representative of three explants. Scale bar = 20 μm.

3.4 Inhibition of class I PI3K signalling potentiates lung branching

To examine the role of the PI3K pathway in branching morphogenesis we used a range of pharmacological agents targeting various elements of this pathway with high selectivity to limit the influence off target effects. We initially applied inhibitors targeting the entire class I family of PI3K to cultures of whole lung explants. Over 48 hours the pan class I inhibitor of PI3K ZSTK474 (Kong and Yamori, 2007) significantly increased branching in a concentration dependent manner compared to DMSO controls (Figure 3.4A,B). This enhancement of branching correlated with a concentration-dependent decrease in levels of phosphorylated Akt (Figure 3.4C), an indirect measure of PI3K activity (Franke et al., 1995). Immunofluorescence staining of the epithelial marker E-Cadherin also revealed that PI3K inhibition by ZSTK474 induced the formation of significantly more, albeit smaller, branches than controls (Figure 3.4D).

As well as the ZSTK474 compound we also applied the less specific pan inhibitor of class I PI3K LY294002 (Vlahos et al., 1994) to cultures of whole lungs as this compound has been used previously to examine PI3K in the branching process of the lungs (Wang et al., 2005), urogenital sinus tissue (Ghosh et al., 2011), and salivary glands (Larsen et al., 2003). At 10 μM LY294002 induced a similar enhancement of branching as seen with the ZSTK474 compound (Figure 3.5). However, at higher concentrations of LY294002 (≥20 μM) we saw a reduction in branching, consistent with the reported effects of this compound on branching.

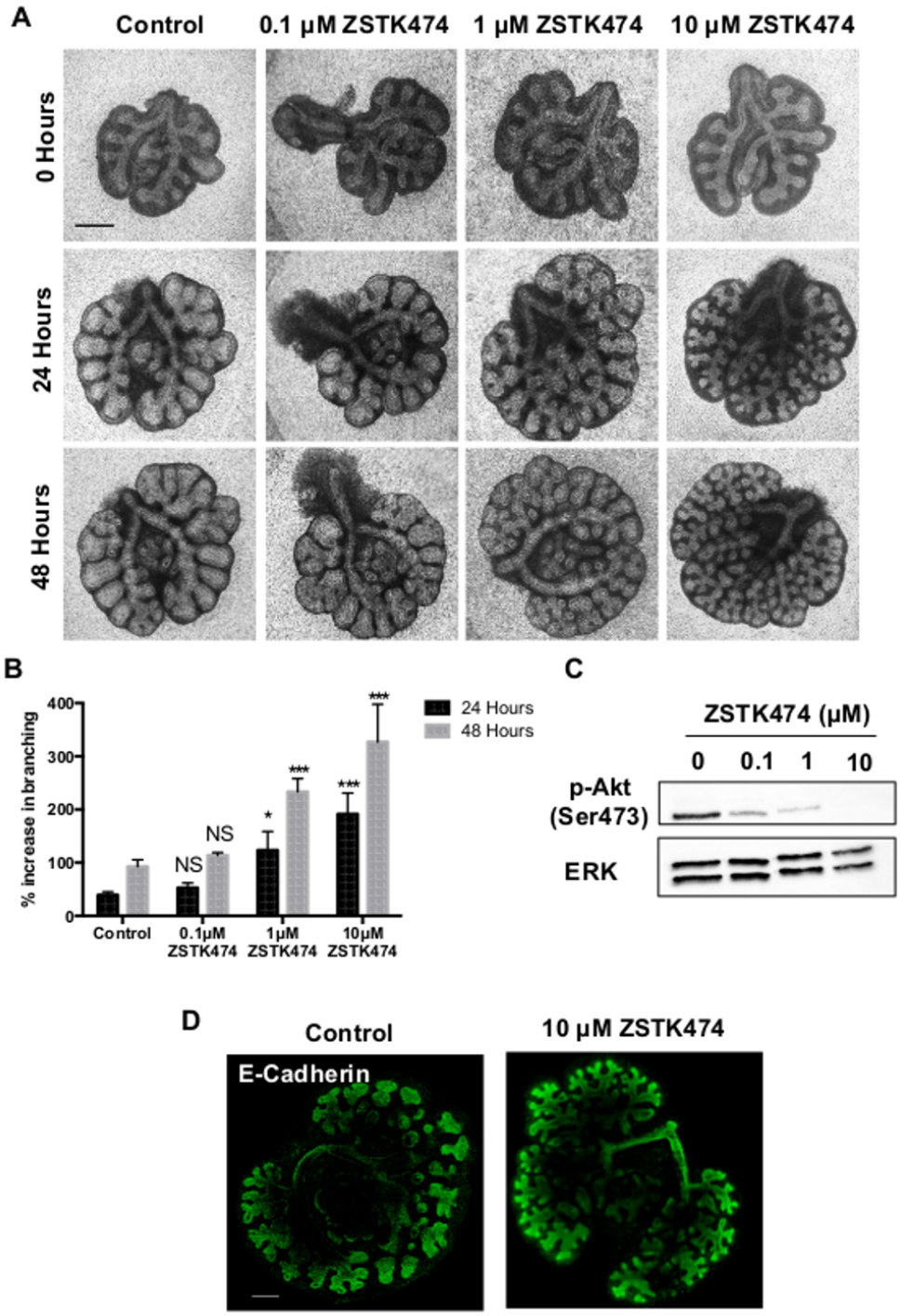

Figure 3.4. Inhibition of PI3K with ZSTK474 promotes epithelial branching in murine lung explants. Light microscope images of E12.5 murine lung explants cultured with either 0.1% DMSO (Control) or 0.1, 1 or 10 μM ZSTK474 over 48 hours. Images representative of at least twelve explants per condition are shown. Scale bar = 0.5 mm **B**. Percentage increase in epithelial branching over 24 and 48 hours relative to the number of branches at initial isolation. Bars show mean ± s.e.m from n=20 **C.** Western blot analysis for levels of phosphorylated Akt (p-Akt) and ERK in explants following 48 hours of culture. Protein bands representative of three separate experiments. **D**. Confocal image of E-Cadherin expression in lung explants cultured with or without 10 μM ZSTK474 for 48 hours. Scale bar = 200 μm. *** P<0.001, * P<0.05, * NS = Not Significant, compared with control.

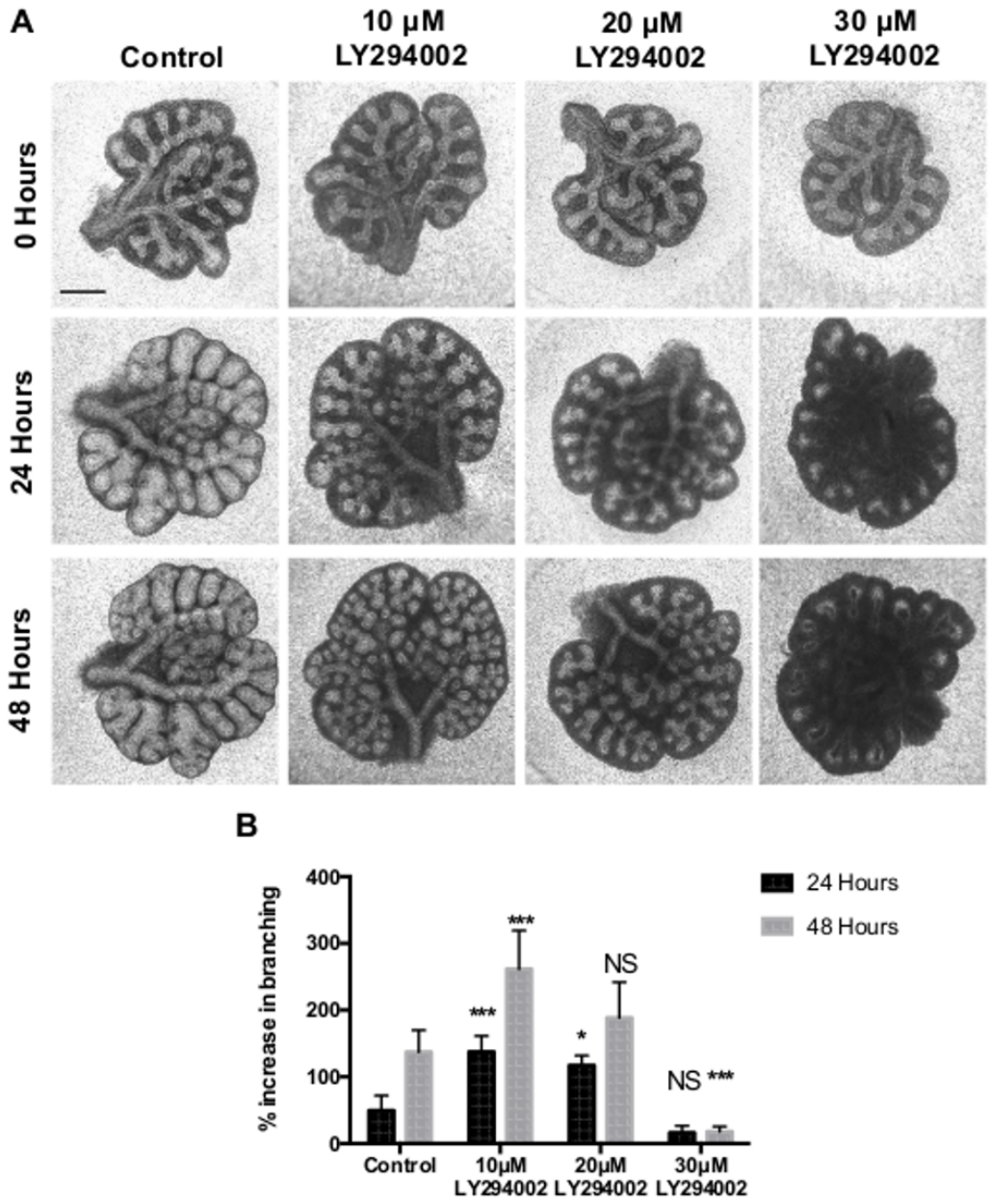

Figure 3.5 LY294002 induces contrasting effects on lung branching. A. Light microscope images of E12.5 murine lung explants cultured with 0.1% DMSO (Control) or 10, 20 or 30 µM LY294002 over 24 and 48 hours. Images are representative of at least nine explants per condition. Scale bar = 0.5 mm **B**. Percentage increase in epithelial branching over 24 and 48 hours relative to the number of branches at initial isolation. Bars show mean ± s.e.m from n=9 *** P<0.001, * P<0.05, NS = Not Significant, compared with control.

Inhibition of downstream signalling components of PI3K potentiates lung branching

To further confirm the involvement of PI3K in the branching process we examined the effect of inhibiting downstream signalling components of PI3K, namely Akt and mTOR. As with ZSTK474, Akt inhibitor VIII (Lindsley et al., 2005) produced a concentration dependent increase in branching (Figure 3.6A,B). This increase in branching was accompanied by a reduction in phosphorylated Akt at the Ser473 position (Figure 3.6C). Phosphorylated Akt at Ser473 can be used as an indirect method of detecting Akt activation due to this residue being phosphorylated by mTORC2 following activation by Akt (Facchinetti et al., 2008).

Increased branching was also seen with the mTORC1/2 inhibitor AZD8055 (Chresta et al., 2010), but not with the mTORC1 inhibitor rapamycin (Guba et al., 2002) (Figure 3.7A,B). Enhanced branching with 0.1 μM AZD8055 compared to controls was also apparent with time-lapse microscopy (Videos 3.1 and 3.3). Following activation of mTORC1 by Akt, mTORC1 phosphorylates S6 ribosomal protein (Julien et al., 2010). S6 ribosomal protein can therefore be used as an indicator of mTORC1 activity. Western blot analysis revealed a reduction in phosphorylated levels of S6 ribosomal protein following culture with either AZD8055 or rapamycin. However, only AZD8055 induced a loss in levels of phosphorylated Akt (Figure 3.7C).

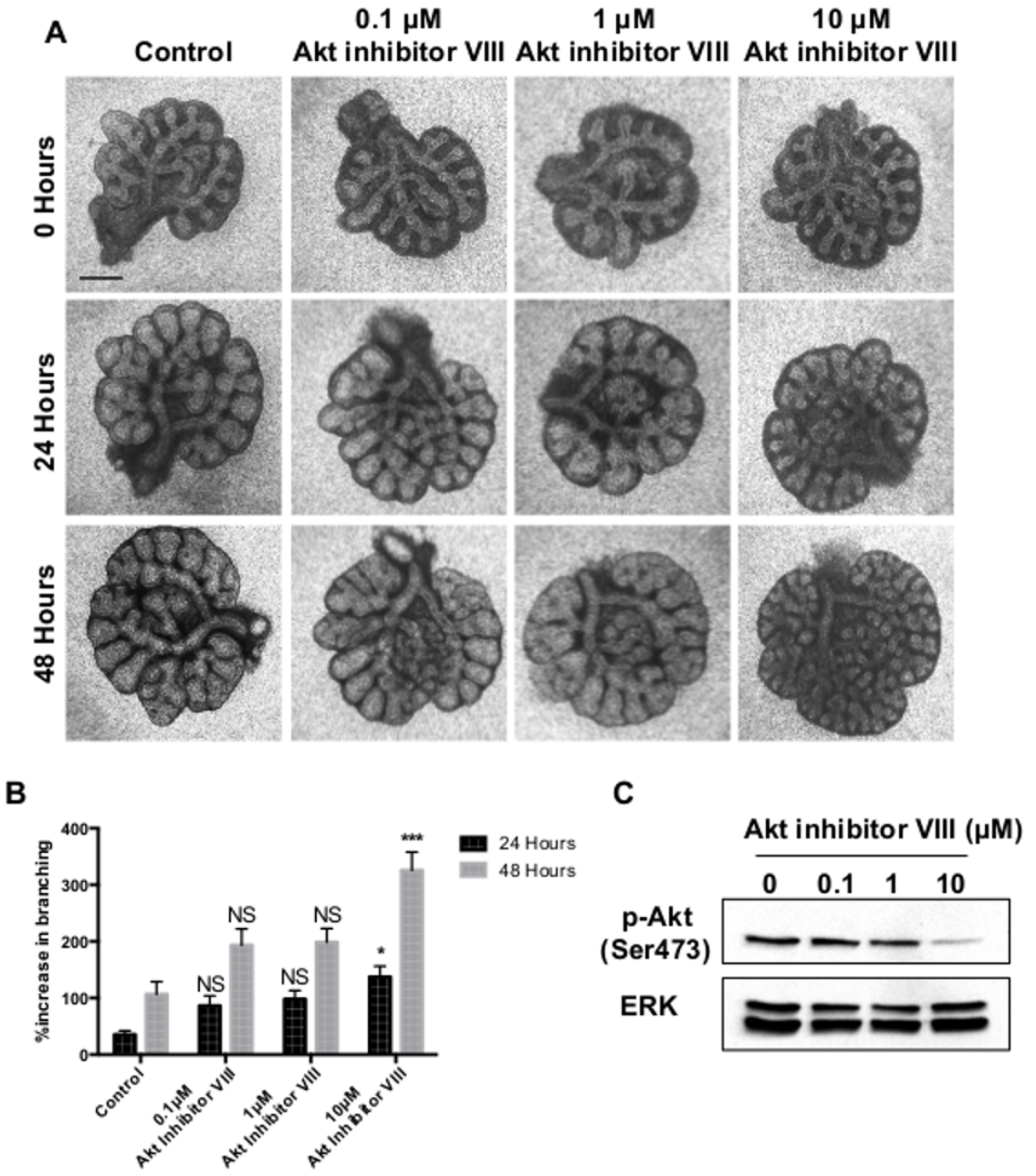

Figure 3.6. Inhibition of Akt promotes epithelial branching. A. Light microscope images of E12.5 murine lung explants cultured with 0.1% DMSO (Control) or 0.1, 1 or 10 μM Akt inhibitor VIII over 48 hours. Images are representative of at least twelve explants per condition. **B.** Percentage increase in epithelial branching over 24 and 48 hours relative to the number of branches at initial isolation. Bars show mean ± s.e.m from n=12 **C**. Western blot analysis for levels of phosphorylated Akt (p-Akt) and ERK in explants following 48 hours of culture. Protein bands representative of three separate experiments. Scale bar = 0.5 mm. * P<0.05, *** P<0.001, compared with control.

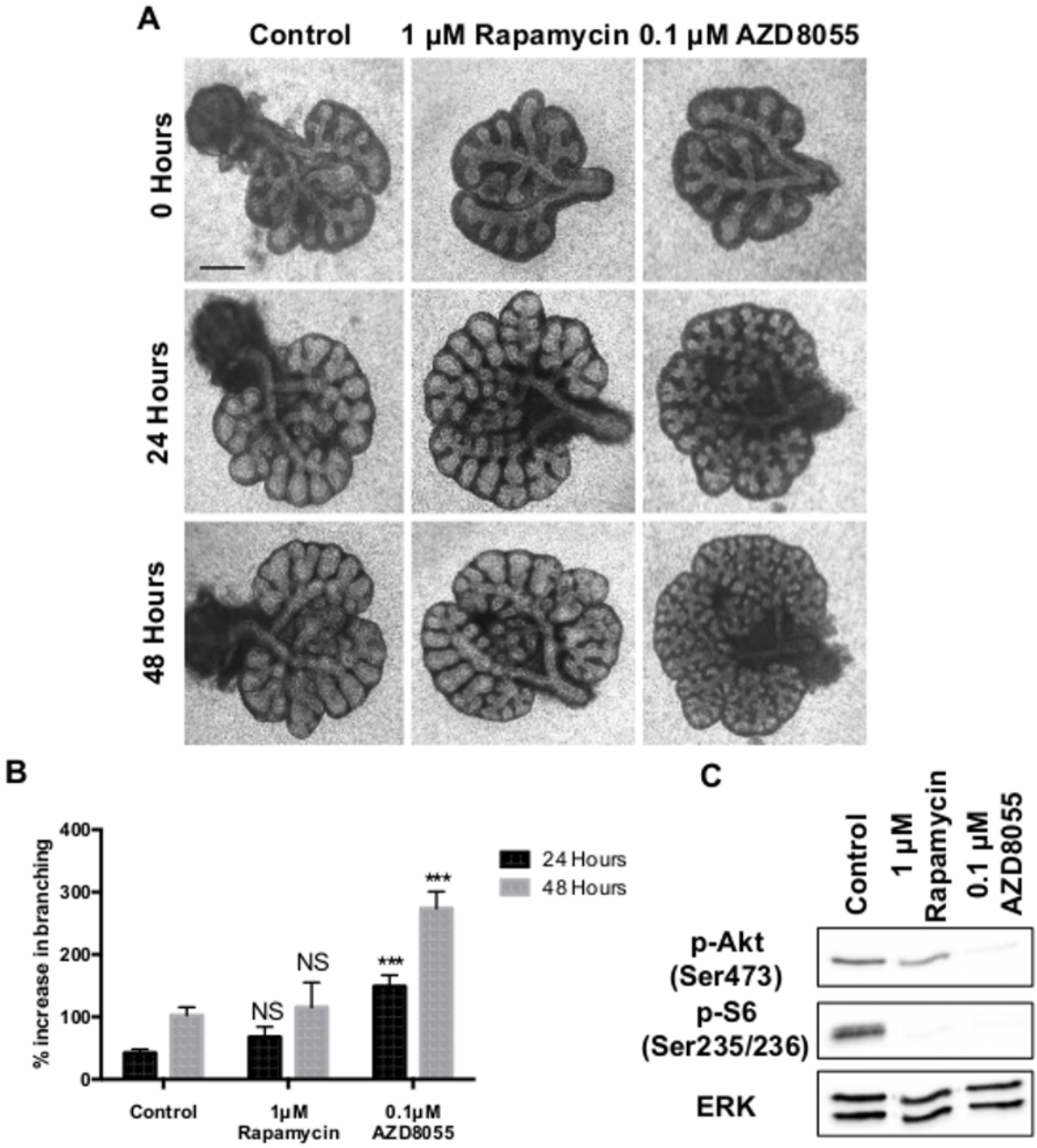

Figure 3.7. Inhibition of mTORC2 but not mTORC1 promotes epithelial branching. A. Light microscope images of E12.5 murine lung explants cultured in either 0.1% DMSO (Control), 1 μM rapamycin or 0.1 μM AZD8055. Images representative of at least twelve explants per condition are shown. **B**. Percentage increase in epithelial branching over 24 and 48 hours relative to the number of branches at initial isolation. Bars show mean ± s.e.m from n=12 C**.** Western blot analysis for levels of phosphorylated S6 ribosomal protein (p-S6), phosphorylated Akt (p-Akt) and ERK in explants cultured for 48 hours. Protein bands representative of three separate experiments Scale bar = 0.5 mm. *** P<0.001, NS = Not Significant, compared with control.

The alpha isoform of PI3K regulates branching morphogenesis in the lung

Given that PI3Kα and PI3Kβ have a divergent role in the branching program of the mammary gland (Utermark et al., 2012), we sought to establish the roles of individual PI3K isoforms in the branching program of the lung. Whole lung explants cultured with a selective inhibitor of PI3Kα, BYL719 (Furet et al., 2013), produced a large enhancement of branching compared with DMSO controls (Figure 3.8A). Consistent with this, BYL719 induced a reduction in levels of phosphorylated Akt (Figure 3.8C). No alteration in branching was seen when whole explants were cultured with a selective inhibitor of PI3Kβ, GSK2636771 (Sanchez et al., 2012), over 48 hours (Figure 3.8). Further, no reduction in phosphorylated Akt was detected from explants cultured with GSK2636771, suggesting a lack of involvement for PI3Kβ in this system.

To confirm these findings we first examined the BYL719 and GSK2636771 compounds over their effective concentration range to determine if the inhibitors were exhibiting off target effects. The BYL719 compound produced a concentration dependent increase in branching (Figure 3.9A), wheras GSK2636771 had no observable effects on branching morphogenesis at concentrations up to 10 μM (Figure 3.9C). To further exclude the possibility of an off target affect and confirm the involvement of PI3Kα we used a second set of PI3Kα and PI3Kβ selective inhibitors. As with BYL719, a concentration dependent enhancement of branching was observed with the PI3Kα inhibitor A66 (Jamieson et al., 2011) (Figure 3.9B). Similarly, no change in branching was seen at concentrations less than 10 μM with the PI3Kβ inhibitor TGX-221 (Figure 3.9D). A small enhancement of branching was seen with TGX-221 at 10 μM. However, this occurred at concentrations where other isoforms of PI3K would be inhibited (Jackson et al., 2005).

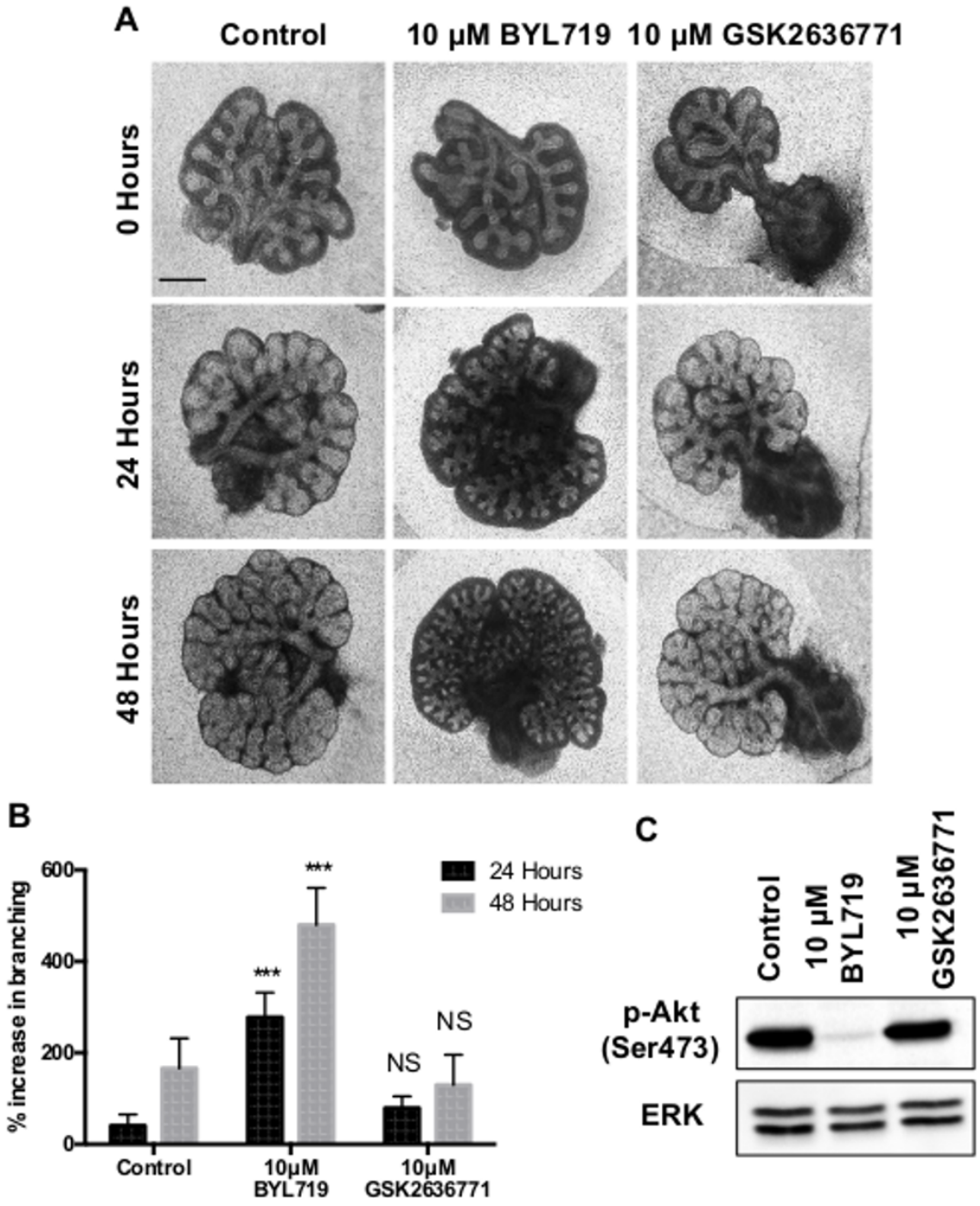

Figure 3.8. PI3Kα, but not PI3Kβ, regulates lung branching morphogenesis. A. Light microscope images of E12.5 murine lung explants cultured with 0.1% DMSO (Control), 10 μM BYL719 or 10 μM GSK2636771. Images representative of at least twelve explants per condition are shown. **B**. Percentage increase in epithelial branching over 24 and 48 hours relative to the number of branches at initial isolation. Bars show mean ± s.e.m from n=12 **C.** Western blot analysis for levels of phosphorylated Akt (p-Akt) and ERK in explants following 48 hours of culture. Protein bands representative of three separate experiments. Scale bar = 0.5 mm. *** P<0.001, NS = Not Significant, compared with control.

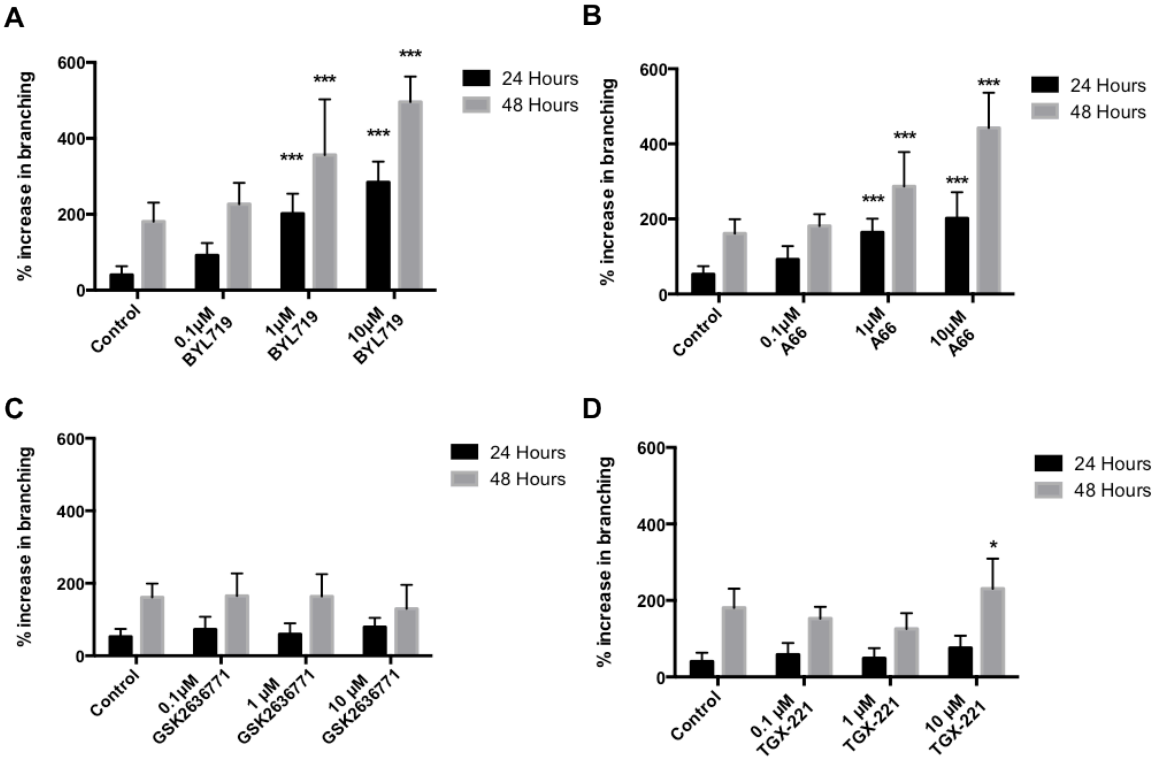

Figure 3.9. Concentration dependent effects of PI3Kα and PI3Kβ selective inhibitors on branching morphogenesis. Percentage increase in branching of E12.5 murine lung explants cultured with 0.1% DMSO (Control) or 0.1, 1 or 10 μM of either the PI3Kα inhibitors BYL719 (**A**) and A66 (**B**) or the PI3Kβ inhibitors GSK2636771 (**C**) and TGX-221 (**D**) over 24 and 48 hours. Bars show mean ± s.e.m from n=12. ***P<0.001 *P<0.05, compared with control.

3.5 Isolated lung epithelium: a model to directly examine the branching epithelium

The whole lung explant model can be cultured with minimal supplementation to the cell culture medium (0.5% FBS in DMEM: F12 medium), easily manipulated pharmacologically, and provides a quantifiable output related to epithelial branching. Despite these advantages the whole explant model suffers from several caveats. Of particular note is that it is difficult to determine if an affect on branching is specific to the lung epithelium or secondary to an effect on the mesenchyme. This caveat is highlighted by work examining the interplay between the branching epithelium and the vasculature of the lung (Lazarus et al., 2011). In this study the lungs of mice expressing a soluble VEGFR under the control of the SPC promoter exhibited reduced vascularisation, and as a consequence reduced

branching, compared to their wild type counterparts. This would imply that inhibiting the growth of the vasculature would have a knock on effect of reducing epithelial branching.

To overcome this caveat we utilised a method to isolate and culture mesenchyme-free embryonic lung epithelium (Del Moral and Warburton, 2010). Terminal branches were removed from isolated E12.5 lung explants and the mesenchyme stripped using fine needles (Figure 3.10A). To confirm that mesenchyme stripping was efficient we examined isolated branch tips stripped of mesenchyme for the presence of mesenchymal cells. Isolated epithelium contained non-epithelial cells as evidenced by the presence of DAPI positive cells that did not express the epithelial marker E-Cadherin (Figure 3.10B, bottom panels). Further, some cells expressed the mesenchymal marker desmin (Figure 3.10B, top panels). This would imply that the stripping process is not entirely efficient and some mesenchymal cells do remain. Nevertheless isolated epithelium failed to grow when placed in culture in non-supplemented cell culture medium suggesting that the remaining mesenchyme is insufficient to maintain the viability of the epithelium (Figure 3.10C).

Isolated lung epithelium requires the addition of growth factors in order to maintain the growth of the isolate. Different growth factors produce different morphological effects on the tissue. FGF7 treatment induces the formation of large cystic structures after 96 hours of culture whereas FGF10 induces the formation of epithelial branches (Bellusci et al., 1997; Cardoso et al., 1997). FGF1 also produces a branched response, but to a lesser extent than FGF10 (Figure 3.10C). The effects of pharmacological agents directly on the lung epithelium can therefore be assessed with respect to the growth factor used in the culture system.

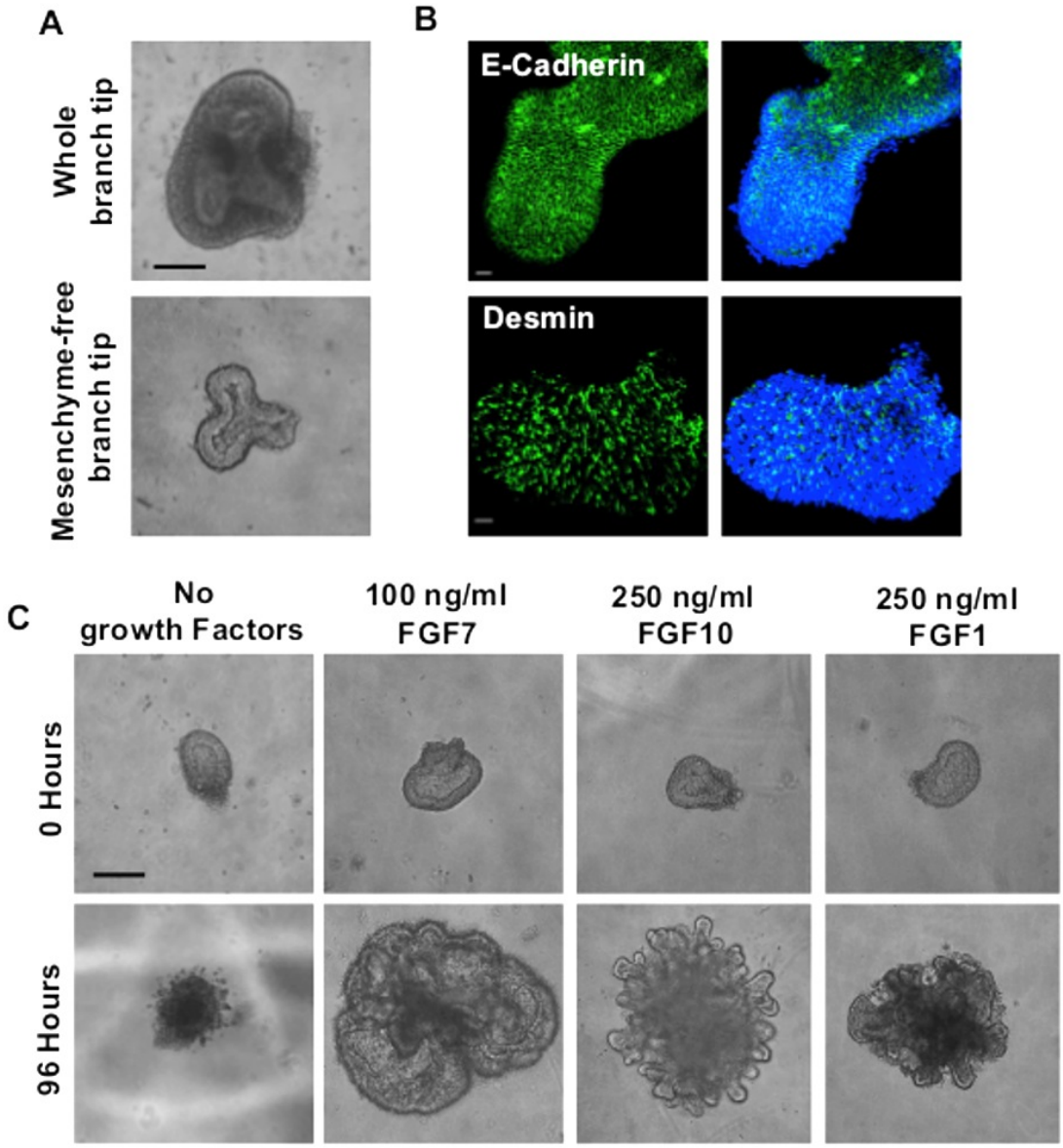

Figure 3.10. Mesenchyme-stripped branch epithelium still shows evidence of intact mesenchymal cells yet requires additional growth factors for development. A. Light microscope images of an isolated E12.5 murine lung branch before (top panel) and after (bottom panel) mesenchyme removal. Scale bar = 200 μm. **B.** Expression of E-Cadherin (top panels) and desmin (bottom panels) in isolated murine lung branches following removal of mesenchyme. Scale bar = 20 μm. **C.** Light microscope images of isolated lung epithelium cultured over 96 hours without additional growth factors or with 100 ng/ml FGF7, 250 ng/ml FGF10 or 100 ng/ml FGF1. Images are representative of at least six isolates. Scale bar = 200 μm.

FGF10 and FGF1 induce inconsistent effects on isolated lung epithelium

Despite initial success with the FGF10 and FGF1 models, FGF10 and FGF1 produced inconsistent responses from isolated epithelium. In the majority of attempts, epithelial isolates cultured with FGF10 or FGF1 would only form into a single tubular structure after 96 hours of culture (Figure 3.11A). Remarkably, this tubular structure underwent periodic waves of contraction (Video 3.4; Figure 3.11B). This is in contrast to the reported branching effects of these growth factors (Bellusci et al., 1997; Cardoso et al., 1997). Due to the inconsistent nature of this culture system, and the strikingly different morphogenic responses compared to those reported in the literature, we were unable to examine the affects of PI3K inhibition on isolates cultured with either FGF10 or FGF1.

As lung bud isolates cultured with either FGF1 or FGF10 underwent periodic waves of contraction we examined the isolates for the presence of smooth muscle. After 96 hours isolates cultured with FGF10 demonstrated an enhanced expression of αSMA, suggesting the presence smooth muscle cells (Figure 3.11C). These αSMA positive cells surrounded the epithelial isolate and are therefore the likely cause of the contractile responses observed. Furthermore, we observed enhanced expression of the mesenchymal marker desmin compared to that present at initial isolation. Together, these observations would suggest that FGF10 at least, induced the proliferation of the remaining mesenchymal cells (Figure 3.11C).

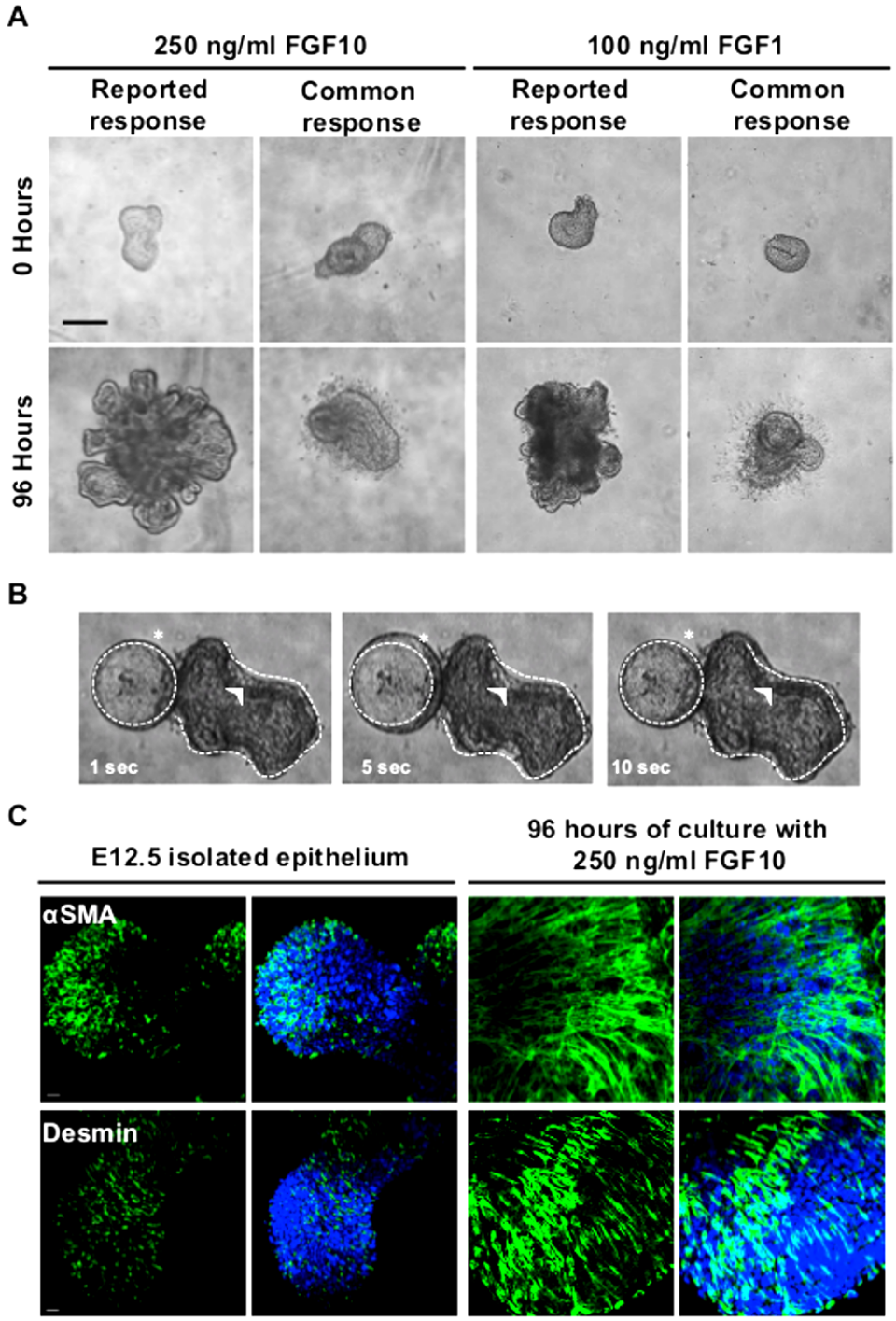

Figure 3.11. FGF10 and FGF1 produce inconsistent responses from isolated lung epithelium. A. Light microscope images of isolated E12.5 murine lung epithelium in culture for 96 hours with 250 ng/ml FGF10 (left panels) or 100 ng/ml FGF1 (right panels). Images demonstrating outcomes consistent with reported responses from FGF10 and FGF1 are shown as well as images demonstrating outcomes that were inconsistent with reported responses. Images are examples from sixty separate isolates. Scale bar = 200 μm. **B**. Still images from a movie depicting the contractile waves exhibited by an isolate cultured with 250 ng/ml FGF10 for 96 hours. Note the reduction in lumen size between 1 and 5 seconds (arrow head, dotted line) and an enlargement of one end of the isolate (asterisk, dotted line) **C.** Fluorescent images of the mesenchymal markers αSMA and desmin acquired at 40x magnification from either freshly mesenchyme-stripped E12.5 lung epithelium or isolates cultured for 96 hours in the presence of 250 ng/ml FGF10. Images are representative of three experiments. Scale bar = 20 μm.

3.6 FGF7-treated lung epithelium develop branches with a defined lumen and organised epithelium following inhibition PI3K signalling

To examine the effects of PI3K directly on the lung epithelium we applied inhibitors of PI3K to isolated lung epithelium cultured in the presence of FGF7. Epithelial isolates cultured with ZSTK474 alone failed to develop (Figure 3.12A), similar to isolates cultured with no supplements. Remarkably, culture of epithelial isolates with FGF7 and ZSTK474 induced the formation of branch-like structures, which were particularly evident at 10 μM (Figure 3.12A). This was strikingly different from the large cystic morphology induced by culture with FGF7 alone (Figure 3.12A). To understand if these branched structures were fully formed branches or a simple scattering of cells we examined the morphology of the isolates by confocal microscopy. Z-stack analysis revealed that these structures contained an intact lumen, as evidenced by the lack of nuclei in the centre of the branch, surrounded by cuboidal epithelial cells. A patchwork of actin was also noted at what appears to be a luminal surface (Figure 3.12B).

Next, we examined if the differentiation of the lung epithelium was affected by inhibition of PI3K. Following culture with FGF7, the isolated lung epithelium ubiquitously expressed SOX9, a marker of distal lung epithelium (Turcatel et al., 2013); Nkx2.1, a transcription factor required for distal lung morphogenesis (Yuan et al., 2000); and pro-SPC, a marker of differentiated lung epithelium (Cardoso et al., 1997). Expression of these markers was not appreciably changed in lung epithelium cultured with FGF7 and ZSTK474 (Figure 3.13).

Similar to the effects observed with isolated lung epithelium co-cultured with FGF7 and ZSTK474, co-culture with FGF7 and the mTORC1/2 inhibito3r AZD8055 elicited the appearance of branch-like structures from the initial isolate. Co-culture of FGF7 with the mTORC1 inhibitor rapamycin produced large cystic structures similar to culture with FGF7 alone (Figure 3.14). This re-enforces the notion that mTORC1 alone is insufficient to promote branching in either the whole explant culture or in isolated lung epithelium. Co-culture of FGF7 and Akt inhibitor VIII induced death of the isolate at concentrations >10 nM (Data not shown).

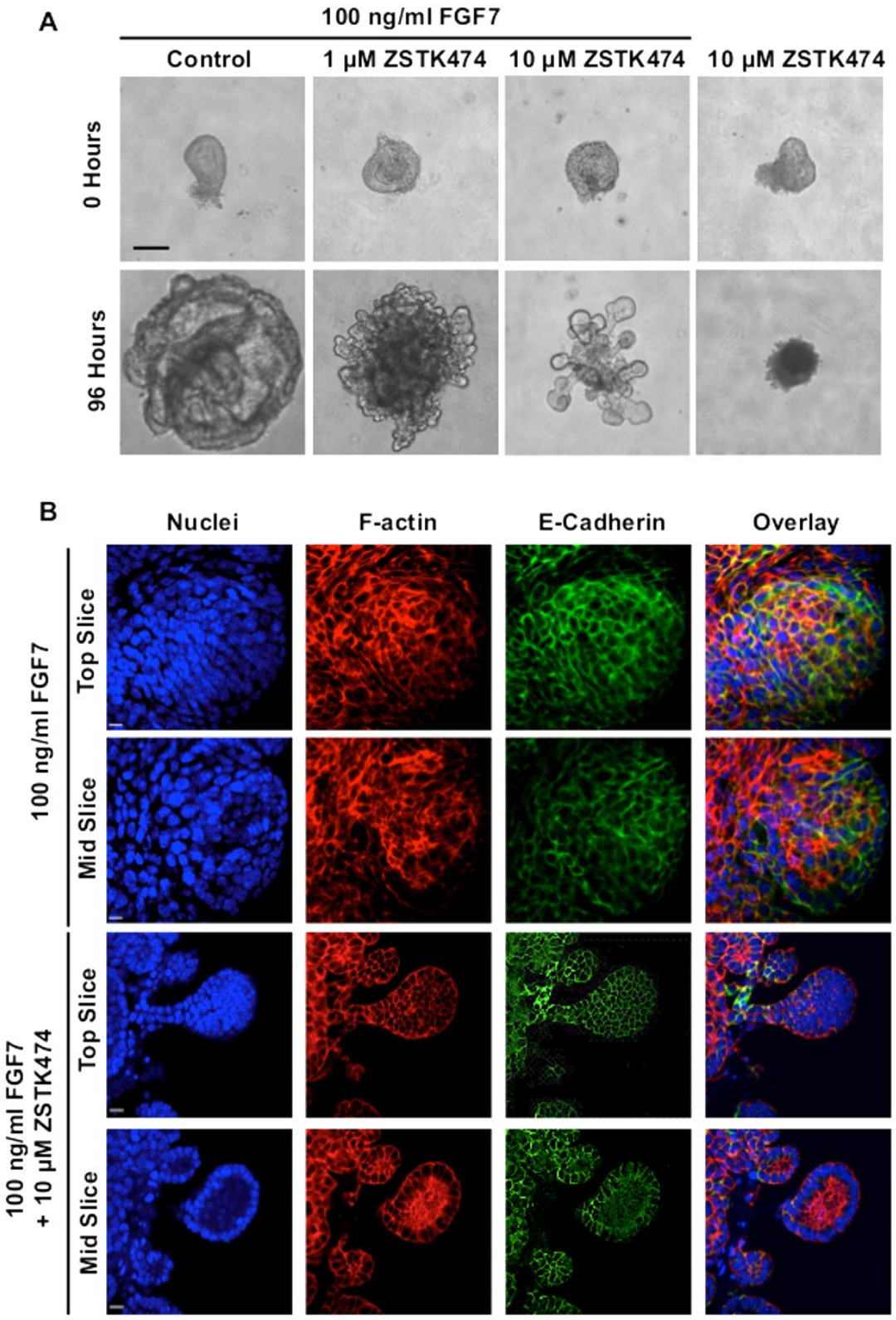

Figure 3.12. FGF7-treated lung epithelium develop branches with defined lumen and organised epithelium following PI3K inhibition. A. Light microscope images of isolated E12.5 murine lung epithelium cultured with either 100 ng/ml FGF7 alone (left panels), 10 μM ZSTK474 alone (right panels) or either 1 or 10 μM ZSTK474 in combination with FGF7 (middle panels) over 96 hours. Images representative of at least twenty isolates are shown. Scale bar = 200 μm. **B**. Z-stack confocal images of top and mid sections from isolated lung epithelium cultured with 100 ng/ml FGF7 alone or in combination with 10 μM ZSTK474 showing expression of the epithelial marker E-Cadherin and actin cytoskeleton.

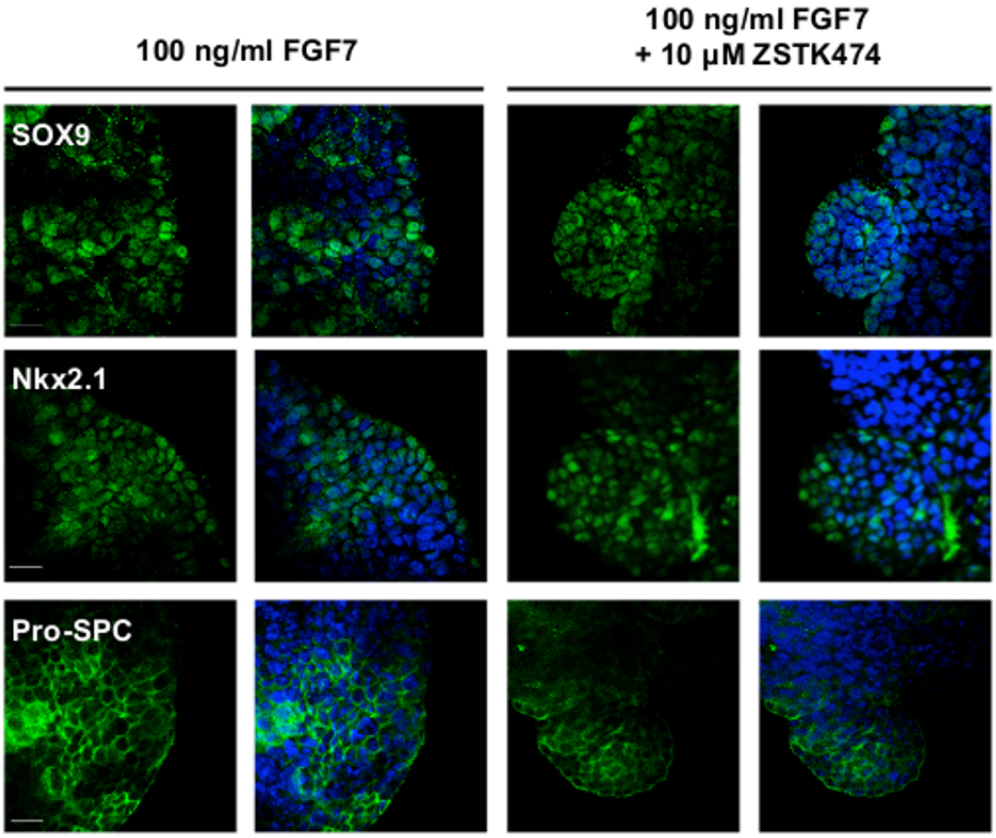

Figure 3.13. PI3K inhibition does not affect the differentiation of lung epithelium in response to FGF7. Immunofluorescence images of the expression of the lung markers SOX9 (top panels), Nkx2.1 (middle panels) and pro-SPC (bottom panels) in isolated lung epithelium cultured for 96 hours with 100 ng/ml FGF7 with or without 10 μM ZSTK474. Images are representative of three experiments. Scale bar = 20 μm.

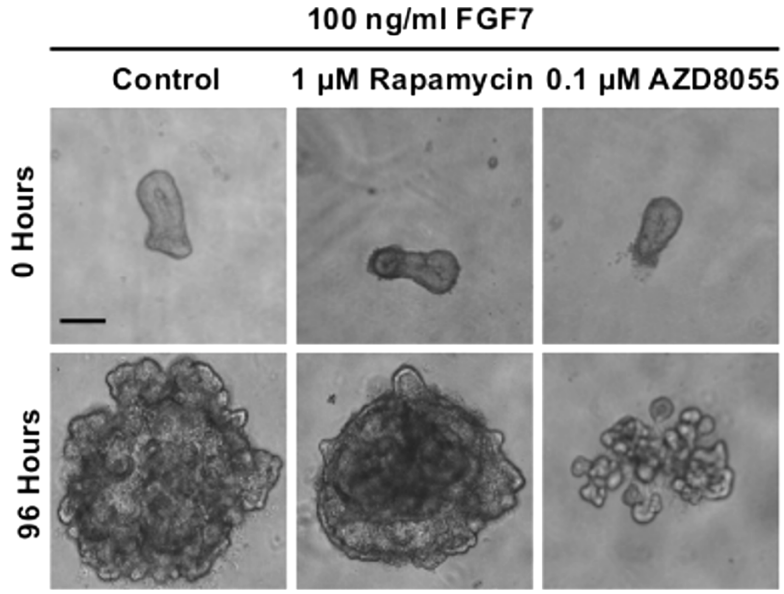

Figure 3.14. FGF7-treated lung epithelium develops branches following mTORC1/2 but not mTORC1 inhibition. Light microscope images of isolated E12.5 murine lung epithelium cultured over 96 hours with 100 ng/ml FGF7 alone (left panels) or in combination with either 1 μM rapamycin (middle panels) or 0.1 μM AZD8055 (right panels). Images are representative of at least twelve isolates. Scale bar = 200 μm.

Inhibition of PI3Kα but not PI3Kβ induces branching in isolated lung epithelium cultured with FGF7

We next wished to confirm if the isoform dependence of PI3K in branching morphogenesis observed in the whole lung explant model applied to isolated lung epithelium as well. To address this question isolated epithelium was cultured with FGF7 in combination with either the PI3Kα inhibitor BYL719 or the PI3Kβ inhibitor GSK2636771. As with ZSTK474, culture of isolated lung epithelium with FGF7 and BYL719 induced the formation of epithelial branches. Addition of both FGF7 and GSK2636771 produced a similar morphological appearance to FGF7 alone (Figure 3.15). This goes further to demonstrate that the branching of lung epithelium is regulated by the alpha, and not beta, isoform of PI3K.

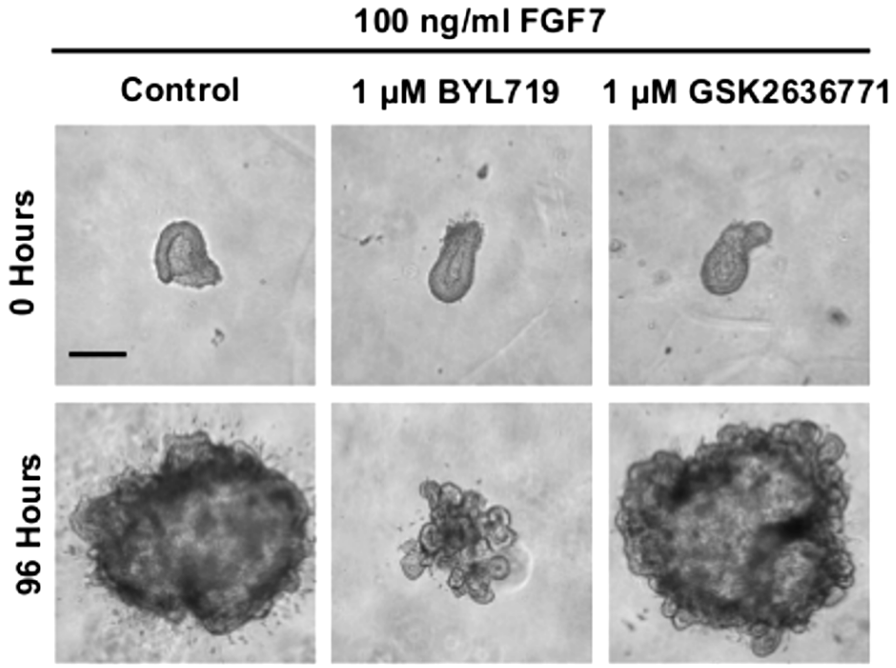

Figure 3.15. Inhibition of PI3Kα but not PI3Kβ induces branching in isolated lung epithelium cultured with FGF7. Light microscope images of isolated E12.5 murine lung epithelium cultured over 96 hours with 100 ng/ml FGF7 alone (left panels) or in combination with either 1 μM BYL719 (middle panels) or 1 μM GSK2636771 (right panels). Images are representative of six isolates per condition. Scale bar = 200 μm.

ZSTK474-induced branching is not a result of altered proliferation

As lung bud isolates cultured with ZSTK474 and FGF7 resulted in outgrowths that were smaller than those cultured with FGF7 alone we reasoned that proliferation may be reduced as PI3K inhibition has been reported to arrest cell growth (Chang et al., 2003). To address this, we examined the expression of two markers of proliferation (Ki67 and phospho-histone H3 (PH3)) in isolated epithelium after 96 hours of culture with FGF7 alone or in combination with ZSTK474. Both isolated lung buds treated with FGF7 alone or in combination ZSTK474 showed uniform appearance of Ki67 after 96 hours of culture. Small, isolated, clusters of cell expressing PH3 were also apparent in both culture conditions although these cells did not appear to be localised to specific regions (Figure 3.16A). To quantify the number of Ki67-positive cells from each treatment group images were processed using ImageJ software as outlined in the materials and methods (Section 2.11). As an example, representative analysis is provided in figure 3.16B showing the conversion of a Ki67 image to a binary image following background and noise reduction prior to the quantification of the number of nuclei using the 'analyse particles' function. Despite the isolates cultured with ZSTK474 and FGF7 being smaller in size than the isolates cultured with just FGF7, the proportion of Ki67-positive cells to the total cell number was not statistically different between the two groups (Figure 3.16C).

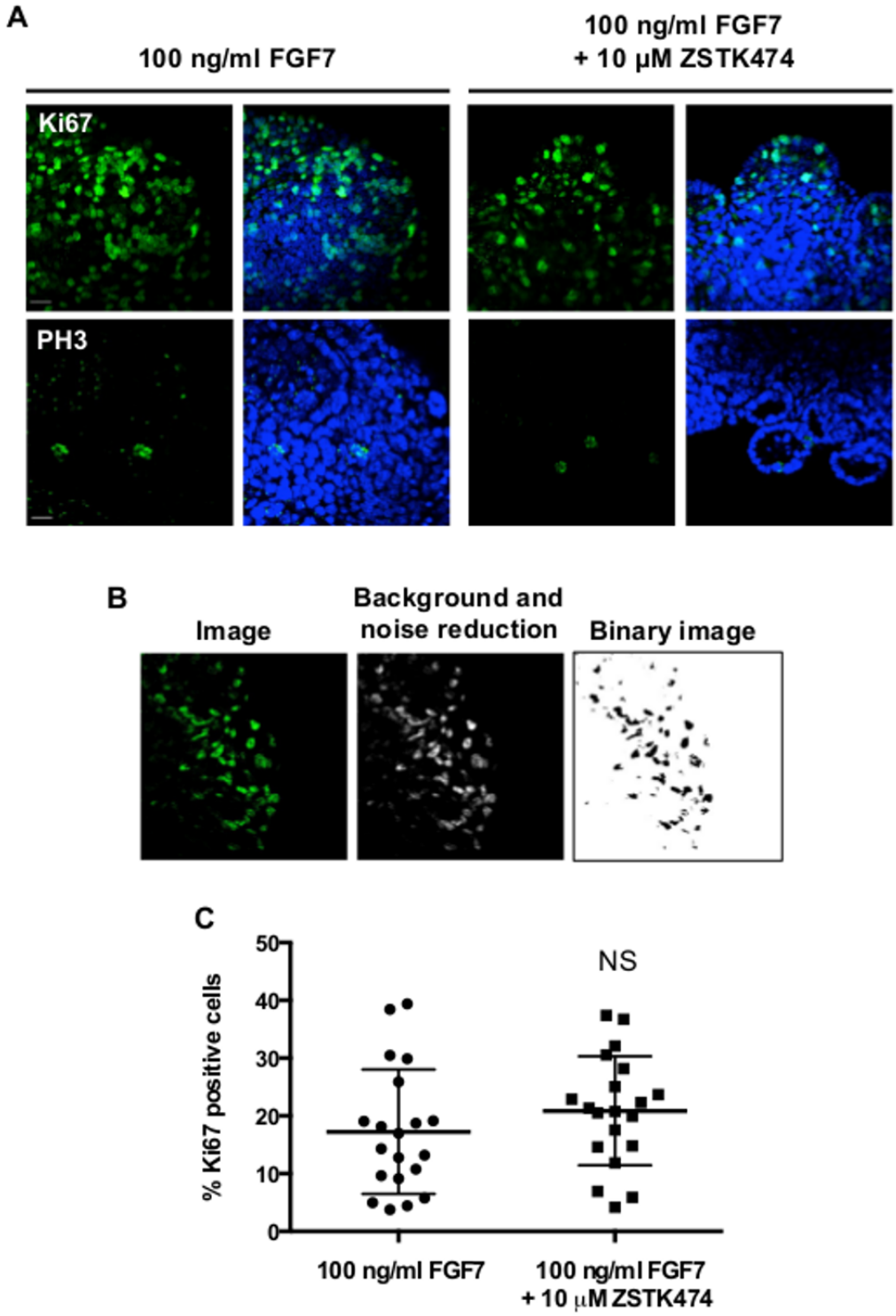

Figure 3.16. FGF7-treated isolated lung epithelium co-cultured with ZSTK474 continues to express markers of proliferation. A. Immunofluorescence images showing the expression of Ki67 (top panels) and phosphorylated-histone H3 (PH3, lower panels) in isolated lung epithelium cultured over 96 hours with 100 ng/ml FGF7 alone or in combination with 10 μM ZSTK474. Images are representative of twenty isolates per condition. **B.** Example of image analysis for the quantification of positive nuclei. A confocal image (right panel) is adjusted to reduce background and noise (middle panel) before being converted to a binary image (right panel). This image is then used to calculate the number of positive nuclei. **C**. Percentage of Ki67 positive cells in isolated lung epithelium cultured with either FGF7 alone or in combination with ZSTK474. Data pooled from twenty images per condition. Scale bar = 20 μm.

3.7 Lentiviral and lipid transfection of embryonic lung cultures

To complement our observations with pharmacological inhibitors we attempted to manipulate our embryonic branching models with lentiviral particles with the hope of introducing shRNA sequences targeting PI3K. To examine the utility of lentiviral infection in these models we initially generated lentiviral particles containing a GFP expression vector. GFP fluorescence following viral infection in embryonic lungs would therefore be an indication of effective delivery and would also demonstrate whether a particular cellular compartment favoured lentiviral infection. To confirm the effective generation of GFP lentiviral particles we infected cultures of A549 cells. 48 hours post infection approximately 86% of the A549 cells expressed GFP protein as analysed by flow cytometry (Figure 3.17A). Following exposure of lung explants to GFP lentiviral particles GFP expression was confined to the mesenchymal component of the lung explants (Figure 3.17B). The lack of epithelial expression of GFP vector therefore limits the use of lentiviral infection in this model. We also applied GFP lentiviral particles to isolated lung epithelium to assess the utility of lentiviral infection in this model. Unlike the application of lentiviral particles to whole explant cultures, lentiviral particles induced the death of isolated lung epithelium (Figure 3.17C).

The utility of siRNA transfection was next examined in the isolated lung epithelium model. Due to the fragile nature of the isolated epithelium and a requirement for the isolate to be placed within a Matrigel dome we tried multiple methods of siRNA transfection (Section 2.3). We incubated isolates with either 10 or 50 nM of siRNA targeting p110α (*PIK3CA*), p110β (*PIK3CB*), p85α (*PIK3R1*) or p85β (*PIK3R2*) in complex with either lipofectamine or jetPRIME transfection reagent prior to the mounting of the isolate into Matrigel. Following from the transfection step the isolates were cultured with FGF7 for 96 hours. None of these transfection strategies produced any obvious morphological changes in response to FGF7 compared with FGF7 alone (Figure 3.18). Equally the use of the transfection reagent 3D-Fect, which was combined with Matrigel in order to prolong the transfection time of the epithelial isolate, produced no obvious morphological change in isolates cultured with FGF7 (Figure 3.18). RNA extracted from 20 isolates following siRNA transfection and culture amounted to <0.3 μg, which was

insufficient for analysis of PI3K transcripts to determine whether PI3K gene expression was silenced.

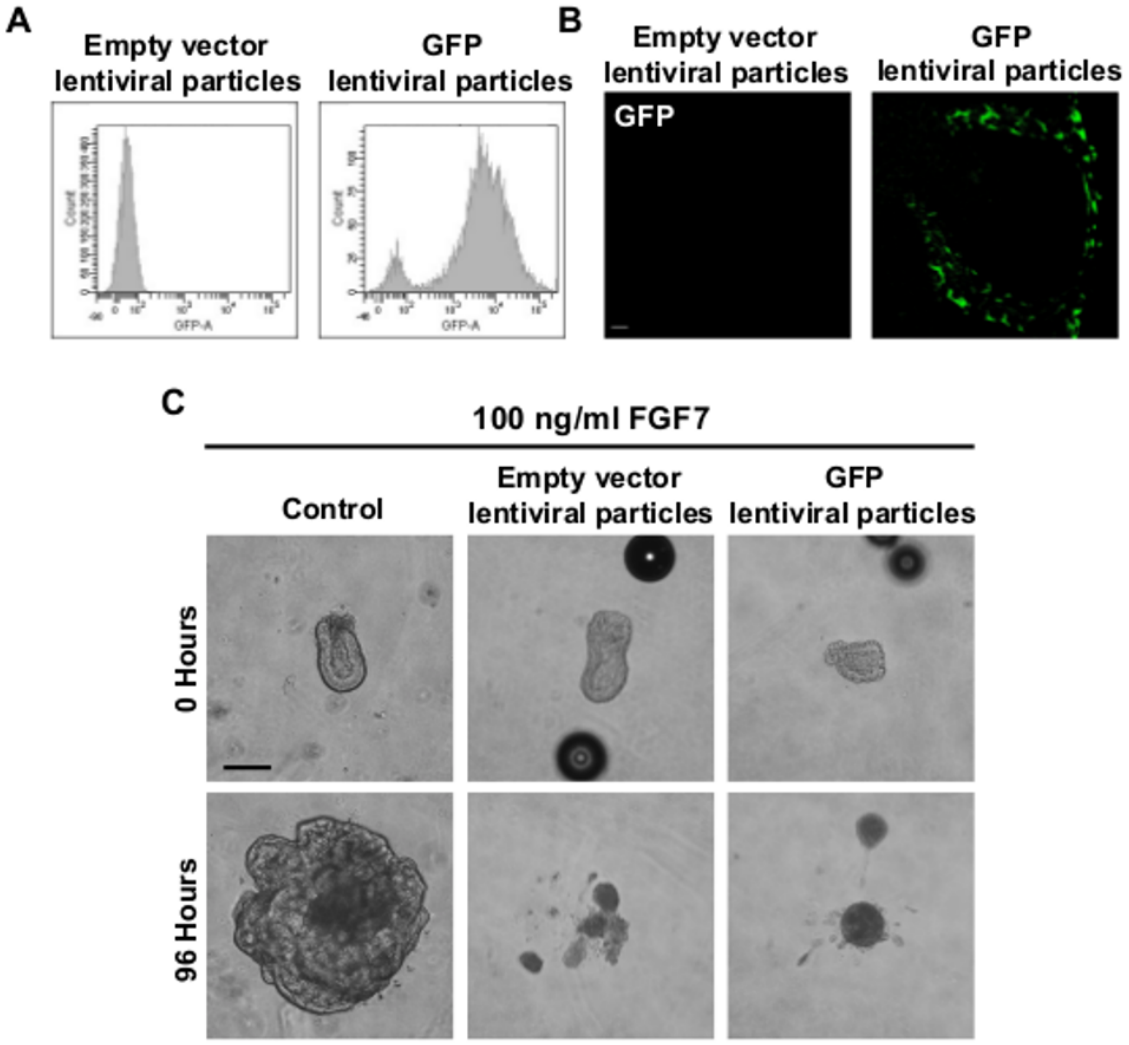

Figure 3.17. Lentiviral gene expression in cultures of embryonic murine lungs. A. FACS analysis for GFP expression in A549 cells 48 hours after infection with GFP lentiviral particles. **B.** GFP expression in E12.5 lung explants 48 after infection with lentiviral particles. Scale bar = 20 μm. **C.** Light microscope pictures of E12.5 isolated lung epithelium cultured for 96 hours in the presence of 100 ng/ml FGF7 following infection with GFP lentiviral particles. Scale bar = 200 μm. FACS plots and images are representative of three independent experiments with three separate harvests of GFP lentiviral particles.

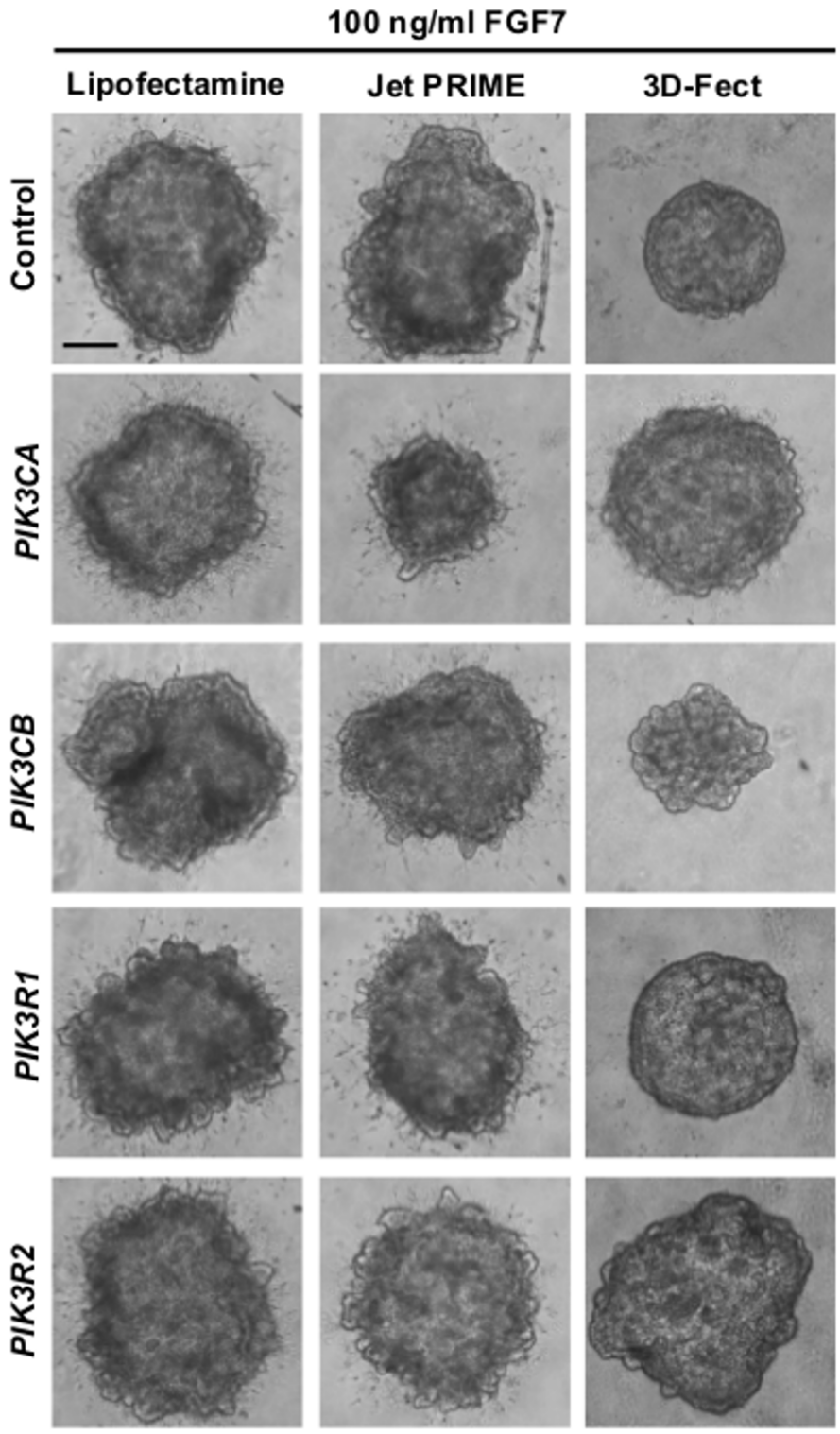

Figure 3.18. siRNA transfection of isolated murine lung epithelium. Light microscope images of isolated E12.5 murine lung epithelium after 96 hours of culture with 100 ng/ml FGF7. Isolates were transfected with siRNA targeting *PIK3CA, PIK3CB, PIK3R1* or *PIK3R2* in complex with either lipofectamine, jet PRIME or 3D-Fect transfection reagents. Images representative of sixty isolates per treatment over three independent experiments. Scale bar = 200 μm.

3.8 Interactions between FGF7 and heparan sulphate

FGF10 and FGF7 both signal through epithelial FGFR2b yet exhibit different morphological effects in isolated lung epithelium. FGF10 promotes directed epithelial branching whereas FGF7 directs a uniform growth of the epithelium. Studies have identified that a key determinant of directed FGF10 signalling is the ability of FGF10, and not FGF7, to bind to locally expressed heparan sulphate. This is highlighted by studies demonstrating that addition of exogenous heparan sulphate to cultures of isolated epithelium perturbs the natural gradient of heparan sulphate. This allows FGF10 to act uniformly across the epithelium, producing a morphological effect similar to FGF7 (Izvolsky et al., 2003).

We therefore wished to confirm that the branching response observed from the culture of isolated epithelium with FGF7 and ZSTK474 was independent of interactions with heparan sulphate. The addition of exogenous heparan sulphate to isolated lung epithelium cultured with FGF7 elicited no obvious change in morphology after 96 hours. Equally, heparan sulphate had no effect on the branching response resulting from co-culture with FGF7 and ZSTK474 (Figure 3.19), suggesting that this branching response is independent of heparan sulphate interactions.

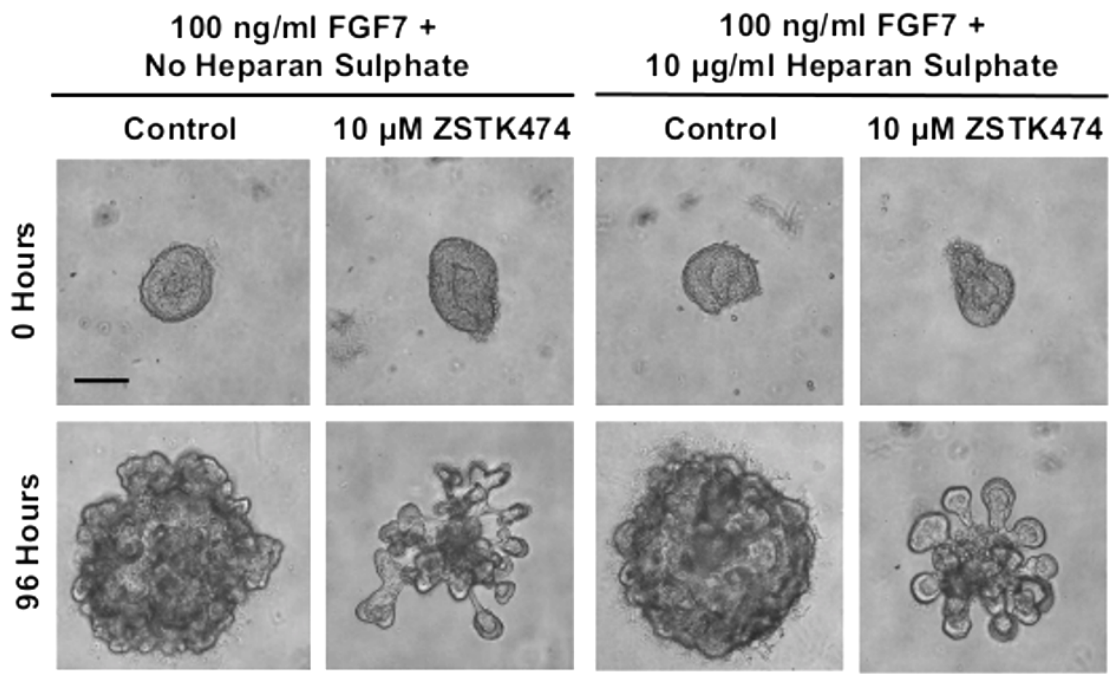

Figure 3.19. Heparan sulphate does not affect FGF7/ZSTK474 induced branching. Light microscope images of isolated E12.5 murine lung epithelium cultured over 96 hours with 100 ng/ml FGF7 alone or in combination with 10 µM ZSTK474 either in the presence of no heparan sulphate (left panels) or with 10 µg/ml heparan sulphate (right panels). Images are representative of six isolates per condition. Scale bar = 200 µm.

3.9 Does FGFR1b function as branching receptor?

The inability of heparan sulphate to affect the actions of FGF7 are unsurprising given that FGF7 natively lacks a binding domain for heparan sulphate (Makarenkova et al., 2009). Given the ubiquitous expression of FGFR2b in the lung epithelium (Cardoso et al., 1997) we hypothesised that a second receptor may be present, localised to sites of branching, that can initiate a branching response. FGFR2b would be inactivated following PI3K inhibition thus uncovering the actions of FGF7 through this second receptor. A potential candidate is FGFR1b as both FGF7 and FGF10 can signal through this receptor (Zhang et al., 2006). Further, high concentrations are required for the activation of this receptor by FGF7 and FGF10, which may account for the high concentrations required for a morphogenic response in cultures of isolated epithelium (Bellusci et al., 1997; Cardoso et al., 1997). FGFR1b expression has been identified at the tips of the branching epithelium of the salivary glands (Steinberg et al., 2005) and kidneys (Meyer et al., 2004), which gives more credence to this hypothesis. Moreover,

branch-like structures have been shown to form from the activation of FGFR1 in mammary organoid cultures (Xian et al., 2005).

To test this hypothesis we first examined the expression of FGFR1 in the branching lung epithelium. 3T3 fibroblast cells were used as a positive control for the expression of FGFR1 by immunofluorescence (Figure 3.20A). Isolated E12.5 murine lung epithelial branch tips showed no expression of FGFR1 by immunofluorescence (Figure 3.18B). We next examined the morphogenic effects of the principle growth factor for FGFR1, FGF2 (Zhang et al., 2006), on isolated lung epithelium. FGF2 induced the formation of large cystic structures of similar morphology to FGF7 over all concentrations tested (Figure 3.20C).

Finally, we studied the effects of the FGFR inhibitor PD173074 (Kunii et al., 2008; Skaper et al., 2000) on the growth of embryonic lungs. PD173074 reduced branching in whole embryonic lung explants in a concentration dependent manner (Figure 3.21A,B). Although branching was inhibited the explants appeared to be healthy given their morphology and the continuation of periodic contractile waves (Video 3.5). As FGFR inhibition reduced epithelial branching we wished to see if the branching response could be rescued through inhibition of PI3K. Culture with both PD173074 and ZSTK474 was found to be toxic to the lung explants (Figure 3.21C). Lung epithelium co-cultured with PD173074 and FGF7 failed to grow and appeared similar to isolated epithelium cultured without growth factors (Figure 3.21D). A similar inhibition of growth was observed when PD173074 was added to isolated epithelium cultured with FGF7 and ZSTK474 (Figure 3.21D).

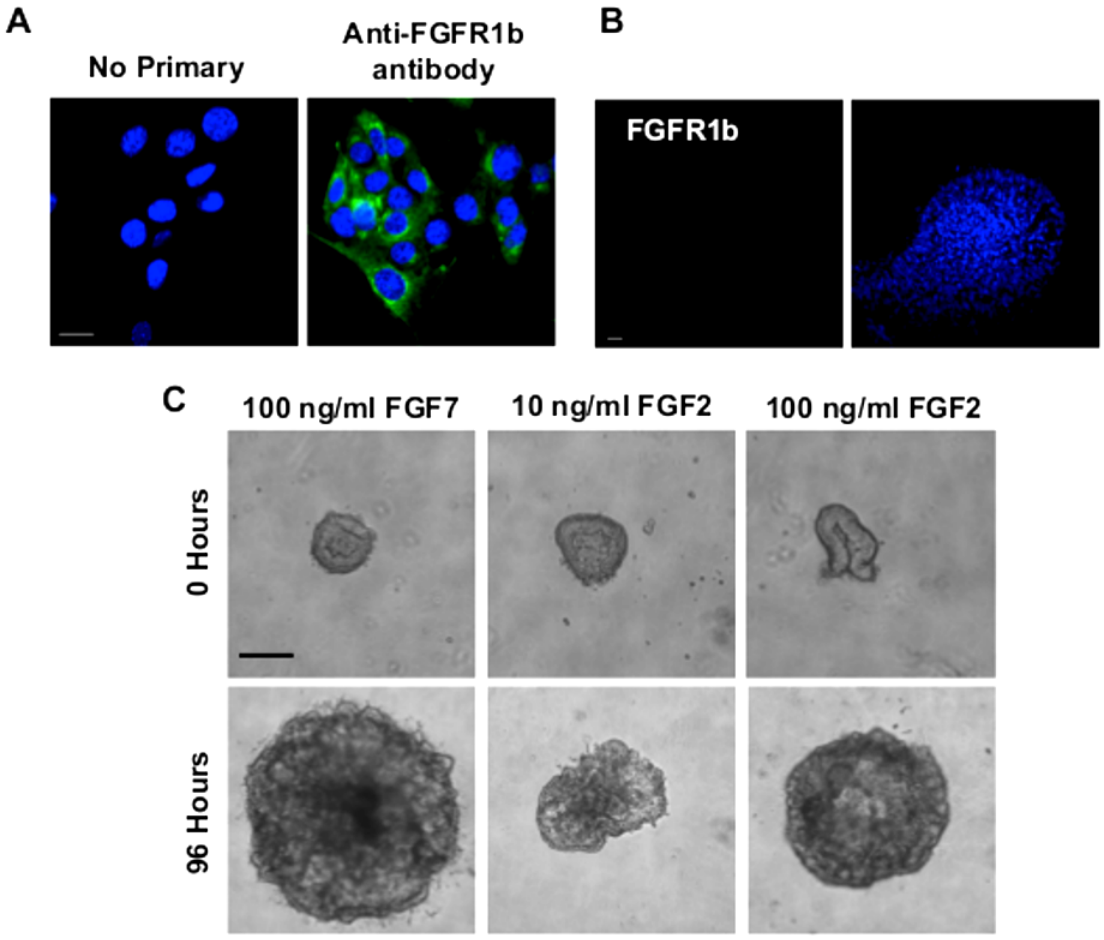

Figure 3.20. FGFR1 is not present at the sites of branching and its activation does not induce branching. A. Fluorescent images of 3T3 cells labelled with no primary antibody or an antibody directed against FGFR1. **B**. FGFR1 expression in an epithelial branch tip isolated from E12.5 murine lung explants. Fluorescent images are representative of three independent experiments. **C.** Light microscope images of isolated E12.5 murine lung epithelium cultured over 96 hours with either 100 ng/ml FGF7 or 10 or 100 ng/ml FGF2. Images are representative of six isolates per condition. Scale bar = 20 μm for fluorescent images and 200 μm for isolated epithelial cultures.

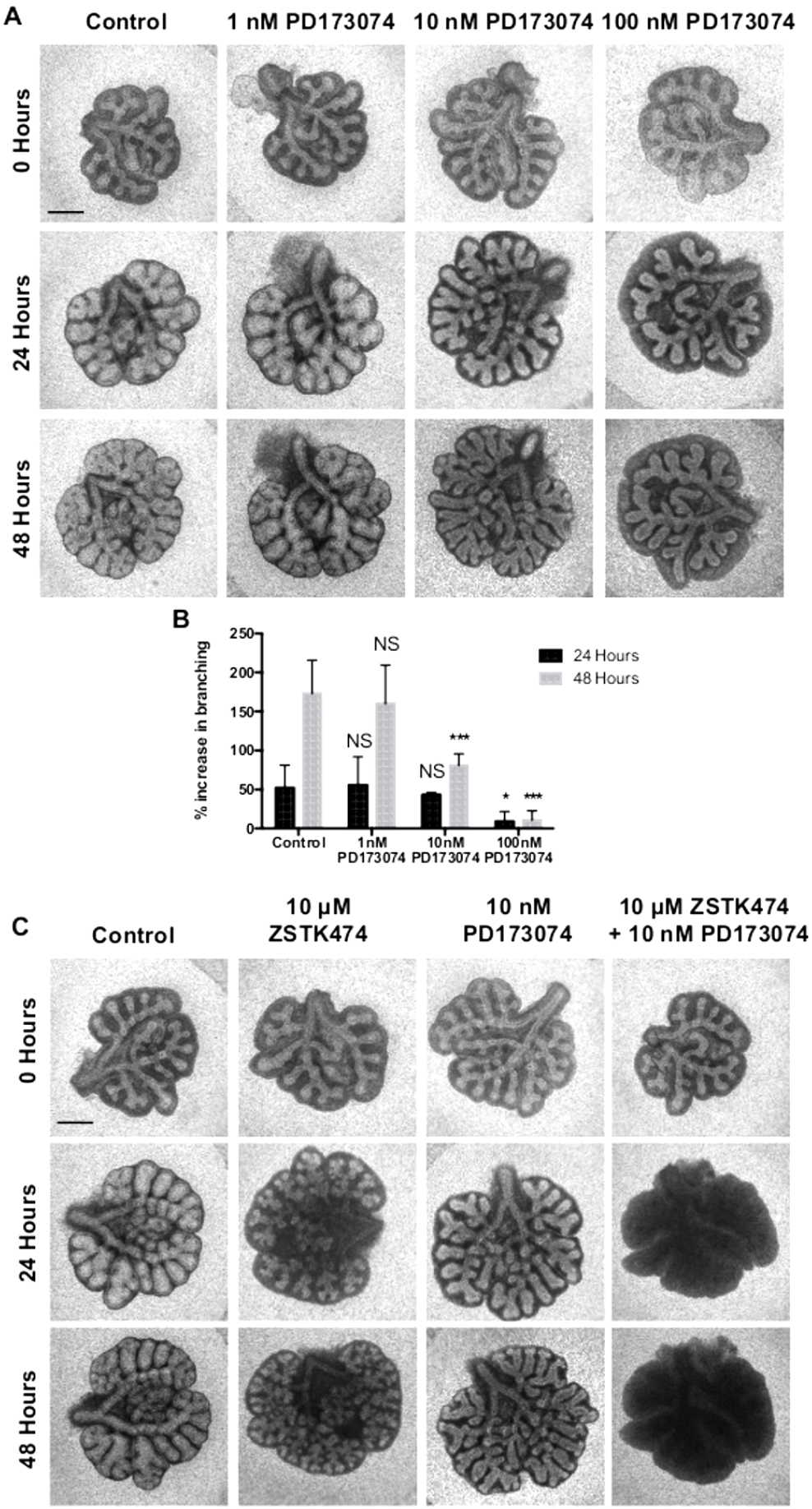
A
Control
1 nM PD173074
10 nM PD173074
100 nM PD173074
0 Hours
24 Hours
48 Hours
B
% increase in branching
250
200
150
100
50
0
NS
NS
NS
***
*
***
24 Hours
48 Hours
Control
1nM PD173074
10nM PD173074
100nM PD173074
C
Control
10 µM ZSTK474
10 nM PD173074
10 µM ZSTK474 + 10 nM PD173074
0 Hours
24 Hours
48 Hours

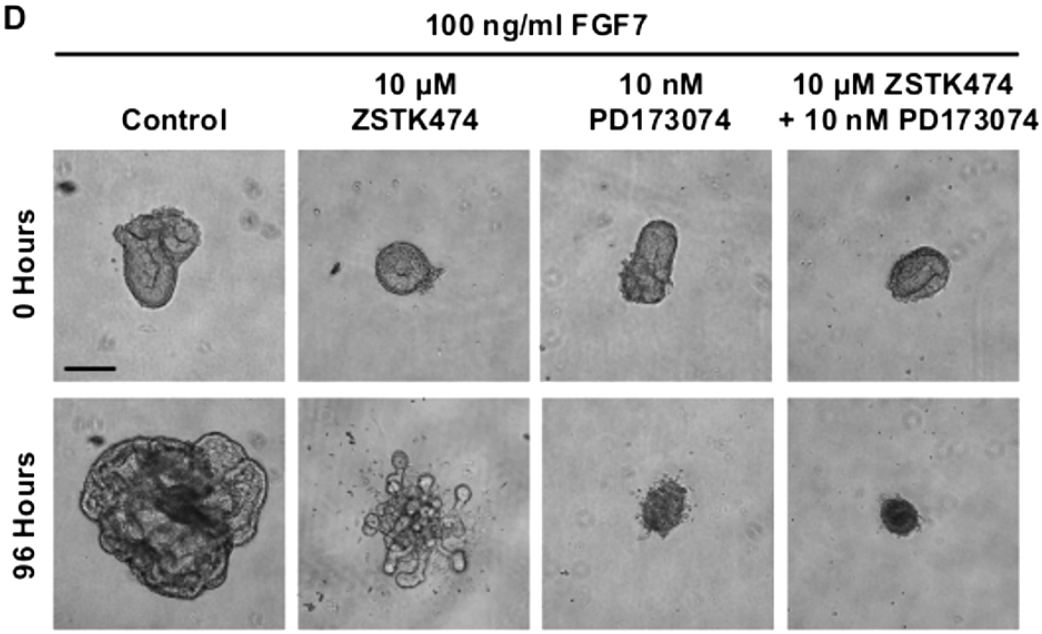

Figure 3.21. Inhibition of FGFR reduces epithelial growth and branching, which is not rescued by inhibition of PI3K. A. Light microscope images of E12.5 murine lung explants cultured with 0.1% DMSO (Control), 1, 10 or 100 nM PD173074 over 48 hours. Images are representative of at least six explants for each of the treatments shown. **B.** Percentage increase in epithelial branching over 24 and 48 hours relative to the number of branches at initial isolation. Bars show mean ± s.e.m from n=6 **C** & **D**. Light microscope images either lung explants (**C**) or isolated lung epithelium (**D**) cultured with 0.1% DMSO (Control), 10 µM ZSTK474, 10 nM PD173074 or with a combination of ZSTK474 and PD173074 over 48 or 96 hours. Images are representative of six explants/isolates per condition. Scale bar = 0.5mm for whole lung explants and 200 µm for isolated epithelial cultures. *** P<0.001, * P<0.05, NS = Not Significant, compared with control.

3.10 β-Catenin and regulation of cell-cell contacts in branching

Epithelial branching in the lung requires the collective migration of epithelial cells towards an FGF10 signal (Park et al., 1998). Work in the migration of the neural crest epithelial cells has identified that the collective migration of epithelial cells requires the transient loss of cell-cell contacts (Theveneau et al., 2013). Indeed, a loss of E-Cadherin mediated cell-cell contacts is pivotal in the acquisition of a migratory phenotype in epithelial cancers (Perl et al., 1998). Moreover, forced expression of E-Cadherin in isolated murine lung epithelium prevents the induction of branching by FGF10 (Liu et al., 2008).

E-Cadherin is anchored to the cell cytoskeleton through β-Catenin. Increasing the interactions between E-cadherin and β-Catenin strengthens the cell-cell contacts (Lickert et al., 2000). Likewise, decreasing this interaction weakens cell-cell

contacts (Behrens et al., 1993). In an epithelial cell there are two pools of β-Catenin protein; a cytoplasmic pool that is constantly turned over until stabilised through Wnt signalling (Aberle et al., 1997; van Noort et al., 2002), and a pool present at the adherens junction. The cytoplasmic pool of β-Catenin is regulated by the kinase GSK3β, which constantly targets β-Catenin for proteasomal degradation until inhibited by Wnt activation (Aberle et al., 1997). The adherens pool can be directly regulated by JNK (Lee et al., 2009). Further, these two pools of β-Catenin can influence each other. Overexpression of *Xenopus* C-Cadherin sequesters β-Catenin from the cytoplasm of cells thus reducing β-Catenin transcriptional activity (Fagotto et al., 1996). Equally, following the disruption of cell-cell contacts, β-Catenin can be released from the cadherin pool and signal following Wnt activation (Kam and Quaranta, 2009). As both GSK3β and JNK can be inhibited by PI3K activity (Aikin et al., 2004; Cross et al., 1995) we hypothesised that inhibition of PI3K may indirectly destabilise the cell-cell contacts between neighbouring epithelial cells thus priming the cells for a branching event.

To investigate this we examined the distribution of E-Cadherin and β-Catenin at the leading edge of a developing branch from isolated lung epithelium cultured with both FGF7 and ZSTK474. We imaged an isolate after 48 hours of culture, when the epithelial branches begin to form, to give the best chance of seeing cell-cell contact disruption. β-Catenin co-localised with E-Cadherin consistently across the tip of a developing branch suggesting that cell-cell contacts were not being disrupted (Figure 3.22).

We next examined the impact of GSK3β on the branching lung utilising the selective GSK3β inhibitor 1m (Bone et al., 2009). Inhibition of GSK3β with 1m reduced branching in whole lung explants although it was difficult to distinguish an epithelial branch from surrounding mesenchyme (Figure 3.23A,B). When applied to isolated lung epithelium cultured with FGF7, 1m induced a more uniform growth of the epithelium than epithelial isolates cultured with FGF7 alone. Equally, when applied to isolated epithelium cultured with FGF7 and ZSTK474, 1m prevented the induction of branches and instead induced the uniform growth of the epithelium similar to FGF7 and 1m albeit of significantly smaller size (Figure 3.23C).

Finally, we investigated the effect of JNK inhibition on the branching response. Although there was a trend for the JNK inhibitor SP600125 to promote branching in lung explants the difference was not statistically significant. Further at concentrations greater than 5 μM SP600125 appeared to be toxic to the explants (Figure 3.24A,B). 5 μM SP600125 also had little effect on the morphology induced by either FGF7 alone or in combination with ZSTK474 when applied to isolated lung epithelium (Figure 3.24C).

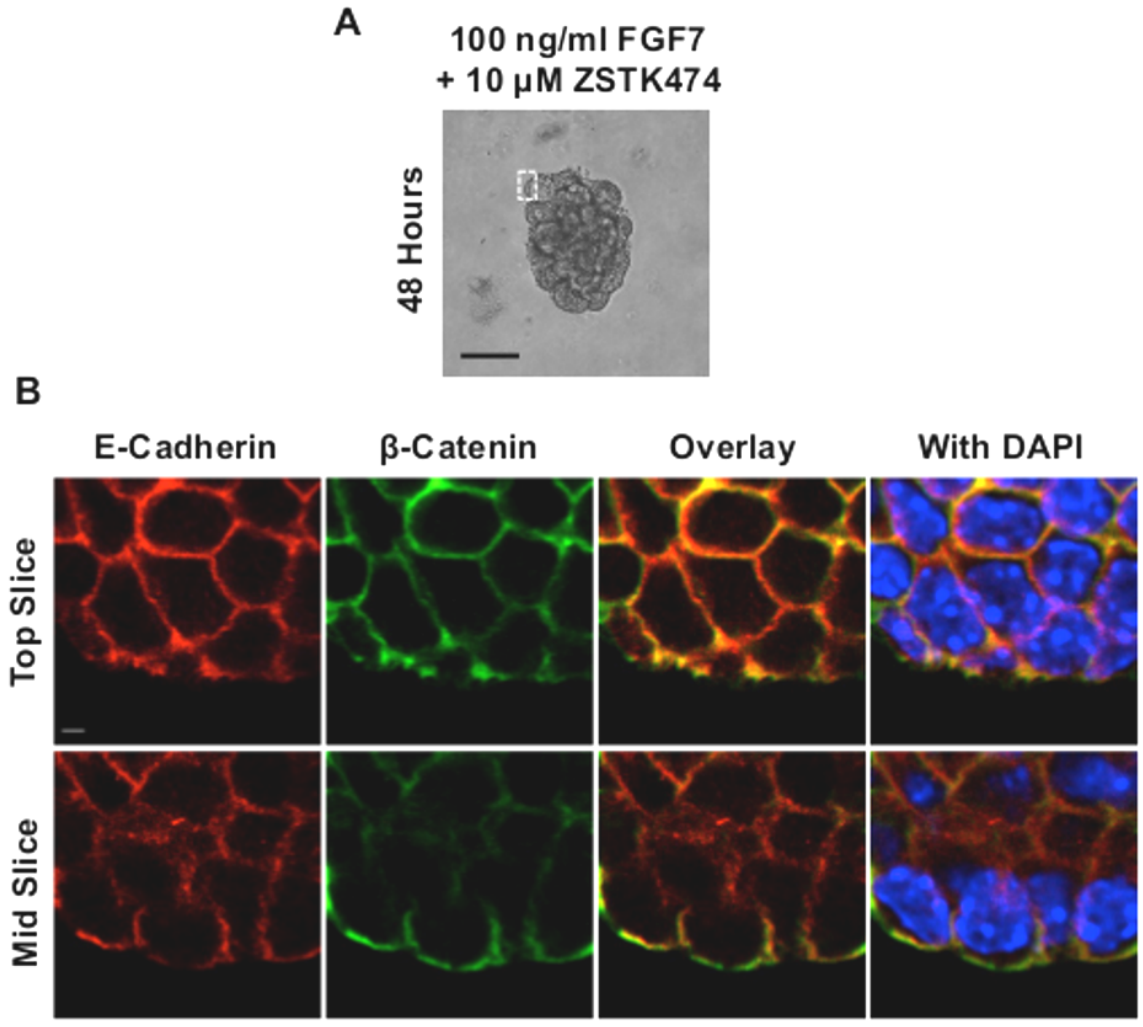

Figure 3.22. Cell-cell contacts between epithelial cells remain intact during branching. A. Light microscope image of isolated E12.5 murine lung epithelium after 48 hours of culture with 100 ng/ml FGF7 and 10 μM ZSTK474. White box represents area of imaging in **B**. Scale bar = 200 μm. **B**. Z-stack confocal images of top and mid sections of **A** showing localisation of E-Cadherin (red) and β-catenin (green). Images taken at 63x magnification with 6x zoom. Images are representative of two independent experiments. Scale bar = 2 μm.

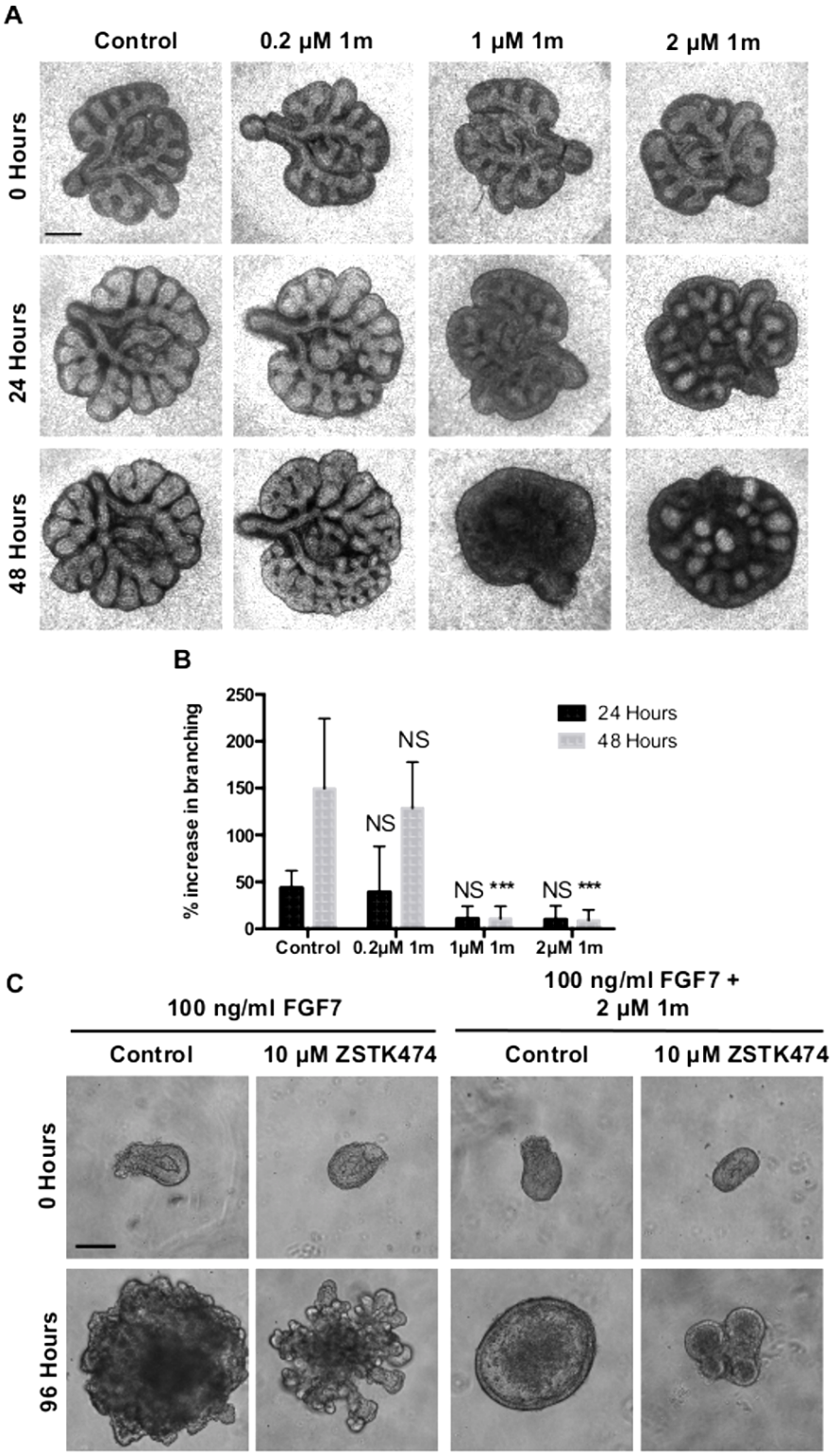

Figure 3.23. Inhibition of GSK3β reduces branching. A. Light microscope images of E12.5 murine lung explants cultured with 0.1% DMSO (Control), 0.2, 1 or 2 μM 1m over 48 hours. Images representative of at least six explants for each condition are shown. Scale bar = 0.5 mm. **B.** Percentage increase in epithelial branching over 24 and 48 hours relative to the number of branches at initial isolation. Bars show mean ± s.e.m from n=6. **C.** Light microscope images of isolated E12.5 murine lung epithelium cultured over 96 hours with 100 ng/ml FGF7 alone or in combination with 10 μM ZSTK474 either in the presence of no 1m (left panels) or with 2 μM 1m (right panels). Images are representative of six isolates per condition. Scale bar = 200 μm.

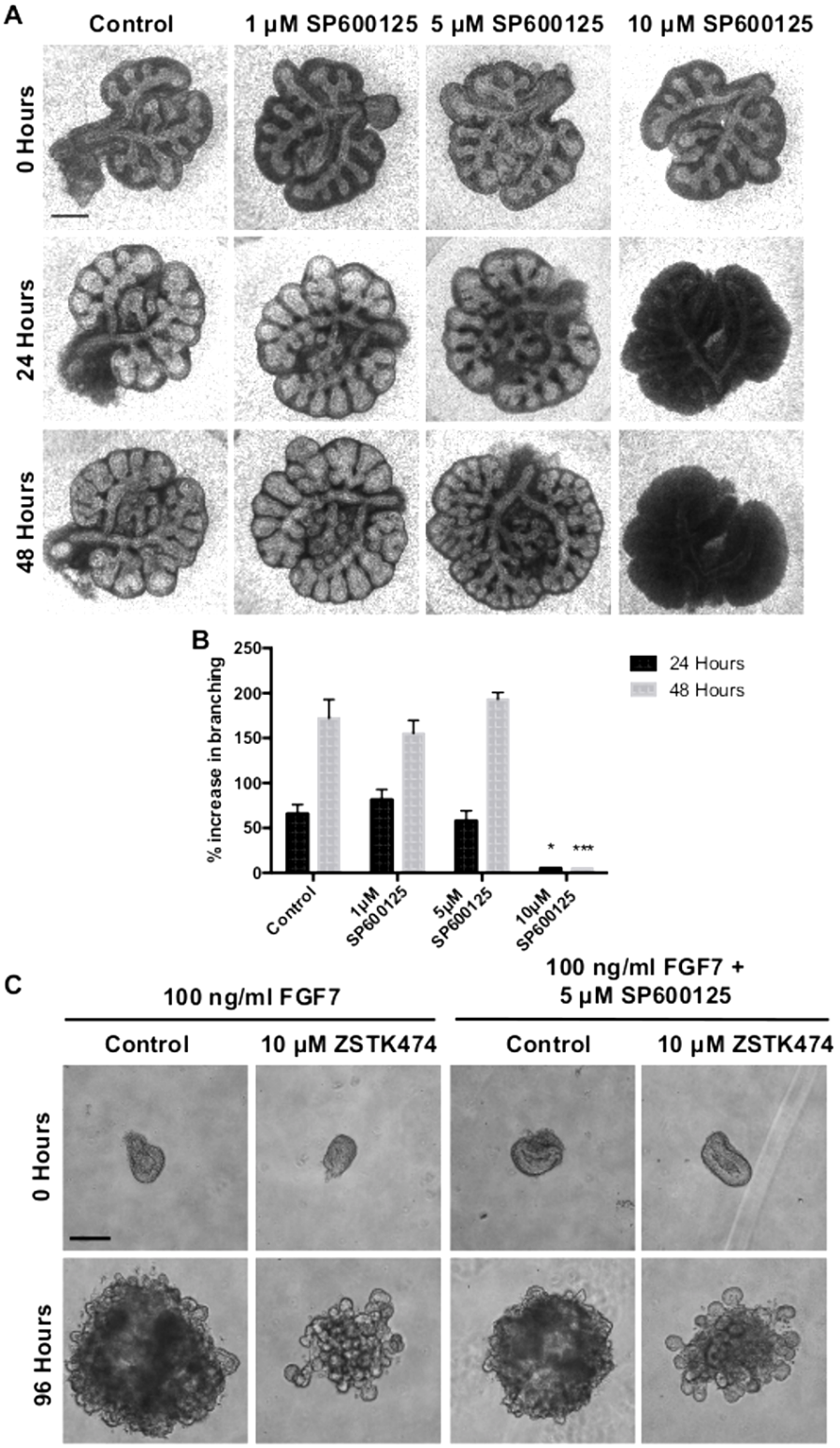

Figure 3.24. Inhibition of JNK has no effect on branching. A. Light microscope images of E12.5 murine lung explants cultured with 0.1% DMSO (Control) or 1, 5 or 10 μM SP600125 over 48 hours. Images representative of at least six explants for each condition are shown. Scale bar = 0.5 mm. **B.** Percentage increase in epithelial branching over 24 and 48 hours relative to the number of branches at initial isolation. Bars show mean ± s.e.m from n=6. **C.** Light microscope images of isolated E12.5 murine lung epithelium cultured over 96 hours with 100 ng/ml FGF7 alone or in combination with 10 μM ZSTK474 either in the presence of no SP600125 (left panels) or with 5 μM SP600125 (right panels). Images are representative of six isolates per condition. Scale bar = 200 μm.

3.11 Summary of results

- Inhibition of PI3Kα does not prevent the induction of EMT but does reduce the activity of the resulting fibroblasts
- Culture of embryonic lungs adequately recapitulates the branching process
- Inhibition of PI3Kα, or its downstream signalling components potentiates epithelial branching in cultures of embryonic lungs
- Contrary to reported results, FGF10 and FGF1 promote growth of residual mesenchymal tissue in isolated lung epithelium
- Inhibition of PI3K results in FGF7 initiating a branched response from isolated lung epithelium
- This induction of branching does not affect the differentiation of the epithelial cells nor does it appear to be the result of altered proliferation.
- Lentiviral and lipid based transfection methods a re largely ineffective in cultures of embryonic lungs
- FGFR1 does not appear to be expressed in the branching lung epithelium
- Cell-cell contacts remain intact in branches that form from isolated lung epithelium as a result of FGF7 treatment and PI3K inhibition
- Inhibition of GSK3β perturbs branching and causes a more uniform growth of isolated lung epithelium
- Inhibition of JNK has little effect on epithelial branching

3.12 Discussion

PI3K in the induction of EMT

EMT is considered a potential source of myofibroblasts in the progression of lung fibrosis. Lung epithelial cells from both mice with experimental fibrosis and patients with idiopathic pulmonary fibrosis have been reported to express markers of both epithelial cells and fibroblasts, indicative of a cell undergoing EMT (Kim et al., 2006; Marmai et al., 2011). Evidence for EMT in the fibrotic process is largely dependent on the observation of cells expressing markers of both epithelial cells and fibroblasts, i.e. cell in a ‘partial EMT’ state, as a cell that has completely undergone EMT would be indistinguishable from other, native, fibroblasts. This has lead to controversy regarding the involvement of EMT in the fibrotic process

with the growing appreciation that, due to the complex 3D nature of the lung, cells that have been identified as in a state of partial EMT may simply be two cells overlapping. Indeed, confocal analysis of lung sections taken from patients with pulmonary fibrosis and lineage tracing studies in mice has failed to identify cells in on

Inhibition of PI3K with either ZSTK474 or PIK-75 did not prevent TGFβ induced EMT in A549 epithelial cells. However, inhibition of PI3Kα did reduce the production of MMP-9 and MMP-2. This would suggest that PI3Kα is not involved in the initial loss of epithelial proteins induced by TGFβ but is responsible for the induction of a fibroblast phenotype. This observation is different from that reported with the LY294002 PI3K inhibitor, which suggested that PI3K inhibition was capable of preventing the induction of EMT (Bakin et al., 2000; Chen et al., 2012; Yan et al., 2009). Further observations with more selective PI3K inhibitors and genetic knockdown approaches will reveal the full extent of PI3K in the EMT process.

It has been reported that the activity of both PI3Kα and PI3Kγ are required for the conversion of fibroblasts to myofibroblasts, i.e. an increase in cell proliferation, αSMA expression and collagen deposition (Conte et al., 2011). This study, and our own would therefore suggest that PI3K inhibition would be an attractive target in pulmonary fibrosis, as inhibition of fibroblast activity would halt the progression of fibrotic lung injury.

Embryonic lung cultures: similarities and differences to lungs *in-utero*

Ex-vivo cultures of whole embryonic lungs, taken at the initial stages of the branching program, recapitulate many elements of the developmental process. They continue to develop epithelial branches in culture and demonstrate the expression and arrangement of various cell types consistent with what has been observed *in-utero*. As well as these similarities between the culture of embryonic lungs and their growth *in-utero* there are many differences. For instance the branching rate, and growth of the explant is greatly diminished in culture compared to the growth *in-utero* (Metzger et al., 2008). Moreover, the pressure apparent during culture is different than that *in-utero*, which greatly affects the branching

response (Unbekandt et al., 2008). The constituents of the cell culture medium used to maintain the cultures of embryonic lungs are also different from the comparative environment *in-utero*. A notable difference is the concentration of calcium, which is usually 1.05 mM in DMEM cell culture medium (equivalent to the levels of calcium found in adult plasma) compared to 1.7 mM found in foetal serum. This higher, foetal, level of calcium reduces branching in lung explant cultures compared to the lower, adult, level (Finney et al., 2008). Despite these differences, cultures of whole embryonic lungs remain an elegant model to study the gross effects of a signalling factor on branching.

The culture of isolated lung epithelium overcomes the additional caveat associated with the whole explant model in that it is difficult to determine if an affect on branching is specific to the lung epithelium or secondary to an effect on the mesenchyme. This model allows for the study of the mechanisms involved in epithelial morphogenesis with respect to the actions of FGF7, FGF10 or FGF1. However, this model lacks any regulation of branching usually provided by the surrounding mesenchyme, therefore branching is non-stereotyped compared to *in-utero*.

The PI3K pathway negatively regulates lung branching morphogenesis

We primarily focussed on the role of the PI3K pathway in the branching program of the lung due to the current conflicting reports of this pathway in the branching process and the strong involvement of this pathway in developmentally related diseases such as cancer and fibrosis. We show here, for the first time, that PI3K plays a negative role in airway branching morphogenesis. This has been demonstrated by a robust increase in murine lung explant branching upon pharmacological inhibition of either PI3K or its downstream effectors Akt and mTOR.

Notably we observed a potentiation of branching with an inhibitor of both the mTORC1 and mTORC2 complexes of mTOR but not with an inhibitor of mTORC1 alone. Once activated mTORC2 can feedback and potentiate Akt activity (Facchinetti et al., 2008), whereas mTORC1 can negatively regulate mTORC2 (Julien et al., 2010). Thus, inhibition of mTORC1 should increase Akt signalling by

removing this inhibitory effect on mTORC2. Moreover, mTORC1 activation of S6K can feedback and negatively regulated PI3K signalling at RTKs (Haruta et al., 2000; O'Reilly et al., 2006). Therefore, inhibition of mTORC1 with rapamycin should in fact potentiate PI3K signalling by removing these negative feedback loops. However, following treatment of lung explants with rapamycin we observed no increase in the levels of phosphorylated Akt compared with controls. This may suggest that these feedback loops are not functional in the branching process. Alternatively it may reflect the observation that prolonged rapamycin treatment inhibits mTORC2 activity, thus reducing Akt activation (Sarbassov et al., 2006). In this instance we might expect to see a potentiation of branching and/or a reduction in the levels of phosphorylated Akt; although the 48-hour assessment of branching may be too early to observe this delayed effect of rapamycin in our system.

In contrast, direct inhibition of both mTORC1 and mTORC2 with AZD8055 would remove the negative feedback of mTORC1 but would also remove the positive effect of mTORC2 on Akt activity. As a consequence the overall net effect would be decreased activation of Akt signalling and thus an increase in branching. The dependence of mTORC2 in this system would be best analysed with a selective inhibitor of mTORC2. However, there is currently no available pharmacological tool with which to assess this.

The observation that inhibition of PI3K potentiates branching in the murine embryonic lung is somewhat surprising given that previous work has suggested a requirement for PI3K signalling. Wang and colleagues observed a reduction in branching in murine lung explants cultured with the pan class I PI3K inhibitor LY294002 (Wang et al., 2005). In our study we observed a similar inhibitory effect with the LY294002 compound at concentrations used by Wang and colleagues (>20 μM). However, this was preceded by an efficient increase in branching at 10 μM. It therefore seems likely that at higher concentrations the actions of LY294002 on the lung explants are a consequence of toxicity and/or inhibition of branching through one of the many off-target effects of the compound (Davies et al., 2000).

The use of isoform-selective inhibitors of this kinase suggests that the alpha isoform of PI3K negatively regulates lung branching. An increase in branching

above that seen with the pan PI3K inhibitor ZSTK474 was observed with the PI3Kα specific inhibitors A66 and BYL719 but not with the PI3Kβ specific inhibitors GSK2636771 and TGX-221. This is in contrast to mammary glands where mice deficient in PI3Kα exhibited decreased mammary branching, and mice deficient in PI3Kβ exhibited potentiated branching (Utermark et al., 2012). The distinct roles of PI3Kα and PI3Kβ in mammary branching may be explained by the fact that PI3Kβ is less active and could compete with the more active PI3Kα for lipid substrate. Deletion of PI3Kβ would therefore potentiate PI3K signalling through increased PI3Kα activity (Utermark et al., 2012).

Using a range of pharmacological agents, targeting PI3K and its downstream signalling components, we have been able to better explore the role of PI3K signalling in airway branching (summarised in Figure 3.25A). Thus our findings more accurately represent the role for the PI3K pathway in lung branching morphogenesis. Although the reported IC50 values for these compounds are usually in the nanomolar range these values are obtained from cell free assays and do not necessarily reflect their potency in cells and tissues. Thus, the higher concentrations required in our study to elicit inhibitory effects likely reflects the influence of cell membrane permeability and compound stability on inhibitor efficiency when using *in-vitro* cell/tissue based assays.

PI3K inhibition alters morphogenic properties of FGF7

A particularly striking observation is that branches form from isolated lung epithelium cultured with FGF7 when PI3K signalling is inhibited. These structures contain a luminal space and organised epithelium confirming that they are not merely a scattering of cells but are fully formed branches. Moreover, PI3K inhibition did not appreciably alter the differentiation of the epithelial cells, which maintained a distal immature type II AEC phenotype, consistent with the state of the lung epithelium at this stage of development (Warburton et al., 2010). This was demonstrated by the continued expression of SOX9, Nkx2.1 (distal markers) and pro-SPC (type II AEC marker) in the lung epithelium following culture with either FGF7 alone or in combination with ZSTK474. SOX9 expression has been noted to prevent the differentiation of the lung epithelium, maintaining the epithelial cells in a branching state (Chang et al., 2013).

This is the first reported observation of FGF7 promoting a branched response in isolated lung epithelium. As the isolates cultured with FGF7 and the inhibitor of PI3K, ZSTK474, were smaller than those cultured with FGF7 alone we examined if proliferation was being affected. In the presence of FGF7 and ZSTK474, lung epithelial isolates continued to express the proliferation markers Ki67 and PH3. The proportion of cells expressing Ki67 was not significantly different between isolates cultured in the presence of FGF7 and ZSTK474 and those cultured with FGF7 alone suggesting that proliferation was not being altered. Interestingly the expression of PH3 was restricted to small populations of cells scattered across the epithelial isolate. This could suggest the presence of distal epithelial stem cells thought to be instrumental in the differentiation of the epithelial cells following branching morphogenesis (Rawlins et al., 2009).

Limitations to the FGF10 and FGF1 models

An unfortunate caveat of this work is that we were unable to assess the impact of PI3K inhibition on the branching response induced natively by FGF10 or FGF1. It would have been interesting to examine if inhibition of PI3K switched FGF10, or FGF1, signalling from a branching response to uniform growth; or simply induced a similar morphology to that seen with FGF7 and an inhibitor of PI3K.

The inability of isolated epithelium to branch in response to FGF10 or FGF1 and instead form a single tubule may imply that the epithelium is adopting a phenotype consistent with the proximal parts of the airway network. This is supported by the observation that smooth muscle cells develop around the tubule and periodically contract. However, this may be an unrelated effect attributed to the culture system. Epithelial cells that comprise the proximal regions of the branched network express the transcription factor SOX2 (Chang et al., 2013). Therefore, if the epithelial cells present in the tubules that develop in response to FGF10 also express SOX2 it would imply that they have adopted a proximal phenotype.

It has been reported that the contractile phenotype expressed in the developing lung requires a pacemaker region that can be influenced by FGF10 (Jesudason et al., 2005). If in our culture system we were developing proximal airway epithelium

surrounded by contractile smooth muscle then it would suggest that a pacemaker region in the lung can develop independently and is not limited to a particular region of the lung.

Transfection of embryonic lungs

We attempted to improve the utility of the whole lung explant model by incorporating a lentiviral expression vector into the cultures. This would have allowed us to express shRNAs to complement our pharmacological data. Further, this would have allowed us to express reporter proteins, such as a GFP labelled PH domain of Akt, which would have allowed us to examine where in a branch the product of PI3K, $PI(3,4,5)P_3$, accumulates. This would have provided answers as to whether PI3K is involved in the elongation of an existing branch, or is required for the initiation of an epithelial branch, as is suggested for mammary branching (Zhu and Nelson, 2013).

Unfortunately, upon infection with lentiviral particles containing a GFP expression vector we only observed fluorescence in the mesenchymal component of the lung explants, suggesting a complete lack of infection of the epithelial cells. A preference for the mesenchymal cells to take up lentiviral particles has also been demonstrated for cultures of salivary gland cultures (Hsu et al., 2012). A solution to this caveat is the injection of transfection material (lentiviral particles or siRNA) directly into the tracheal lumen of lung explants (Lee et al., 2014). The material is then dispersed throughout the airway network and is predominantly incorporated into epithelial cells. However, this technique is difficult, requiring the precise microinjection of transfection material. Further, a study using fluorescently tagged siRNA has suggested that the microinjection technique does not uniformly disperse the material across the epithelium, with the majority been taken up by the proximal branches closest to the trachea and little ending up in the terminal branches (Lee et al., 2014).

A more elegant solution has recently been demonstrated for salivary gland cultures and could theoretically be applied to lung cultures as well (Sequeira et al., 2013). In this system the mesenchyme is removed from the epithelial tissue of the salivary gland. The epithelial tissue is then directly infected with a viral construct

before the mesenchymal tissue is repositioned around the epithelium. When placed in culture at the air liquid interface the mesenchymal tissue appears to reform around the epithelium and the salivary gland continues to branch normally. By this means, viral constructs are reported to be preferentially expressed in salivary gland epithelial cells and their effect on branching can be adequately assessed (Sequeira et al., 2013). Although this technique seems relatively straightforward it remains to be determined if this could be applied to cultures of embryonic lungs. It is currently unknown if the lung mesenchyme can reform around the epithelium once removed and subsequently propagate branching. Further, it has been demonstrated that different viral particles (e.g. adenoviral and lentiviral) have different efficacies in cultures of lung and salivary glands (Hsu et al., 2012). Therefore, an appropriate viral infection method specific for the lung epithelium would also need to be determined.

We also attempted to transfect isolated epithelium with siRNA targeting different elements of PI3K. Following transfection with siRNA we did not see any morphological change in response to FGF7 from isolated epithelium. This may either be due to ineffective transfection, or that knockdown of PI3K in this instance had no effect on FGF7 activity. Given that we were unable to acquire enough RNA to assess knockdown by siRNA we could not determine which outcome is correct. Nevertheless, given the amount of pharmacological data we acquired it would seem likely that we were not achieving efficient knockdown. To expand on this work it would first be prudent to ensure that the transfection method of choice was adequate for isolated lung epithelium. This could be examined by using a fluorescently labelled siRNA to visualise the level of incorporation of the siRNA into the epithelium.

Mechanisms of FGF7 induced branching through inhibition of PI3K

There have been numerous reports to date involving the alteration of FGF10 signalling to produce a morphological effect similar to FGF7 but we are the first to demonstrate the opposite. These studies have primarily altered FGF10 signalling by interfering with the interactions between heparan sulphate and FGF10 (Izvolsky et al., 2003; Makarenkova et al., 2009; Patel et al., 2008), or overexpressing E-Cadherin (Liu et al., 2008), in isolated branching epithelium. FGF7 lacks a

heparan-binding domain and should therefore act independently of heparan sulphate (Makarenkova et al., 2009). Indeed, the addition of heparan sulphate to isolated epithelium cultured with FGF7 and ZSTK474 failed to perturb branching. Our work is therefore also the first example of a branching response that is independent of heparan sulphate.

The canonical branching receptor FGFR2b is expressed ubiquitously across the lung epithelium (Cardoso et al., 1997). We therefore hypothesised that a second receptor could function in the branching response whose expression is restricted to the sites of branching. A prospective candidate was FGFR1b as this receptor is found only at the branching tips in the branching salivary glands (Steinberg et al., 2005), and the forced activation of this receptor is sufficient to induce branching in mammary organoid cultures (Xian et al., 2005). Despite this evidence we were unable to identify the expression of FGFR1 in the branch ends of isolated embryonic lungs. There is the possibility that the antibody was not specific for the FGFR1b isoform of FGFR1, and only bound to the relevant FGFR1 isoform present in 3T3 cells. Further, the typical FGFR1 agonist, FGF2, was unable to induce branching in cultures of isolated lung epithelium, instead inducing a morphology similar to FGF7. FGF2 can also signal through FGFR2b, albeit at high concentrations (Ornitz et al., 1996). Inhibition of FGFR with PD173074 was able to obstruct epithelial branching. However, PD173074 is not specific for a particular FGFR (Kunii et al., 2008) so the reduction in branching observed is likely due to its inhibitory action on FGFR2b. Alternatively, as PD173074 can also inhibit VEGFR signalling (Mohammadi et al., 1998), this inhibition of branching may be a result of a knock-on effect from a reduction in angiogenesis (Lazarus et al., 2011). Nevertheless, inhibition of PI3K could not rescue the branching response, suggesting that PI3K functions downstream of FGFR.

We then investigated if inhibition of PI3K was disrupting the contacts between neighbouring epithelial cells, thus promoting branching. Confocal analysis of a developing branch from isolated lung epithelium cultured with both FGF7 and ZSTK474 demonstrated consistent co-localisation between E-Cadherin and β-Catenin, indicating that cell-cell contacts were not being disrupted. As this analysis was performed on fixed tissue it does not address whether disruptions caused by

PI3K inhibition are a transient event. Indeed, a transient loss of cell-cell contacts in the migration of epithelial cells has been reported in the migration of cells that from the neural crest (Theveneau et al., 2013). A transient loss in cell-cell contacts could be examined by expressing fluorescently labelled E-Cadherin and β-Catenin within isolated lung epithelium and then live imaging the cell-cell contacts as a branch develops.

We then examined if the regulators of β-Catenin, GSK3β and JNK, were influential in the branching response. Inhibition of GSK3β appeared to inhibit the branching of whole lung explants. Wnt signalling is required for proliferation and growth of the lung mesenchyme, mesenchymal deletion of β-catenin results in arrested lung growth and reduced branching (Yin et al., 2008). Therefore, overactive β-Catenin bought about through inhibition of GSK3β may cause hyper-proliferation of the mesenchymal cells that would have a knock-on effect of perturbing epithelial branching. Equally, hyperactive β-Catenin signalling in the lung epithelium reduces branching and causes an enlargement of the terminal air space. (Okubo and Hogan, 2004). We saw a similar morphological effect when we cultured isolated lung epithelium with FGF7 and an inhibitor of GSK3β. This effect was reduced with inhibition of PI3K. However, in the presence of a GSK3β inhibitor, PI3K inhibition was unable to initiate branching. This may suggest that PI3K inhibition induces branching via activation of GSK3β. Alternatively the effects of disrupting Wnt signalling via GSK3β inhibition may supersede the effect of PI3K inhibition.

We also examined the effect of JNK on lung branching as this kinase appears to directly regulated the pool of β-Catenin present at the adherens junctions (Lee et al., 2009). JNK inhibition failed to significantly effect either the branching of whole embryonic lung explants or the morphological effects induced by FGF7 with or without ZSTK474 in isolated lung epithelium. A non-requirement for JNK has also been reported for mammary gland branching (Cellurale et al., 2012). Others have reported a reduction in branching following JNK inhibition caused through an induction of apoptosis (Wu et al., 2009). We observed a similar cell death in explants treated with 10 μM of the JNK inhibitor compared with controls. However, we believe that this is likely due to the toxicity of the compound at these concentrations and not as a result of JNK inhibition.

A requirement for PI3K in the signalling output of FGF10 and FGF7 through FGFR2b has recently been reported from Hela cells overexpressing this receptor. Stimulation of FGFR2b by FGF10 resulted in the p85 subunit of PI3K being recruited to the receptor, separate from the classical Grb2/Gab1 interactions. Following internalisation, this interaction with PI3K led to the receptor being recycled to the cell membrane. In contrast, FGF7/FGFR2b signalling failed to recruit PI3K to this site and, upon internalisation, the receptor was degraded. Removal of this novel PI3K binding site from FGFR2b resulted in the degradation of the receptor following FGF10 simulation, producing a signalling outcome similar to FGF7 (Francavilla et al., 2013). PI3K, acting as a switch for FGFR2b trafficking, therefore appears to be a critical determinant for the signalling output of a ligand. Of particular note is that inhibition of PI3K with LY294002 was shown to promote the recycling of FGFR2b following stimulation by FGF7 (Francavilla et al., 2013). This work therefore lends a possible explanation as to how inhibition of PI3K is sufficient to promote branching from isolated lung epithelium cultured with FGF7. When PI3K signalling is inhibited, the FGFR2b receptor would be recycled, not degraded, following stimulation by FGF7. The net effect of this would then be an FGF10-like signalling event, i.e. a branching response.

This hypothesis could be examined in cultures of embryonic lungs by determining whether FGFR2b enters the recycling or late endosomes following stimulation with either FGF10 or FGF7. A shift from late to recycling endosomes following inhibition of PI3K would support the idea that PI3K acts to direct endosomal sorting of FGFR2b, which in turn determines the morphogenic outcome. To achieve this the proportion of FGFR2b entering either recycling or late endosomes could be visualised by immunofluorescence staining. Alternatively, using transfection methods outlined above, fluorescently labelled Rab11 (recycling endosomes, (Ullrich et al., 1996)), Rab7 (late endosomes, (Soldati et al., 1995)) and FGFR2b could be incorporated into cultures of embryonic lungs. The proportion of FGFR2b in the different endosomal compartments could then be imaged in real time. This would provide information as to whether PI3K is required for the regulation of branch initiation, elongation, or both.

FGF10 and FGF7 both act to regulate branching in the lung and salivary glands. In the lung, FGF10 promotes branch initiation and elongation (Bellusci et al., 1997) whereas FGF7 induces the formation of cysts (Cardoso et al., 1997). In the salivary gland FGF10 serves to promote bud elongation and FGF7 promotes branch budding (Makarenkova et al., 2009). Differences in FGF actions on the branching epithelium may therefore account for the reported differences in the function of PI3K in the salivary glands and lungs. In the salivary gland inhibition of PI3K would shift the action of FGF7 from a budding response to an elongation response (Figure 3.26). This reduction in budding may have the net effect of reducing branching, which is what is seen when PI3K is inhibited in salivary gland explant cultures (Larsen et al., 2003).

We propose that, in a setting where PI3K signalling is inhibited in the developing airways, FGF7 produced in the mesenchyme acting through FGFR2b is modulated to produce a signalling outcome similar to FGF10. This would have the net effect of inducing the formation of branches that would not otherwise develop (Figure 3.25B). Local reduction in PI3K activity in the branching epithelium may therefore add a novel mode of regulation during branching morphogenesis.

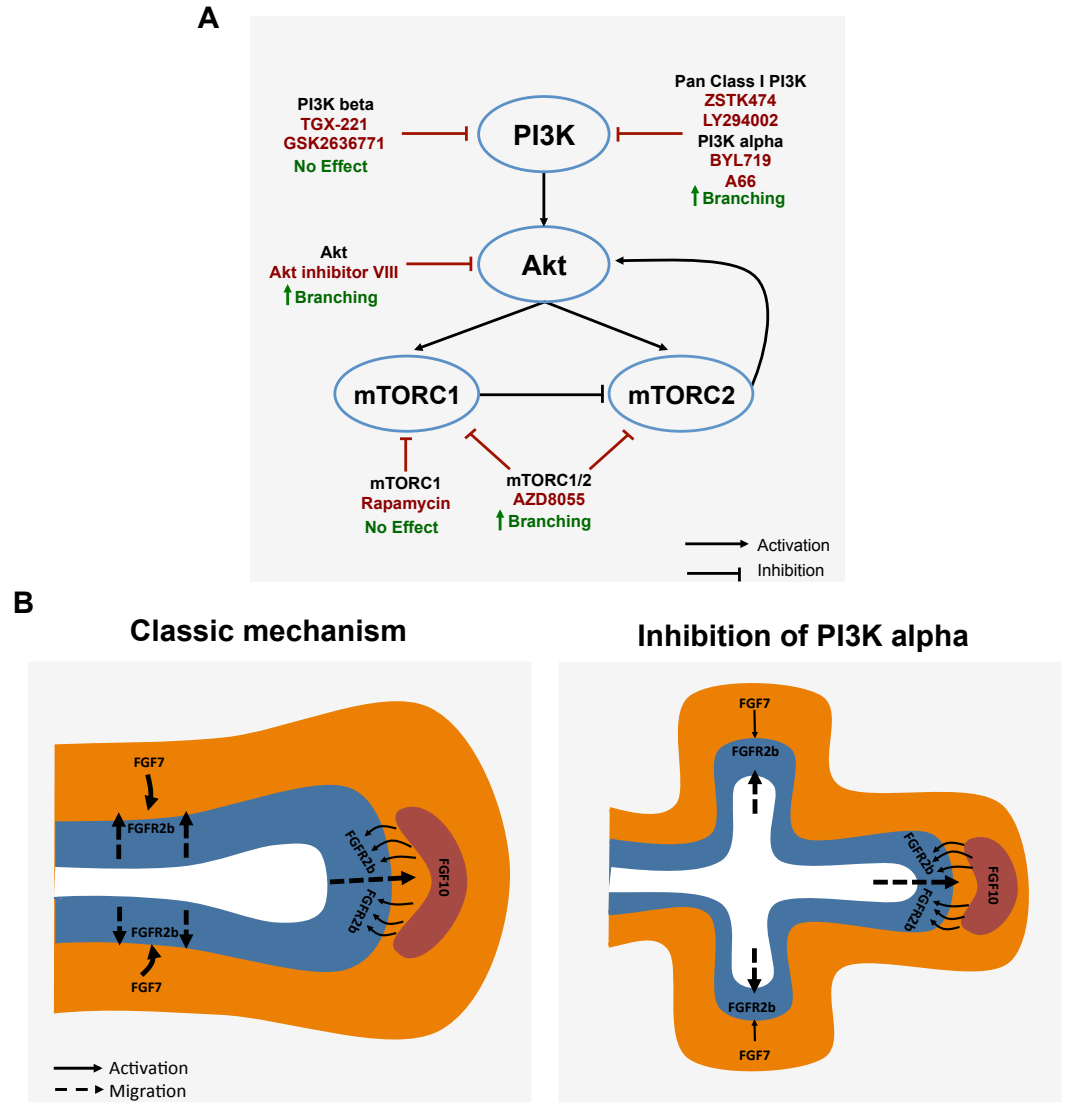

Figure 3.25. PI3K inhibition promotes branching morphogenesis through manipulation of FGF7 signalling. A. Sites of intervention for PI3K signalling and apparent effects of kinase activities on branching morphogenesis. Inhibitory pharmacological compounds are presented in red text with apparent biological effect in green. Pharmacological inhibition of either PI3Kα, Akt or dual inhibition of mTORC1/2 potentiates epithelial branching. Inhibition of either PI3Kβ or mTORC1 has no observable effects on branching. **B**. FGF10 and FGF7 signalling during lung branching morphogenesis. Lung epithelium is represented as blue with the surrounding mesenchyme as orange. Red represents FGF10 producing cells. Classically, FGF10 promotes branching whereas FGF7 induces the enlargement of the epithelium (left panel). In a setting where PI3K is inhibited (right panel) FGF7 signalling through FGFR2b is switched to an FGF10 signalling event. This has the outcome of inducing the formation of branches that would not otherwise develop.

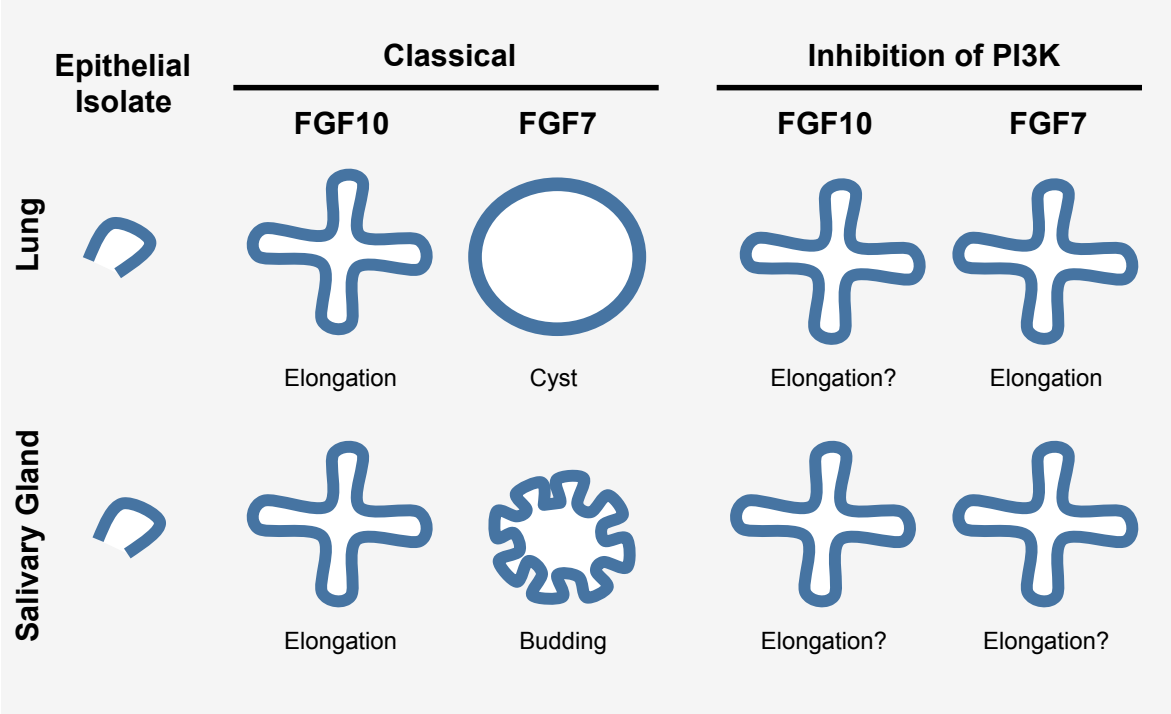

Figure 3.26. Proposed action of PI3K on the morphogenic responses of FGF10 and FGF7 in embryonic lung and salivary gland epithelium. Classically, FGF10 promotes branch elongation in both lung and salivary gland epithelium. FGF7 induces the formation of cystic structures in lung epithelium and branch budding in salivary gland. Following PI3K inhibition the elongation effect to FGF10 is potentially unaffected whereas the responses of FGF7 are switched to that of branch elongation.

Chapter 4: Immunogenicity of Cell-Penetrating Peptides

4.1 Background

CPPs are small peptides capable to transporting an otherwise cell impermeant cargo into the cytoplasm of mammalian cells. Originally derived from natural sources, many CPPs have been engineered for therapeutic applications and a number are currently in clinical trials for tissue scarring and cancer (Milletti, 2012). Despite appearing to be well tolerated in the clinic there is the possibility that these CPPs have inherent immunogenic properties that would make them impractical for therapeutic use. This seems plausible as many CPPs were originally derived, and contain protein sequences, from immunogenic substances. This is the case for the CPP HIV-TAT, which originated from a HIV protein (Frankel and Pabo, 1988) and several CPPs that have been derived from components present in animal venom (Gurrola et al., 2010; Rádis-Baptista and Kerkis, 2011).

Surprisingly, there is currently very little work into the possible immunogenic properties possessed by CPPs. Animals that have been administered CPPs show little immune response either at the site of administration or in the plasma (Khafagy et al., 2013; Suhorutsenko et al., 2011). However, one study has reported an innate immune response from mice that had been administered the CPP penetratin conjugated to an siRNA (Moschos et al., 2007). Interestingly, neither penetratin alone nor HIV-TAT induced a similar immune response. This may be due to inherent differences in immunogenicity between CPPs or results from differences in intracellular transport between a CPP: Cargo complex and a CPP alone.

The application of CPPs therapeutically would ideally be through a non-invasive route i.e. through the skin, airway or oral route. Through this course, CPPs would first encounter the epithelial cells that form a barrier between the body and the outside environment. It is these cells that would likely respond to any immunogenic properties possessed by the CPP molecule, potentially through pattern-recognition receptors. We therefore sought to examine the immunogenic potential of three of the most commonly used CPPs (HIV-TAT, Antennapedia and Transportan) on epithelial cell lines representing the skin, airways and intestine.

4.2 HIV-TAT, Antennapedia and Transportan effectively deliver a cargo into epithelial cells

We first examined the effectiveness of our CPPs by examining the uptake of a fluorescently labelled BSA cargo into epithelial cells. After 2 hours of incubation with CPP: BSA-568 complexes, using concentrations of CPP reported to deliver a protein based cargo, a fluorescent signal indicative of BSA incorporation was observed in A431 (epidermal), A549 (alveolar) and Caco-2 (intestinal) epithelial cells (Figure 4.1). A fluorescent signal was also observed from cells exposed to BSA-568 alone. Although this signal was comparatively weak compared to CPPs it would suggest that the epithelial cells were actively taking up some BSA.

To estimate the amount of CPP-mediated delivery of BSA-568 to the epithelial cell lines the fluorescence intensity of each image was measured relative to the number of cells in the field of view. This was compared to the fluorescent signal obtained similarly from cells exposed to the BSA-568 cargo alone, with the fold increase being used to estimate the extent of CPP-mediated uptake for a specific CPP and cell type (Figure 4.1). Although not statistically different, there was a trend for Antennapedia to be the most effective, although inconsistent, CPP for the delivery of this protein cargo, with HIV-TAT being the least.

We also examined the CPP-mediated delivery of a fluorescently labelled siRNA targeting Sjögren syndrome antigen B (SSB) to A549 cells. Following 2 hours of culture a strong fluorescent signal indicative of siRNA entry was observed from cells incubated with Antennapedia: siRNA complexes. A comparatively weak signal was seen from cells incubated with Transportan: siRNA complexes and very little uptake was observed following incubation with HIV-TAT: siRNA complexes (Figure 4.2A). After 48 hours of incubation, protein isolated from A549 cell was analysed for SSB knockdown by western blotting. Despite confocal microscopy demonstrating incorporation of SSB siRNA into A549 cells we could not detect any knockdown effect (Figure 4.2B).

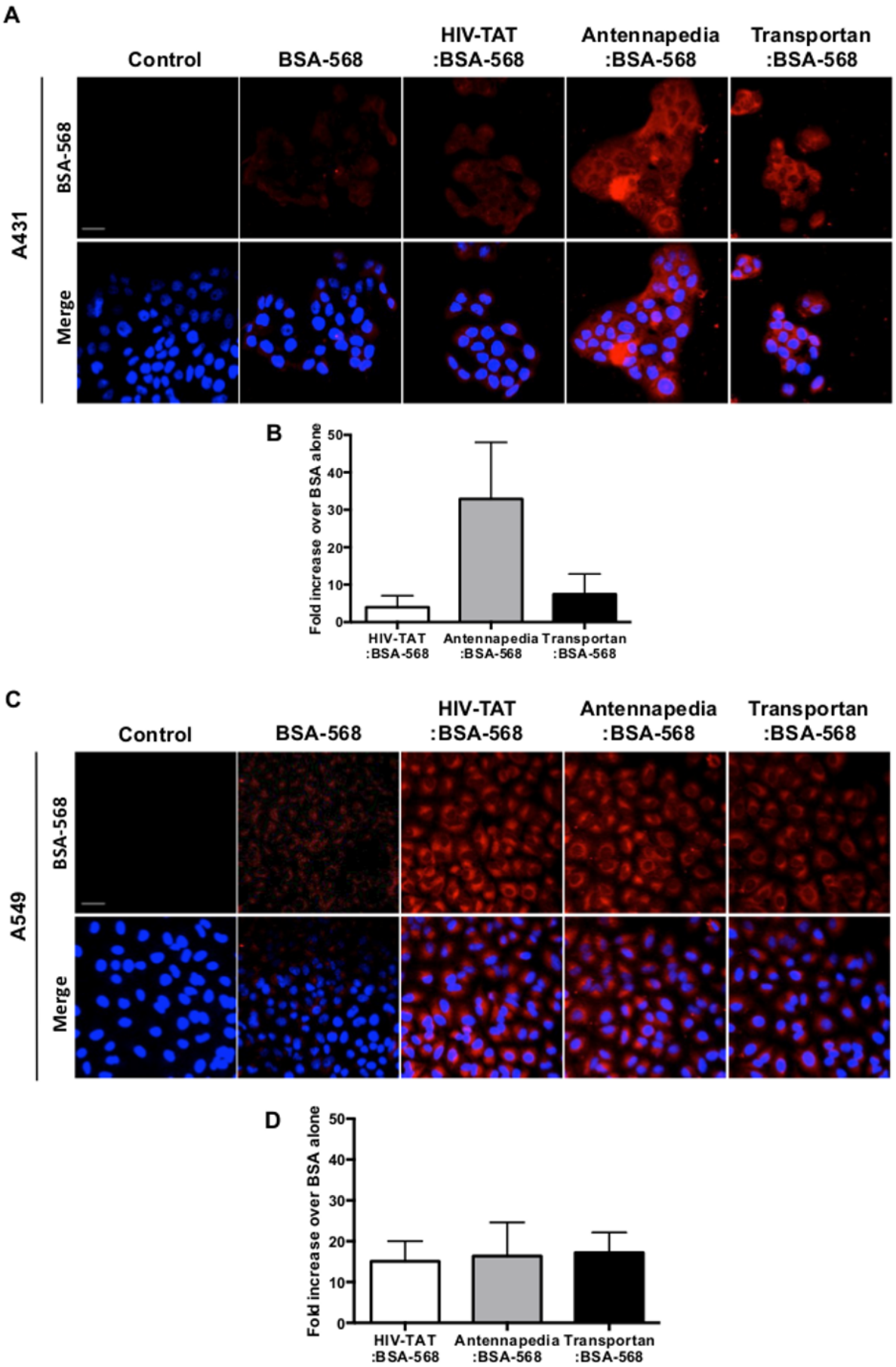
A
Control
BSA-568
HIV-TAT :BSA-568
Antennapedia :BSA-568
Transportan :BSA-568
A431
BSA-568
Merge
B
Fold increase over BSA alone
50
40
30
20
10
0
HIV-TAT :BSA-568
Antennapedia :BSA-568
Transportan :BSA-568
C
Control
BSA-568
HIV-TAT :BSA-568
Antennapedia :BSA-568
Transportan :BSA-568
A549
BSA-568
Merge
D
Fold increase over BSA alone
50
40
30
20
10
0
HIV-TAT :BSA-568
Antennapedia :BSA-568
Transportan :BSA-568

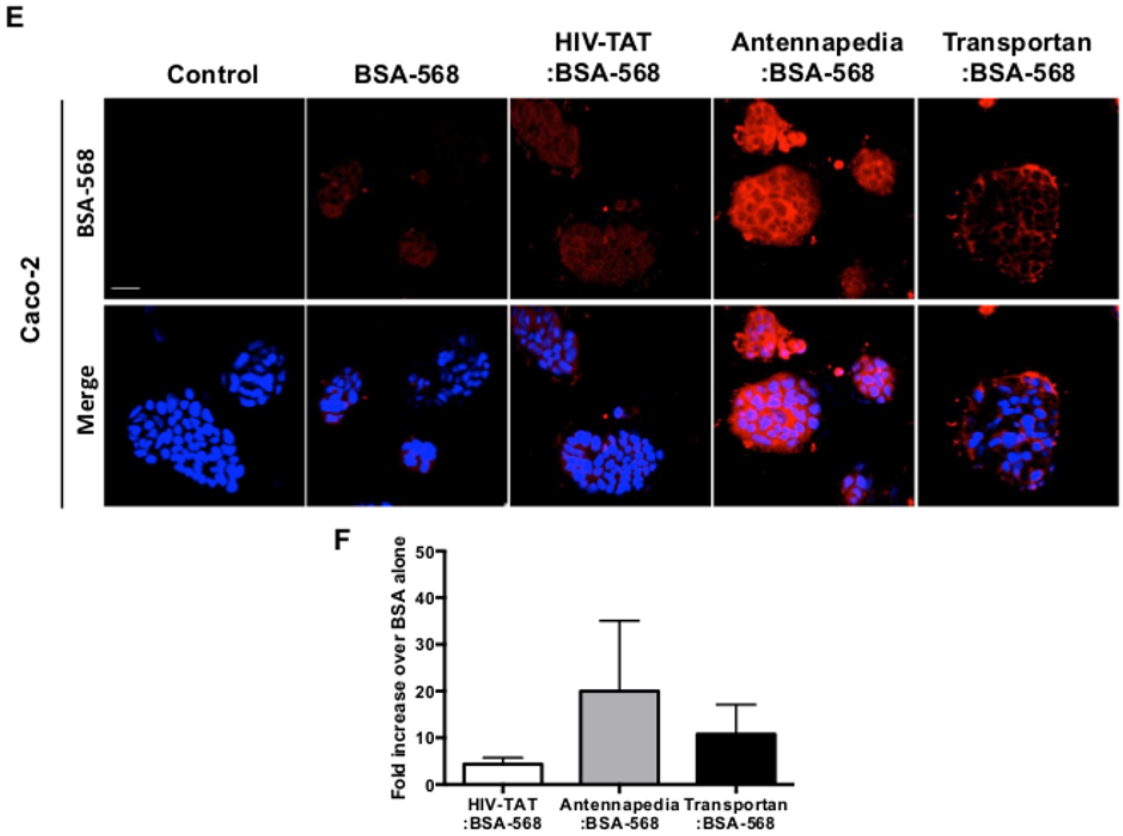

Figure 4.1. **CPPs mediate the entry of a protein cargo into epithelial cells.** Fluorescent images of A431 (**A**), A549 (**C**) and Caco-2 (**E**) epithelial cells exposed to BSA-568 (1 μM) alone or in complex with the CPPs HIV-TAT (20 μM), Antennapedia (20 μM) and Transportan (10 μM) for 2 hours. Images are representative of three independent experiments. Scale bar = 20 μm. The amount of CPP mediated delivery of BSA-568 to A431 (**B**), A549 (**D**) and Caco-2 (**F**) was estimated by comparing the increase in mean fluorescence intensity per cell from each CPP relative to BSA-568 alone. Data was pooled from fifteen separate images taken across three independent experiments.

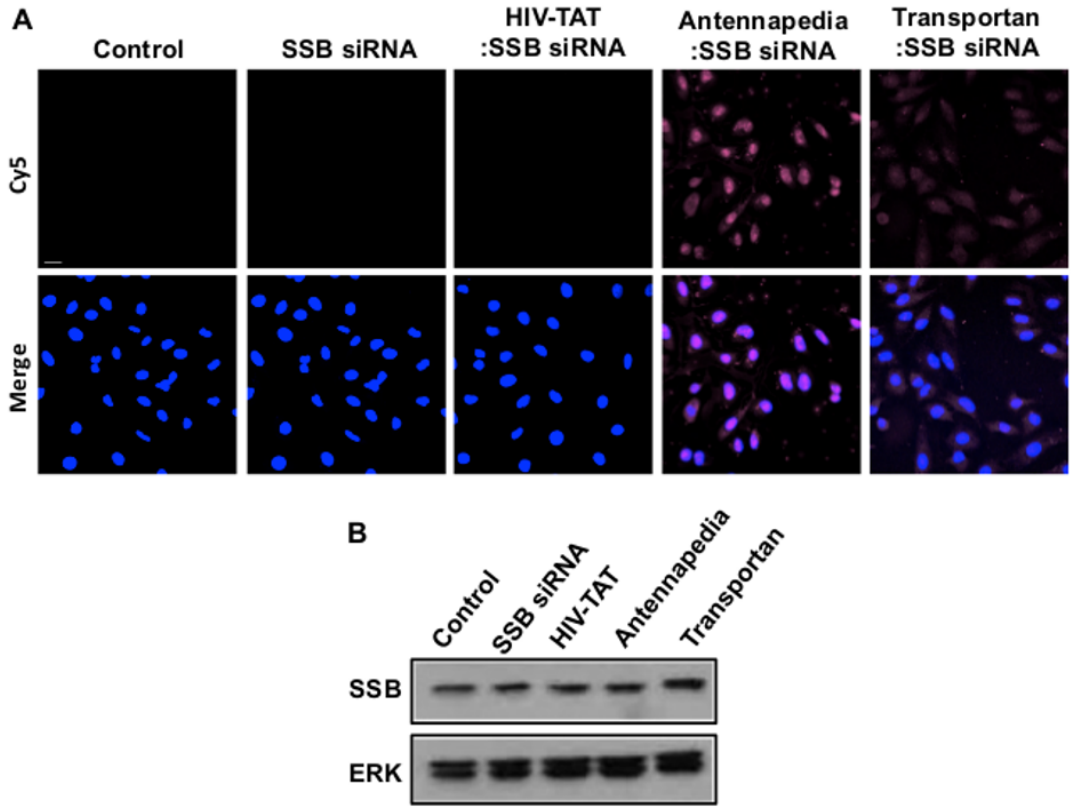

Figure 4.2. CPPs transport siRNA molecules into A549 cells but do not induce a knockdown effect. A. Fluorescent images of A549 cells exposed to VivoTag680 tagged SSB siRNA (10 nM) either alone or in complex with HIV-TAT (20 μM), Antennapedia (20 μM) or Transportan (10 μM) for 2 hours. Images are representative of two independent experiments. Scale bar = 20 μm. **B** Western blot analysis for levels of SSB and ERK following 48 hours of exposure of A549 cells to CPP: SSB siRNA complexes. Protein bands are representative of two independent experiments.

4.3 CPPs do not affect cell viability

It has been reported that CPPs at high concentrations can be cytotoxic to cells (Hansen et al., 2012; Kilk et al., 2009; Watkins et al., 2009). It was therefore prudent to establish if the concentrations of CPPs selected for these studies were exhibiting such an effect on the cells. We examined the effect of both CPPs alone and in complex with a cargo on cell viability as the interactions between a CPP and its cargo have been suggested to affect the transport of a CPP within a cell (Madani et al., 2011; Moschos et al., 2007). Compared to cargo alone we observed no change in cell viability for any of the CPPs examined across each of the cell types used as measured by MTT assay (Figure 4.3).

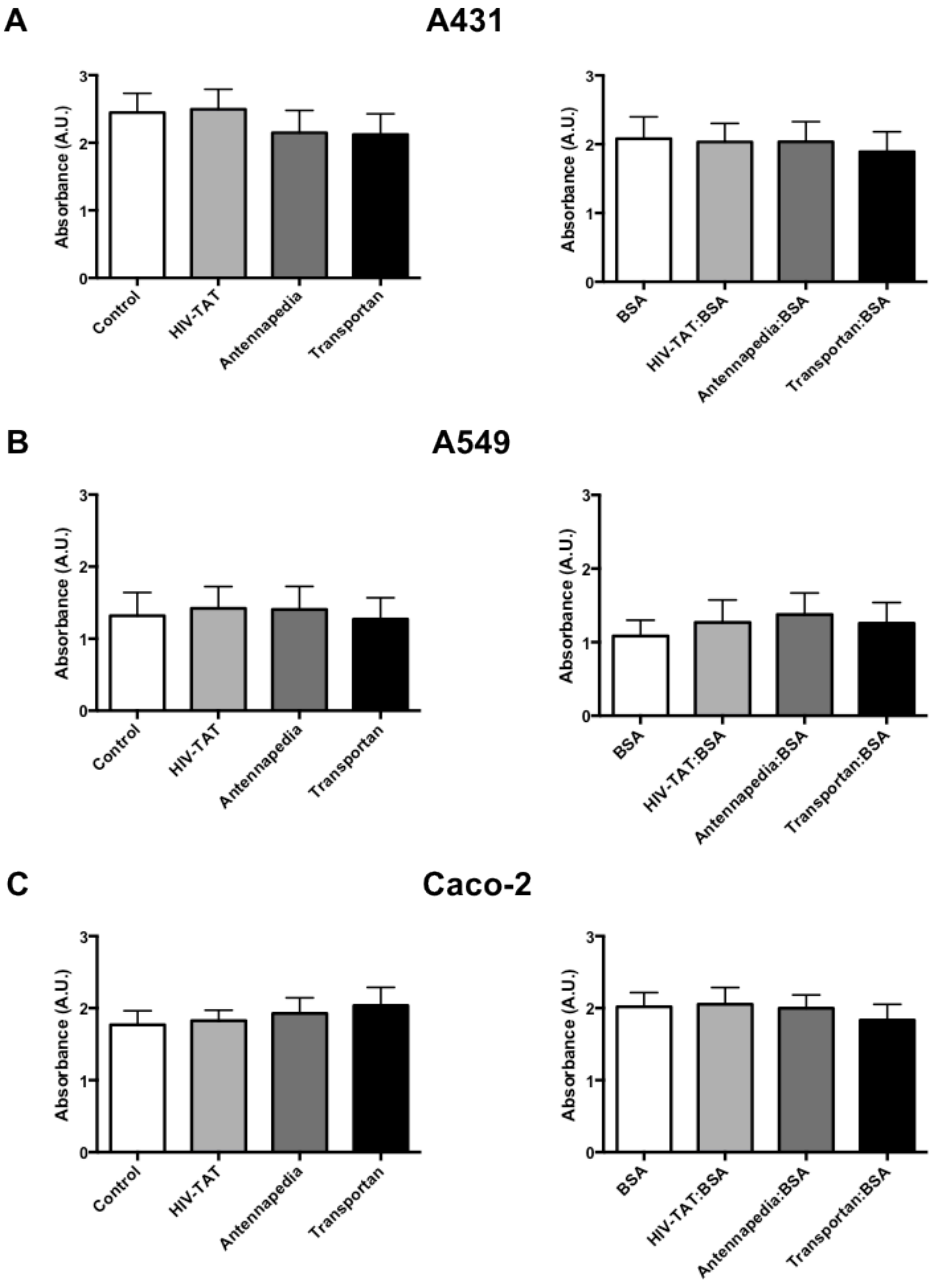

Figure 4.3. Epithelial cell viability is unaffected flowing exposure to CPP complexes. A431 (**A**), A549 (**B**) and Caco-2 (**C**) cells were exposed to HIV-TAT (20 μM), Antennapedia (20 μM) or Transportan (10 μM) either alone (left panels) or in complex with BSA (1 μM; right panels). After 72 hours of culture cells were assessed for viability by MTT assay. Values are expressed as mean ± s.e.m pooled from three independent experiments measured in triplicate.

4.4 CPPs do not activate the NFκB signalling pathway

We reasoned that if CPPs were having an immunogenic response in epithelial cells then they would most likely activate pattern recognition receptors. Once activated pattern recognition receptors signal via NFκB to induce the production of pro-inflammatory cytokines (Medzhitov et al., 1997). We therefore examined NFκB activation in epithelial cells after 2 hours of exposure to CPP: cargo complexes. Western blot analysis failed to detect any increase in phosphorylated levels of the p65 subunit of NFκB for any of the CPPs examined compared to cargo alone for the three epithelial cell lines examined (Figure 4.4). 2 ng/ml TNFα failed to induce an increase in phosphorylated NFκB but as the protein was extracted 2 hours post application of CPP complexes this may have been too late to observe an activation of NFκB signalling.

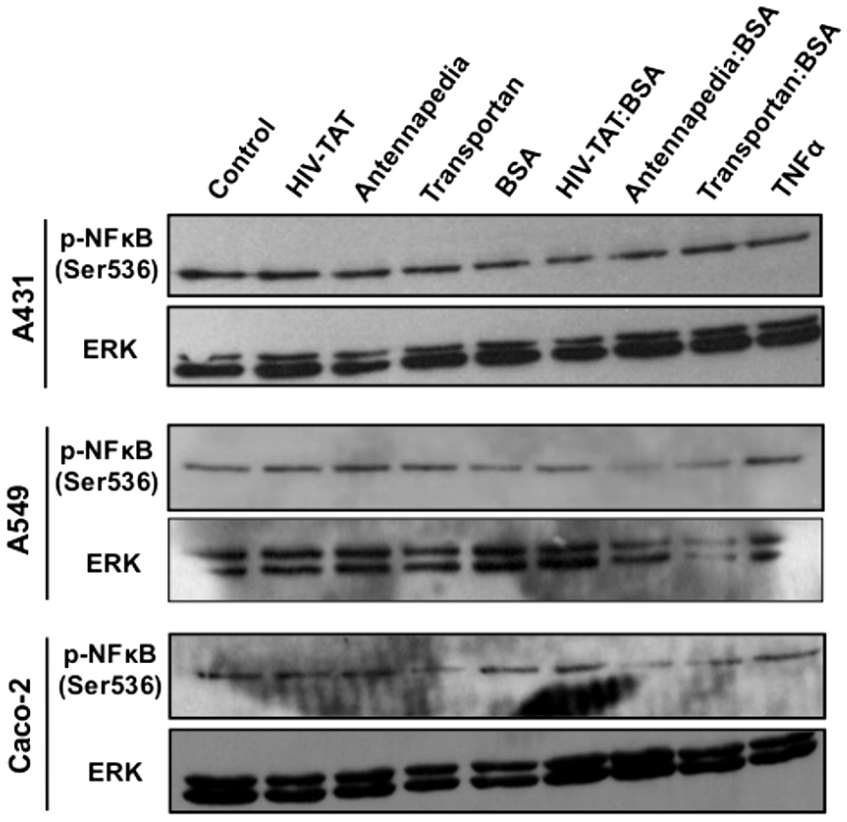

Figure 4.4. The NFκB pathway is not activated in epithelial cells following exposure to CPP complexes. A431 (Top panels), A549 (middle panels) and Caco-2 (bottom panels) cells were exposed to HIV-TAT (20 μM), Antennapedia (20 μM) or Transportan (10 μM) either alone or in complex with BSA (1 μM) for 2 hours. 2 ng/ml TNFα was used as a positive control. Cells were subsequently analysed for expression of phosphorylated NFκB. Expression of ERK is shown as a gel loading control. Protein bands are representative from three independent experiments.

4.5 CPPs do not induce the production of inflammatory mediators from epithelial cells

Epithelial cells release ‘danger signals’ in response to an immunogen in order to recruit inflammatory cells (Parker and Prince, 2011; Vareille et al., 2011). These include IL-6, which induces the activation of neutrophils (Borish et al., 1989), and IL-8, which promotes neutrophil recruitment (Atkins et al., 1977). Both of these cytokines are also released in response to pattern-recognition receptor activation (Adachi et al., 1998; Mukaida et al., 1990). Therefore if CPPs are indeed immunogenic then epithelial cells should release at least IL-6 and IL-8 in response. We collected supernatant from epithelial cells 72 hours after initial exposure to the CPPs alone, or in combination with a BSA protein cargo, in order to detect an early or delayed immune response. We also applied TNFα to the epithelial cells to induce the production of IL-6 and IL-8 as a positive control (Mukaida et al., 1990). We observed no difference in IL-6 (Figure 4.5) or IL-8 release (Figure 4.6) compared to cargo alone from any of the CPPs examined across the cell types tested. A431 and A549 cells demonstrated a robust increase in the release of IL-6 and IL-8 in response to TNFα. However, Caco-2 cells showed comparative low levels of IL-6 and IL-8 release in response to TNFα.

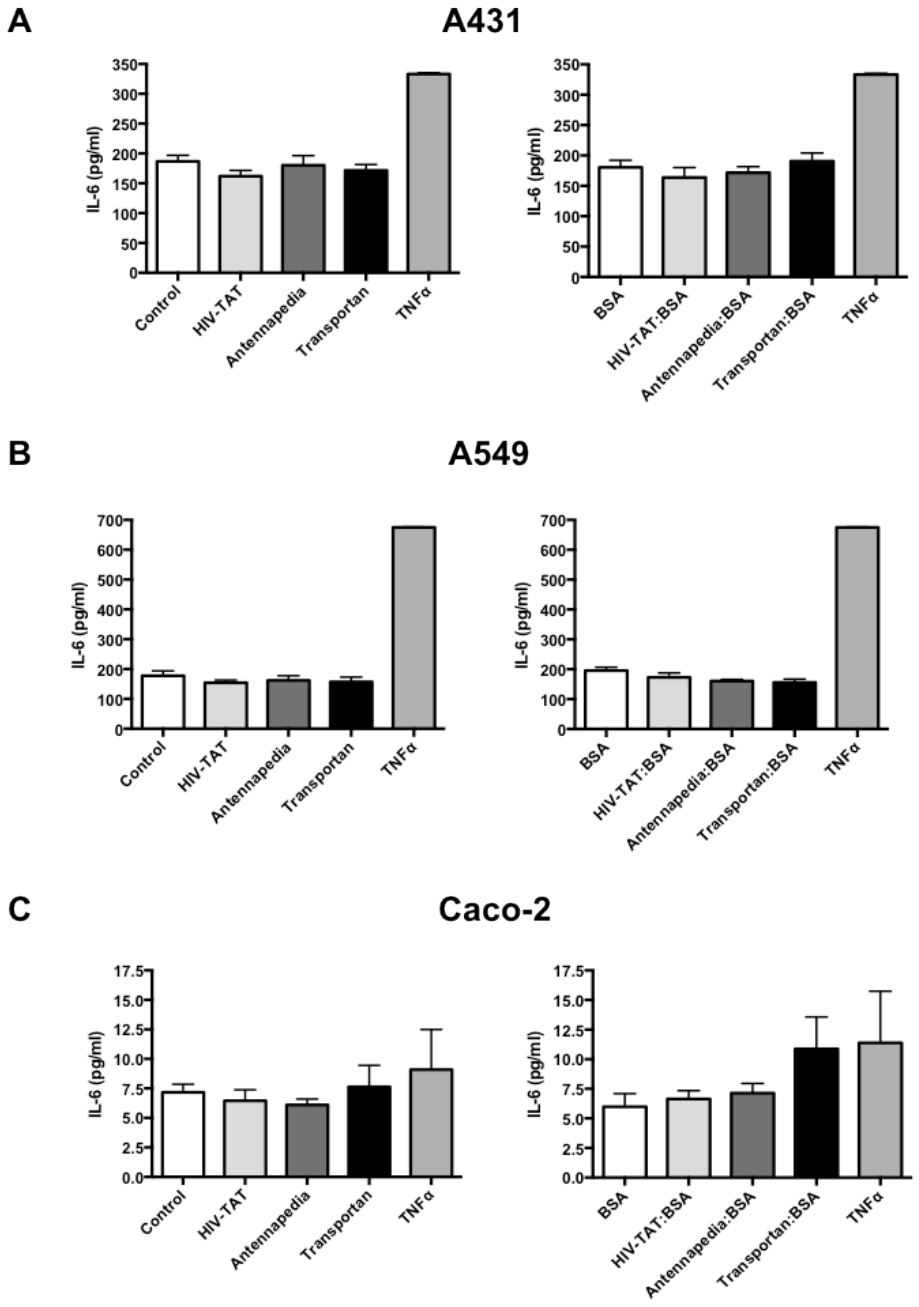

Figure 4.5. IL-6 production from epithelial cells is unchanged following exposure to CPP complexes. A431 (**A**), A549 (**B**) and Caco-2 (**C**) cells were exposed for 72 hours to the CPPs HIV-TAT (20 μM), Antennapedia (20 μM) or Transportan (10 μM) either alone (left panels) or in complex with a BSA protein cargo (1 μM; right panels). An ELISA based assay was used to evaluate IL-6 content from collected cell supernatants. 2 ng/ml TNFα was used as a positive control. Values are expressed as mean ± s.e.m pooled from three independent experiments measured in triplicate.

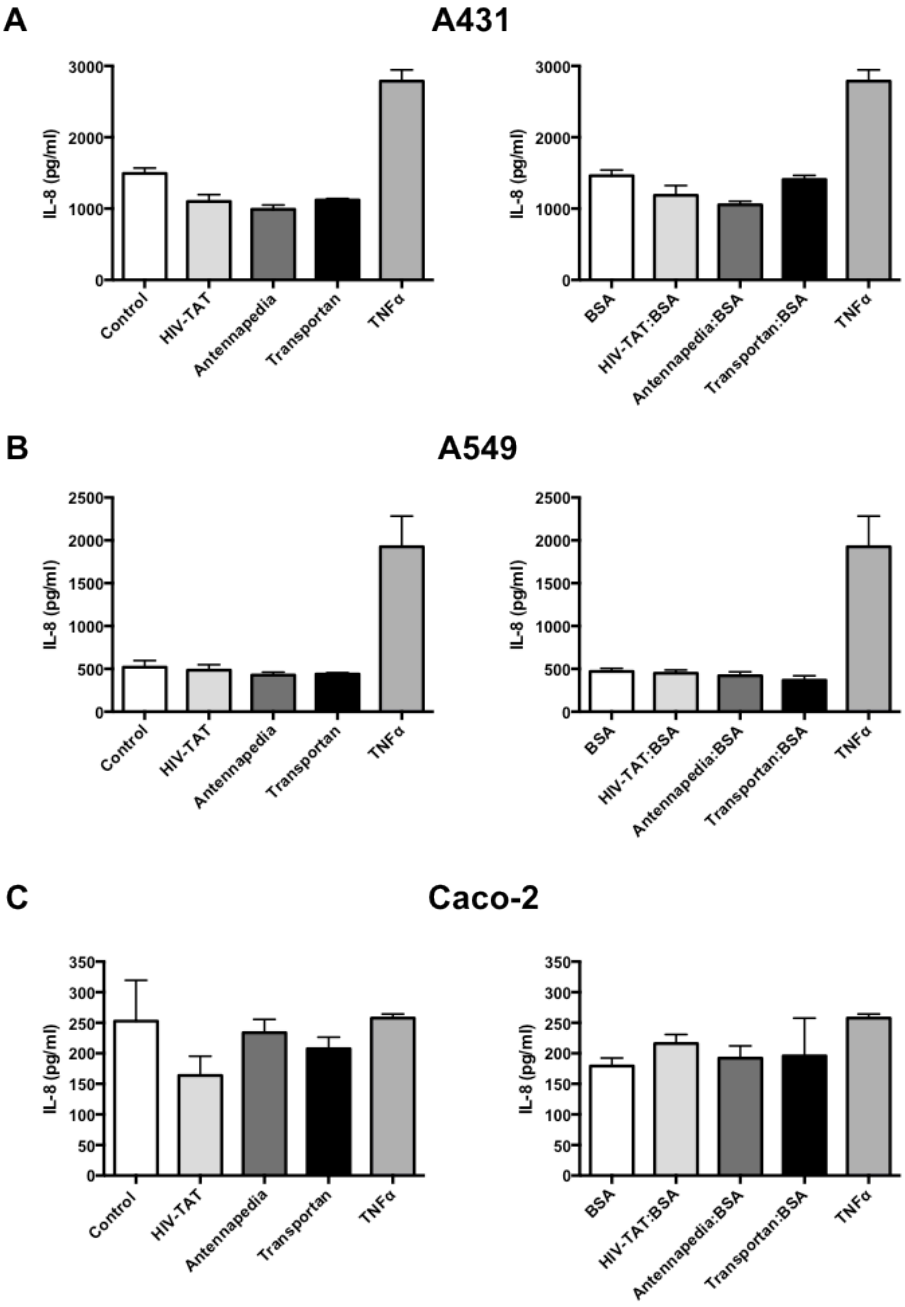

Figure 4.6. IL-8 production from epithelial cells is unchanged following exposure to CPP complexes. A431 (**A**), A549 (**B**) and Caco-2 (**C**) cells were exposed for 72 hours to the CPPs HIV-TAT (20 μM), Antennapedia (20 μM) or Transportan (10 μM) either alone (left panels) or in complex with a BSA protein cargo (1 μM; right panels). An ELISA based assay was used to evaluate IL-8 content from collected cell supernatants. 2 ng/ml TNFα was used as a positive control. Values are expressed as mean ± s.e.m pooled from three independent experiments measured in triplicate.

4.6 Summary of results

- The CPPs HIV-TAT, Antennapedia and Transportan can effectively deliver a fluorescently labelled BSA cargo into epithelial cells.
- CPPs can also deliver an siRNA cargo into cells. However, this delivery does not lead to efficient knockdown.
- The concentrations of CPPs used to deliver a cargo into cells do not affect epithelial cell viability after 72 hours of culture.
- NFκB signalling in epithelial cells does not appear to be activated following exposure to CPPs either alone or in complex with a protein cargo.
- Neither IL-6 nor IL-8 release is significantly affected 72 hours post exposure to CPPs either alone or in complex with a protein cargo.

4.7 Discussion

In this chapter we have demonstrated that CPPs can deliver a protein based cargo into epithelial cells lines representing the skin, airways and intestine. We observed a small amount of uptake from cells exposed to the labelled BSA cargo alone. It has been reported that epithelial cells can take up small amounts of BSA by clatherin-mediated endocytosis (Yumoto et al., 2012). This may suggest that the fluorescent signal from cells exposed to CPP: BSA complexes was simply the result of cellular uptake of the BSA cargo alone. However the large fold increase in fluorescence intensity between BSA alone and CPP: BSA complexes would suggest that BSA entry was being significantly enhanced by CPPs. We observed different levels of uptake for a fluorescently tagged BSA cargo between the CPPs HIV-TAT, Antennapedia and Transportan. This is consistent with previous observations that different CPPs can utilise separate routes of cargo delivery and therefore have different delivery efficacies (Lundin et al., 2008).

We also examined the ability of CPPs to deliver an siRNA cargo into A549 epithelial cells. Although we also observed siRNA in cells exposed to either Antennapedia or Transportan we were not able to detect a knockdown of the SSB protein. This lack of knockdown is probably the result of the CPP: siRNA complexes being retained in endosomes, thereby preventing the siRNA construct

from interacting with the cytoplasmic endoribonuclease Dicer to initiate knockdown. The retention of CPPs and their cargos within endosomes is a common caveat of CPP-mediated delivery (Rudolph et al., 2003). As a result, many of the CPPs in development today contain modifications to promote endosomal escape (Lo and Wang, 2008; Lundberg et al., 2007). To demonstrate the delivery of siRNA into cells with these CPPs an endosomolytic agent such as chloroquine would have to be added to the cells in order to release the CPP: siRNA complexes from endosomes (Rudolph et al., 2003). This would have been impractical for this study, as endosomolytic compounds may have affected the cellular response to a CPP. For instance, chloroquine has been demonstrated to have both anti- and pro- inflammatory responses (Fox, 1993; Park et al., 2003).

CPP-mediated cargo entry into epithelial cells did not appear to initiate an immune reaction from the epithelial cells examined in this study as evidenced by a lack of activation of NFκB signalling, and no increase in IL-6 or IL-8 release. Although this is not the complete repertoire of potential pro-inflammatory signalling molecules than can be released from epithelial cells in response to an immunogen or material that incites an inflammatory response, this outcome provides an indication that an overt immune response was not induced. We observed that the intestinal cell line, Caco-2, produced far less basal IL-6 and IL-8 compared to A431 and A549 cells and failed to respond to TNFα. The intestinal lining is host to a plethora of resident microbes. Intestinal cells therefore exhibit a level of tolerance to pro-inflammatory signals such as lipopolysaccharide and TNFα (Schuerer-Maly et al., 1994; Vitkus et al., 1998). The lack of response exhibited by Caco-2 cells is therefore likely the result of this native tolerance to pro-inflammatory signals.

The observation that the CPPs tested in this study do not induce an immune response is somewhat surprising given their derivation from harmful substances such as viruses and venoms (Frankel and Pabo, 1988; Gurrola et al., 2010; Rádis-Baptista and Kerkis, 2011); it would seem reasonable to presume that these CPP sequences could be recognised by cells as materials that could lead to infection and/or cell damage. Our data supporting that these CPPs can be used to deliver a protein cargo without acute cytotoxic or inflammatory outcomes is important for the

continued use of these molecules as therapeutic tools to enhance the cytoplasmic delivery of therapeutic agents.

In pharmaceutical applications involving topical delivery, the concentrations of CPPs are likely to be maximal for epithelial cells at the site of administration. Therefore epithelial cells would be a likely initiator of an immune response if CPPs were indeed immunogenic. Beyond epithelial cells, antigen-presenting cells are also a likely source of an immune response, as these cells would encounter CPPs in tissues and/or the vasculature following topical application. This has been examined elsewhere. CPPs added to the monocytic cell line THP-1 showed no release of pro-inflammatory cytokines (Suhorutsenko et al., 2011). Nevertheless, it remains to be established if CPPs can be presented to adaptive immune cells via major histocompatibility complex molecules. This would determine if CPPs could induce an adaptive immune response. A potential way to examine this would be to expose isolated antigen presenting cells to CPPs and then culture these with naïve $CD4^+$ T lymphocytes. The T lymphocytes could then be examined for activation, and skewing toward a particular T helper subset in response to CPP presentation by antigen presenting cells.

It has been established that the mechanism by which a CPP can enter a cell is dependent on the type of CPP and the cargo used (Lundin et al., 2008). Therefore, depending on the type of cargo, a CPP may be directed to an area of the cell where it interacts with a pattern recognition receptor that recognises the CPP sequence. This is plausible as several pattern recognition receptors, including toll-like receptors 3, 7, 8 and 9 are found in intracellular compartments (Brinkmann et al., 2007). Each type of cargo; oligonucleotides, plasmid DNA, protein etc., should therefore be examined when in complex with a CPP to give a more complete picture of the immunogenic potential of CPPs.

Future work could examine outcomes elicited by CPPs *in-vivo* where the full repertoire of possible immune responses can be observed. This has been examined for a few CPPs utilising protein (Khafagy et al., 2013), DNA (Suhorutsenko et al., 2011), and siRNA (Moschos et al., 2007) based cargos. Nevertheless, because of the variety of CPPs and cargos currently in

development, it would be prudent for researchers to investigate the immunogenicity of their own CPP with a particular cargo and a specific method of administration, since the nature of these events may be unique to their system.

Chapter 5: Bacterial Toxins as Drug Delivery Vehicles

5.1 Background

Bacterial toxins such as PEx, Chx and Dtx have been repurposed for therapeutic applications by replacing the receptor-binding domain of the toxin with a cell-specific antibody; thus creating highly toxic, cell specific immunotoxins (Pastan et al., 2006). The continuing success of these immunotoxins, as evidenced by the increasing number entering clinical trials, has spurred research into novel applications for these bacterial toxins. Bacterial toxins may be modified to transport a therapeutic cargo into target cells by exploiting their ability to be transported to the cell cytosol following internalisation (Mohammed et al., 2012). Although an intriguing idea, a potential obstacle for this approach is that, as toxins can exploit multiple pathways within cells (Smith et al., 2006a), it is conceivable that substantial amounts of toxin may be lost to degradative pathways that would result in an ineffective amount of therapeutic reaching the cytosol.

Identification of factors that influence the sorting of bacterial toxins within cells will likely help to overcome this caveat as toxins will be able to be further modified to exploit the most efficient route to the cytoplasm. A potential candidate is the lipid ganglioside GM1, the native receptor for cholera toxin, as structural changes to this lipid have been demonstrate to influence the intracellular target of cholera toxin. For example, the C16:1 ceramide chain variant of GM1 targets cholera toxin to the Golgi whereas the C18:0 variant directs transport to lysosomes (Chinnapen et al., 2012). This may be also true for PEx, which has been identified to bind to GM1 (R. Mrsny, unpublished observations) separately from its native receptor CD91 (Kounnas et al., 1992).

Naturally, PEx is secreted by *Pseudomonas aeruginosa* present at mucosal linings as a method of host immune evasion. PEx is passively transported across the polarised epithelial cells that comprise this lining and subsequently targets antigen presenting cells present in the sub-mucosal space (Mrsny et al., 2002). This observation suggests that a therapeutic cargo could be attached to a toxin as a means to transport the therapeutic across an epithelial barrier. This would allow the administration of macromolecule therapeutics through the airway (or possibly by the oral route) that would otherwise have to be administered by injection.

Questions remain as to whether these toxins would retain their ability to transport across epithelial surfaces while carrying a therapeutic cargo or if the cargo would still be biologically active following transcytosis.

In this chapter we sought to examine the utility of bacterial toxins as drug delivery vehicles. Using fluorescently labelled toxins in order to observe their transport within cells, we examined the role GM1 has in the cellular localisation of two bacterial toxins, PEx and Chx. Furthermore, we assessed the ability of these toxins to deliver an siRNA cargo to cells and whether such a cargo could be transported across epithelial monolayers.

5.2 PEx and Chx can enter and be transported within A431 epithelial cells

We initially examined whether the modified, fluorescently labelled, PEx and Chx retained their ability to be endocytosed into cells and were capable of being transported to distinct intracellular locations. PEx and Chx were tagged with Alexa Fluor 568 at a free cysteine residue introduced in place of the REDL sequence at the C-terminus (provided by Professor Randall Mrsny). These labelled toxins were added to non-polarised A431 epidermal cells expressing GFP-tagged markers that defined different intracellular compartments (Chinnapen et al., 2012). After 2 hours both PEx-568 and Chx-568 were present in the early endosomes (Rab5, (Bucci et al., 1992)), suggesting that they were endocytosed. Equally PEx and Chx were found in late endosomes (Rab7, (Soldati et al., 1995)) suggesting a proportion of the toxins were transported to lysosomal compartments. PEx and Chx were also present in sorting endosomes (Rab11, (Ullrich et al., 1996)), an element of the retrograde pathway. Comparatively little PEx-568 and Chx-568 was observed in the Golgi network (Golgin97, (Griffith et al., 1997)) and the ER (Sec61, (Deshaies et al., 1991)) (Figure 5.1). These observations demonstrate that both PEx-568 and Chx-568 are capable of entering non-polarised cells by endocytic mechanisms.

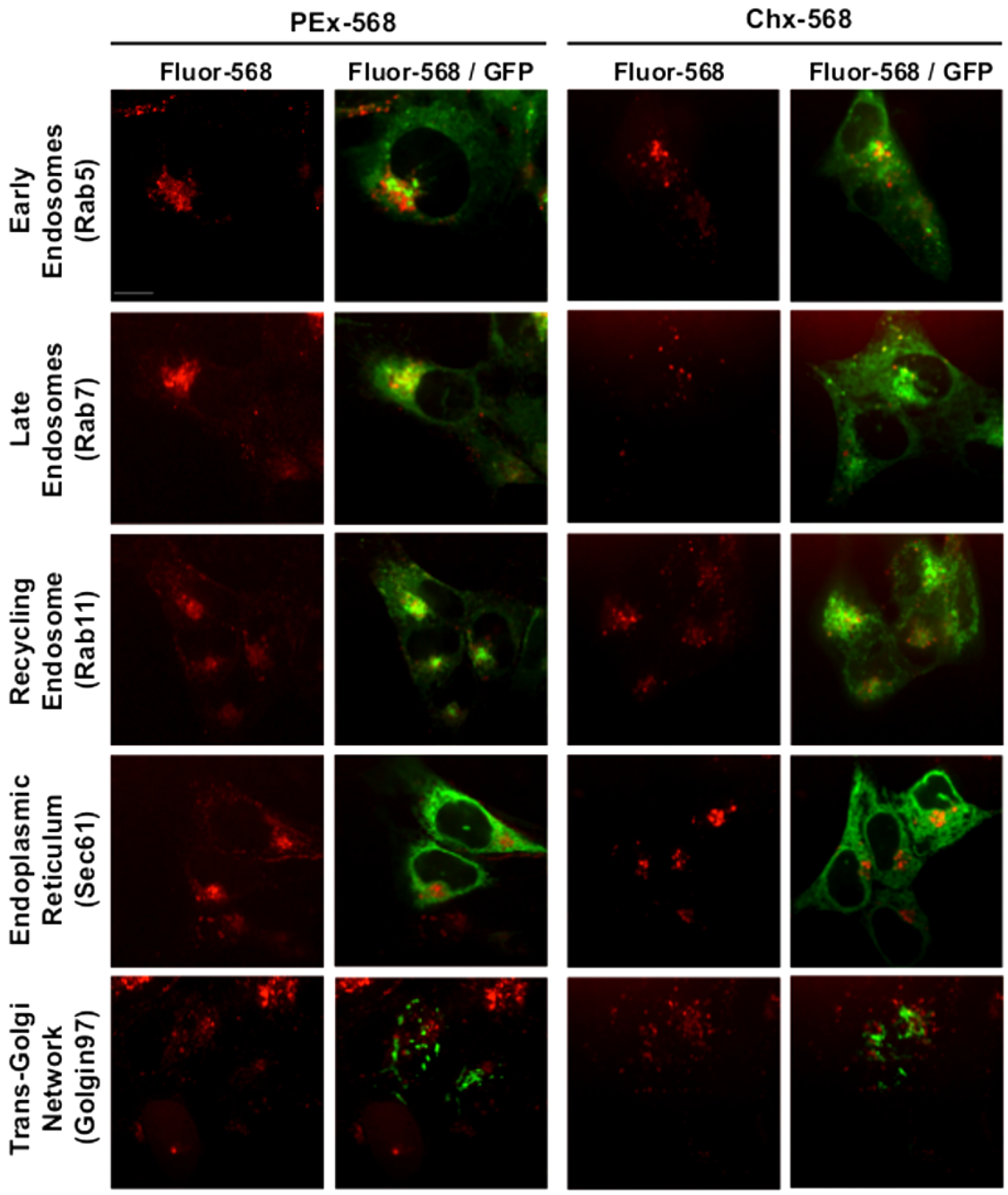

Figure 5.1. PEx and Chx enter non-polarised epithelial cells by endocytosis and are transported via the retrograde pathway. Fluorescent images of 20 µg/ml PEx-568 (left panels) and Chx-568 (right panels) within non-polarised A431 epidermal cells expressing either GFP tagged Rab5, Rab7, Rab11, Sec61 or Golgin97 after 2 hours. Images are representative of ten images taken over three independent experiments. Scale bar = 10 µm.

5.3 GM1 influences the intracellular transport of PEx

MEF cells deficient in GD2 synthase lack the capability to produce GM1 (Chinnapen et al., 2012). These cells are therefore incapable of internalising cholera toxin, which uses GM1 as a cell entry receptor (Holmgren et al., 1975). These $MEF^{GM1-/-}$ cells can be loaded with different structural variants of the ceramide chain of GM1 to assess the dependence of GM1 characteristics on cell entry and intracellular transport of a bacterial toxin. To confirm the efficiency of GM1 loading we incubated $MEF^{GM1-/-}$ cells with the B subunit of cholera toxin conjugated to Alexa Fluor 568 (CTB-568). CTB-568 was capable of being internalised into cells loaded with either the C16:1 or C18:0 variants of GM1. We observed a greater localisation of CTB-568 to the Golgi network in cells loaded with C16:1 GM1 compared to those loaded with C18:0 (Figure 5.2). This is consistent with the reported role for GM1 structure in the transport of CTB within cells (Chinnapen et al., 2012).

We next examined the influence of GM1 on the transport of PEx and Chx. After 2 hours of incubation, a very low level of fluorescent signal for Chx-568 was observed in un-loaded $MEF^{GM1-/-}$ cells. Incubation of CHx-568 with $MEF^{GM1-/-}$ cells loaded with either the C16:1 or C18:0 variants of GM1 demonstrated marginally greater levels of intracellular toxin, but no localisation to the Golgi network (Figure 5.3). Conversely, PEx was found to enter un-loaded $MEF^{GM1-/-}$ cells equally well to $MEF^{GM1-/-}$ cells loaded with either C16:1 or C18:0 (Figure 5.4A). To calculate the relative amount of PEx-568 that entered the Golgi network images were analysed using iMAB software as outlined in the materials and methods (Section 2.11). An example of the masks generated for PEx-568, the Golgi network, and the co-localisation between the two signals is represented in figure 5.4B. There was no difference in the relative amount of PEx present in the Golgi network between $MEF^{GM1-/-}$ cells and those loaded with C18:0. However, a significant increase in the amount of PEx in the Golgi network was observed for $MEF^{GM1-/-}$ cells loaded with C16:1 compared with unloaded $MEF^{GM1-/-}$ cells (Figure 5.4C).

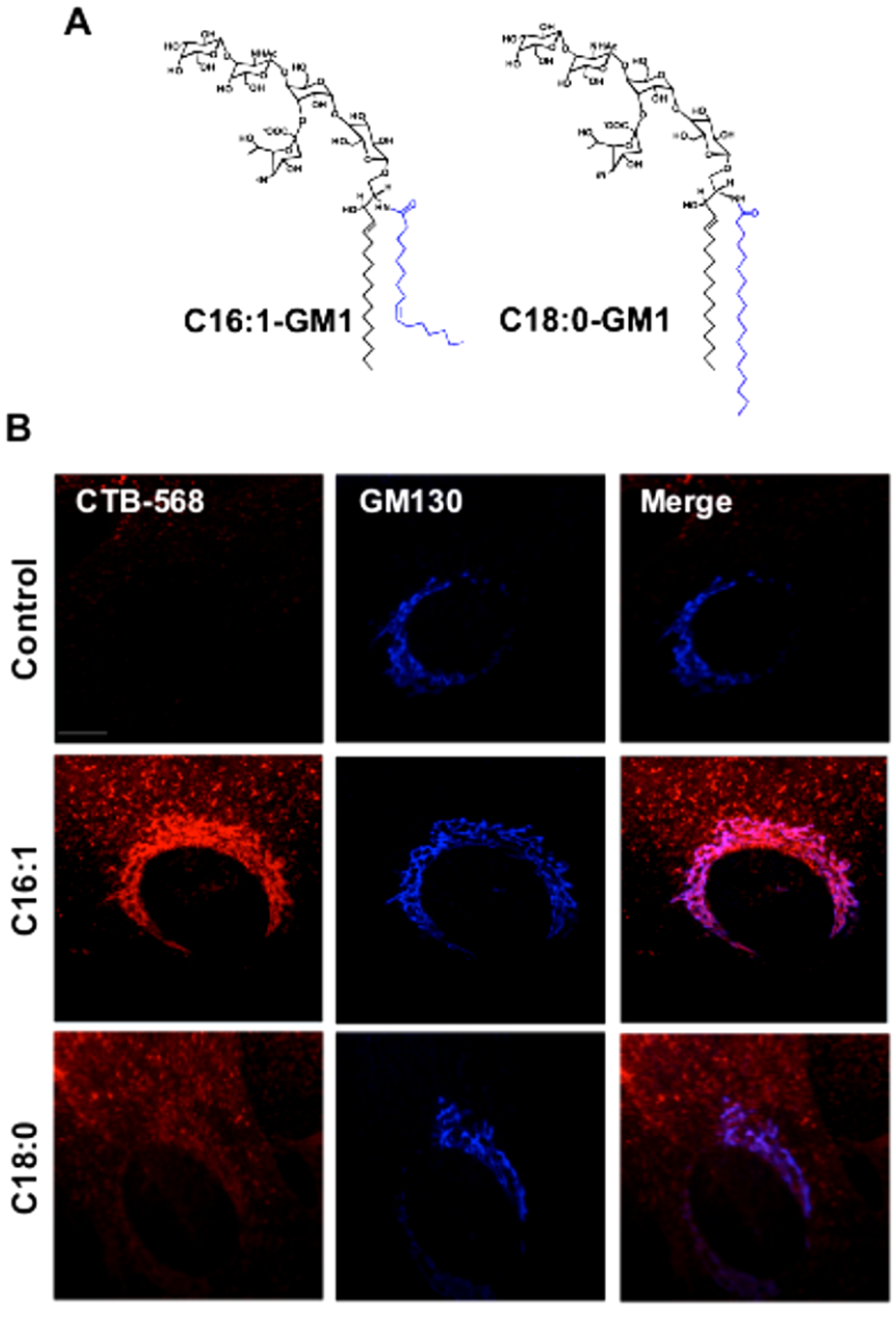

Figure 5.2. GM1 is required for CTB entry into cells and transport to the Golgi network. A. Schematic illustration of C16:1 and C18:0 ceramide chain structures of GM1. Adapted from (Chinnapen et al., 2012). **B**. Fluorescent images of 20 nM CTB-568 after 2 hours of incubation with $MEF^{GM1-/-}$ cells alone (Control) or $MEF^{GM1-/-}$ cells loaded with either 5 μM C16:1 or 7.5 μM C18:0 GM1. Expression of GM130 was used to visualise the Golgi network. Images are representative of twelve images acquired from three independent experiments. Scale bar = 10 μm.

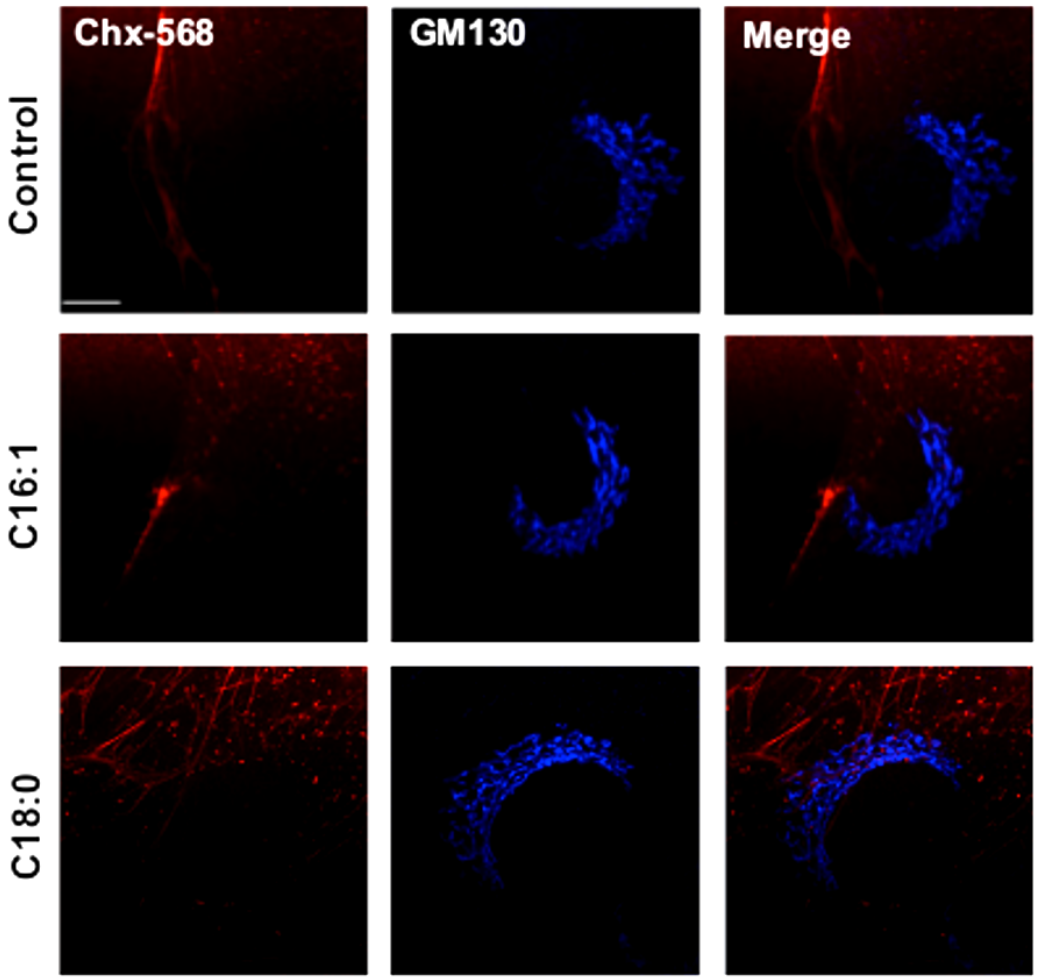

Figure 5.3. Chx transport is not dependent upon GM1 ceramide chain composition. Fluorescent images of 20 µg/ml Chx-568 after 2 hours of incubation with $MEF^{GM1-/-}$ cells alone (Control) or $MEF^{GM1-/-}$ cells loaded with either 5 µM C16:1 or 7.5 µM C18:0 GM1. Expression of GM130 was used to visualise the Golgi network. Images are representative of twelve images acquired from three independent experiments. Scale bar = 10 µm.

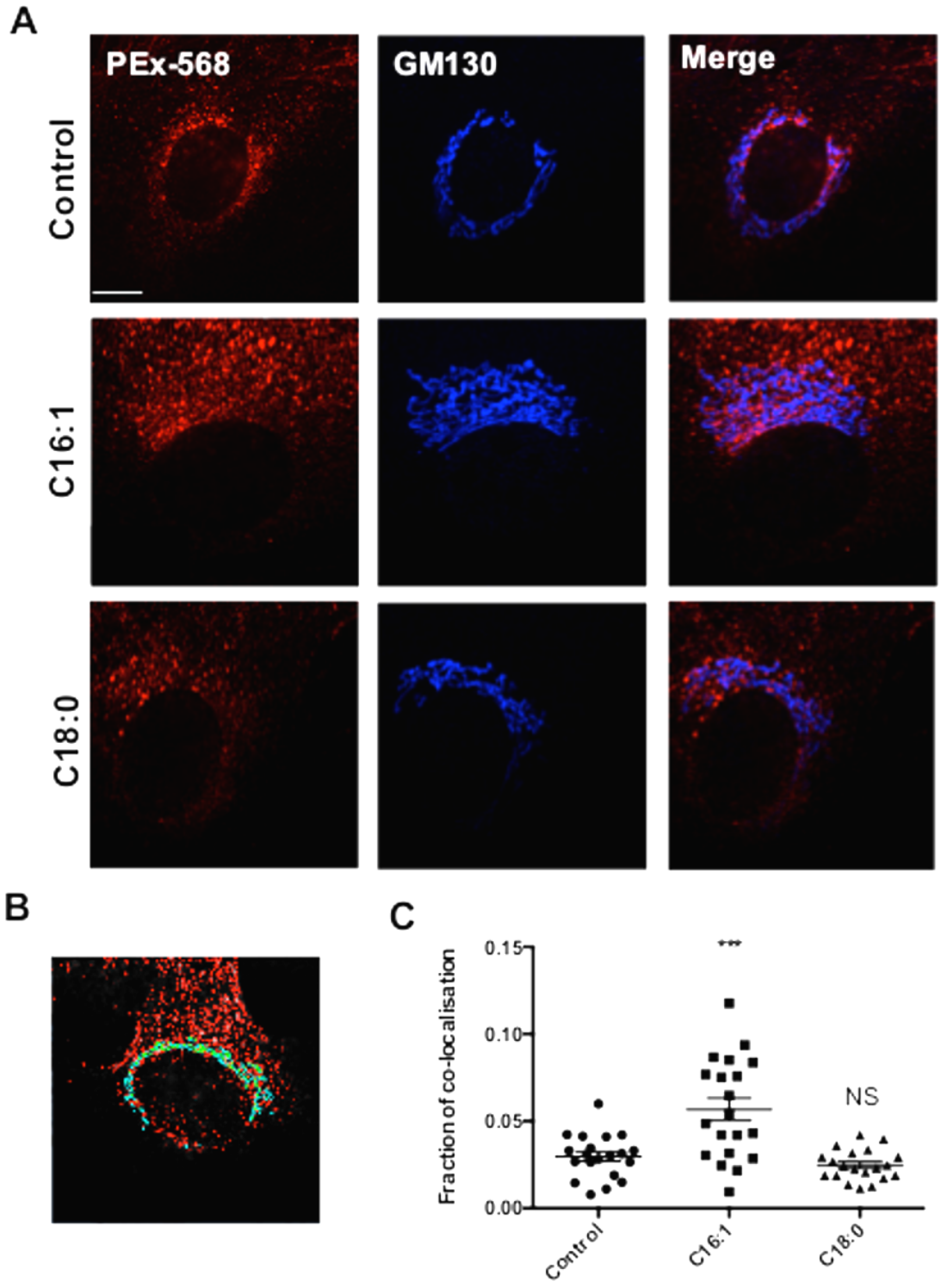

Figure 5.4. The C16:1 ceramide chain variant of GM1 enhances PEx transport to the Golgi network. A. Fluorescent images of 20 µg/ml PEx-568 after 2 hours of incubation with $MEF^{GM1-/-}$ cells alone (Control) or $MEF^{GM1-/-}$ cells loaded with either 5 µM C16:1 or 7.5 µM C18:0 GM1. Expression of GM130 was used to visualise the Golgi network. Images representative of twenty images acquired from three independent experiments. Scale bar = 10 µm. **B.** Example of mask generation using iMAB software. Masks are generated for areas of fluorescence for PEx-568 (Red), GM130 (Blue) and where both signals overlap (Green) **C.** Quantification of PEx-568 co-localisation with the Golgi network in MEF cells deficient in GM1 (Control) or loaded with either C16:1 or C18:0. *** P<0.001, NS = Not Significant, compared with control.

5.4 PEx and Chx do not utilise the same cell surface receptor for cell entry

The differences observed for PEx and Chx entry into MEFs is surprising as they were both thought to interact with CD91 given their sequence homology and the available cell data to date (Jørgensen et al., 2008). To understand if Chx does in fact use CD91 as a receptor we compared the entry of Chx-568 into CHO cells deficient in CD91 with PEx-568. After 2 hours of incubation a signal for PEx-568 was observed in wild type CHO cells (Figure 5.4). Conversely, PEx-568 was not detected in $CHO^{CD91-/-}$ cells, thus confirming a need for CD91 in the entry pathway for PEx (Kounnas et al., 1992). Unlike PEx, Chx was not detected in either wild type CHO or $CHO^{CD91-/-}$ cells (Figure 5.5).

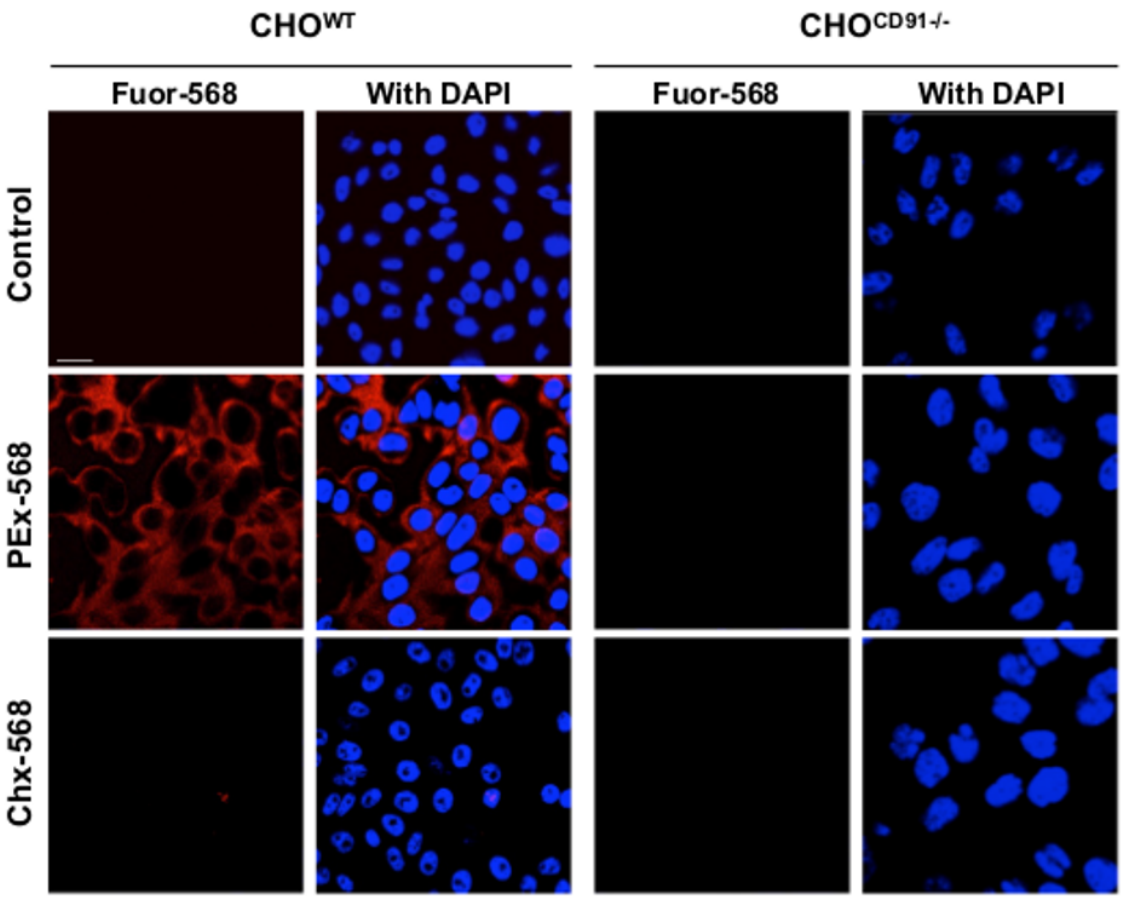

Figure 5.5. Chx does not share the same cell entry receptor as PEx. Fluorescent images of wild type and $CD91^{-/-}$ CHO cells incubated for 2 hours with HBSS (Control), or 20 µg/ml of either PEx-568 or Chx-568. Images are representative of two independent experiments. Scale bar = 20 µm

5.5 Transcytosis of PEx and Chx across polarised monolayers of Caco-2 cells

We next examined if PEx and Chx could be transported across polarised monolayers of Caco-2 epithelial cells, recapitulating the transport of these toxins across mucosal surfaces present at the airways and intestinal tract (Daugherty et al., 2000). Although PEx is an airway toxin Caco-2 cells were chosen for these experiments as they secrete less mucus than Calu-3 cells (Haghi et al., 2010), their respiratory counterpart. Mucus production would have interfered with toxin transcytosis preventing an adequate interpretation of their effectiveness. To assess the integrity of Caco-2 monolayers fluorescently labelled 4 kDa dextran was applied to the apical compartment, any subsequent fluorescent signal present in the basolateral compartment would therefore be proportional to the integrity of the monolayer. After 30 minutes of incubation with FITC labelled dextran a large fluorescent signal was measured in the basolateral compartment of transwells devoid of cells. Comparatively little dextran was measured in the basolateral compartment of transwells containing confluent monolayers of Caco-2 cells, thus confirming the integrity of the epithelial barrier (Figure 5.6A).

Transport of PEx and Chx across monolayers was assessed by initially applying 20 µg/ml of either PEx-568 or Chx-568 to the apical surface of Caco-2 cells and then measuring the amount of fluorescence present in the basolateral compartment after 15, 30, 60, 120 and 240 minutes. These values were then adjusted for background flourescence and the relative integrity of each respective monolayer assessed by the extent of 4 kDa dextran transport as outlined in the materials and methods (section 2.9). This type of correction for non-specific macromolecular transport not only corrected for monolayer-to-monolayer differences but could also be used to ensure that the forms PEx and Chx used in these studies had not negatively affected monolayer integrity. Both PEx and Chx were able to transport across polarised Caco-2 monolayers over 4 hours (Figure 5.6B). Although there was a trend for a higher amount of PEx to cross the cells compared to Chx this difference was not statistically different.

To determine if PEx and Chx could influence the transport of the other we assessed the transport of fluorescently labelled PE/Chx when incubated with increasing amounts of unlabelled Chx/PEx at the apical surface of Caco-2 monolayers. Both 20 and 200 µg of unlabelled Chx was able to greatly reduce the transport of PEx-568 across Caco-2 monolayers, which was significant at 120 and 240 minutes in the presence of 200 µg unlabelled Chx (Figure 5.6C). Conversely 20 µg of unlabelled PEx had no effect on the transport of Chx-568. Surprisingly, 200 µg of unlabelled PEx significantly enhanced the amount of Chx-568 that transported across monolayers at 120 and 240 minutes (Figure 5.6C).

Given that GM1 can influence the transport of PEx within non-polarised cells we wished to examine if GM1 could affect the transport of either PEx or Chx, across polarised Caco-2 cells. To examine this we applied PEx-568 and Chx-568 to the apical surface of Caco-2 monolayers along with equal amounts of CTB. If GM1 was involved in the transport of PEx or Chx, CTB should compete for GM1 and thus influence PEx and Chx transport. In the presence of 20 µg/ml of CTB the amount of PEx-568 that crossed polarised Caco-2 cells was significantly reduced compared to PEx-568 alone 30 minutes following application (Figure 5.7A). Conversely, 20 µg/ml of CTB increased the amount of Chx-568 that transported across Caco-2 cells compared to Chx-568 alone, which was significant at 240 minutes (Figure 5.7B).

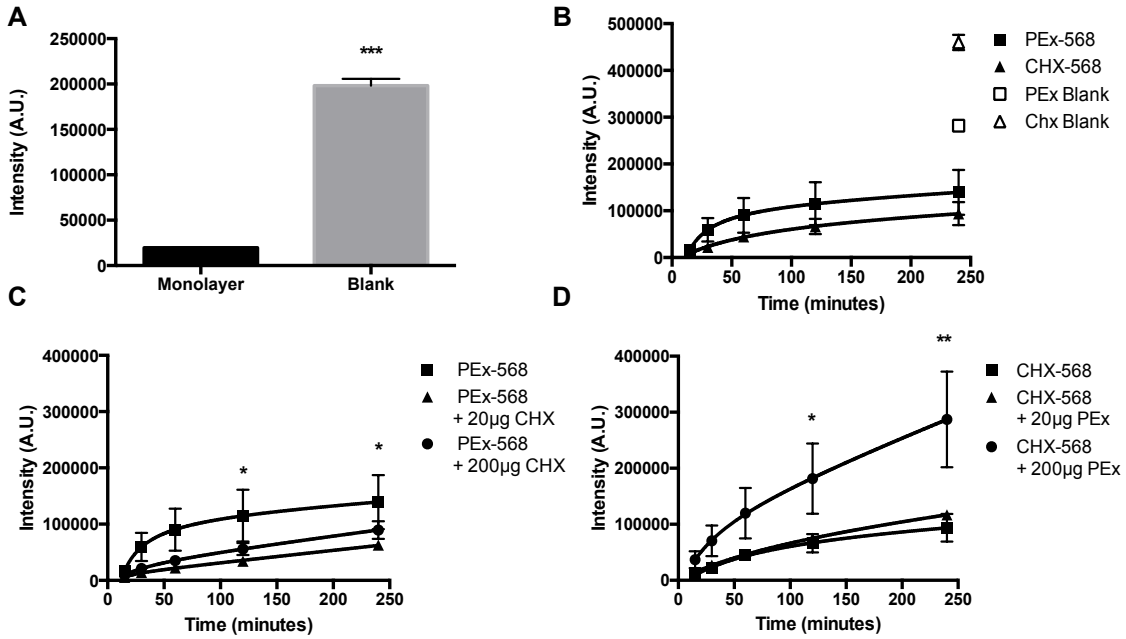

Figure 5.6. PEx and Chx transport across polarised epithelial cells. A. Amount of FITC-labelled 4 kDa dextran present in the basolateral compartment 30 minutes after apical addition to blank Transwells compared to Transwells supporting a confluent monolayer of Caco-2 cells **B**. Relative amount of 20 µg/ml of either PEx-568 (squares) or Chx-568 (triangles) present in the basolateral compartment over 240 minutes following initial application to the apical compartment of Caco-2 monolayers. The amount of PEx-568 (open squares) or Chx-568 (open triangles) that moved across blank transwells after 240 minutes of incubation is depicted. **C**. Relative amount of 20 µg/ml PEx-568 transported across Caco-2 monolayers over 240 minutes either alone (squares) or in the presence of either 20 (triangles) or 200 (circles) µg/ml of unlabelled Chx. **D**. Relative amount of 20 µg/ml Chx-568 transported across Caco-2 monolayers over 240 minutes either alone (squares) or in the presence of either 20 (triangles) or 200 (circles) µg/ml of unlabelled PEx. Data presented as mean ± s.e.m for each time point pooled from two independent experiments, totalling six individual wells. * P<0.05, ** P<0.01, *** P<0.001, compared to control at respective time point where appropriate.

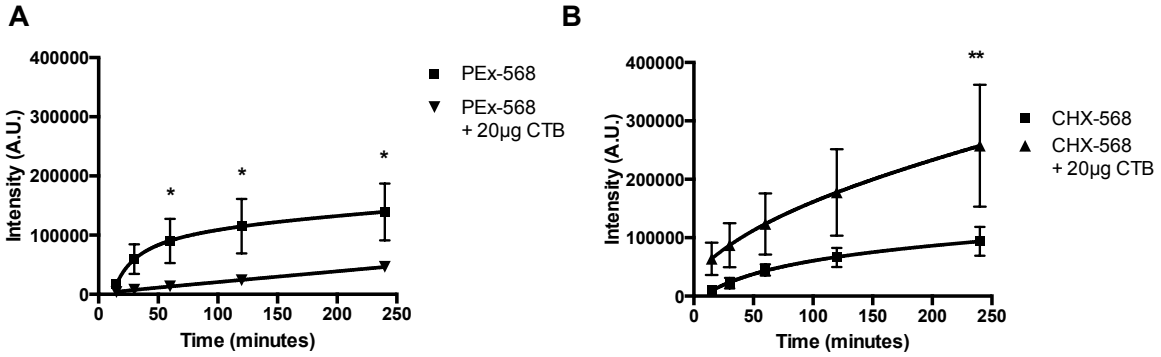

Figure 5.7. GM1 influences PEx and Chx transport across polarised epithelial cells. A. Relative amount of 20 µg/ml PEx-568 transported across Caco-2 monolayers either alone (squares) or in the presence of 20 µg/ml CTB (triangles) over 240 minutes. **B**. Relative amount of 20 µg/ml Chx-568 transported across polarised Caco-2 cells either alone (squares) or in the presence of 20 µg/ml CTB (triangles) over 240 minutes. Data presented as mean ± s.e.m fluorescence for each time point pooled from two independent experiments, totalling six individual wells. * P< 0.05, ** P<0.01, compared to control at respective time point.

5.6 PEx can transport and deliver an siRNA cargo into macrophages

The final facet of this project sought to examine the utility of using bacterial toxins as a delivery vehicle for therapeutics. We attached a siRNA targeting Sjögren syndrome antigen B (SSB) at the C-terminus of non-toxic PEx using the same conjugation strategy and chemistry used to attach the Alexa 568 dye. The siRNA duplex itself was labelled with the VivoTag680s that allowed its fate to be monitored. We initially examined these constructs in J774.2 macrophages as macrophages (or other antigen presenting cells) are the end targets for PEx as part of the immune evasion employed by *Pseudomonas aeruginosa* (Mrsny et al., 2002). Both siRNA alone and PEx tagged with either Alexa Fluor 488 or VivoTag680 SSB siRNA was observed in J774.2 macrophages 1 hour after administration (Figure 5.8A). This signal persisted 24 hours post administration although the signal was diminished. After 48 hours of incubation with the constructs we observed a knockdown of SSB protein from macrophages cultured with PEx conjugated to the SSB siRNA but not from macrophages cultured with SSB siRNA alone (Figure 5.8B). This would indicate that PEx-siRNA was not phagocytosed, but instead entered macrophages through CD91 mediated endocytosis and was transported to the cytoplasm where the siRNA could elicit a knockdown effect.

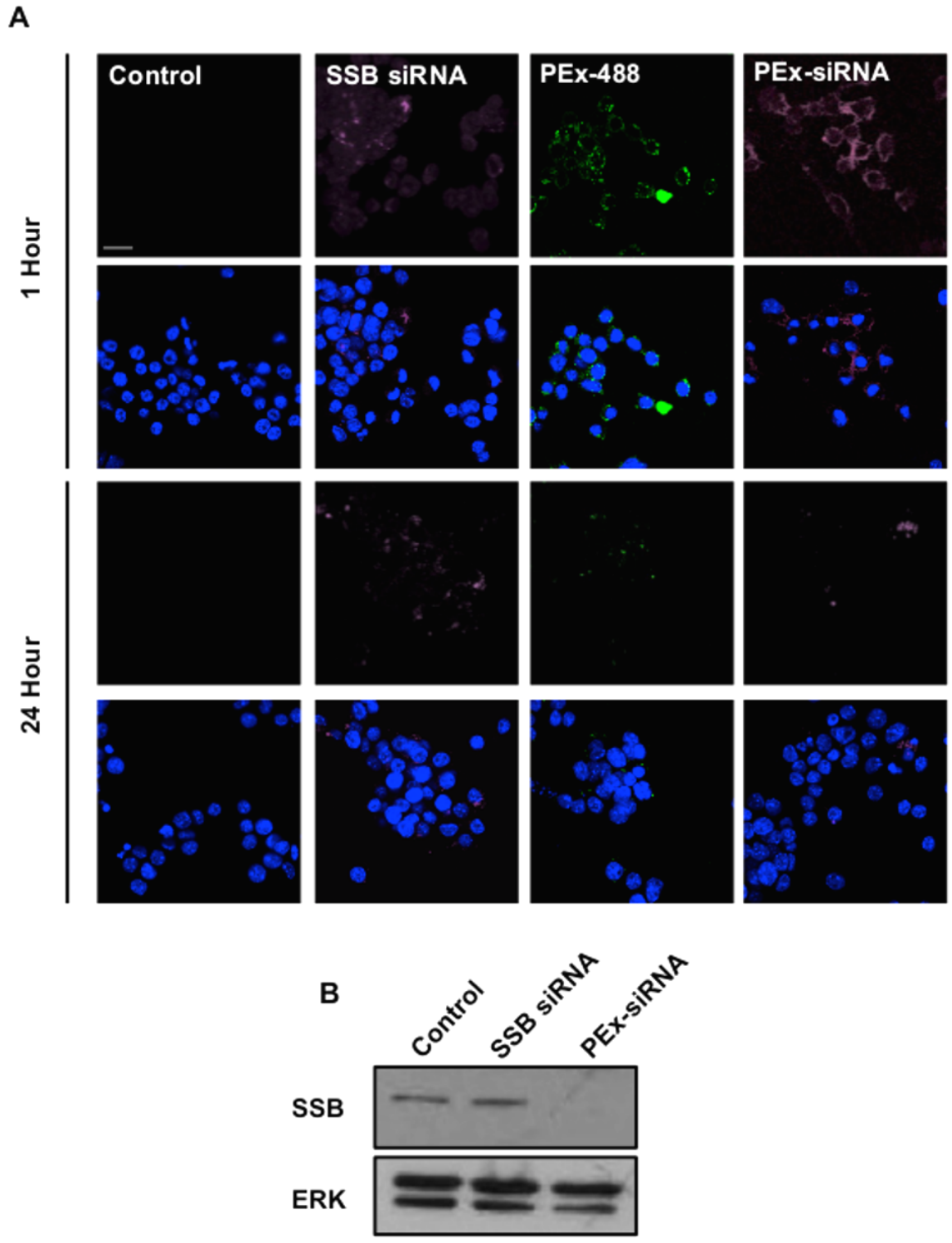

Figure 5.8. PEx can deliver an siRNA cargo into macrophages to elicit a knockdown effect. A. Fluorescent images of J774.2 macrophages incubated for 1 or 24 hours with HBSS (Control), VivoTag680 tagged SSB siRNA (SSB siRNA; 10 nM), PEx tagged with Alexa Fluor 488 (PEx-488; 20 µg/ml) or an equivalent fluorescent amount of PEx tagged with VivoTag680 tagged SSB siRNA (PEx-siRNA). Images are representative of three independent experiments. Scale bar = 20 µm **B**. Western blot analysis for levels of SSB and ERK from J774.2 macrophages incubated with either SSB siRNA alone or PEx tagged with SSB siRNA for 48 hours. Protein bands representative of three separate experiments.

PEx and Chx can transport an siRNA cargo across polarised Caco-2 cells and subsequently deliver a cargo into macrophages

Next, we examined if an siRNA cargo could be transported across polarised monolayers of Caco-2 cells. PEx, or Chx, conjugated to a VivoTag680 tagged SSB siRNA was applied to the apical surface of Caco-2 monolayers. After 2 hours both PEx-siRNA and Chx-siRNA was observed in Caco-2 monolayers although their localisation differed (Figure 5.9A). PEx-siRNA appeared to be transported throughout the cytoplasm of polarised Caco-2 cells, whereas Chx-siRNA was observed within the periphery of the cells. To explore this further we examined the co-localisation of labelled bacterial toxins with the tight junction marker occludin. PEx-siRNA weakly co-localised with occludin whereas Chx-siRNA strongly co-localised (Figure 5.9B).

Once we established that an siRNA cargo could be transported through polarised epithelial cells by PEx and Chx we next sought to establish if these toxins could still deliver an siRNA cargo to cells present in the basolateral compartment. 2 hours after the apical addition of labelled toxins to Caco-2 monolayers no siRNA or PEx-siRNA was detected in J774.2 macrophages present in the basolateral compartment of Transwell chambers. However, after 24 hours PEx-siRNA, but not siRNA alone, was observed in macrophages (Figure 5.10A). Moreover, knockdown of SSB was observed in J774.2 macrophages cultured in the basolateral compartment of Caco-2 monolayers incubated with PEx-siRNA but not in those cultured with monolayers exposed to siRNA alone (Figure 5.10B).

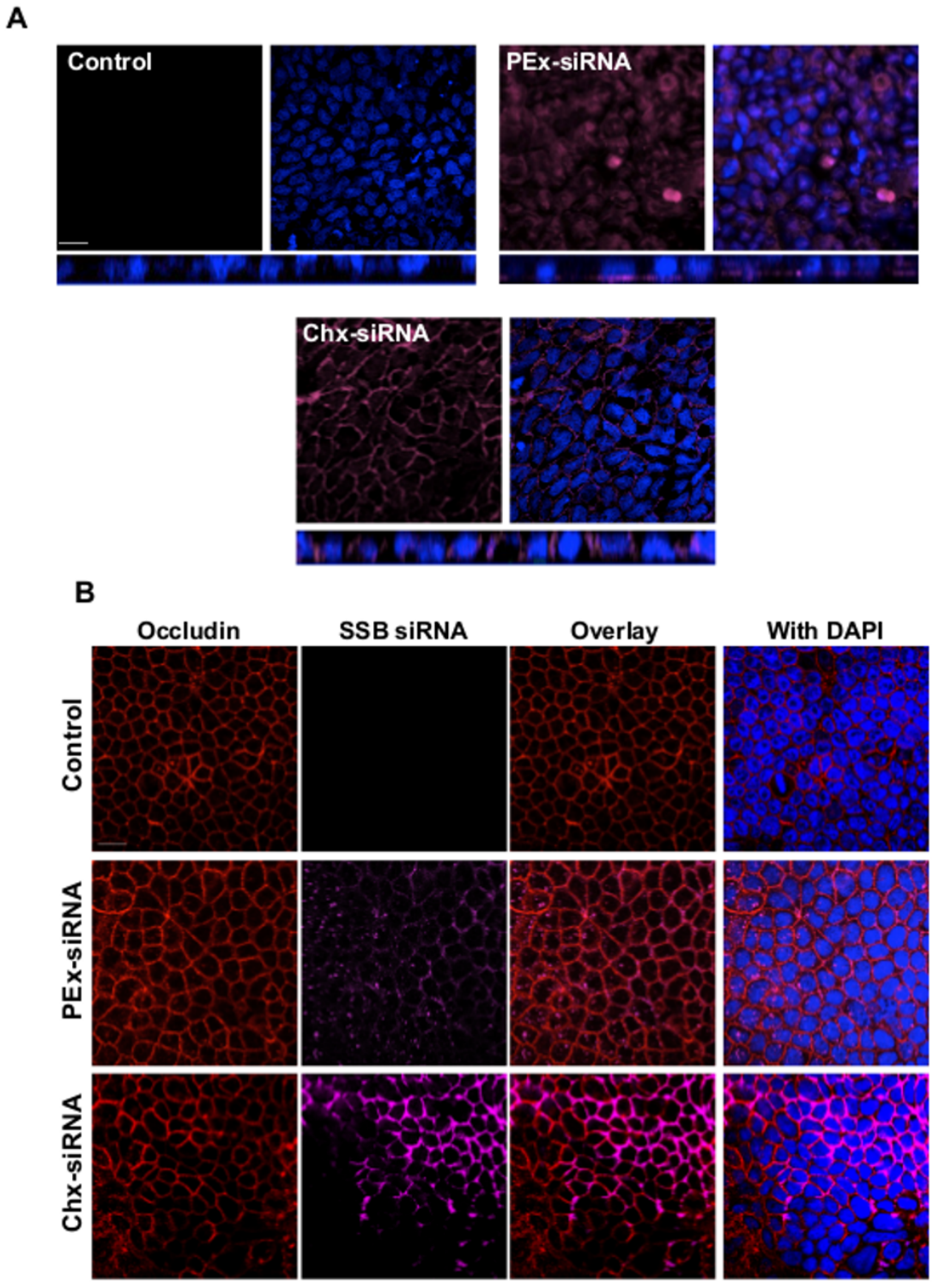

Figure 5.9. PEx and Chx can transport an siRNA cargo across polarised epithelial cells. A. Confocal images of Caco-2 monolayers following incubation with VivoTag680 tagged siRNA (Control) coupled to either PEx (PEx-siRNA) or Chx (Chx-siRNA). Z-stack images of siRNA conjugates crossing Caco-2 monolayers after 2 hours are displayed below. Images are representative of two independent experiments. Z-stack = 5 µm. **B.** Expression of occludin in Caco-2 cells incubated with siRNA conjugates over 2 hours. Images acquired from a single experiment. Scale bar = 20 µm

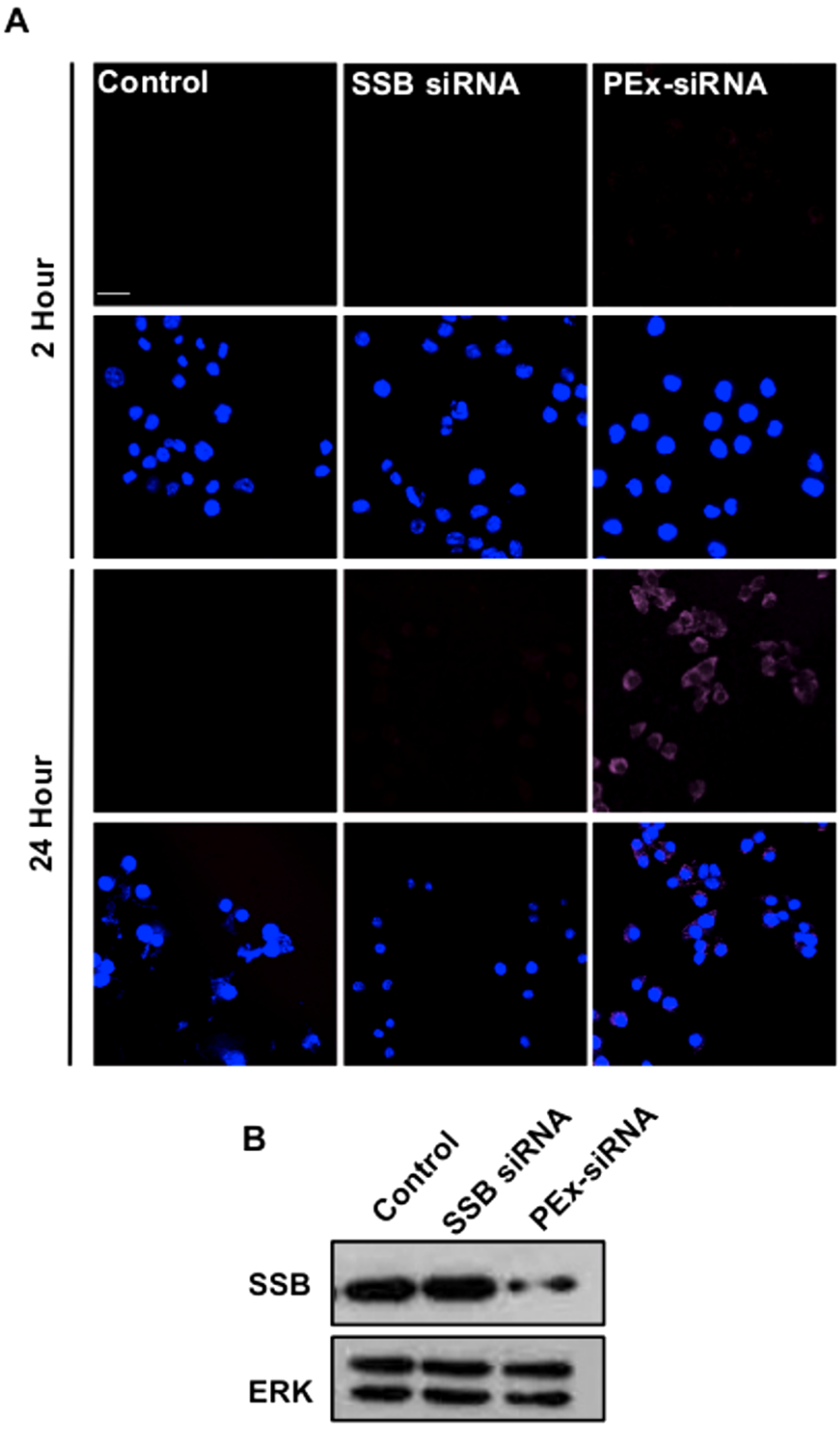

Figure 5.10. PEx can deliver a functional siRNA cargo to macrophages following transport across polarised epithelial cells. Fluorescent images of J774.2 macrophages following transport of VivoTag680 tagged SSB siRNA alone (SSB siRNA; 10 nM) or an equivalent fluorescent amount conjugated of PEx conjugated to VivoTag680 tagged SSB siRNA (PEx-siRNA) across polarised monolayers of Caco-2 cells at 2 and 24 hours. Images acquired from a single experiment. Scale bar = 20 μm. Western blot analysis for levels of SSB and ERK from J774.2 macrophages present in the basolateral compartment of Caco-2 monolayers incubated with either SSB siRNA alone or PEx tagged with SSB siRNA for 48 hours. Protein bands are representative from a single experiment.

5.7 Summary of results

- Fluorescently labelled PEx and Chx are able to enter non-polarised epithelial cells and are capable of being sorted through the retrograde pathway.
- PEx transport to the Golgi network is influenced by the ganglioside GM1. The C16:1 ceramide chain variant of GM1 enhances transport to the Golgi, whereas the C18:0 variant did not appear to influence transport to the Golgi.
- Minimal amounts of Chx enter $MEF^{GM1-/-}$ compared to PEx, which is only marginally increased following GM1 loading.
- Despite structural similarities PEx and Chx do not share the same cell surface receptor.
- Both PEx and Chx are capable of transcytosis across polarised monolayers of Caco-2 epithelial cells.
- Chx can impair the transport of PEx across monolayers, whereas PEx can enhance Chx transport.
- CTB impairs PEx, yet enhances Chx transport across polarised monolayers of Caco-2 cells.
- PEx can efficiently transport an siRNA cargo into macrophages and elicit a knockdown effect.
- PEx can transport an siRNA cargo across monolayers of epithelial cells and then a functional form of this cargo into macrophages present in the basolateral compartment where the siRNA can elicit an effect.

5.8 Discussion

Cellular receptor for Chx

Fluorescently labelled PEx and Chx are both capable of entering the epithelial cell line A431 wherein they appeared to be transported to endosomal compartments. The fact that we observed a fluorescent signal within these intracellular compartments would suggest that we are observing the transport of the complete toxin and not just the fluorescent cargo that may have separated. Comparatively little toxin was observed in the Golgi network and ER, inconsistent with the

reported intracellular transport pathway (Smith et al., 2006a). In order to effectively couple a cargo onto PEx and Chx the C-terminus had to be modified to include a fee cysteine residue required for coupling. This modification removed the REDL sequence that is required for effective transport of a toxin to the ER. Therefore, the lack of signal in the ER is likely due to the absence of this REDL sequence. However, this REDL sequence may not be completely necessary for PEx transport to the cytoplasm as studies utilising the translocation domain of PEx, and therefore lacking the REDL sequence, fused to GFP has been demonstrated to effectively enter the cytoplasm (Mohammed et al., 2012). As transport to the ER occurs after entry into the Golgi network (Smith et al., 2006a), a comparatively weak signal for toxin in the Golgi in these cells may reflect the small fraction of internalised toxin that reaches the retrograde pathway (Kreitman and Pastan, 1998; Yamaizumi et al., 1978).

Upon examining these bacterial toxins in $MEF^{GM1-/-}$ cells we were able to observe cellular entry with PEx and Chx, although the signal with Chx was significantly less. This is surprising as PEx and Chx are both thought to share the same cell surface receptor, CD91 (Jørgensen et al., 2008; Kounnas et al., 1992). We confirmed that CD91 is the required receptor for PEx by demonstrating the entry of PEx into wild type CHO cells but not those deficient in CD91. We also demonstrated that Chx is incapable of entering wild type CHO cells, which further supports that the receptor for Chx is not CD91.

As we have demonstrated that Chx can effectively enter both A431 and Caco-2 epithelial cells a way to determine the receptor(s) for Chx would be to pull down the epithelial membrane proteins that Chx binds to. Once identified, these proteins could then be individually knocked out and Chx entry evaluated. However, a caveat to this approach is that it would not identify if the receptor for Chx is a lipid, which is the case for CTB that utilises the ganglioside GM1 for cell entry (Holmgren et al., 1975).

GM1 and the intracellular transport of PEx in non-polarised cells

We examined the influence of GM1 on the transport of bacterial toxins with a goal of identifying mechanisms that could be exploited to enhance the cytoplasmic delivery of a toxin. Loading cells with the C16:1 ceramide chain variant of GM1 greatly enhanced the localisation of PEx to the Golgi network compared to cells which lacked GM1. Moreover, cells loaded with the C18:0 ceramide chain variant of GM1 did not show a similar enhancement of PEx localisation to the Golgi network. Chinnapen and colleagues have demonstrated that different structural variants of GM1 can transport to distinct intracellular locations, with C16:1 predominantly transporting to the Golgi network whereas C18:0 transports to late endosomes (Chinnapen et al., 2012). Our work therefore demonstrates that GM1 can also influence the transport of PEx and does not simply enhance cellular entry. Further, the observation that PEx can be still be transported to, albeit less so, the Golgi network in the absence of C16:1 GM1 would support the idea that PEx can exploit multiple pathways within a cell (Smith et al., 2006a).

We hypothesis that GM1 is required for at least one of the intracellular pathways proposed by Smith and colleagues. PEx can be transported either via an Arf1 or a Rab6 dependent pathway. As the Rab6 dependent pathway appears to be associated with detergent resistant membrane components (Smith et al., 2006a), of which GM1 is a component, it would seem likely that in GM1 deficient cells PEx transports exclusively through the Arf1 dependent pathway. This could be demonstrated by knocking down either Rab6 or Arf1 in GM1 deficient MEFs. If our hypothesis is correct, then the transport of PEx to the Golgi network should be prevented following knockdown of Arf1 and unaffected in Rab6 deficient cells. Further, PEx localisation to the Golgi network should not be enhanced by C16:1 GM1 in Rab6 deficient cells.

Moreover it would be important to determine at which stage in the transport process GM1 can influence PEx. This could be inferred by examining the binding of PEx to GM1 at different pH levels. An appropriate pH to examine would be pH 6.8 as this is the pH of the airway surface and is therefore relevant to the natural activity of PEx (Jayaraman et al., 2001), which is derived from the respiratory pathogen *Pseudomonas aeruginosa*. This would be compared with binding at pH

5.5, which is representative of endosomal pH (Geisow and Evans, 1984). This method could also be used to examine if GM1 can bind, and therefore influence, Chx. In this instance Chx binding to GM1 could be compared between endosomal pH (pH 5.5) and a pH relative to the intestinal tract (pH 6 – 7) as Chx is derived from the intestinal pathogen *Vibrio cholerae* (Fallingborg, 1999).

Although we have identified that GM1 can influence the transport of PEx to the Golgi network it still remains to be established if GM1 can influence the toxicity of PEx. This could be examined by measuring inhibition of protein synthesis following the application of the toxic form of PEx to MEF cells either deficient in GM1 or loaded with the C16:1 ceramide chain variant.

Transcytosis of PEx and Chx

In this study we have developed an *in-vitro* system with which to assess the transcytosis of PEx and Chx across polarised epithelium. As well as PEx and Chx, CTB is capable of undergoing transcytosis across polarised epithelial cells (Lencer et al., 1995). Once internalised CTB is either transported to the basolateral surface or enters the retrograde pathway leading to the Golgi network (Saslowsky et al., 2013). These two pathways are independent and it has been demonstrated that the amount of CTB that undergoes transcytosis can be enhanced though inhibition of the retrograde pathway.

PEx and Chx appear to affect the transport of the other. Excess Chx reduces the transcytosis of PEx, whereas excess PEx actually enhances Chx transcytosis. This may suggest that there are two transport routes for these toxins within polarised epithelial cells; one that leads to transcytosis, and one that leads to an intracellular compartment. If Chx has a preference for the transcytotic pathway over PEx then an excess of Chx would push PEx down the intracellular pathway thus reducing PEx transcytosis. Equally, if PEx has a preference for the intracellular pathway then an excess of PEx would make more Chx available for transcytosis. However, this explanation assumes that the two toxins share the same intracellular pathway.

We observed different distributions of Chx and PEx within polarised epithelial cells, Chx appeared to be transported within the periphery of the cells whereas PE transported across the cytoplasm. This may suggest that the two toxins are transported differently across polarised epithelium. Alternatively it may reflect a preference of Chx for the transcytosis pathway and PEx for an intracellular pathway. Brefeldin A is a protein transport inhibitor that blocks entry into the retrograde pathway (Chinnapen et al., 2012; Saslowsky et al., 2013). If the observed distribution of the toxins is due to their preference for one pathway over another then a similar distribution of PEx to Chx would be observed in cells treated with Brefeldin A as this would push more PEx into the transcytosis pathway. If not, then it would suggest that the two toxins travel via different intracellular pathways.

The sorting of CTB to either the transcytotic or retrograde pathway in polarised cells appears to be influenced by the structure of GM1; with the C16:1 ceramide chain variant promoting transcytosis (Saslowsky et al., 2013). This also appears to be true for PEx transcytosis as CTB was able to reduce the transcytosis of PEx. This is also consistent with a requirement for GM1 in the transport of PEx within non-polarised cells. Surprisingly CTB was able to enhance the transcytosis of Chx suggesting a difference in GM1 interactions between Chx and PEx. These observations could be explored further by utilising Caco-2 cells deficient in GM1. This model would allow for the characterisation of different GM1 structures on the transport of toxins across polarised cells.

We examined transcytosis of these toxins in Caco-2 cells, an intestinal cell line, which more accurately reflects the natural environment for the intestinal toxin Chx over the respiratory toxin PEx. Therefore a preference for Chx over PEx for the transcytotic pathway may simply be a reflection of the system used. A way to examine this further would be to study the transcytosis of these toxins in an airway epithelial cell line such as Calu-3 cells, although the mucus produced from Calu-3 monolayers would need to be removed with a mucolytic such as N-acetylcystine.

Transcytosis Pathway for PEx and Chx

The intracellular pathway for PEx and Chx transcytosis remains to be established and would have implications for the use of these toxins as therapeutic agents. As mentioned, a possible caveat for this therapeutic approach in non-polarised cells at least is the possibility of losing an effective amount of toxin to lysosomal degradation. The same may be true for transcytosis so it would be important to determine how much of an applied toxin is effectively transported to the basolateral side.

Aside from bacterial toxins, immunoglobulins are capable of undergoing transcytosis from the apical to basolateral surface of epithelia (Dickinson et al., 1999; Sakagami et al., 2006). This mechanism serves to transfer maternal IgG to the foetus and neonate and extend the half life of circulating IgG in the adult (Roopenian and Akilesh, 2007). It seems possible that bacterial toxins such as PEx and Chx could exploit this type of natural transcytosis mechanism to mediate their transfer across mucosal surfaces.

During *Pseudomonas aeruginosa* infection the bacterium crosses mucosal surfaces to invade the blood stream and avoid the host immune system. It has been reported that in order for *Pseudomonas aeruginosa* to undergo transcytosis the bacterium requires the recruitment of basolateral proteins to the apical surface of polarised epithelial cells (Kierbel et al., 2007). This process is dependent on the activity of PI3K, which has previously been reported to be sufficient to transform the apical surface of polarised epithelium to basolateral (Gassama-Diagne et al., 2006). As part of the host immune response dimeric IgA is secreted into the luminal space by epithelial cells. To achieve this dimeric IgA enters polarised epithelial cells through interactions with the polymeric immunoglobulin receptor present on the basolateral surface of epithelial cells. Dimeric IgA is then transported across the epithelium and is secreted on the apical side (Apodaca et al., 1994; Mostov et al., 1984). This mechanism is exploited by the pathogen *Streptococcus pneumonia* in host invasion (Zhang et al., 2000). Given the requirement of basolateral proteins for *Pseudomonas aeruginosa* invasion, and a dependency of PI3K for effective dimeric IgA transcytosis (Cardone and Mostov, 1995), we hypothesis that *Pseudomonas aeruginosa* (and possibly PEx) also

exploits this transcytosis mechanism. However, this hypothesis would require that PEx alone is sufficient to induce a switch of an apical surface to basolateral.

Bacterial toxin mediated cargo delivery

The primary aim of this project was to examine the potential use of bacterial toxins as drug carriers. We have been able to demonstrate that PEx is capable of both transporting an siRNA cargo across polarised epithelial cells by transcytosis and delivering said cargo into cells present in the basolateral compartment. The observation that knockdown can be achieved is particularly promising and suggests that PEx was able to transport the siRNA to the cytosol of a cell, which would be required for a therapeutic effect. However, it remains to be determined if the PEx-siRNA construct could induce knockdown in the polarised monolayer of cells. This would seem unlikely as the natural, toxic; PEx can be transported across polarised epithelial cells without inducing the death of the cells. Together these data suggests that toxins can be used in place of other cell delivery reagents that are limited by their retention in endosomal compartments (Plank et al., 1994; Rudolph et al., 2003). Cytoplasmic delivery of a cargo has been previously reported with PEx (Mohammed et al., 2012), but we are the first to demonstrate a therapeutic effect.

The repertoire of cargos that can be delivered by bacterial toxins remains to be elucidated. Given that these toxins require sorting within vesicles it is likely that there is a size limit to the overall toxin that may preclude certain macromolecule cargos from being used with this system. Another consideration for the therapeutic use of these toxins is whether their immunogenic properties will hinder their use. This is a common problem for the related immunotoxins, as a patient develops neutralising antibodies following prolonged use (Posey et al., 2002). The removal of B cell epitopes reduces the immunogenicity of immunotoxins (Onda et al., 2008; Onda et al., 2011), which may be applicable to toxins repurposed for drug delivery.

Chapter 6: General Discussion

6.1 PI3K in lung branching morphogenesis

Overview

This thesis began by examining how the PI3K pathway, a critical mediator of a number of disease processes, operates during the development of the lung. This builds on the appreciation that developmental pathways can become reactivated in, and contribute to, the pathogenesis of a number of lung diseases (Shi et al., 2009). We utilised a range of pharmacological agents targeting different elements of the PI3K signalling cascade to ensure that the observations made were due to inhibition of PI3K signalling and not a result of off-target effects. Using these compounds and *ex-vivo* culture models of whole embryonic lungs we were able to identify a novel role for PI3K in the epithelial branching program of the lung. We discovered that inhibition of either PI3Kα, or its downstream signalling components Akt and mTORC2, greatly enhanced the branching potential of isolated embryonic lung cultures. This was a surprising observation as similar experiments have reported the opposite effects of PI3K inhibition in other epithelial branching organs such as the salivary glands (Larsen et al., 2003), mammary glands (Utermark et al., 2012), urogenital sinus tissue (Ghosh et al., 2011), and ureteric bud (Tang et al., 2002). Moreover, PI3K activation in the salivary gland, mimicked through exogenous application of PI(3,4,5)P (Larsen et al., 2003), has been shown to promote branching, further supporting a positive role for PI3K in branching.

To understand why our observations conflicted with the literature we examined the PI3K pathway in preparations of isolated branching epithelium stimulated with the morphogen FGF7. In this context we observed that inhibition of PI3K was sufficient to dramatically alter the morphogenic properties of FGF7 from the formation of epithelial cysts to the formation of numerous epithelial branches resembling the morphogenic response to the related factor FGF10. The unique effect of PI3K on the branching program of the lung could therefore be explained by the different responses to FGF7 and FGF10 between the lung and salivary gland epithelium. In the salivary glands FGF7 initiates the formation of numerous small branches whereas FGF10 promotes branch elongation (Makarenkova et al., 2009). If PI3K inhibition switches FGF7 signalling to that of FGF10 then the budding response would be lost in salivary glands, and as a result there would be fewer branches.

This has implications for the use of PI3K directed therapies for regenerative medicine in that a therapeutic effect in one organ may have a deleterious effect in another.

To attempt to explain how inhibition of PI3K alters the morphogenic properties of FGF7 we examined the influence of heparan sulphate, the FGFR1b receptor and the regulation of cell-cell contacts. Heparan sulphate has been reported to be critical for the branching response elicited by FGF10 (Izvolsky et al., 2003). However, removal of the heparan sulphate gradient failed to perturb the branching response achieved through FGF7 in the presence of an inhibitor of PI3K singalling. FGFR1b was considered to be a branching receptor due to the ubiquitous expression across the lung epithelium of the canonical branching receptor FGFR2b (Cardoso et al., 1997), and because FGFR1 has been reported to be expressed in the branch tips of the developing salivary glands and ureteric bud (Meyer et al., 2004; Steinberg et al., 2005). We were unable to identify the expression of FGFR1b in isolated lung epithelium. Moreover, we also failed to observe a branching response with the FGFR1 agonist FGF2. Together these results would suggest that FGFR1b was redundant in this system. Finally, we examined the impact of PI3K on cell-cell contacts and branching as regulation of the cell-cell contacts has been reported to be required for the collective migration of epithelial cells (Theveneau et al., 2013). Additionally, E-Cadherin cell-cell contacts can be regulated by JNK and GSK3β, which can themselves be controlled by PI3K activity (Aberle et al., 1997; Aikin et al., 2004; Cross et al., 1995; Lee et al., 2009). We observed no disruption of cell-cell contacts in the branching tip of isolated lung epithelium. However, inhibition of GSK3β, and potentially enhanced cell-cell contacts, resulted in a more uniform cyst structure in response to FGF7 and prevented the induction of branches in response to FGF7 and PI3K inhibition. Inhibition of JNK, on the other hand, failed to affect the branching response.

Future directions

The difficulties associated with manipulating this model genetically, either through direct transfection of genetic material or viral infection, limit the use of this model. However, new approaches are emerging that will overcome this caveat that will give more power to this physiologically relevant model of lung development. These include novel infection techniques with which to directly infect the epithelium of a branching organ (Sequeira et al., 2013). Alternatively as we have demonstrated a robust method of genetic delivery to cells using modified bacterial toxins this may present an alternative means to introduce genetic tools into embryonic lung tissue. This model does not require the removal and subsequent reinstatement of the mesenchymal tissue as required by Sequeira and colleagues, which may damage the growth of the whole explant. Moreover, as these bacterial toxins can be modified to replace the receptor-binding domain with an antibody, this approach has the added benefit of allowing a specific subset of cells within the explant to be targeted.

A mechanistic explanation for how PI3K inhibition can alter the signalling event of FGF7 to that of FGF10 has been reported that warrants further investigation in models of branching morphogenesis. Francavilla and colleagues reported that PI3K can control the sorting of internalised FGFR2b to either the recycling or late endosomes (Francavilla et al., 2013). FGF10 was shown to promote the recycling of FGFR2b whereas FGF7 promoted the degradation. The recycling of FGFR2b required the scaffolding properties of the p85 subunit of PI3K, which was recruited to the receptor solely in response to FGF10 interactions. However, inhibition of PI3K was demonstrated to be able to promote the recycling of FGFR2b following FGF7 stimulation (Francavilla et al., 2013), thus providing a mechanism for the observations from our experiments.

It would be valuable to establish if a similar mechanism exists in the branching epithelium. This would be best achieved by expressing fluorescently tagged constructs of FGFR2b and elements of the recycling and late endosomes in isolated lung epithelium. The transport of internalised FGFR2b could then be visualised in real time in response to FGF7 with or without an inhibitor of PI3K signalling. Moreover the same experiment could be preformed in isolated salivary

gland epithelium to establish if the conflicting reports of PI3K inhibition on the branching response between organs are indeed as a result of differences in FGF signalling.

The finding that FGFR2b sorting is critical in the morphogenic output of a factor would give more importance to the signals that drive endosomal sorting in development and disease. Identification of whether distinct signalling pathways are activated in separate endosomal compartments would provide answers as to how sorting can effect the morphogenic output of a growth factor. Given the involvement of the class II and III PI3K family members in endosomal transport (Ikonomov et al., 2006; Schu et al., 1993; Xu et al., 2001), these kinases may also be able to direct branching morphogenesis through the manipulation of FGF signalling.

Aside from the branching response, an intriguing question in the development of the branched airway network is how the airway lumen forms during successive branch generations and expands to such a size as to minimise the work required to overcome flow resistance and reduce the amount dead space volume (Murray, 1926; Weibel and Gomez, 1962). As observed in the whole explant model the proximal branches of a developing lung are surrounded by smooth muscle generated from the FGF10 producing cells of the mesenchyme (Agha et al., 2014). These cells periodically contract, forcing fluid back and forth along the luminal space (Schittny et al., 2000). An exciting prospect that warrants further investigation is that the fluid that surges through the lumen during each contractile wave serves to test the luminal space for efficiency. The epithelium may be capable of responding to these mechanical cues and altering their growth accordingly to optimise the luminal space. If correct then lung disorders may arise from inefficient airway peristalsis that induces the formation of inadequate lumen. During an asthma attack the smooth muscle that lines the airways contracts, restricting airflow. Given that the same smooth muscle is active in this model of embryonic lung branching this model could potentially be used to assess drugs designed to reduce the muscular contraction during an asthmatic attack.

In this study we have explored the role of disease-associated pathways in developmental processes using physiologically relevant models. Beyond examining signalling pathways these models could potentially be used to recreate the diseased environment. During the fibrotic process myofibroblasts secrete a range of factors to promote matrix reorganisation and the proliferation and differentiation of surrounding fibroblasts (Scotton and Chambers, 2007). It would be interesting to see what effect the application of conditioned media from fibrotic myofibroblasts, or the myofibroblasts themselves, has on cultures of lung explants. An induction of a fibrotic process in the explants would be exciting and would allow for a physiologically relevant model with which to test potential anti-fibrotic drugs. However, given that a prominent pro-fibrotic cytokine released from myofibroblasts is TGFβ (Popova et al., 2010), the effects of these cells on embryonic lung explants may likely be akin to the reported effects of TGFβ on lung branching (Xing et al., 2008).

6.2 Immunogenicity of CPPs

Overview

The second facet of this thesis sought to determine if CPPs, a widely used transfection carrier that is emerging in the clinic, have underlying immunogenic properties. Given their initial derivation from proteins isolated from viruses and venoms (Frankel and Pabo, 1988; Gurrola et al., 2010; Rádis-Baptista and Kerkis, 2011), it seem reasonable to presume that these CPP protein sequences could be recognised by cells to initiate an immune response, making it surprising that their potential immunogenic nature has not been explored in great detail in the literature. We have demonstrated that three commonly used CPPs were capable of delivering a fluorescent cargo to epithelial cells *in-vitro* albeit with different efficacies. These CPPs did not affect the viability of the epithelial cells, which has been reported for CPPs at high concentrations (Hansen et al., 2012; Kilk et al., 2009; Watkins et al., 2009). After initial application, these CPPs did not appear to activate NFκB signalling, a commonly activated inflammatory pathway. Furthermore, prolonged exposure (72 hours) of cells to these CPPs failed to incite the release of the pro-inflammatory cytokines IL-6 and IL-8. Together this would

suggest that CPPs are not immunogenic, at least towards epithelial cells in an *in-vitro* system.

Future directions

A limitation of this study is that it was performed in an *in-vitro* system; this therefore removed the ability to examine the full immune response including whether a CPP could be 'presented' to adaptive immune cells. As mentioned, this could be examined *in-vitro* by exposing antigen presenting cells with CPPs and observing if these cells are then capable of activating cells of the adaptive immune system.

Multiple studies have reported that CPPs can be transported to different intracellular locations dependent on the CPP and the type of cargo (Lundin et al., 2008; Moschos et al., 2007). It is therefore possible that the CPPs in this study failed to induce an immune response, as they did not transport to an area of the cell where they would be recognised as immunogenic. It would therefore seem prudent to test each individual type of CPP: Cargo complex for immunogenic potential before the therapeutic reaches the clinic.

6.3 Bacterial toxins as drug delivery tools

Overview

The final part of this thesis examined the intracellular transport of two bacterial toxins and explored their potential as therapeutic delivery agents. We have demonstrated that PEx and Chx are internalised by epithelial cells and are subsequently transported to intracellular locations consistent with their intoxication pathway. Interestingly we determined that the ganglioside GM1 is influential in the intracellular transport of PEx, with the C16:1 ceramide chain variant enhancing the localisation of PEx to the Golgi network.

We have also studied the transcytosis of these bacterial toxins across polarised monolayers of Caco-2 cells. Both PEx and Chx were able to transport across Caco-2 cells from the apical side and be released into the basolateral compartment. We briefly explored the transcytosis pathway for these toxins by

studying the impact of one on the transport of the other. We identified that these toxins can compete with each other and that Chx can disrupt PEx transcytosis whereas PEx can enhance Chx transcytosis. This was also apparent with CTB, implying that GM1 may also affect the transcytosis pathway. Indeed, a role for GM1 structure has been identified in the transcytosis pathway of CTB (Saslowsky et al., 2013).

Finally, we were able to combine these two approaches to demonstrate that PEx, when coupled with an siRNA cargo, can effectively transport across a polarised monolayer of cells and deliver the cargo into cells present in the basolateral compartment. A particularly striking finding is that this siRNA construct could then initiate knockdown of a target protein within cells.

Future directions

During this study we discovered that the receptor for Chx is not the same as PEx, which was assumed based on the similarities between the structure of the two toxins (Jørgensen et al., 2008). Future work should endeavour to identify the cellular receptor for Chx entry, as this will be critical for identifying which cells a Chx based therapeutic could target.

It would be also be beneficial to identify the transcytosis pathway for PEx and Chx. In nature *Streptococcus pneumonia* has evolved to exploit natural transcytosis pathways in the body to aid in host invasion (Zhang et al., 2000). It would therefore seem reasonable that PEx and Chx evolved to exploit similar pathways. A likely candidate is the neonatal Fc receptor, which transports IgG from the apical to the basolateral surface of mucosal linings (Dickinson et al., 1999; Sakagami et al., 2006). An alternative is the polymeric immunoglobulin receptor, which naturally transports dimeric IgA from the basolateral surface of mucosal linings and secretes dimeric IgA into the mucosa (Apodaca et al., 1994; Mostov et al., 1984). This second prospect is more appealing given that *Pseudomonas aeruginosa* requires the translocation of basolateral proteins to the apical surface in order to transport across polarised epithelium (Kierbel et al., 2007).

We have established that bacterial toxins can effectively transport a cargo across polarised epithelial surfaces and deliver said cargo into cells present on the basolateral side. The next step would be to demonstrate the same effect *in-vivo*. It would be important to see if a bacterial toxin applied to the mucosal surface of the airways or intestine is capable of overcoming the added barrier of mucosa and fluid flux to be transported either into the bloodstream or the surrounding tissue. Moreover, the repertoire of potential cargos needs to be determined, answering whether there is a size limit for a therapeutic cargo.

Finally, there is the potential to further tailor bacterial toxins for therapeutic use by removing both the receptor binding domain and the toxic domain and replacing with a cell-specific immunoglobulin and drug cargo respectively. This would allow for the intracellular delivery of a drug cargo to a specific cell type of interest.

6.4 Concluding remarks

Developmental pathways that orchestrate the growth of an organ can show a resurgence in the diseased state. These developmental pathways control the remodelling of an organ to a degree where function becomes impaired. An example of this is TGFβ, which is critical for lung growth. Too much or too little of this factor greatly perturbs the branching program of the developing lung. Signalling of this factor is also overactive in fibrosis where it is seen as one of the predominant pathogenic signals (Shi et al., 2009). Insight into how signalling pathways (that act to remodel an organ during disease) function in the development of an organ will aid in the understanding of how the remodelling occurs and will lead to novel therapeutic strategies for regenerative medicine.

We have identified a novel role for PI3K in the development of the lung that will have implications for the use of PI3K based therapies particularly because we have observed a contrasting effect of PI3K than what is seen in other epithelial branching organs. As we have examined a process that involves the migration of epithelial cells this work will have particular impact on epithelial cancers, where PI3K signalling is consistently found to be overactive (Engelman, 2009).

We have provided evidence to suggest that CPPs are passive entities that do no incite an immune response. However, more work is needed before we can know for sure if they do not exhibit immunogenic properties. As these CPPs progress through clinical trials covering a range of CPPs and cargos across many diseases more data will emerge regarding their safety.

The repurposing of bacterial toxins as drug carriers is an exciting prospect. We have demonstrated the proof of concept, showing that toxins can deliver an active cargo into cells wherein they can exhibit a therapeutic effect. Historically these toxins have been detrimental to society, but with the generation of these toxins as drug carriers and the continued success of related immunotoxins we will see them take on a new, beneficial, role.

References

Aberle, H., Bauer, A., Stappert, J., Kispert, A. and Kemler, R. (1997). beta-catenin is a target for the ubiquitin-proteasome pathway. *EMBO J.* **16**, 3797–3804.

Adachi, O., Kawai, T., Takeda, K., Matsumoto, M., Tsutsui, H., Sakagami, M., Nakanishi, K. and Akira, S. (1998). Targeted disruption of the MyD88 gene results in loss of IL-1- and IL-18-mediated function. *Immunity* **9**, 143–150.

Agha, El, E., Herold, S., Alam, D. A., Quantius, J., Mackenzie, B., Carraro, G., Moiseenko, A., Chao, C.-M., Minoo, P., Seeger, W., et al. (2014). Fgf10-positive cells represent a progenitor cell population during lung development and postnatally. *Development* **141**, 296–306.

Aikin, R., Maysinger, D. and Rosenberg, L. (2004). Cross-talk between phosphatidylinositol 3-kinase/AKT and c-jun NH2-terminal kinase mediates survival of isolated human islets. *Endocrinology* **145**, 4522–4531.

Akinc, A., Thomas, M., Klibanov, A. M. and Langer, R. (2005). Exploring polyethylenimine-mediated DNA transfection and the proton sponge hypothesis. *J Gene Med* **7**, 657–663.

Alessi, D. R., James, S. R., Downes, C. P., Holmes, A. B., Gaffney, P. R., Reese, C. B. and Cohen, P. (1997). Characterization of a 3-phosphoinositide-dependent protein kinase which phosphorylates and activates protein kinase Balpha. *Curr. Biol.* **7**, 261–269.

Ali, K., Camps, M., Pearce, W. P., Ji, H., Rückle, T., Kuehn, N., Pasquali, C., Chabert, C., Rommel, C. and Vanhaesebroeck, B. (2008). Isoform-specific functions of phosphoinositide 3-kinases: p110 delta but not p110 gamma promotes optimal allergic responses in vivo. *J. Immunol.* **180**, 2538–2544.

Alves, I. D., Goasdoué, N., Correia, I., Aubry, S., Galanth, C., Sagan, S., Lavielle, S. and Chassaing, G. (2008). Membrane interaction and perturbation mechanisms induced by two cationic cell penetrating peptides with distinct charge distribution. *Biochim. Biophys. Acta* **1780**, 948–959.

Anon. (2013). Pirfenidone. First, do no harm. *Prescrire Int* **22**, 117–119.

Apodaca, G., Katz, L. A. and Mostov, K. E. (1994). Receptor-mediated transcytosis of IgA in MDCK cells is via apical recycling endosomes. *J. Cell Biol.* **125**, 67–86.

Arcaro, A. and Wymann, M. P. (1993). Wortmannin is a potent phosphatidylinositol 3-kinase inhibitor: the role of phosphatidylinositol 3,4,5-trisphosphate in neutrophil responses. *Biochem. J.* **296 (Pt 2)**, 297–301.

Asselin-Labat, M.-L., Sutherland, K. D., Barker, H., Thomas, R., Shackleton, M., Forrest, N. C., Hartley, L., Robb, L., Grosveld, F. G., van der Wees, J., et al. (2007). Gata-3 is an essential regulator of mammary-gland morphogenesis and luminal-cell differentiation. *Nat. Cell Biol.* **9**, 201–209.

Atkins, P. C., Norman, M., Weiner, H. and Zweiman, B. (1977). Release of neutrophil chemotactic activity during immediate hypersensitivity reactions in humans. *Ann. Intern. Med.* **86**, 415–418.

Baiz, D., Hassan, S., Choi, Y. A., Flores, A., Karpova, Y., Yancey, D., Pullikuth, A., Sui, G., Sadelain, M., Debinski, W., et al. (2013). Combination of the PI3K inhibitor ZSTK474 with a PSMA-targeted immunotoxin accelerates apoptosis and regression of prostate cancer. *Neoplasia* **15**, 1172–1183.

Bakin, A. V., Tomlinson, A. K., Bhowmick, N. A., Moses, H. L. and Arteaga, C. L. (2000). Phosphatidylinositol 3-kinase function is required for transforming growth factor beta-mediated epithelial to mesenchymal transition and cell migration. *J. Biol. Chem.* **275**, 36803–36810.

Barnes, P. J. (2004). The size of the problem of managing asthma. *Respir Med* **98 Suppl B**, S4–8.

Behrens, J., Vakaet, L., Friis, R., Winterhager, E., Van Roy, F., Mareel, M. M. and Birchmeier, W. (1993). Loss of epithelial differentiation and gain of invasiveness correlates with tyrosine phosphorylation of the E-cadherin/beta-catenin complex in cells transformed with a temperature-sensitive v-SRC gene. *J. Cell Biol.* **120**, 757–766.

Bellusci, S., Grindley, J., Emoto, H., Itoh, N. and Hogan, B. L. (1997). Fibroblast growth factor 10 (FGF10) and branching morphogenesis in the embryonic mouse lung. *Development* **124**, 4867–4878.

Berlose, J. P., Convert, O., Derossi, D., Brunissen, A. and Chassaing, G. (1996). Conformational and associative behaviours of the third helix of antennapedia homeodomain in membrane-mimetic environments. *Eur. J. Biochem.* **242**, 372–386.

Bilancio, A., Okkenhaug, K., Camps, M., Emery, J. L., Rückle, T., Rommel, C. and Vanhaesebroeck, B. (2006). Key role of the p110delta isoform of PI3K in B-cell antigen and IL-4 receptor signaling: comparative analysis of genetic and pharmacologic interference with p110delta function in B cells. *Blood* **107**, 642–650.

Birchmeier, C., Birchmeier, W. and Brand-Saberi, B. (1996). Epithelial-mesenchymal transitions in cancer progression. *Acta Anat (Basel)* **156**, 217–226.

Biswas, K., Yoshioka, K., Asanuma, K., Okamoto, Y., Takuwa, N., Sasaki, T. and Takuwa, Y. (2013). Essential role of class II phosphatidylinositol-3-kinase-C2α in sphingosine 1-phosphate receptor-1-mediated signaling and migration in endothelial cells. *J. Biol. Chem.* **288**, 2325–2339.

Bohnacker, T., Marone, R., Collmann, E., Calvez, R., Hirsch, E. and Wymann, M. P. (2009). PI3Kgamma adaptor subunits define coupling to degranulation and cell motility by distinct PtdIns(3,4,5)P3 pools in mast cells. *Sci Signal* **2**, ra27.

Bone, H. K., Damiano, T., Bartlett, S., Perry, A., Letchford, J., Ripoll, Y. S., Nelson, A. S. and Welham, M. J. (2009). Involvement of GSK-3 in regulation of murine embryonic stem cell self-renewal revealed by a series of bisindolylmaleimides. *Chem. Biol.* **16**, 15–27.

Borish, L., Rosenbaum, R., Albury, L. and Clark, S. (1989). Activation of neutrophils by recombinant interleukin 6. *Cell. Immunol.* **121**, 280–289.

Brinkmann, M. M., Spooner, E., Hoebe, K., Beutler, B., Ploegh, H. L. and Kim, Y.-M. (2007). The interaction between the ER membrane protein UNC93B and TLR3, 7, and 9 is crucial for TLR signaling. *J. Cell Biol.* **177**, 265–275.

Brondello, J. M., Pouysségur, J. and McKenzie, F. R. (1999). Reduced MAP kinase phosphatase-1 degradation after p42/p44MAPK-dependent phosphorylation. *Science* **286**, 2514–2517.

Brunn, G. J., Williams, J., Sabers, C., Wiederrecht, G., Lawrence, J. C. and Abraham, R. T. (1996). Direct inhibition of the signaling functions of the mammalian target of rapamycin by the phosphoinositide 3-kinase inhibitors, wortmannin and LY294002. *EMBO J.* **15**, 5256–5267.

Bucci, C., Parton, R. G., Mather, I. H., Stunnenberg, H., Simons, K., Hoflack, B. and Zerial, M. (1992). The small GTPase rab5 functions as a regulatory factor in the early endocytic pathway. *Cell* **70**, 715–728.

Cano, A., Pérez-Moreno, M. A., Rodrigo, I., Locascio, A., Blanco, M. J., del Barrio, M. G., Portillo, F. and Nieto, M. A. (2000). The transcription factor snail controls epithelial-mesenchymal transitions by repressing E-cadherin expression. *Nat. Cell Biol.* **2**, 76–83.

Cardone, M. and Mostov, K. (1995). Wortmannin inhibits transcytosis of dimeric IgA by the polymeric immunoglobulin receptor. *FEBS Lett.* **376**, 74–76.

Cardoso, W. V., Itoh, A., Nogawa, H., Mason, I. and Brody, J. S. (1997). FGF-1 and FGF-7 induce distinct patterns of growth and differentiation in embryonic lung epithelium. *Dev. Dyn.* **208**, 398–405.

Carpenter, G. and Ji, Q. S. (1999). Phospholipase C-gamma as a signal-transducing element. *Exp. Cell Res.* **253**, 15–24.

Castranova, V., Rabovsky, J., Tucker, J. H. and Miles, P. R. (1988). The alveolar type II epithelial cell: a multifunctional pneumocyte. *Toxicol. Appl. Pharmacol.* **93**, 472–483.

Cellurale, C., Girnius, N., Jiang, F., Cavanagh-Kyros, J., Lu, S., Garlick, D. S., Mercurio, A. M. and Davis, R. J. (2012). Role of JNK in mammary gland development and breast cancer. *Cancer Res.* **72**, 472–481.

Chang, D. R., Martinez Alanis, D., Miller, R. K., Ji, H., Akiyama, H., McCrea, P. D. and Chen, J. (2013). Lung epithelial branching program antagonizes alveolar differentiation. *Proc. Natl. Acad. Sci. U.S.A.* **110**, 18042–18051.

Chang, F., Lee, J. T., Navolanic, P. M., Steelman, L. S., Shelton, J. G., Blalock, W. L., Franklin, R. A. and McCubrey, J. A. (2003). Involvement of PI3K/Akt pathway in cell cycle progression, apoptosis, and neoplastic transformation: a target for cancer chemotherapy. *Leukemia* **17**, 590–603.

Chell, V., Balmanno, K., Little, A. S., Wilson, M., Andrews, S., Blockley, L., Hampson, M., Gavine, P. R. and Cook, S. J. (2013). Tumour cell responses to new fibroblast growth factor receptor tyrosine kinase inhibitors and identification of a gatekeeper mutation in FGFR3 as a mechanism of acquired resistance. *Oncogene* **32**, 3059–3070.

Chen, H., Sun, J., Buckley, S., Chen, C., Warburton, D., Wang, X.-F. and Shi, W. (2005). Abnormal mouse lung alveolarization caused by Smad3 deficiency is a developmental antecedent of centrilobular emphysema. *Am. J. Physiol. Lung Cell Mol. Physiol.* **288**, L683–91.

Chen, X.-F., Zhang, H.-J., Wang, H.-B., Zhu, J., Zhou, W.-Y., Zhang, H., Zhao, M.-C., Su, J.-M., Gao, W., Zhang, L., et al. (2012). Transforming growth factor-β1 induces epithelial-to-mesenchymal transition in human lung cancer cells via PI3K/Akt and MEK/Erk1/2 signaling pathways. *Mol. Biol. Rep.* **39**, 3549–3556.

Chinnapen, D. J.-F., Hsieh, W.-T., Welscher, te, Y. M., Saslowsky, D. E., Kaoutzani, L., Brandsma, E., D'Auria, L., Park, H., Wagner, J. S., Drake, K. R., et al. (2012). Lipid sorting by ceramide structure from plasma membrane to ER for the cholera toxin receptor ganglioside GM1. *Dev. Cell* **23**, 573–586.

Chresta, C. M., Davies, B. R., Hickson, I., Harding, T., Cosulich, S., Critchlow, S. E., Vincent, J. P., Ellston, R., Jones, D., Sini, P., et al. (2010). AZD8055 is a potent, selective, and orally bioavailable ATP-competitive mammalian target of rapamycin kinase inhibitor with in vitro and in vivo antitumor activity. *Cancer Res.* **70**, 288–298.

Collier, R. J. (1975). Diphtheria toxin: mode of action and structure. *Bacteriol Rev* **39**, 54–85.

Colvin, J. S., White, A. C., Pratt, S. J. and Ornitz, D. M. (2001). Lung hypoplasia and neonatal death in Fgf9-null mice identify this gene as an essential regulator of lung mesenchyme. *Development* **128**, 2095–2106.

Conte, E., Fruciano, M., Fagone, E., Gili, E., Caraci, F., Iemmolo, M., Crimi, N. and Vancheri, C. (2011). Inhibition of PI3K prevents the proliferation and differentiation of human lung fibroblasts into myofibroblasts: the role of class I P110 isoforms. *PLoS ONE* **6**, e24663.

Crackower, M. A., Oudit, G. Y., Kozieradzki, I., Sarao, R., Sun, H., Sasaki, T., Hirsch, E., Suzuki, A., Shioi, T., Irie-Sasaki, J., et al. (2002). Regulation of myocardial contractility and cell size by distinct PI3K-PTEN signaling pathways. *Cell* **110**, 737–749.

Crombez, L., Aldrian-Herrada, G., Konate, K., Nguyen, Q. N., McMaster, G. K.,

Brasseur, R., Heitz, F. and Divita, G. (2009). A new potent secondary amphipathic cell-penetrating peptide for siRNA delivery into mammalian cells. *Mol. Ther.* **17**, 95–103.

Cross, D. A., Alessi, D. R., Cohen, P., Andjelkovich, M. and Hemmings, B. A. (1995). Inhibition of glycogen synthase kinase-3 by insulin mediated by protein kinase B. *Nature* **378**, 785–789.

Cross, M. J., Lu, L., Magnusson, P., Nyqvist, D., Holmqvist, K., Welsh, M. and Claesson-Welsh, L. (2002). The Shb adaptor protein binds to tyrosine 766 in the FGFR-1 and regulates the Ras/MEK/MAPK pathway via FRS2 phosphorylation in endothelial cells. *Mol. Biol. Cell* **13**, 2881–2893.

Datta, S. R., Dudek, H., Tao, X., Masters, S., Fu, H., Gotoh, Y. and Greenberg, M. E. (1997). Akt phosphorylation of BAD couples survival signals to the cell-intrinsic death machinery. *Cell* **91**, 231–241.

Daugherty, A. L., McKee, M. L., FitzGerald, D. J. and Mrsny, R. J. (2000). Epithelial application of Pseudomonas aeruginosa exotoxin A results in a selective targeting to cells in the liver, spleen and lymph node. *J Control Release* **65**, 297–302.

Davenport, T. G., Jerome-Majewska, L. A. and Papaioannou, V. E. (2003). Mammary gland, limb and yolk sac defects in mice lacking Tbx3, the gene mutated in human ulnar mammary syndrome. *Development* **130**, 2263–2273.

Davies, S. P., Reddy, H., Caivano, M. and Cohen, P. (2000). Specificity and mechanism of action of some commonly used protein kinase inhibitors. *Biochem. J.* **351**, 95–105.

De Leij, L., Haar, Ter, J. G., Schwander, E., Berendsen, H. H. and The, T. H. (1987). Small Cell Lung Cancer and Embryonic Lung Epithelium Share Monoclonal Antibody Defined Neuroendocrine-related Antigens. *Chest* **91**, 9S–11S.

De Moerlooze, L., Spencer-Dene, B., Revest, J. M., Hajihosseini, M., Rosewell, I. and Dickson, C. (2000). An important role for the IIIb isoform of fibroblast growth factor receptor 2 (FGFR2) in mesenchymal-epithelial signalling during mouse organogenesis. *Development* **127**, 483–492.

Del Moral, P.-M. and Warburton, D. (2010). Explant culture of mouse embryonic whole lung, isolated epithelium, or mesenchyme under chemically defined conditions as a system to evaluate the molecular mechanism of branching morphogenesis and cellular differentiation. *Methods Mol. Biol.* **633**, 71–79.

Derossi, D., Joliot, A. H., Chassaing, G. and Prochiantz, A. (1994). The third helix of the Antennapedia homeodomain translocates through biological membranes. *J. Biol. Chem.* **269**, 10444–10450.

Deshaies, R. J., Sanders, S. L., Feldheim, D. A. and Schekman, R. (1991). Assembly of yeast Sec proteins involved in translocation into the endoplasmic reticulum into a membrane-bound multisubunit complex. *Nature* **349**, 806–808.

Dickinson, B. L., Badizadegan, K., Wu, Z., Ahouse, J. C., Zhu, X., Simister, N. E., Blumberg, R. S. and Lencer, W. I. (1999). Bidirectional FcRn-dependent IgG transport in a polarized human intestinal epithelial cell line. *J. Clin. Invest.* **104**, 903–911.

Diehl, J. A., Cheng, M., Roussel, M. F. and Sherr, C. J. (1998). Glycogen synthase kinase-3beta regulates cyclin D1 proteolysis and subcellular localization. *Genes Dev.* **12**, 3499–3511.

Ding, W., Bellusci, S., Shi, W. and Warburton, D. (2003). Functional analysis of the human Sprouty2 gene promoter. *Gene* **322**, 175–185.

Domin, J., Harper, L., Aubyn, D., Wheeler, M., Florey, O., Haskard, D., Yuan, M. and Zicha, D. (2005). The class II phosphoinositide 3-kinase PI3K-C2beta regulates cell migration by a PtdIns3P dependent mechanism. *J. Cell. Physiol.* **205**, 452–462.

Dosio, F., Stella, B., Cerioni, S., Gastaldi, D. and Arpicco, S. (2014). Advances in anticancer antibody-drug conjugates and immunotoxins. *Recent Pat Anticancer Drug Discov* **9**, 35–65.

Du, X., Youle, R. J., FitzGerald, D. J. and Pastan, I. (2010). Pseudomonas exotoxin A-mediated apoptosis is Bak dependent and preceded by the degradation of Mcl-1. *Molecular and Cellular Biology* **30**, 3444–3452.

Duband, J. L., Monier, F., Delannet, M. and Newgreen, D. (1995). Epithelium-mesenchyme transition during neural crest development. *Acta Anat (Basel)* **154**, 63–78.

Dull, T., Zufferey, R., Kelly, M., Mandel, R. J., Nguyen, M., Trono, D. and Naldini, L. (1998). A third-generation lentivirus vector with a conditional packaging system. *J. Virol.* **72**, 8463–8471.

Edling, C. E., Selvaggi, F., Buus, R., Maffucci, T., Di Sebastiano, P., Friess, H., Innocenti, P., Kocher, H. M. and Falasca, M. (2010). Key role of phosphoinositide 3-kinase class IB in pancreatic cancer. *Clin. Cancer Res.* **16**, 4928–4937.

Engelman, J. A. (2009). Targeting PI3K signalling in cancer: opportunities, challenges and limitations. *Nat. Rev. Cancer* **9**, 550–562.

Engelman, J. A., Jänne, P. A., Mermel, C., Pearlberg, J., Mukohara, T., Fleet, C., Cichowski, K., Johnson, B. E. and Cantley, L. C. (2005). ErbB-3 mediates phosphoinositide 3-kinase activity in gefitinib-sensitive non-small cell lung cancer cell lines. *Proc. Natl. Acad. Sci. U.S.A.* **102**, 3788–3793.

Facchinetti, V., Ouyang, W., Wei, H., Soto, N., Lazorchak, A., Gould, C., Lowry, C., Newton, A. C., Mao, Y., Miao, R. Q., et al. (2008). The mammalian target of rapamycin complex 2 controls folding and stability of Akt and protein kinase C. *EMBO J.* **27**, 1932–1943.

Fagotto, F., Funayama, N., Gluck, U. and Gumbiner, B. M. (1996). Binding to

cadherins antagonizes the signaling activity of beta-catenin during axis formation in Xenopus. *J. Cell Biol.* **132**, 1105–1114.

Fallingborg, J. (1999). Intraluminal pH of the human gastrointestinal tract. *Dan Med Bull* **46**, 183–196.

Featherstone, N. C., Connell, M. G., Fernig, D. G., Wray, S., Burdyga, T. V., Losty, P. D. and Jesudason, E. C. (2006). Airway smooth muscle dysfunction precedes teratogenic congenital diaphragmatic hernia and may contribute to hypoplastic lung morphogenesis. *Am. J. Respir. Cell Mol. Biol.* **35**, 571–578.

Finch, P. W., Cunha, G. R., Rubin, J. S., Wong, J. and Ron, D. (1995). Pattern of keratinocyte growth factor and keratinocyte growth factor receptor expression during mouse fetal development suggests a role in mediating morphogenetic mesenchymal-epithelial interactions. *Dev. Dyn.* **203**, 223–240.

Finney, B. A., del Moral, P. M., Wilkinson, W. J., Cayzac, S., Cole, M., Warburton, D., Kemp, P. J. and Riccardi, D. (2008). Regulation of mouse lung development by the extracellular calcium-sensing receptor, CaR. *J. Physiol. (Lond.)* **586**, 6007–6019.

Fittipaldi, A., Ferrari, A., Zoppé, M., Arcangeli, C., Pellegrini, V., Beltram, F. and Giacca, M. (2003). Cell membrane lipid rafts mediate caveolar endocytosis of HIV-1 Tat fusion proteins. *J. Biol. Chem.* **278**, 34141–34149.

FitzGerald, D. J., Willingham, M. C. and Pastan, I. (1986). Antitumor effects of an immunotoxin made with Pseudomonas exotoxin in a nude mouse model of human ovarian cancer. *Proc. Natl. Acad. Sci. U.S.A.* **83**, 6627–6630.

Flaumenhaft, R., Moscatelli, D. and Rifkin, D. B. (1990). Heparin and heparan sulfate increase the radius of diffusion and action of basic fibroblast growth factor. *J. Cell Biol.* **111**, 1651–1659.

Foley, B. T., Moehring, J. M. and Moehring, T. J. (1995). Mutations in the elongation factor 2 gene which confer resistance to diphtheria toxin and Pseudomonas exotoxin A. Genetic and biochemical analyses. *J. Biol. Chem.* **270**, 23218–23225.

Foster, J. G., Blunt, M. D., Carter, E. and Ward, S. G. (2012). Inhibition of PI3K signaling spurs new therapeutic opportunities in inflammatory/autoimmune diseases and hematological malignancies. *Pharmacol. Rev.* **64**, 1027–1054.

Fox, R. I. (1993). Mechanism of action of hydroxychloroquine as an antirheumatic drug. *Semin. Arthritis Rheum.* **23**, 82–91.

Francavilla, C., Rigbolt, K. T. G., Emdal, K. B., Carraro, G., Vernet, E., Bekker-Jensen, D. B., Streicher, W., Wikström, M., Sundström, M., Bellusci, S., et al. (2013). Functional Proteomics Defines the Molecular Switch Underlying FGF Receptor Trafficking and Cellular Outputs. *Mol. Cell*.

Franke, T. F., Kaplan, D. R., Cantley, L. C. and Toker, A. (1997). Direct regulation of the Akt proto-oncogene product by phosphatidylinositol-3,4-

bisphosphate. *Science* **275**, 665–668.

Franke, T. F., Yang, S. I., Chan, T. O., Datta, K., Kazlauskas, A., Morrison, D. K., Kaplan, D. R. and Tsichlis, P. N. (1995). The protein kinase encoded by the Akt proto-oncogene is a target of the PDGF-activated phosphatidylinositol 3-kinase. *Cell* **81**, 727–736.

Frankel, A. D. and Pabo, C. O. (1988). Cellular uptake of the tat protein from human immunodeficiency virus. *Cell* **55**, 1189–1193.

Fruman, D. A. and Rommel, C. (2014). PI3K and cancer: lessons, challenges and opportunities. *Nat Rev Drug Discov* **13**, 140–156.

Furet, P., Guagnano, V., Fairhurst, R. A., Imbach-Weese, P., Bruce, I., Knapp, M., Fritsch, C., Blasco, F., Blanz, J., Aichholz, R., et al. (2013). Discovery of NVP-BYL719 a potent and selective phosphatidylinositol-3 kinase alpha inhibitor selected for clinical evaluation. *Bioorganic & Medicinal Chemistry Letters* **23**, 3741–3748.

Futaki, S., Suzuki, T., Ohashi, W., Yagami, T., Tanaka, S., Ueda, K. and Sugiura, Y. (2001). Arginine-rich peptides. An abundant source of membrane-permeable peptides having potential as carriers for intracellular protein delivery. *J. Biol. Chem.* **276**, 5836–5840.

Gao, X., Zhang, Y., Arrazola, P., Hino, O., Kobayashi, T., Yeung, R. S., Ru, B. and Pan, D. (2002). Tsc tumour suppressor proteins antagonize amino-acid-TOR signalling. *Nat. Cell Biol.* **4**, 699–704.

Garami, A., Zwartkruis, F. J. T., Nobukuni, T., Joaquin, M., Roccio, M., Stocker, H., Kozma, S. C., Hafen, E., Bos, J. L. and Thomas, G. (2003). Insulin activation of Rheb, a mediator of mTOR/S6K/4E-BP signaling, is inhibited by TSC1 and 2. *Mol. Cell* **11**, 1457–1466.

Garlich, J. R., De, P., Dey, N., Su, J. D., Peng, X., Miller, A., Murali, R., Lu, Y., Mills, G. B., Kundra, V., et al. (2008). A vascular targeted pan phosphoinositide 3-kinase inhibitor prodrug, SF1126, with antitumor and antiangiogenic activity. *Cancer Res.* **68**, 206–215.

Gassama-Diagne, A., Yu, W., Beest, ter, M., Martin-Belmonte, F., Kierbel, A., Engel, J. and Mostov, K. (2006). Phosphatidylinositol-3,4,5-trisphosphate regulates the formation of the basolateral plasma membrane in epithelial cells. *Nat. Cell Biol.* **8**, 963–970.

Geisow, M. J. and Evans, W. H. (1984). pH in the endosome. Measurements during pinocytosis and receptor-mediated endocytosis. *Exp. Cell Res.* **150**, 36–46.

Gerbal-Chaloin, S., Gondeau, C., Aldrian-Herrada, G., Heitz, F., Gauthier-Rouvière, C. and Divita, G. (2007). First step of the cell-penetrating peptide mechanism involves Rac1 GTPase-dependent actin-network remodelling. *Biol. Cell* **99**, 223–238.

Ghosh, S., Lau, H., Simons, B. W., Powell, J. D., Meyers, D. J., De Marzo, A. M., Berman, D. M. and Lotan, T. L. (2011). PI3K/mTOR signaling regulates prostatic branching morphogenesis. *Developmental Biology* **360**, 329–342.

Giannotta, M., Ruggiero, C., Grossi, M., Cancino, J., Capitani, M., Pulvirenti, T., Consoli, G. M. L., Geraci, C., Fanelli, F., Luini, A., et al. (2012). The KDEL receptor couples to Gαq/11 to activate Src kinases and regulate transport through the Golgi. *EMBO J.* **31**, 2869–2881.

Glogau, R., Blitzer, A., Brandt, F., Kane, M., Monheit, G. D. and Waugh, J. M. (2012). Results of a randomized, double-blind, placebo-controlled study to evaluate the efficacy and safety of a botulinum toxin type A topical gel for the treatment of moderate-to-severe lateral canthal lines. *J Drugs Dermatol* **11**, 38–45.

Gontan, C., de Munck, A., Vermeij, M., Grosveld, F., Tibboel, D. and Rottier, R. (2008). Sox2 is important for two crucial processes in lung development: branching morphogenesis and epithelial cell differentiation. *Developmental Biology* **317**, 296–309.

Gordon, V. M., Klimpel, K. R., Arora, N., Henderson, M. A. and Leppla, S. H. (1995). Proteolytic activation of bacterial toxins by eukaryotic cells is performed by furin and by additional cellular proteases. *Infect. Immun.* **63**, 82–87.

Griffith, K. J., Chan, E. K., Lung, C. C., Hamel, J. C., Guo, X., Miyachi, K. and Fritzler, M. J. (1997). Molecular cloning of a novel 97-kd Golgi complex autoantigen associated with Sjögren's syndrome. *Arthritis Rheum.* **40**, 1693–1702.

Guba, M., Breitenbuch, von, P., Steinbauer, M., Koehl, G., Flegel, S., Hornung, M., Bruns, C. J., Zuelke, C., Farkas, S., Anthuber, M., et al. (2002). Rapamycin inhibits primary and metastatic tumor growth by antiangiogenesis: involvement of vascular endothelial growth factor. *Nat. Med.* **8**, 128–135.

Guillermet-Guibert, J., Bjorklof, K., Salpekar, A., Gonella, C., Ramadani, F., Bilancio, A., Meek, S., Smith, A. J. H., Okkenhaug, K. and Vanhaesebroeck, B. (2008). The p110beta isoform of phosphoinositide 3-kinase signals downstream of G protein-coupled receptors and is functionally redundant with p110gamma. *Proc. Natl. Acad. Sci. U.S.A.* **105**, 8292–8297.

Guo, J.-P., Coppola, D. and Cheng, J. Q. (2011). IKBKE protein activates Akt independent of phosphatidylinositol 3-kinase/PDK1/mTORC2 and the pleckstrin homology domain to sustain malignant transformation. *J. Biol. Chem.* **286**, 37389–37398.

Guo, L., Degenstein, L. and Fuchs, E. (1996). Keratinocyte growth factor is required for hair development but not for wound healing. *Genes Dev.* **10**, 165–175.

Gurrola, G. B., Capes, E. M., Zamudio, F. Z., Possani, L. D. and Valdivia, H. H. (2010). Imperatoxin A, a Cell-Penetrating Peptide from Scorpion Venom, as a Probe of Ca-Release Channels/Ryanodine Receptors. *Pharmaceuticals (Basel)* **3**, 1093–1107.

Guterstam, P., Madani, F., Hirose, H., Takeuchi, T., Futaki, S., Andaloussi, El, S., Gräslund, A. and Langel, U. (2009). Elucidating cell-penetrating peptide mechanisms of action for membrane interaction, cellular uptake, and translocation utilizing the hydrophobic counter-anion pyrenebutyrate. *Biochim. Biophys. Acta* **1788**, 2509–2517.

Hacohen, N., Kramer, S., Sutherland, D., Hiromi, Y. and Krasnow, M. A. (1998). sprouty encodes a novel antagonist of FGF signaling that patterns apical branching of the Drosophila airways. *Cell* **92**, 253–263.

Haghi, M., Young, P. M., Traini, D., Jaiswal, R., Gong, J. and Bebawy, M. (2010). Time- and passage-dependent characteristics of a Calu-3 respiratory epithelial cell model. *Drug Dev Ind Pharm* **36**, 1207–1214.

Hakomori, S. (2003). Structure, organization, and function of glycosphingolipids in membrane. *Curr. Opin. Hematol.* **10**, 16–24.

Hanas, R. and Ludvigsson, J. (1997). Experience of pain from insulin injections and needle‐phobia in young patients with IDDM. *Practical Diabetes International*.

Hansen, A., Schäfer, I., Knappe, D., Seibel, P. and Hoffmann, R. (2012). Intracellular toxicity of proline-rich antimicrobial peptides shuttled into mammalian cells by the cell-penetrating peptide penetratin. *Antimicrob. Agents Chemother.* **56**, 5194–5201.

Harada, K., Truong, A. B., Cai, T. and Khavari, P. A. (2005). The class II phosphoinositide 3-kinase C2beta is not essential for epidermal differentiation. *Molecular and Cellular Biology* **25**, 11122–11130.

Harris, D. P., Vogel, P., Wims, M., Moberg, K., Humphries, J., Jhaver, K. G., DaCosta, C. M., Shadoan, M. K., Xu, N., Hansen, G. M., et al. (2011). Requirement for class II phosphoinositide 3-kinase C2alpha in maintenance of glomerular structure and function. *Molecular and Cellular Biology* **31**, 63–80.

Harris, S. J., Parry, R. V., Westwick, J. and Ward, S. G. (2008). Phosphoinositide lipid phosphatases: natural regulators of phosphoinositide 3-kinase signaling in T lymphocytes. *J. Biol. Chem.* **283**, 2465–2469.

Haruta, T., Uno, T., Kawahara, J., Takano, A., Egawa, K., Sharma, P. M., Olefsky, J. M. and Kobayashi, M. (2000). A rapamycin-sensitive pathway down-regulates insulin signaling via phosphorylation and proteasomal degradation of insulin receptor substrate-1. *Mol. Endocrinol.* **14**, 783–794.

Hassan, R., Williams-Gould, J., Watson, T., Pai-Scherf, L. and Pastan, I. (2004). Pretreatment with rituximab does not inhibit the human immune

response against the immunogenic protein LMB-1. *Clin. Cancer Res.* **10**, 16–18.

Hieda, Y., Iwai, K., Morita, T. and Nakanishi, Y. (1996). Mouse embryonic submandibular gland epithelium loses its tissue integrity during early branching morphogenesis. *Dev. Dyn.* **207**, 395–403.

Hinz, B. and Gabbiani, G. (2010). Fibrosis: recent advances in myofibroblast biology and new therapeutic perspectives. *F1000 Biol Rep* **2**, 78.

Hisatomi, K., Mukae, H., Sakamoto, N., Ishimatsu, Y., Kakugawa, T., Hara, S., Fujita, H., Nakamichi, S., Oku, H., Urata, Y., et al. (2012). Pirfenidone inhibits TGF-β1-induced over-expression of collagen type I and heat shock protein 47 in A549 cells. *BMC Pulm Med* **12**, 24.

Holmgren, J., Lönnroth, I., Månsson, J. and Svennerholm, L. (1975). Interaction of cholera toxin and membrane GM1 ganglioside of small intestine. *Proc. Natl. Acad. Sci. U.S.A.* **72**, 2520–2524.

Holz, M. K. and Blenis, J. (2005). Identification of S6 kinase 1 as a novel mammalian target of rapamycin (mTOR)-phosphorylating kinase. *J. Biol. Chem.* **280**, 26089–26093.

Hsu, J. C., Di Pasquale, G., Harunaga, J. S., Onodera, T., Hoffman, M. P., Chiorini, J. A. and Yamada, K. M. (2012). Viral gene transfer to developing mouse salivary glands. *J. Dent. Res.* **91**, 197–202.

Huang, C.-H., Mandelker, D., Schmidt-Kittler, O., Samuels, Y., Velculescu, V. E., Kinzler, K. W., Vogelstein, B., Gabelli, S. B. and Amzel, L. M. (2007). The structure of a human p110alpha/p85alpha complex elucidates the effects of oncogenic PI3Kalpha mutations. *Science* **318**, 1744–1748.

Igarashi, M., Finch, P. W. and Aaronson, S. A. (1998). Characterization of recombinant human fibroblast growth factor (FGF)-10 reveals functional similarities with keratinocyte growth factor (FGF-7). *J. Biol. Chem.* **273**, 13230–13235.

Iglewski, B. H., Liu, P. V. and Kabat, D. (1977). Mechanism of action of Pseudomonas aeruginosa exotoxin Aiadenosine diphosphate-ribosylation of mammalian elongation factor 2 in vitro and in vivo. *Infect. Immun.* **15**, 138–144.

Ikonomov, O. C., Sbrissa, D. and Shisheva, A. (2006). Localized PtdIns 3,5-P2 synthesis to regulate early endosome dynamics and fusion. *Am. J. Physiol., Cell Physiol.* **291**, C393–404.

Inoki, K., Li, Y., Zhu, T., Wu, J. and Guan, K.-L. (2002). TSC2 is phosphorylated and inhibited by Akt and suppresses mTOR signalling. *Nat. Cell Biol.* **4**, 648–657.

Iyer, S. N., Gurujeyalakshmi, G. and Giri, S. N. (1999). Effects of pirfenidone on transforming growth factor-beta gene expression at the transcriptional level in

bleomycin hamster model of lung fibrosis. *J. Pharmacol. Exp. Ther.* **291**, 367–373.

Izvolsky, K. I., Shoykhet, D., Yang, Y., Yu, Q., Nugent, M. A. and Cardoso, W. V. (2003). Heparan sulfate-FGF10 interactions during lung morphogenesis. *Developmental Biology* **258**, 185–200.

Jackson, M. E., Simpson, J. C., Girod, A., Pepperkok, R., Roberts, L. M. and Lord, J. M. (1999). The KDEL retrieval system is exploited by Pseudomonas exotoxin A, but not by Shiga-like toxin-1, during retrograde transport from the Golgi complex to the endoplasmic reticulum. *J. Cell. Sci.* **112 (Pt 4)**, 467–475.

Jackson, S. P., Schoenwaelder, S. M., Goncalves, I., Nesbitt, W. S., Yap, C. L., Wright, C. E., Kenche, V., Anderson, K. E., Dopheide, S. M., Yuan, Y., et al. (2005). PI 3-kinase p110beta: a new target for antithrombotic therapy. *Nat. Med.* **11**, 507–514.

Jamieson, S., Flanagan, J. U., Kolekar, S., Buchanan, C., Kendall, J. D., Lee, W. J., Rewcastle, G. W., Denny, W. A., Singh, R., Dickson, J., et al. (2011). A drug targeting only p110α can block phosphoinositide 3-kinase signalling and tumour growth in certain cell types. *Biochem. J.* **438**, 53–62.

Jayaraman, S., Song, Y. and Verkman, A. S. (2001). Airway surface liquid pH in well-differentiated airway epithelial cell cultures and mouse trachea. *Am. J. Physiol., Cell Physiol.* **281**, C1504–11.

Jesudason, E. C., Smith, N. P., Connell, M. G., Spiller, D. G., White, M. R. H., Fernig, D. G. and Losty, P. D. (2006). Peristalsis of airway smooth muscle is developmentally regulated and uncoupled from hypoplastic lung growth. *Am. J. Physiol. Lung Cell Mol. Physiol.* **291**, L559–65.

Jesudason, E. C., Smith, N. P., Connell, M. G., Spiller, D. G., White, M. R. H., Fernig, D. G. and Losty, P. D. (2005). Developing rat lung has a sided pacemaker region for morphogenesis-related airway peristalsis. *Am. J. Respir. Cell Mol. Biol.* **32**, 118–127.

Jiao, C.-Y., Delaroche, D., Burlina, F., Alves, I. D., Chassaing, G. and Sagan, S. (2009). Translocation and endocytosis for cell-penetrating peptide internalization. *J. Biol. Chem.* **284**, 33957–33965.

Joanne, P., Galanth, C., Goasdoué, N., Nicolas, P., Sagan, S., Lavielle, S., Chassaing, G., Amri, El, C. and Alves, I. D. (2009). Lipid reorganization induced by membrane-active peptides probed using differential scanning calorimetry. *Biochim. Biophys. Acta* **1788**, 1772–1781.

Jones, S. W., Christison, R., Bundell, K., Voyce, C. J., Brockbank, S. M. V., Newham, P. and Lindsay, M. A. (2005). Characterisation of cell-penetrating peptide-mediated peptide delivery. *Br. J. Pharmacol.* **145**, 1093–1102.

Joshi, S. and Kotecha, S. (2007). Lung growth and development. *Early Hum. Dev.* **83**, 789–794.

Julien, L. A., Carriere, A., Moreau, J. and Roux, P. P. (2010). mTORC1-Activated S6K1 Phosphorylates Rictor on Threonine 1135 and Regulates mTORC2 Signaling. *Molecular and Cellular Biology* **30**, 908–921.

Jørgensen, R., Purdy, A. E., Fieldhouse, R. J., Kimber, M. S., Bartlett, D. H. and Merrill, A. R. (2008). Cholix toxin, a novel ADP-ribosylating factor from Vibrio cholerae. *J. Biol. Chem.* **283**, 10671–10678.

Kam, Y. and Quaranta, V. (2009). Cadherin-bound beta-catenin feeds into the Wnt pathway upon adherens junctions dissociation: evidence for an intersection between beta-catenin pools. *PLoS ONE* **4**, e4580.

Kanai, M., Göke, M., Tsunekawa, S. and Podolsky, D. K. (1997). Signal transduction pathway of human fibroblast growth factor receptor 3. Identification of a novel 66-kDa phosphoprotein. *J. Biol. Chem.* **272**, 6621–6628.

Keen, J. H., Willingham, M. C. and Pastan, I. H. (1979). Clathrin-coated vesicles: isolation, dissociation and factor-dependent reassociation of clathrin baskets. *Cell* **16**, 303–312.

Khafagy, E.-S., Kamei, N., Nielsen, E. J. B., Nishio, R. and Takeda-Morishita, M. (2013). One-month subchronic toxicity study of cell-penetrating peptides for insulin nasal delivery in rats. *Eur J Pharm Biopharm* **85**, 736–743.

Kierbel, A., Gassama-Diagne, A., Rocha, C., Radoshevich, L., Olson, J., Mostov, K. and Engel, J. (2007). Pseudomonas aeruginosa exploits a PIP3-dependent pathway to transform apical into basolateral membrane. *J. Cell Biol.* **177**, 21–27.

Kilk, K., Mahlapuu, R., Soomets, U. and Langel, U. (2009). Analysis of in vitro toxicity of five cell-penetrating peptides by metabolic profiling. *Toxicology* **265**, 87–95.

Kim, K. K., Kugler, M. C., Wolters, P. J., Robillard, L., Galvez, M. G., Brumwell, A. N., Sheppard, D. and Chapman, H. A. (2006). Alveolar epithelial cell mesenchymal transition develops in vivo during pulmonary fibrosis and is regulated by the extracellular matrix. *Proc. Natl. Acad. Sci. U.S.A.* **103**, 13180–13185.

Klämbt, C., Glazer, L. and Shilo, B. Z. (1992). breathless, a Drosophila FGF receptor homolog, is essential for migration of tracheal and specific midline glial cells. *Genes Dev.* **6**, 1668–1678.

Knight, Z. A., Gonzalez, B., Feldman, M. E., Zunder, E. R., Goldenberg, D. D., Williams, O., Loewith, R., Stokoe, D., Balla, A., Toth, B., et al. (2006). A pharmacological map of the PI3-K family defines a role for p110alpha in insulin signaling. *Cell* **125**, 733–747.

Kong, D. and Yamori, T. (2007). ZSTK474 is an ATP-competitive inhibitor of class I phosphatidylinositol 3 kinase isoforms. *Cancer Sci.* **98**, 1638–1642.

Kotecha, S. (2000). Lung growth: implications for the newborn infant. *Arch. Dis. Child. Fetal Neonatal Ed.* **82**, F69–74.

Kouhara, H., Hadari, Y. R., Spivak-Kroizman, T., Schilling, J., Bar-Sagi, D., Lax, I. and Schlessinger, J. (1997). A lipid-anchored Grb2-binding protein that links FGF-receptor activation to the Ras/MAPK signaling pathway. *Cell* **89**, 693–702.

Kounnas, M. Z., Morris, R. E., Thompson, M. R., FitzGerald, D. J., Strickland, D. K. and Saelinger, C. B. (1992). The alpha 2-macroglobulin receptor/low density lipoprotein receptor-related protein binds and internalizes Pseudomonas exotoxin A. *J. Biol. Chem.* **267**, 12420–12423.

Kovalenko, D., Yang, X., Nadeau, R. J., Harkins, L. K. and Friesel, R. (2003). Sef inhibits fibroblast growth factor signaling by inhibiting FGFR1 tyrosine phosphorylation and subsequent ERK activation. *J. Biol. Chem.* **278**, 14087–14091.

Kreitman, R. J. and Pastan, I. (1998). Accumulation of a recombinant immunotoxin in a tumor in vivo: fewer than 1000 molecules per cell are sufficient for complete responses. *Cancer Res.* **58**, 968–975.

Kunii, K., Davis, L., Gorenstein, J., Hatch, H., Yashiro, M., Di Bacco, A., Elbi, C. and Lutterbach, B. (2008). FGFR2-amplified gastric cancer cell lines require FGFR2 and Erbb3 signaling for growth and survival. *Cancer Res.* **68**, 2340–2348.

Lam, E. W.-F., Francis, R. E. and Petkovic, M. (2006). FOXO transcription factors: key regulators of cell fate. *Biochem. Soc. Trans.* **34**, 722–726.

Lao, D.-H., Chandramouli, S., Yusoff, P., Fong, C. W., Saw, T. Y., Tai, L. P., Yu, C. Y., Leong, H. F. and Guy, G. R. (2006). A Src homology 3-binding sequence on the C terminus of Sprouty2 is necessary for inhibition of the Ras/ERK pathway downstream of fibroblast growth factor receptor stimulation. *J. Biol. Chem.* **281**, 29993–30000.

Larsen, M., Hoffman, M. P., Sakai, T., Neibaur, J. C., Mitchell, J. M. and Yamada, K. M. (2003). Role of PI 3-kinase and PIP3 in submandibular gland branching morphogenesis. *Developmental Biology* **255**, 178–191.

Lazarus, A., Del Moral, P.-M., Ilovich, O., Mishani, E., Warburton, D. and Keshet, E. (2011). A perfusion-independent role of blood vessels in determining branching stereotypy of lung airways. *Development* **138**, 2359–2368.

Lee, K. S., Lee, H. K., Hayflick, J. S., Lee, Y. C. and Puri, K. D. (2006). Inhibition of phosphoinositide 3-kinase delta attenuates allergic airway inflammation and hyperresponsiveness in murine asthma model. *FASEB J.* **20**, 455–465.

Lee, M. K., Smith, S. M., Banerjee, M. M., Li, C., Minoo, P., Volpe, M. V. and Nielsen, H. C. (2014). The p66Shc adapter protein regulates the morphogenesis and epithelial maturation of fetal mouse lungs. *Am. J. Physiol.*

Lung Cell Mol. Physiol. **306**, L316–25.

Lee, M.-H., Koria, P., Qu, J. and Andreadis, S. T. (2009). JNK phosphorylates beta-catenin and regulates adherens junctions. *FASEB J.* **23**, 3874–3883.

Lemichez, E., Bomsel, M., Devilliers, G., vanderSpek, J., Murphy, J. R., Lukianov, E. V., Olsnes, S. and Boquet, P. (1997). Membrane translocation of diphtheria toxin fragment A exploits early to late endosome trafficking machinery. *Mol. Microbiol.* **23**, 445–457.

Lencer, W. I., Moe, S., Rufo, P. A. and Madara, J. L. (1995). Transcytosis of cholera toxin subunits across model human intestinal epithelia. *Proc. Natl. Acad. Sci. U.S.A.* **92**, 10094–10098.

Lewis, M. J. and Pelham, H. R. (1990). A human homologue of the yeast HDEL receptor. *Nature* **348**, 162–163.

Li, X., Brunton, V. G., Burgar, H. R., Wheldon, L. M. and Heath, J. K. (2004). FRS2-dependent SRC activation is required for fibroblast growth factor receptor-induced phosphorylation of Sprouty and suppression of ERK activity. *J. Cell. Sci.* **117**, 6007–6017.

Liao, R. G., Jung, J., Tchaicha, J., Wilkerson, M. D., Sivachenko, A., Beauchamp, E. M., Liu, Q., Pugh, T. J., Pedamallu, C. S., Hayes, D. N., et al. (2013). Inhibitor-sensitive FGFR2 and FGFR3 mutations in lung squamous cell carcinoma. *Cancer Res.* **73**, 5195–5205.

Lickert, H., Bauer, A., Kemler, R. and Stappert, J. (2000). Casein kinase II phosphorylation of E-cadherin increases E-cadherin/beta-catenin interaction and strengthens cell-cell adhesion. *J. Biol. Chem.* **275**, 5090–5095.

Lin, A., Piao, H.-L., Zhuang, L., Sarbassov, D. D., Ma, L. and Gan, B. (2014). FoxO Transcription Factors Promote AKT Ser473 Phosphorylation and Renal Tumor Growth in Response to Pharmacologic Inhibition of the PI3K-AKT Pathway. *Cancer Res.* **74**, 1682–1693.

Lindsley, C. W., Zhao, Z., Leister, W. H., Robinson, R. G., Barnett, S. F., Defeo-Jones, D., Jones, R. E., Hartman, G. D., Huff, J. R., Huber, H. E., et al. (2005). Allosteric Akt (PKB) inhibitors: discovery and SAR of isozyme selective inhibitors. *Bioorganic & Medicinal Chemistry Letters* **15**, 761–764.

Liu, Y., Martinez, L., Ebine, K. and Abe, M. K. (2008). Role for mitogen-activated protein kinase p38 alpha in lung epithelial branching morphogenesis. *Developmental Biology* **314**, 224–235.

Lo, S. L. and Wang, S. (2008). An endosomolytic Tat peptide produced by incorporation of histidine and cysteine residues as a nonviral vector for DNA transfection. *Biomaterials* **29**, 2408–2414.

Lois, C., Hong, E. J., Pease, S., Brown, E. J. and Baltimore, D. (2002). Germline transmission and tissue-specific expression of transgenes delivered by lentiviral vectors. *Science* **295**, 868–872.

Lundberg, P., El-Andaloussi, S., Sütlü, T., Johansson, H. and Langel, U. (2007). Delivery of short interfering RNA using endosomolytic cell-penetrating peptides. *FASEB J.* **21**, 2664–2671.

Lundin, P., Johansson, H., Guterstam, P., Holm, T., Hansen, M., Langel, U. and Andaloussi, El, S. (2008). Distinct uptake routes of cell-penetrating peptide conjugates. *Bioconjug. Chem.* **19**, 2535–2542.

Madani, F., Lindberg, S., Langel, U., Futaki, S. and Gräslund, A. (2011). Mechanisms of cellular uptake of cell-penetrating peptides. *J Biophys* **2011**, 414729.

Maffucci, T., Cooke, F. T., Foster, F. M., Traer, C. J., Fry, M. J. and Falasca, M. (2005). Class II phosphoinositide 3-kinase defines a novel signaling pathway in cell migration. *J. Cell Biol.* **169**, 789–799.

Mailleux, A. A., Kelly, R., Veltmaat, J. M., De Langhe, S. P., Zaffran, S., Thiery, J. P. and Bellusci, S. (2005). Fgf10 expression identifies parabronchial smooth muscle cell progenitors and is required for their entry into the smooth muscle cell lineage. *Development* **132**, 2157–2166.

Mailleux, A. A., Tefft, D., Ndiaye, D., Itoh, N., Thiery, J. P., Warburton, D. and Bellusci, S. (2001). Evidence that SPROUTY2 functions as an inhibitor of mouse embryonic lung growth and morphogenesis. *Mech. Dev.* **102**, 81–94.

Makarenkova, H. P., Hoffman, M. P., Beenken, A., Eliseenkova, A. V., Meech, R., Tsau, C., Patel, V. N., Lang, R. A. and Mohammadi, M. (2009). Differential interactions of FGFs with heparan sulfate control gradient formation and branching morphogenesis. *Sci Signal* **2**, ra55.

Mandelbrot, B. B. (1983). *The Fractal Geometry of Nature*. Macmillan.

Manders, E., Verbeek, F. J. and Aten, J. A. (1993). Measurement of co-localization of objects in dual-colour confocal images. *Journal of Microscopy*.

Mandl, M., Slack, D. N. and Keyse, S. M. (2005). Specific inactivation and nuclear anchoring of extracellular signal-regulated kinase 2 by the inducible dual-specificity protein phosphatase DUSP5. *Molecular and Cellular Biology* **25**, 1830–1845.

Manning, B. D. and Cantley, L. C. (2007). AKT/PKB signaling: navigating downstream. *Cell* **129**, 1261–1274.

Manning, G., Whyte, D. B., Martinez, R., Hunter, T. and Sudarsanam, S. (2002). The protein kinase complement of the human genome. *Science* **298**, 1912–1934.

Marek, L., Ware, K. E., Fritzsche, A., Hercule, P., Helton, W. R., Smith, J. E., McDermott, L. A., Coldren, C. D., Nemenoff, R. A., Merrick, D. T., et al. (2009). Fibroblast growth factor (FGF) and FGF receptor-mediated autocrine signaling in non-small-cell lung cancer cells. *Mol. Pharmacol.* **75**, 196–207.

Marmai, C., Sutherland, R. E., Kim, K. K., Dolganov, G. M., Fang, X., Kim, S. S., Jiang, S., Golden, J. A., Hoopes, C. W., Matthay, M. A., et al. (2011). Alveolar epithelial cells express mesenchymal proteins in patients with idiopathic pulmonary fibrosis. *Am. J. Physiol. Lung Cell Mol. Physiol.* **301**, L71–8.

Marsh, J. W. (1988). Antibody-mediated routing of diphtheria toxin in murine cells results in a highly efficacious immunotoxin. *J. Biol. Chem.* **263**, 15993–15999.

Martin-Belmonte, F., Gassama, A., Datta, A., Yu, W., Rescher, U., Gerke, V. and Mostov, K. (2007). PTEN-mediated apical segregation of phosphoinositides controls epithelial morphogenesis through Cdc42. *Cell* **128**, 383–397.

Mason, I. J., Fuller-Pace, F., Smith, R. and Dickson, C. (1994). FGF-7 (keratinocyte growth factor) expression during mouse development suggests roles in myogenesis, forebrain regionalisation and epithelial-mesenchymal interactions. *Mech. Dev.* **45**, 15–30.

McKee, M. L. and FitzGerald, D. J. (1999). Reduction of furin-nicked Pseudomonas exotoxin A: an unfolding story. *Biochemistry* **38**, 16507–16513.

McLean, B. A., Zhabyeyev, P., Pituskin, E., Paterson, I., Haykowsky, M. J. and Oudit, G. Y. (2013). PI3K inhibitors as novel cancer therapies: implications for cardiovascular medicine. *J. Card. Fail.* **19**, 268–282.

Medzhitov, R., Preston-Hurlburt, P. and Janeway, C. A. (1997). A human homologue of the Drosophila Toll protein signals activation of adaptive immunity. *Nature* **388**, 394–397.

Metzger, R. J., Klein, O. D., Martin, G. R. and Krasnow, M. A. (2008). The branching programme of mouse lung development. *Nature* **453**, 745–750.

Meyer, T. N., Schwesinger, C., Bush, K. T., Stuart, R. O., Rose, D. W., Shah, M. M., Vaughn, D. A., Steer, D. L. and Nigam, S. K. (2004). Spatiotemporal regulation of morphogenetic molecules during in vitro branching of the isolated ureteric bud: toward a model of branching through budding in the developing kidney. *Developmental Biology* **275**, 44–67.

Miettinen, P. J., Ebner, R., Lopez, A. R. and Derynck, R. (1994). TGF-beta induced transdifferentiation of mammary epithelial cells to mesenchymal cells: involvement of type I receptors. *J. Cell Biol.* **127**, 2021–2036.

Miki, T., Bottaro, D. P., Fleming, T. P., Smith, C. L., Burgess, W. H., Chan, A. M. and Aaronson, S. A. (1992). Determination of ligand-binding specificity by alternative splicing: two distinct growth factor receptors encoded by a single gene. *Proc. Natl. Acad. Sci. U.S.A.* **89**, 246–250.

Milletti, F. (2012). Cell-penetrating peptides: classes, origin, and current landscape. *Drug Discov. Today* **17**, 850–860.

Min, H., Danilenko, D. M., Scully, S. A., Bolon, B., Ring, B. D., Tarpley, J. E.,

DeRose, M. and Simonet, W. S. (1998). Fgf-10 is required for both limb and lung development and exhibits striking functional similarity to Drosophila branchless. *Genes Dev.* **12**, 3156–3161.

Misawa, H., Ohtsubo, M., Copeland, N. G., Gilbert, D. J., Jenkins, N. A. and Yoshimura, A. (1998). Cloning and characterization of a novel class II phosphoinositide 3-kinase containing C2 domain. *Biochem. Biophys. Res. Commun.* **244**, 531–539.

Mohammadi, M., Froum, S., Hamby, J. M., Schroeder, M. C., Panek, R. L., Lu, G. H., Eliseenkova, A. V., Green, D., Schlessinger, J. and Hubbard, S. R. (1998). Crystal structure of an angiogenesis inhibitor bound to the FGF receptor tyrosine kinase domain. *EMBO J.* **17**, 5896–5904.

Mohammadi, M., Honegger, A. M., Rotin, D., Fischer, R., Bellot, F., Li, W., Dionne, C. A., Jaye, M., Rubinstein, M. and Schlessinger, J. (1991). A tyrosine-phosphorylated carboxy-terminal peptide of the fibroblast growth factor receptor (Flg) is a binding site for the SH2 domain of phospholipase C-gamma 1. *Molecular and Cellular Biology* **11**, 5068–5078.

Mohammed, A. F., Abdul-Wahid, A., Huang, E. H.-B., Bolewska-Pedyczak, E., Cydzik, M., Broad, A. E. and Gariépy, J. (2012). The Pseudomonas aeruginosa exotoxin A translocation domain facilitates the routing of CPP-protein cargos to the cytosol of eukaryotic cells. *J Control Release* **164**, 58–64.

Moir, L. M., Trian, T., Ge, Q., Shepherd, P. R., Burgess, J. K., Oliver, B. G. G. and Black, J. L. (2011). Phosphatidylinositol 3-kinase isoform-specific effects in airway mesenchymal cell function. *J. Pharmacol. Exp. Ther.* **337**, 557–566.

Moschos, S. A., Jones, S. W., Perry, M. M., Williams, A. E., Erjefalt, J. S., Turner, J. J., Barnes, P. J., Sproat, B. S., Gait, M. J. and Lindsay, M. A. (2007). Lung delivery studies using siRNA conjugated to TAT(48-60) and penetratin reveal peptide induced reduction in gene expression and induction of innate immunity. *Bioconjug. Chem.* **18**, 1450–1459.

Mostov, K. E., Friedlander, M. and Blobel, G. (1984). The receptor for transepithelial transport of IgA and IgM contains multiple immunoglobulin-like domains. *Nature* **308**, 37–43.

Mrsny, R. J., Daugherty, A. L., McKee, M. L. and FitzGerald, D. J. (2002). Bacterial toxins as tools for mucosal vaccination. *Drug Discov. Today* **7**, 247–258.

Mukaida, N., Mahe, Y. and Matsushima, K. (1990). Cooperative interaction of nuclear factor-kappa B- and cis-regulatory enhancer binding protein-like factor binding elements in activating the interleukin-8 gene by pro-inflammatory cytokines. *J. Biol. Chem.* **265**, 21128–21133.

Murray, C. D. (1926). The Physiological Principle of Minimum Work: II. Oxygen Exchange in Capillaries. *Proc. Natl. Acad. Sci. U.S.A.* **12**, 299–304.

Naber, H. P. H., Drabsch, Y., Snaar-Jagalska, B. E., Dijke, ten, P. and van

Laar, T. (2013). Snail and Slug, key regulators of TGF-β-induced EMT, are sufficient for the induction of single-cell invasion. *Biochem. Biophys. Res. Commun.* **435**, 58–63.

Naglich, J. G., Metherall, J. E., Russell, D. W. and Eidels, L. (1992). Expression cloning of a diphtheria toxin receptor: identity with a heparin-binding EGF-like growth factor precursor. *Cell* **69**, 1051–1061.

Nakase, I., Niwa, M., Takeuchi, T., Sonomura, K., Kawabata, N., Koike, Y., Takehashi, M., Tanaka, S., Ueda, K., Simpson, J. C., et al. (2004). Cellular uptake of arginine-rich peptides: roles for macropinocytosis and actin rearrangement. *Mol. Ther.* **10**, 1011–1022.

Nakase, I., Tadokoro, A., Kawabata, N., Takeuchi, T., Katoh, H., Hiramoto, K., Negishi, M., Nomizu, M., Sugiura, Y. and Futaki, S. (2007). Interaction of arginine-rich peptides with membrane-associated proteoglycans is crucial for induction of actin organization and macropinocytosis. *Biochemistry* **46**, 492–501.

Nashed, B. F., Zhang, T., Al-Alwan, M., Srinivasan, G., Halayko, A. J., Okkenhaug, K., Vanhaesebroeck, B., Hayglass, K. T. and Marshall, A. J. (2007). Role of the phosphoinositide 3-kinase p110delta in generation of type 2 cytokine responses and allergic airway inflammation. *Eur. J. Immunol.* **37**, 416–424.

Nawshad, A. and Hay, E. D. (2003). TGFbeta3 signaling activates transcription of the LEF1 gene to induce epithelial mesenchymal transformation during mouse palate development. *J. Cell Biol.* **163**, 1291–1301.

Nieto, M. A., Sargent, M. G., Wilkinson, D. G. and Cooke, J. (1994). Control of cell behavior during vertebrate development by Slug, a zinc finger gene. *Science* **264**, 835–839.

Nobukuni, T., Joaquin, M., Roccio, M., Dann, S. G., Kim, S. Y., Gulati, P., Byfield, M. P., Backer, J. M., Natt, F., Bos, J. L., et al. (2005). Amino acids mediate mTOR/raptor signaling through activation of class 3 phosphatidylinositol 3OH-kinase. *Proc. Natl. Acad. Sci. U.S.A.* **102**, 14238–14243.

Norris, F. A., Atkins, R. C. and Majerus, P. W. (1997). The cDNA cloning and characterization of inositol polyphosphate 4-phosphatase type II. Evidence for conserved alternative splicing in the 4-phosphatase family. *J. Biol. Chem.* **272**, 23859–23864.

O'Neal, D. P., Hirsch, L. R., Halas, N. J., Payne, J. D. and West, J. L. (2004). Photo-thermal tumor ablation in mice using near infrared-absorbing nanoparticles. *Cancer Lett.* **209**, 171–176.

O'Reilly, K. E., Rojo, F., She, Q.-B., Solit, D., Mills, G. B., Smith, D., Lane, H., Hofmann, F., Hicklin, D. J., Ludwig, D. L., et al. (2006). mTOR inhibition induces upstream receptor tyrosine kinase signaling and activates Akt. *Cancer*

Res. **66**, 1500–1508.

Ochs, M., Nyengaard, J. R., Jung, A., Knudsen, L., Voigt, M., Wahlers, T., Richter, J. and Gundersen, H. J. G. (2004). The number of alveoli in the human lung. *Am. J. Respir. Crit. Care Med.* **169**, 120–124.

Okkenhaug, K. (2013). Signaling by the phosphoinositide 3-kinase family in immune cells. *Annu. Rev. Immunol.* **31**, 675–704.

Okubo, T. and Hogan, B. L. M. (2004). Hyperactive Wnt signaling changes the developmental potential of embryonic lung endoderm. *J. Biol.* **3**, 11.

Olive, K. P., Jacobetz, M. A., Davidson, C. J., Gopinathan, A., McIntyre, D., Honess, D., Madhu, B., Goldgraben, M. A., Caldwell, M. E., Allard, D., et al. (2009). Inhibition of Hedgehog signaling enhances delivery of chemotherapy in a mouse model of pancreatic cancer. *Science* **324**, 1457–1461.

Olsen, E., Duvic, M., Frankel, A., Kim, Y., Martin, A., Vonderheid, E., Jegasothy, B., Wood, G., Gordon, M., Heald, P., et al. (2001). Pivotal phase III trial of two dose levels of denileukin diftitox for the treatment of cutaneous T-cell lymphoma. *J. Clin. Oncol.* **19**, 376–388.

Onda, M., Beers, R., Xiang, L., Lee, B., Weldon, J. E., Kreitman, R. J. and Pastan, I. (2011). Recombinant immunotoxin against B-cell malignancies with no immunogenicity in mice by removal of B-cell epitopes. *Proc. Natl. Acad. Sci. U.S.A.* **108**, 5742–5747.

Onda, M., Beers, R., Xiang, L., Nagata, S., Wang, Q.-C. and Pastan, I. (2008). An immunotoxin with greatly reduced immunogenicity by identification and removal of B cell epitopes. *Proc. Natl. Acad. Sci. U.S.A.* **105**, 11311–11316.

Ong, S. H., Guy, G. R., Hadari, Y. R., Laks, S., Gotoh, N., Schlessinger, J. and Lax, I. (2000). FRS2 proteins recruit intracellular signaling pathways by binding to diverse targets on fibroblast growth factor and nerve growth factor receptors. *Molecular and Cellular Biology* **20**, 979–989.

Ong, S. H., Hadari, Y. R., Gotoh, N., Guy, G. R., Schlessinger, J. and Lax, I. (2001). Stimulation of phosphatidylinositol 3-kinase by fibroblast growth factor receptors is mediated by coordinated recruitment of multiple docking proteins. *Proc. Natl. Acad. Sci. U.S.A.* **98**, 6074–6079.

Ornitz, D. M., Xu, J., Colvin, J. S., McEwen, D. G., MacArthur, C. A., Coulier, F., Gao, G. and Goldfarb, M. (1996). Receptor specificity of the fibroblast growth factor family. *J. Biol. Chem.* **271**, 15292–15297.

Orr-Urtreger, A., Bedford, M. T., Burakova, T., Arman, E., Zimmer, Y., Yayon, A., Givol, D. and Lonai, P. (1993). Developmental localization of the splicing alternatives of fibroblast growth factor receptor-2 (FGFR2). *Developmental Biology* **158**, 475–486.

Owens, D. E. and Peppas, N. A. (2006). Opsonization, biodistribution, and pharmacokinetics of polymeric nanoparticles. *Int J Pharm* **307**, 93–102.

Palmada, M., Speil, A., Jeyaraj, S., Böhmer, C. and Lang, F. (2005). The serine/threonine kinases SGK1, 3 and PKB stimulate the amino acid transporter ASCT2. *Biochem. Biophys. Res. Commun.* **331**, 272–277.

Papini, E., Rappuoli, R., Murgia, M. and Montecucco, C. (1993). Cell penetration of diphtheria toxin. Reduction of the interchain disulfide bridge is the rate-limiting step of translocation in the cytosol. *J. Biol. Chem.* **268**, 1567–1574.

Park, J., Kwon, D., Choi, C., Oh, J.-W. and Benveniste, E. N. (2003). Chloroquine induces activation of nuclear factor-kappaB and subsequent expression of pro-inflammatory cytokines by human astroglial cells. *J. Neurochem.* **84**, 1266–1274.

Park, W. S., Heo, W. D., Whalen, J. H., O'Rourke, N. A., Bryan, H. M., Meyer, T. and Teruel, M. N. (2008). Comprehensive identification of PIP3-regulated PH domains from C. elegans to H. sapiens by model prediction and live imaging. *Mol. Cell* **30**, 381–392.

Park, W. Y., Miranda, B., Lebeche, D., Hashimoto, G. and Cardoso, W. V. (1998). FGF-10 is a chemotactic factor for distal epithelial buds during lung development. *Developmental Biology* **201**, 125–134.

Parker, D. and Prince, A. (2011). Innate immunity in the respiratory epithelium. *Am. J. Respir. Cell Mol. Biol.* **45**, 189–201.

Pastan, I., Hassan, R., FitzGerald, D. J. and Kreitman, R. J. (2006). Immunotoxin therapy of cancer. *Nat. Rev. Cancer* **6**, 559–565.

Patel, V. N., Likar, K. M., Zisman-Rozen, S., Cowherd, S. N., Lassiter, K. S., Sher, I., Yates, E. A., Turnbull, J. E., Ron, D. and Hoffman, M. P. (2008). Specific heparan sulfate structures modulate FGF10-mediated submandibular gland epithelial morphogenesis and differentiation. *J. Biol. Chem.* **283**, 9308–9317.

Patki, V., Virbasius, J., Lane, W. S., Toh, B. H., Shpetner, H. S. and Corvera, S. (1997). Identification of an early endosomal protein regulated by phosphatidylinositol 3-kinase. *Proc. Natl. Acad. Sci. U.S.A.* **94**, 7326–7330.

Patrucco, E., Notte, A., Barberis, L., Selvetella, G., Maffei, A., Brancaccio, M., Marengo, S., Russo, G., Azzolino, O., Rybalkin, S. D., et al. (2004). PI3Kgamma modulates the cardiac response to chronic pressure overload by distinct kinase-dependent and -independent effects. *Cell* **118**, 375–387.

Pearse, B. M. (1976). Clathrin: a unique protein associated with intracellular transfer of membrane by coated vesicles. *Proc. Natl. Acad. Sci. U.S.A.* **73**, 1255–1259.

Perl, A. K., Wilgenbus, P., Dahl, U., Semb, H. and Christofori, G. (1998). A causal role for E-cadherin in the transition from adenoma to carcinoma. *Nature* **392**, 190–193.

Plank, C., Oberhauser, B., Mechtler, K., Koch, C. and Wagner, E. (1994). The influence of endosome-disruptive peptides on gene transfer using synthetic virus-like gene transfer systems. *J. Biol. Chem.* **269**, 12918–12924.

Popova, A. P., Bozyk, P. D., Goldsmith, A. M., Linn, M. J., Lei, J., Bentley, J. K. and Hershenson, M. B. (2010). Autocrine production of TGF-beta1 promotes myofibroblastic differentiation of neonatal lung mesenchymal stem cells. *Am. J. Physiol. Lung Cell Mol. Physiol.* **298**, L735–43.

Posey, J. A., Khazaeli, M. B., Bookman, M. A., Nowrouzi, A., Grizzle, W. E., Thornton, J., Carey, D. E., Lorenz, J. M., Sing, A. P., Siegall, C. B., et al. (2002). A phase I trial of the single-chain immunotoxin SGN-10 (BR96 sFv-PE40) in patients with advanced solid tumors. *Clin. Cancer Res.* **8**, 3092–3099.

Post, M., Souza, P., Liu, J., Tseu, I., Wang, J., Kuliszewski, M. and Tanswell, A. K. (1996). Keratinocyte growth factor and its receptor are involved in regulating early lung branching. *Development* **122**, 3107–3115.

Potter, C. J., Pedraza, L. G. and Xu, T. (2002). Akt regulates growth by directly phosphorylating Tsc2. *Nat. Cell Biol.* **4**, 658–665.

Pritchard, C., Mecham, B., Dumpit, R., Coleman, I., Bhattacharjee, M., Chen, Q., Sikes, R. A. and Nelson, P. S. (2009). Conserved gene expression programs integrate mammalian prostate development and tumorigenesis. *Cancer Res.* **69**, 1739–1747.

Rawlins, E. L., Clark, C. P., Xue, Y. and Hogan, B. L. M. (2009). The Id2+ distal tip lung epithelium contains individual multipotent embryonic progenitor cells. *Development* **136**, 3741–3745.

Rádis-Baptista, G. and Kerkis, I. (2011). Crotamine, a small basic polypeptide myotoxin from rattlesnake venom with cell-penetrating properties. *Curr. Pharm. Des.* **17**, 4351–4361.

Richard, J. P., Melikov, K., Brooks, H., Prevot, P., Lebleu, B. and Chernomordik, L. V. (2005). Cellular uptake of unconjugated TAT peptide involves clathrin-dependent endocytosis and heparan sulfate receptors. *J. Biol. Chem.* **280**, 15300–15306.

Richard, J. P., Melikov, K., Vives, E., Ramos, C., Verbeure, B., Gait, M. J., Chernomordik, L. V. and Lebleu, B. (2003). Cell-penetrating peptides. A reevaluation of the mechanism of cellular uptake. *J. Biol. Chem.* **278**, 585–590.

Rock, J. R., Barkauskas, C. E., Cronce, M. J., Xue, Y., Harris, J. R., Liang, J., Noble, P. W. and Hogan, B. L. M. (2011). Multiple stromal populations contribute to pulmonary fibrosis without evidence for epithelial to mesenchymal transition. *Proc. Natl. Acad. Sci. U.S.A.* **108**, E1475–83.

Rockich, B. E., Hrycaj, S. M., Shih, H. P., Nagy, M. S., Ferguson, M. A. H., Kopp, J. L., Sander, M., Wellik, D. M. and Spence, J. R. (2013). Sox9 plays multiple roles in the lung epithelium during branching morphogenesis. *Proc.*

Natl. Acad. Sci. U.S.A. **110**, E4456–64.

Rodriguez-Viciana, P., Warne, P. H., Dhand, R., Vanhaesebroeck, B., Gout, I., Fry, M. J., Waterfield, M. D. and Downward, J. (1994). Phosphatidylinositol-3-OH kinase as a direct target of Ras. *Nature* **370**, 527–532.

Roopenian, D. C. and Akilesh, S. (2007). FcRn: the neonatal Fc receptor comes of age. *Nat. Rev. Immunol.* **7**, 715–725.

Rothbard, J. B., Jessop, T. C. and Wender, P. A. (2005). Adaptive translocation: the role of hydrogen bonding and membrane potential in the uptake of guanidinium-rich transporters into cells. *Adv. Drug Deliv. Rev.* **57**, 495–504.

Rothberg, K. G., Heuser, J. E., Donzell, W. C., Ying, Y. S., Glenney, J. R. and Anderson, R. G. (1992). Caveolin, a protein component of caveolae membrane coats. *Cell* **68**, 673–682.

Rubin, C., Zwang, Y., Vaisman, N., Ron, D. and Yarden, Y. (2005). Phosphorylation of carboxyl-terminal tyrosines modulates the specificity of Sprouty-2 inhibition of different signaling pathways. *J. Biol. Chem.* **280**, 9735–9744.

Rudin, C. M., Durinck, S., Stawiski, E. W., Poirier, J. T., Modrusan, Z., Shames, D. S., Bergbower, E. A., Guan, Y., Shin, J., Guillory, J., et al. (2012). Comprehensive genomic analysis identifies SOX2 as a frequently amplified gene in small-cell lung cancer. *Nat. Genet.* **44**, 1111–1116.

Rudolph, C., Plank, C., Lausier, J., Schillinger, U., Müller, R. H. and Rosenecker, J. (2003). Oligomers of the arginine-rich motif of the HIV-1 TAT protein are capable of transferring plasmid DNA into cells. *J. Biol. Chem.* **278**, 11411–11418.

Ruotsalainen, T., Joensuu, H., Mattson, K. and Salven, P. (2002). High pretreatment serum concentration of basic fibroblast growth factor is a predictor of poor prognosis in small cell lung cancer. *Cancer Epidemiol. Biomarkers Prev.* **11**, 1492–1495.

Rusten, T. E., Rodahl, L. M. W., Pattni, K., Englund, C., Samakovlis, C., Dove, S., Brech, A. and Stenmark, H. (2006). Fab1 phosphatidylinositol 3-phosphate 5-kinase controls trafficking but not silencing of endocytosed receptors. *Mol. Biol. Cell* **17**, 3989–4001.

Ryser, H. J., Mandel, R. and Ghani, F. (1991). Cell surface sulfhydryls are required for the cytotoxicity of diphtheria toxin but not of ricin in Chinese hamster ovary cells. *J. Biol. Chem.* **266**, 18439–18442.

Sakagami, M., Omidi, Y., Campbell, L., Kandalaft, L. E., Morris, C. J., Barar, J. and Gumbleton, M. (2006). Expression and transport functionality of FcRn within rat alveolar epithelium: a study in primary cell culture and in the isolated perfused lung. *Pharm. Res.* **23**, 270–279.

Samuels, Y., Wang, Z., Bardelli, A., Silliman, N., Ptak, J., Szabo, S., Yan, H.,

Gazdar, A., Powell, S. M., Riggins, G. J., et al. (2004). High frequency of mutations of the PIK3CA gene in human cancers. *Science* **304**, 554.

Sanchez, R. M., Erhard, K., Hardwicke, M. A., Lin, H., McSurdy-Freed, J., Plant, R., Raha, K., Rominger, C. M., Schaber, M. D., Spengler, M. D., et al. (2012). Synthesis and structure-activity relationships of 1,2,4-triazolo[1,5-a]pyrimidin-7(3H)-ones as novel series of potent β isoform selective phosphatidylinositol 3-kinase inhibitors. *Bioorganic & Medicinal Chemistry Letters* **22**, 3198–3202.

Sarbassov, D. D., Ali, S. M., Sengupta, S., Sheen, J.-H., Hsu, P. P., Bagley, A. F., Markhard, A. L. and Sabatini, D. M. (2006). Prolonged rapamycin treatment inhibits mTORC2 assembly and Akt/PKB. *Mol. Cell* **22**, 159–168.

Sarbassov, D. D., Guertin, D. A., Ali, S. M. and Sabatini, D. M. (2005). Phosphorylation and regulation of Akt/PKB by the rictor-mTOR complex. *Science* **307**, 1098–1101.

Sarnovsky, R., Tendler, T., Makowski, M., Kiley, M., Antignani, A., Traini, R., Zhang, J., Hassan, R. and FitzGerald, D. J. (2010). Initial characterization of an immunotoxin constructed from domains II and III of cholera exotoxin. *Cancer Immunol. Immunother.* **59**, 737–746.

Sasaki, T., Irie-Sasaki, J., Jones, R. G., Oliveira-dos-Santos, A. J., Stanford, W. L., Bolon, B., Wakeham, A., Itie, A., Bouchard, D., Kozieradzki, I., et al. (2000). Function of PI3Kgamma in thymocyte development, T cell activation, and neutrophil migration. *Science* **287**, 1040–1046.

Saslowsky, D. E., Welscher, te, Y. M., Chinnapen, D. J.-F., Wagner, J. S., Wan, J., Kern, E. and Lencer, W. I. (2013). Ganglioside GM1-mediated transcytosis of cholera toxin bypasses the retrograde pathway and depends on the structure of the ceramide domain. *J. Biol. Chem.* **288**, 25804–25809.

Sawyer, C., Sturge, J., Bennett, D. C., O'Hare, M. J., Allen, W. E., Bain, J., Jones, G. E. and Vanhaesebroeck, B. (2003). Regulation of breast cancer cell chemotaxis by the phosphoinositide 3-kinase p110delta. *Cancer Res.* **63**, 1667–1675.

Schaeffer, E. M., Marchionni, L., Huang, Z., Simons, B., Blackman, A., Yu, W., Parmigiani, G. and Berman, D. M. (2008). Androgen-induced programs for prostate epithelial growth and invasion arise in embryogenesis and are reactivated in cancer. *Oncogene* **27**, 7180–7191.

Schittny, J. C., Miserocchi, G. and Sparrow, M. P. (2000). Spontaneous peristaltic airway contractions propel lung liquid through the bronchial tree of intact and fetal lung explants. *Am. J. Respir. Cell Mol. Biol.* **23**, 11–18.

Schu, P. V., Takegawa, K., Fry, M. J., Stack, J. H., Waterfield, M. D. and Emr, S. D. (1993). Phosphatidylinositol 3-kinase encoded by yeast VPS34 gene essential for protein sorting. *Science* **260**, 88–91.

Schuerer-Maly, C. C., Eckmann, L., Kagnoff, M. F., Falco, M. T. and Maly, F. E.

(1994). Colonic epithelial cell lines as a source of interleukin-8: stimulation by inflammatory cytokines and bacterial lipopolysaccharide. *Immunology* **81**, 85–91.

Scotton, C. J. and Chambers, R. C. (2007). Molecular targets in pulmonary fibrosis: the myofibroblast in focus. *Chest* **132**, 1311–1321.

Sequeira, S. J., Gervais, E. M., Ray, S. and Larsen, M. (2013). Genetic modification and recombination of salivary gland organ cultures. *J Vis Exp* e50060.

Shi, W., Xu, J. and Warburton, D. (2009). Development, repair and fibrosis: what is common and why it matters. *Respirology* **14**, 656–665.

Shimizu, T., Tolcher, A. W., Papadopoulos, K. P., Beeram, M., Rasco, D. W., Smith, L. S., Gunn, S., Smetzer, L., Mays, T. A., Kaiser, B., et al. (2012). The clinical effect of the dual-targeting strategy involving PI3K/AKT/mTOR and RAS/MEK/ERK pathways in patients with advanced cancer. *Clin. Cancer Res.* **18**, 2316–2325.

Shirakihara, T., Horiguchi, K., Miyazawa, K., Ehata, S., Shibata, T., Morita, I., Miyazono, K. and Saitoh, M. (2011). TGF-β regulates isoform switching of FGF receptors and epithelial-mesenchymal transition. *EMBO J.* **30**, 783–795.

Sime, P. J., Xing, Z., Graham, F. L., Csaky, K. G. and Gauldie, J. (1997). Adenovector-mediated gene transfer of active transforming growth factor-beta1 induces prolonged severe fibrosis in rat lung. *J. Clin. Invest.* **100**, 768–776.

Sioud, M. (2006). Innate sensing of self and non-self RNAs by Toll-like receptors. *Trends Mol Med* **12**, 167–176.

Skaper, S. D., Kee, W. J., Facci, L., Macdonald, G., Doherty, P. and Walsh, F. S. (2000). The FGFR1 inhibitor PD 173074 selectively and potently antagonizes FGF-2 neurotrophic and neurotropic effects. *J. Neurochem.* **75**, 1520–1527.

Smith, D. C., Spooner, R. A., Watson, P. D., Murray, J. L., Hodge, T. W., Amessou, M., Johannes, L., Lord, J. M. and Roberts, L. M. (2006a). Internalized Pseudomonas exotoxin A can exploit multiple pathways to reach the endoplasmic reticulum. *Traffic* **7**, 379–393.

Smith, T. G., Karlsson, M., Lunn, J. S., Eblaghie, M. C., Keenan, I. D., Farrell, E. R., Tickle, C., Storey, K. G. and Keyse, S. M. (2006b). Negative feedback predominates over cross-regulation to control ERK MAPK activity in response to FGF signalling in embryos. *FEBS Lett.* **580**, 4242–4245.

Soldati, T., Rancaño, C., Geissler, H. and Pfeffer, S. R. (1995). Rab7 and Rab9 are recruited onto late endosomes by biochemically distinguishable processes. *J. Biol. Chem.* **270**, 25541–25548.

Steinberg, Z., Myers, C., Heim, V. M., Lathrop, C. A., Rebustini, I. T., Stewart,

J. S., Larsen, M. and Hoffman, M. P. (2005). FGFR2b signaling regulates ex vivo submandibular gland epithelial cell proliferation and branching morphogenesis. *Development* **132**, 1223–1234.

Stockley, R. A. and Turner, A. M. (2013). α-1-Antitrypsin deficiency: clinical variability, assessment, and treatment. *Trends Mol Med*.

Suhorutsenko, J., Oskolkov, N., Arukuusk, P., Kurrikoff, K., Eriste, E., Copolovici, D.-M. and Langel, U. (2011). Cell-penetrating peptides, PepFects, show no evidence of toxicity and immunogenicity in vitro and in vivo. *Bioconjug. Chem.* **22**, 2255–2262.

Sun, H., Oudit, G. Y., Ramirez, R. J., Costantini, D. and Backx, P. H. (2004). The phosphoinositide 3-kinase inhibitor LY294002 enhances cardiac myocyte contractility via a direct inhibition of Ik,slow currents. *Cardiovasc. Res.* **62**, 509–520.

Sutherland, D., Samakovlis, C. and Krasnow, M. A. (1996). branchless encodes a Drosophila FGF homolog that controls tracheal cell migration and the pattern of branching. *Cell* **87**, 1091–1101.

Sutterlüty, H., Mayer, C.-E., Setinek, U., Attems, J., Ovtcharov, S., Mikula, M., Mikulits, W., Micksche, M. and Berger, W. (2007). Down-regulation of Sprouty2 in non-small cell lung cancer contributes to tumor malignancy via extracellular signal-regulated kinase pathway-dependent and -independent mechanisms. *Mol. Cancer Res.* **5**, 509–520.

Takeda, Y., Tsujino, K., Kijima, T. and Kumanogoh, A. (2014). Efficacy and safety of pirfenidone for idiopathic pulmonary fibrosis. *Patient Prefer Adherence* **8**, 361–370.

Tang, M.-J., Cai, Y., Tsai, S.-J., Wang, Y.-K. and Dressler, G. R. (2002). Ureteric bud outgrowth in response to RET activation is mediated by phosphatidylinositol 3-kinase. *Developmental Biology* **243**, 128–136.

Taylor, G. S., Maehama, T. and Dixon, J. E. (2000). Myotubularin, a protein tyrosine phosphatase mutated in myotubular myopathy, dephosphorylates the lipid second messenger, phosphatidylinositol 3-phosphate. *Proc. Natl. Acad. Sci. U.S.A.* **97**, 8910–8915.

Tefft, J. D., Lee, M., Smith, S., Leinwand, M., Zhao, J., Bringas, P., Crowe, D. L. and Warburton, D. (1999). Conserved function of mSpry-2, a murine homolog of Drosophila sprouty, which negatively modulates respiratory organogenesis. *Curr. Biol.* **9**, 219–222.

Tessier, M. and Woodgett, J. R. (2006). Role of the Phox homology domain and phosphorylation in activation of serum and glucocorticoid-regulated kinase-3. *J. Biol. Chem.* **281**, 23978–23989.

Theveneau, E., Steventon, B., Scarpa, E., Garcia, S., Trepat, X., Streit, A. and Mayor, R. (2013). Chase-and-run between adjacent cell populations promotes directional collective migration. *Nat. Cell Biol.* **15**, 763–772.

Thomas, M. J., Smith, A., Head, D. H., Milne, L., Nicholls, A., Pearce, W., Vanhaesebroeck, B., Wymann, M. P., Hirsch, E., Trifilieff, A., et al. (2005). Airway inflammation: chemokine-induced neutrophilia and the class I phosphoinositide 3-kinases. *Eur. J. Immunol.* **35**, 1283–1291.

Tibolla, G., Piñeiro, R., Chiozzotto, D., Mavrommati, I., Wheeler, A. P., Norata, G. D., Catapano, A. L., Maffucci, T. and Falasca, M. (2013). Class II phosphoinositide 3-kinases contribute to endothelial cells morphogenesis. *PLoS ONE* **8**, e53808.

Tiozzo, C., De Langhe, S., Yu, M., Londhe, V. A., Carraro, G., Li, M., Li, C., Xing, Y., Anderson, S., Borok, Z., et al. (2009). Deletion of Pten expands lung epithelial progenitor pools and confers resistance to airway injury. *Am. J. Respir. Crit. Care Med.* **180**, 701–712.

Turcatel, G., Rubin, N., Menke, D. B., Martin, G., Shi, W. and Warburton, D. (2013). Lung mesenchymal expression of Sox9 plays a critical role in tracheal development. *BMC Biol.* **11**, 117.

Turner, N. and Grose, R. (2010). Fibroblast growth factor signalling: from development to cancer. *Nat. Rev. Cancer* **10**, 116–129.

Tünnemann, G., Martin, R. M., Haupt, S., Patsch, C., Edenhofer, F. and Cardoso, M. C. (2006). Cargo-dependent mode of uptake and bioavailability of TAT-containing proteins and peptides in living cells. *FASEB J.* **20**, 1775–1784.

Ullrich, O., Reinsch, S., Urbé, S., Zerial, M. and Parton, R. G. (1996). Rab11 regulates recycling through the pericentriolar recycling endosome. *J. Cell Biol.* **135**, 913–924.

Unbekandt, M., Del Moral, P.-M., Sala, F. G., Bellusci, S., Warburton, D. and Fleury, V. (2008). Tracheal occlusion increases the rate of epithelial branching of embryonic mouse lung via the FGF10-FGFR2b-Sprouty2 pathway. *Mech. Dev.* **125**, 314–324.

Utermark, T., Rao, T., Cheng, H., Wang, Q., Lee, S. H., Wang, Z. C., Iglehart, J. D., Roberts, T. M., Muller, W. J. and Zhao, J. J. (2012). The p110α and p110β isoforms of PI3K play divergent roles in mammary gland development and tumorigenesis. *Genes Dev.* **26**, 1573–1586.

van Noort, M., Meeldijk, J., van der Zee, R., Destree, O. and Clevers, H. (2002). Wnt signaling controls the phosphorylation status of beta-catenin. *J. Biol. Chem.* **277**, 17901–17905.

Vanhaesebroeck, B., Welham, M. J., Kotani, K., Stein, R., Warne, P. H., Zvelebil, M. J., Higashi, K., Volinia, S., Downward, J. and Waterfield, M. D. (1997). P110delta, a novel phosphoinositide 3-kinase in leukocytes. *Proc. Natl. Acad. Sci. U.S.A.* **94**, 4330–4335.

Vareille, M., Kieninger, E., Edwards, M. R. and Regamey, N. (2011). The airway epithelium: soldier in the fight against respiratory viruses. *Clin. Microbiol. Rev.*

24, 210–229.

Vitkus, S. J., Hanifin, S. A. and McGee, D. W. (1998). Factors affecting Caco-2 intestinal epithelial cell interleukin-6 secretion. *In Vitro Cell. Dev. Biol. Anim.* **34**, 660–664.

Vivès, E., Brodin, P. and Lebleu, B. (1997). A truncated HIV-1 Tat protein basic domain rapidly translocates through the plasma membrane and accumulates in the cell nucleus. *J. Biol. Chem.* **272**, 16010–16017.

Vlahos, C. J., Matter, W. F., Hui, K. Y. and Brown, R. F. (1994). A specific inhibitor of phosphatidylinositol 3-kinase, 2-(4-morpholinyl)-8-phenyl-4H-1-benzopyran-4-one (LY294002). *J. Biol. Chem.* **269**, 5241–5248.

Volckaert, T., Campbell, A., Dill, E., Li, C., Minoo, P. and De Langhe, S. (2013). Localized Fgf10 expression is not required for lung branching morphogenesis but prevents differentiation of epithelial progenitors. *Development* **140**, 3731–3742.

Walker, E. H., Pacold, M. E., Perisic, O., Stephens, L., Hawkins, P. T., Wymann, M. P. and Williams, R. L. (2000). Structural determinants of phosphoinositide 3-kinase inhibition by wortmannin, LY294002, quercetin, myricetin, and staurosporine. *Mol. Cell* **6**, 909–919.

Wang, J., Ito, T., Udaka, N., Okudela, K., Yazawa, T. and Kitamura, H. (2005). PI3K-AKT pathway mediates growth and survival signals during development of fetal mouse lung. *Tissue Cell* **37**, 25–35.

Warburton, D., El-Hashash, A., Carraro, G., Tiozzo, C., Sala, F., Rogers, O., De Langhe, S., Kemp, P. J., Riccardi, D., Torday, J., et al. (2010). Lung organogenesis. *Curr. Top. Dev. Biol.* **90**, 73–158.

Warner, J. O., Marguet, C., Rao, R., Roche, W. R. and Pohunek, P. (1998). Inflammatory mechanisms in childhood asthma. *Clin. Exp. Allergy* **28 Suppl 5**, 71–5– discussion 90–1.

Watkins, C. L., Brennan, P., Fegan, C., Takayama, K., Nakase, I., Futaki, S. and Jones, A. T. (2009). Cellular uptake, distribution and cytotoxicity of the hydrophobic cell penetrating peptide sequence PFVYLI linked to the proapoptotic domain peptide PAD. *J Control Release* **140**, 237–244.

Weaver, M., Batts, L. and Hogan, B. L. M. (2003). Tissue interactions pattern the mesenchyme of the embryonic mouse lung. *Developmental Biology* **258**, 169–184.

Wei, J., Jones, J., Kang, J., Card, A., Krimm, M., Hancock, P., Pei, Y., Ason, B., Payson, E., Dubinina, N., et al. (2011). RNA-induced silencing complex-bound small interfering RNA is a determinant of RNA interference-mediated gene silencing in mice. *Mol. Pharmacol.* **79**, 953–963.

Wei, X., Han, J., Chen, Z.-Z., Qi, B.-W., Wang, G.-C., Ma, Y.-H., Zheng, H., Luo, Y.-F., Wei, Y.-Q. and Chen, L.-J. (2010). A phosphoinositide 3-kinase-gamma

inhibitor, AS605240 prevents bleomycin-induced pulmonary fibrosis in rats. *Biochem. Biophys. Res. Commun.* **397**, 311–317.

Weibel, E. R. (2009). What makes a good lung? *Swiss Med Wkly* **139**, 375–386.

WEIBEL, E. R. and GOMEZ, D. M. (1962). Architecture of the human lung. Use of quantitative methods establishes fundamental relations between size and number of lung structures. *Science* **137**, 577–585.

WHO | The top 10 causes of death WHO | The top 10 causes of death. *WHO*.

Willis, B. C., Liebler, J. M., Luby-Phelps, K., Nicholson, A. G., Crandall, E. D., Bois, du, R. M. and Borok, Z. (2005). Induction of epithelial-mesenchymal transition in alveolar epithelial cells by transforming growth factor-beta1: potential role in idiopathic pulmonary fibrosis. *Am. J. Pathol.* **166**, 1321–1332.

Wirth, A., Jung, M., Bies, C., Frien, M., Tyedmers, J., Zimmermann, R. and Wagner, R. (2003). The Sec61p complex is a dynamic precursor activated channel. *Mol. Cell* **12**, 261–268.

Wojtalla, A., Fischer, B., Kotelevets, N., Mauri, F. A., Sobek, J., Rehrauer, H., Wotzkow, C., Tschan, M. P., Seckl, M. J., Zangemeister-Wittke, U., et al. (2013). Targeting the phosphoinositide 3-kinase p110-α isoform impairs cell proliferation, survival, and tumor growth in small cell lung cancer. *Clin. Cancer Res.* **19**, 96–105.

Wong, A., Lamothe, B., Lee, A., Schlessinger, J., Lax, I. and Li, A. (2002). FRS2 alpha attenuates FGF receptor signaling by Grb2-mediated recruitment of the ubiquitin ligase Cbl. *Proc. Natl. Acad. Sci. U.S.A.* **99**, 6684–6689.

Wu, S., Kasisomayajula, K., Peng, J. and Bancalari, E. (2009). Inhibition of JNK enhances TGF-beta1-activated Smad2 signaling in mouse embryonic lung. *Pediatr. Res.* **65**, 381–386.

Wurmser, A. E. and Emr, S. D. (1998). Phosphoinositide signaling and turnover: PtdIns(3)P, a regulator of membrane traffic, is transported to the vacuole and degraded by a process that requires lumenal vacuolar hydrolase activities. *EMBO J.* **17**, 4930–4942.

Xian, W., Schwertfeger, K. L., Vargo-Gogola, T. and Rosen, J. M. (2005). Pleiotropic effects of FGFR1 on cell proliferation, survival, and migration in a 3D mammary epithelial cell model. *J. Cell Biol.* **171**, 663–673.

Xing, Y., Li, C., Hu, L., Tiozzo, C., Li, M., Chai, Y., Bellusci, S., Anderson, S. and Minoo, P. (2008). Mechanisms of TGFbeta inhibition of LUNG endodermal morphogenesis: the role of TbetaRII, Smads, Nkx2.1 and Pten. *Developmental Biology* **320**, 340–350.

Xu, Y., Hortsman, H., Seet, L., Wong, S. H. and Hong, W. (2001). SNX3 regulates endosomal function through its PX-domain-mediated interaction with PtdIns(3)P. *Nat. Cell Biol.* **3**, 658–666.

Yakes, F. M., Chinratanalab, W., Ritter, C. A., King, W., Seelig, S. and Arteaga, C. L. (2002). Herceptin-induced inhibition of phosphatidylinositol-3 kinase and Akt Is required for antibody-mediated effects on p27, cyclin D1, and antitumor action. *Cancer Res.* **62**, 4132–4141.

Yamaizumi, M., Mekada, E., Uchida, T. and Okada, Y. (1978). One molecule of diphtheria toxin fragment A introduced into a cell can kill the cell. *Cell* **15**, 245–250.

Yan, G., Fukabori, Y., McBride, G., Nikolaropolous, S. and McKeehan, W. L. (1993). Exon switching and activation of stromal and embryonic fibroblast growth factor (FGF)-FGF receptor genes in prostate epithelial cells accompany stromal independence and malignancy. *Molecular and Cellular Biology* **13**, 4513–4522.

Yan, W., Fu, Y., Tian, D., Liao, J., Liu, M., Wang, B., Xia, L., Zhu, Q. and Luo, M. (2009). PI3 kinase/Akt signaling mediates epithelial-mesenchymal transition in hypoxic hepatocellular carcinoma cells. *Biochem. Biophys. Res. Commun.* **382**, 631–636.

Yanagi, S., Kishimoto, H., Kawahara, K., Sasaki, T., Sasaki, M., Nishio, M., Yajima, N., Hamada, K., Horie, Y., Kubo, H., et al. (2007). Pten controls lung morphogenesis, bronchioalveolar stem cells, and onset of lung adenocarcinomas in mice. *J. Clin. Invest.* **117**, 2929–2940.

Yin, Y., White, A. C., Huh, S.-H., Hilton, M. J., Kanazawa, H., Long, F. and Ornitz, D. M. (2008). An FGF-WNT gene regulatory network controls lung mesenchyme development. *Developmental Biology* **319**, 426–436.

Yu, W., Ruest, L.-B. and Svoboda, K. K. H. (2009). Regulation of epithelial-mesenchymal transition in palatal fusion. *Exp. Biol. Med. (Maywood)* **234**, 483–491.

Yuan, B., Li, C., Kimura, S., Engelhardt, R. T., Smith, B. R. and Minoo, P. (2000). Inhibition of distal lung morphogenesis in Nkx2.1(-/-) embryos. *Dev. Dyn.* **217**, 180–190.

Yumoto, R., Suzuka, S., Oda, K., Nagai, J. and Takano, M. (2012). Endocytic uptake of FITC-albumin by human alveolar epithelial cell line A549. *Drug Metab. Pharmacokinet.* **27**, 336–343.

Yusoff, P., Lao, D.-H., Ong, S. H., Wong, E. S. M., Lim, J., Lo, T. L., Leong, H. F., Fong, C. W. and Guy, G. R. (2002). Sprouty2 inhibits the Ras/MAP kinase pathway by inhibiting the activation of Raf. *J. Biol. Chem.* **277**, 3195–3201.

Zalman, L. S. and Wisnieski, B. J. (1984). Mechanism of insertion of diphtheria toxin: peptide entry and pore size determinations. *Proc. Natl. Acad. Sci. U.S.A.* **81**, 3341–3345.

Zhang, J. R., Mostov, K. E., Lamm, M. E., Nanno, M., Shimida, S., Ohwaki, M. and Tuomanen, E. (2000). The polymeric immunoglobulin receptor translocates pneumococci across human nasopharyngeal epithelial cells. *Cell*

102, 827–837.

Zhang, X., Ibrahimi, O. A., Olsen, S. K., Umemori, H., Mohammadi, M. and Ornitz, D. M. (2006). Receptor specificity of the fibroblast growth factor family. The complete mammalian FGF family. *J. Biol. Chem.* **281**, 15694–15700.

Zhao, J., Shi, W., Wang, Y.-L., Chen, H., Bringas, P., Datto, M. B., Frederick, J. P., Wang, X.-F. and Warburton, D. (2002). Smad3 deficiency attenuates bleomycin-induced pulmonary fibrosis in mice. *Am. J. Physiol. Lung Cell Mol. Physiol.* **282**, L585–93.

Zhao, J., Sime, P. J., Bringas, P., Tefft, J. D., Buckley, S., Bu, D., Gauldie, J. and Warburton, D. (1999). Spatial-specific TGF-beta1 adenoviral expression determines morphogenetic phenotypes in embryonic mouse lung. *Eur. J. Cell Biol.* **78**, 715–725.

Zhao, L. and Vogt, P. K. (2008). Helical domain and kinase domain mutations in p110alpha of phosphatidylinositol 3-kinase induce gain of function by different mechanisms. *Proc. Natl. Acad. Sci. U.S.A.* **105**, 2652–2657.

Zhou, X., Takatoh, J. and Wang, F. (2011). The mammalian class 3 PI3K (PIK3C3) is required for early embryogenesis and cell proliferation. *PLoS ONE* **6**, e16358.

Zhu, W. and Nelson, C. M. (2013). PI3K regulates branch initiation and extension of cultured mammary epithelia via Akt and Rac1 respectively. *Developmental Biology* **379**, 235–245.

Zvelebil, M., Oliemuller, E., Gao, Q., Wansbury, O., Mackay, A., Kendrick, H., Smalley, M. J., Reis-Filho, J. S. and Howard, B. A. (2013). Embryonic mammary signature subsets are activated in Brca1-/- and basal-like breast cancers. *Breast Cancer Res.* **15**, R25.

Appendix

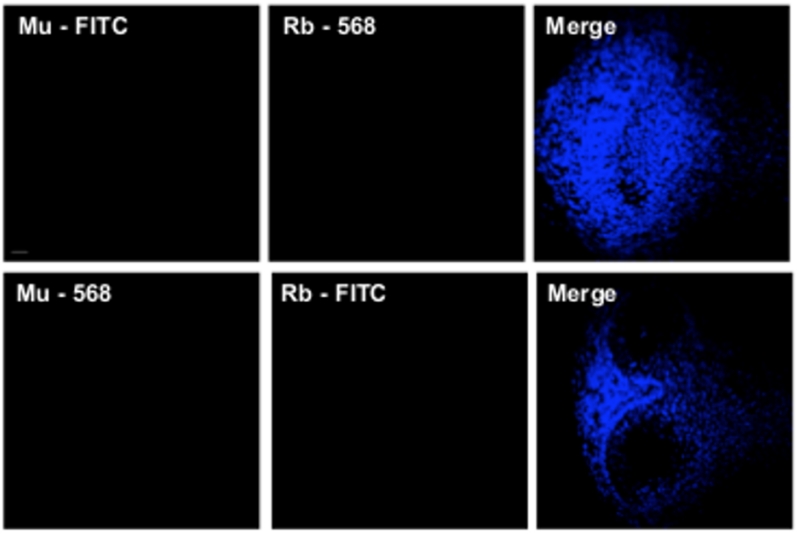

Figure A1. No primary antibody controls for embryonic lung explant immunofluorescence. Confocal images of indicated fluorescent secondary antibodies from isolated E12.5 murine lung explants cultured for 48 hours. Explants were processed for immunofluorescence as outlined in section 2.11 with the exception that there was no primary antibody step. Images are representative of three independent experiments. Scale bar = 20 μm.

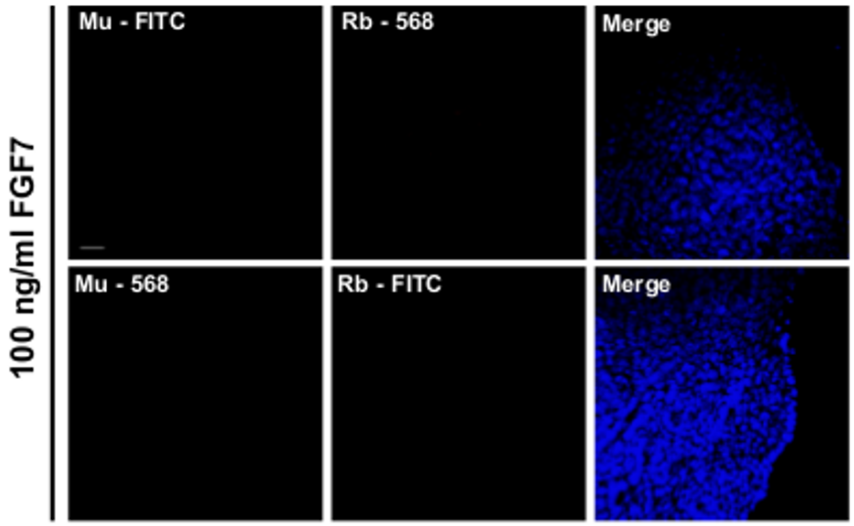

Figure A2. No primary antibody controls for isolated embryonic lung epithelium immunofluorescence. Confocal images of indicated fluorescent secondary antibodies from isolated E12.5 murine lung epithelium cultured for 96 hours with 100 ng/ml FGF7. Isolates were processed for immunofluorescence as outlined in section 2.11 with the exception that there was no primary antibody step. Images are representative of three independent experiments. Scale bar = 20 μm.

Video legends

Video 3.1. E12.5 murine lung explants continue to branch in culture. Time-lapse video of an E12.5 murine lung explant cultured over 48 hours. The video is representative of at least 12 explants. Scale bar = 50 μm.

Video 3.2. Embryonic murine lungs exhibit periodic waves of contraction along epithelial branches. Video clip of a peristaltic wave in cultured embryonic lung explants. Contractile waves appear roughly once every 30 seconds. The video is representative of at least 24 explants.

Video 3.3. AZD8055 potentiates epithelial branching in cultures of E12.5 murine embryonic lungs. Time-lapse video of an E12.5 murine lung explant cultured over 48 hours with 0.1μM of the mTORC2 inhibitor AZD8055. The video is representative of at least 12 explants. Scale bar = 50 μm.

Video 3.4. Isolated murine lung epithelium cultured with FGF10 develops smooth muscle that periodically contracts. Video clip of contractile wave present in isolated E12.5 murine lung epithelium cultured with 250 ng/ml FGF10 at 96 hours of culture. The video is representative of at least 20 epithelial isolates.

Video 3.5. Contractile waves persist in murine lung explants cultured with an inhibitor of FGFR. Video clip of contractile waves present in an E12.5 lung explant at 48 hours of culture with 100 nM of the FGFR inhibitor PD173074. The explant in the video is representative of at least 6 explants.

Publications

Published:

Carter E, Lau CY, Tosh D, Ward SG, Mrsny R. (2013) Cell penetrating peptides fail to induce an innate immune response in epithelial cells in vitro: Implications for continued therapeutic use. Eur J Pharm Biopharm. 85: 12-9

Foster JG, **Carter E**, Kilty I, MacKenzie AB, Ward SG. (2012) Mitochondrial superoxide generation enhances P2X7R-mediated loss of cell surface CD62L on Naïve human CD4+ T Lymphocytes. Journal of Immunology.190, 1551-9

Foster JG, Blunt MD, **Carter E**, Ward SG. (2012) Inhibition of PI3K Signaling Spurs New Therapeutic Opportunities in Inflammatory/Autoimmune Diseases and Hematological Malignancies. Pharmacological Reviews. 64, 1027-54

Submitted:

Carter E, Miron-Buchacra G, Goldoni S, Danahay H, Westwick J, Watson ML, Tosh D, Ward SG. (2014) Phosphoinositide 3-kinase Alpha-dependent regulation of Branching Morphogenesis in Murine Embryonic Lung: Evidence for a Role in Determining the Morphogenic Properties of FGF7.

Cravo A, **Carter E**, Erkan M, Furutani-Seiki M, Harvey E, Mrsny R (2014) Identification of Occludin as a Cell-Cell Contact Sensor for the Hippo Pathway.

Conferences

Gordon Research Conference; Lung Development, Injury & Repair. Andover, NH, USA. August 2013. Inhibition of Phosphoinositide 3-kinase/Akt Signalling Promotes Branching Morphogenesis in the Lung and Alters the Morphogenic Properties of FGF7. **Carter E,** Watson ML, Tosh D, Ward SG.